TECHNISCHE UNIVERSITÄT DARMSTADT

„Thermal Switching of the Opacity of Polymer Films for the Use in Thermo-Responsive Papers“

at the Department of Chemistry
of the Technischen Universität Darmstadt

submitted in fulfilment of the requirements for the degree of
Doctor rerum naturalium
(Dr. rer. nat.)

Doctoral thesis
by Sunna Möhle-Saul

First assessor: Prof. Dr. Markus Biesalski

Second assessor: Prof. Dr. Annette Andrieu-Brunsen

Darmstadt 2024

Date of submission: 28th March 2024

Day of the oral examination: 3rd June 2024

Möhle-Saul, Sunna: Thermal Switching of the Opacity of Polymer Films for the Use in Thermo-Responsive Papers

Darmstadt, Technische Universität Darmstadt,
Year thesis published in TUprints 2024
Date of the viva voce: 03.06.2024

Declarations / Erklärungen

§8 Abs. 1 lit. c der Promotionsordnung der TU Darmstadt
Ich versichere hiermit, dass die elektronische Version meiner Dissertation mit der schriftlichen Version übereinstimmt und für die Durchführung des Promotionsverfahrens vorliegt.

§8 Abs. 1 lit. d der Promotionsordnung der TU Darmstadt
Ich versichere hiermit, dass zu einem vorherigen Zeitpunkt noch keine Promotion versucht wurde und zu keinem früheren Zeitpunkt an einer in- oder ausländischen Hochschule eingereicht wurde. In diesem Fall sind nähere Angaben über Zeitpunkt, Hochschule, Dissertationsthema und Ergebnis dieses Versuchs mitzuteilen.

§9 Abs. 1 der Promotionsordnung der TU Darmstadt
Ich versichere hiermit, dass die vorliegende Dissertation selbstständig und nur unter Verwendung der angegebenen Quellen verfasst wurde.

§9 Abs. 2 der Promotionsordnung der TU Darmstadt
Die Arbeit hat bisher noch nicht zu Prüfungszwecken gedient.

Darmstadt, den 27. März 2024

(Sunna Möhle-Saul)

Abstract / Zusammenfassung

„Thermal Switching of the Opacity of Polymer Films for the Use in Thermo-Responsive Papers"

Thermal papers have become an integral part of everyday life: they are used in cash register receipts, parcel labels and admission tickets. Wherever information needs to be recorded quickly, cheaply and for a limited period of time. However, traditional thermal papers are subject to criticism because their color developer systems can contain substances that are potentially harmful to health and the environment. Therefore, there are already alternative papers based not on the chemical development of color, but on the physical effect of switching a highly light-scattering structure from opaque to transparent. The goal of this work is to find another alternative for an opaque-transparent film applied to paper that can be thermally switched. For this purpose, systems of crystalline low molecular weight substances in polymer matrices are investigated. The components are formulated in different configurations and coated onto substrates. The thermal switchability in the opacity of the resulting films is determined by measuring the optical density before and after thermal switching. Natural waxes such as fatty acids and tristearin and synthetic waxes as well as binary organic eutectic mixtures are investigated as low molecular weight crystalline substances. By measuring the scattering parameters, it is determined whether mixtures in a eutectic composition have a higher scattering effect than their non-eutectic compositions. In the course of the work, promising systems are identified that can serve as basis for possible thermally switchable coatings.

Zusammenfassung: „Thermisches Schalten der Opazität von Polymerfilmen für die Verwendung in Thermo-Responsiven Papieren"

Thermopapiere sind aus dem Alltag nicht mehr wegzudenken. Fast jeder hatte schon einen Kassenzettel, ein Paketetikett oder Eintrittskarte in der Hand. Überall dort, wo schnell, günstig und für eine begrenzte Dauer Informationen festgehalten werden müssen. Klassische Thermopapiere stehen allerdings in der Kritik, da deren Farbentwicklersysteme Substanzen enthalten können, die potentiell gesundheitlich oder auch umwelttoxisch bedenklich sind. Daher gibt es bereits alternative Papiere, die nicht auf die chemische Entwicklung von Farbe basieren, sondern auf den physikalischen Effekt, eine stark lichtstreuende Struktur von opak zu transparent zu schalten. In dieser Arbeit soll eine weitere Alternative für einen opak-transparenten Film gefunden werden, der auf Papier aufgebracht wird und thermisch schaltbar ist. Hierfür werden Systeme aus kristallinen niedermolekulare Substanzen in Polymermatrices untersucht. Die Komponenten werden in unterschiedlichen Konfigurationen formuliert und auf Substrate beschichtet. Die thermische Schaltbarkeit in der Opazität der resultierenden Filme wird durch die Messung der optischen Dichte vor und nach dem thermischen Schalten ermittelt. Als

niedermolekulare kristalline Substanz werden natürliche Wachse wie Fettsäuren und Tristearin und synthetisches Wachs, aber auch binäre organische eutektische Mischungen untersucht. Durch die Messung der Streuparameter wird ermittelt, ob Mischungen in einer eutektischen Zusammensetzung eine erhöhte Streuwirkung aufweisen als ihre nicht-eutektischen Mischungen. Im Laufe der Arbeit werden vielversprechende Systeme aufgezeigt, die als Basis für mögliche thermisch-schaltbare Beschichtungen fungieren können.

Acknowledgments / Danksagung

In erster Linie möchte ich Prof. Markus Biesalski danken. Die Möglichkeit in deinem Arbeitskreis zu arbeiten und zu forschen war mir eine Ehre. Die zahlreichen Diskussionen und vielen Ideen halfen nicht nur bei der Bewältigung der Promotion, sondern auch der persönlichen Entwicklung.

Der Papierfabrik Koehler SE, insbesondere Dr. Michael Horn und Dr. Timo Stalling danke ich für die Möglichkeit mit dieser Arbeit ein relevantes Thema bearbeiten zu dürfen. Der stete Austausch, die Zusammenarbeit und die Erfahrung auf die ich bauen durfte waren essentiell für die Arbeit.

Was ist ein Arbeitskreis ohne die vielzähligen Doktorandinnen, Doktoranden, Studierenden und einer guten Organisation? Danke an die guten Seelen im Sekretariat, Bärbel und Vanessa und Chefin der Labore Martina. Ohne deinen unermüdlichen Einsatz für Ordnung, Sauberkeit und stets gute Ideen und Tipps bei der Laborarbeit würden die Versuche nur halb so gut laufen.
Die Sinter-Experimente in dieser Arbeit wurden mir von Dr. Dieter Spiehl zur Verfügung gestellt, danke dir dafür und für die gute und fruchtbare Zusammenarbeit in unserem gemeinsamen Projekt.
Außerdem danke ich meinen lieben Kolleginnen und Kollegen, die immer ein offenes Ohr für sämtliche Probleme hatten, sei es fachlich oder privat. Besonders die entspannten Abende auf dem Balkon, im Biergarten, kreative Weihnachtsvideo-Drehs und gemeinsame Ausflüge habe ich in guter Erinnerung. Es war eine gute Zeit und ich freue mich schon auf die regelmäßigen jährlichen Zusammenkünfte, z.B. mit dem CCCD e.V.
Viktor, Tobias und Sandra: Danke für eure gute Arbeit im Rahmen eurer F-Praktika. Es war mir eine Freude euch zu betreuen.

Ein besonderer Dank geht außerdem an meine Familie: meinem Mann Sebastian, meinen Eltern Chestin und Michael, meiner Schwiegerfamilie, meinen besten Schwestern Solveig und Berit-Johanna, sowie meinem Neffen Mattis.

Table of Content

Abbreviations

General

CMC	Critical micelle concentration
DIC	Differential interference contrast
DLS	Dynamic light scattering
DSC	Differential scanning calorimetry
GPC	Gel permeation chromatography
LCST	Lower critical solution temperature
OD	Optical density
PCM	Phase change material
PSA	Pressure sensitive adhesive
RID	Refractive index detector
RMSE	Root mean square
rpm	Revolutions per minute
RT	Room temperature
SEM	Scanning electron microscope
STD	Standard deviation
UCST	Upper critical solution temperature
WLI	White light interferometry

Chemicals

BA	Benzoic acid
BAc	Behenic acid
BPA	Bisphenol-A
BPF	Bisphenol-F
BPS	Bisphenol-S
DCM	Dichloromethane
DMO	Dimethyl oxalate
EC	9-Ethylcarbazole
FAc	Fatty acid
*i*PS	Isotactic polystyrene
MEK	Methyl ethyl ketone
PAc	Palmitic acid
PCL	Polycaprolactone

PDMS	Polydimethylsiloxane
PET	Polyethylene terepthalate
PLA	Polylactic acid
P4MS	Poly-4-methylstyrene
PMMA	Polymethyl methacrylate
PS	Polystyrene
P(S-SS$_x$)	Polystyrene styrenesulfonate
SAc	Stearic acid
SAN	Styrene-acrylonitrile resin
THF	Tetrahydrofuran
TS	Tristearin

Formula Symbols

α	Dimensionless size parameter
λ	Wavelength / nm
a	Auxiliary parameter for the calculation of R
d_P	Particle circumference / nm
$h\nu$	Energy of photons / eV
I	Intensity of the transmitted light
I_0	Intensity of the incident light
J	Intensity of reflected light
k	Density related light absorption coefficient / m^2kg^{-1}
m	Mass / kg
m_A	Grammage / kg m^{-2}
n	Refractive index
n_{Dx}	Refractive index for sodium D-line at x °C
OD	Optical density
R	Reflection factor
R_∞	Intrinsic reflection factor
R_{gs}	Reflection factor of black background → 0
R_{gv}	Reflection factor of white background
R_v	Reflection factor of sample in front of white background
s	Density related light scattering coefficient / m^2kg^{-1}
Tr	Transparency
T_C	Crystallization temperature / °C

T_{CP}	Cloud point temperature / °C
T_E	Eutectic temperature / °C
T_g	Glass transition temperature / °C
T_m	Melting temperature / °C
w	Thickness of paper / μm

1 Introduction

When people think of thermal paper and cash register receipts, they often associate them with papers that come with shopping and fade quickly if not stored carefully. Why are they used despite these disadvantages compared to ink-printed paper?

Thermal paper and printers are commonly used for quick and temporary printing needs. The printing speed is usually 150 - 400 mm per second, depending on the thermal paper used, the resolution required and the technical capabilities of the printer.[1,2] Additionally to fast printing speeds, the printers need little to no maintenance. Only the roll of paper or labels has to be replaced, since no ribbons, ink or cartridges are needed. The print head of a thermal printer consists of many small thermocouples: during the printing process, current is passed through the heating elements and, depending on the voltage, higher or lower temperatures can be generated. The paper is fed past the print head and the paper is heated at the desired locations where the printing pixels are formed because the functional coating on the paper is thermochromatic, i.e. it changes its color due to the effect of local heating.[1,3,4]

In 2021 the global thermal paper demand was approximately 1 200 000 t.[5] It is used not only for sales slips, but also for barcode labels in logistics, parking and movie tickets as well as label makers for the home use. The disadvantages of thermal papers are that the contrast of the print fades over time since it is sensitive to UV and heat and only one color can be used. But is has also come into disrepute in recent years due to the use of potentially harmful substances it can contain and the risk of transfer due to the daily contact with users. In addition to the health risk, standard thermal paper cannot be easily recycled. Due to the color developers they contain, sales slips belong in the residual waste so that the critical substances do not end up in recycled paper products (e.g. sanitary and graphic paper). This is usually difficult to implement in reality, as it is haptically the same as normal paper. Shipping labels, for example, are rarely detached from packages and disposed of separately. So thermal papers are either disposed of in the wrong waste stream or, if done correctly, withdrawn from the material cycle, which makes it not sustainable. This is why efforts are being made to find alternatives that use different or no chemical color developers at all. A standard thermal paper composition is schematically displayed in Figure 1.1. The paper usually has grammages from 30-100 g m^{-2} and is coated with an insulation layer to concentrate the energy from the thermal printer in the functional layer, a functional thermochromatic layer and sometimes an additionally protective coating.[6,7] The thermochromatic layer consists of a dye system which includes leuco dyes, color developers and sensitizers/co-solvents. Leuco dyes are most commonly Fluoran dyes which have two chemical forms, the colorless leuco form and a colorful form. The reversible transformation can be triggered by heat, light or pH. In thermal papers the leuco dyes react with a color developer, which are weak organic acids (proton donors), to be transformed in the colorful form. The additional sensitizer or co-solvents are melting point regulators and are used so that the chemical reaction can take place at moderate temperatures.[8–11]

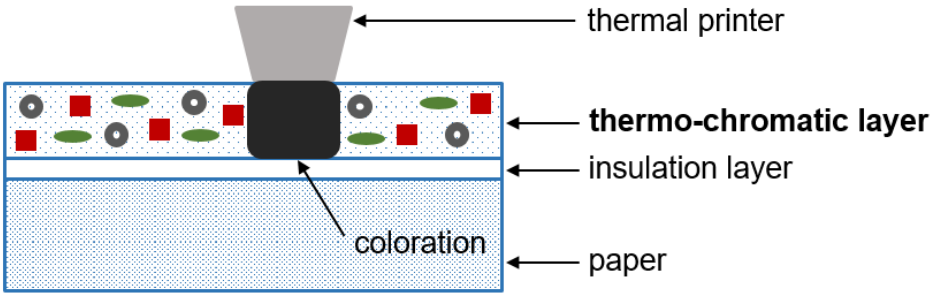

Figure 1.1: Schematic structure of a classic thermal paper based on a dye and color developer system.[9]

Figure 1.2 shows examples of the components of classic thermal papers. As displayed, many are small molecules which leads to limitations: the most common used color developer bisphenol A shows a detectable binding affinity to estrogen receptors which enables them to function as endocrine disruptors which may lead to a broad range of health issues.[12] Since small molecules can migrate to the surface of the papers and are in direct contact to skin and foodstuff, the substances come into contact with the users. These risks lead to the EU-wide ban on bisphenol A for use in thermal papers. This has been in force since 2020.[13,14]

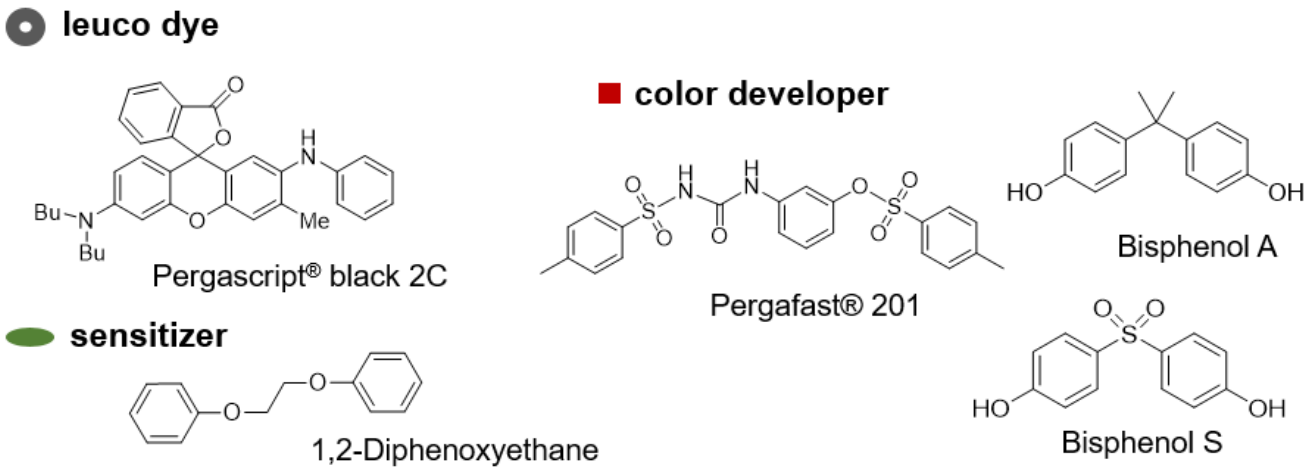

Figure 1.2: Examples for components in a classic thermal paper. Leuco dyes like Pergascript (BASF)[15] are fluoran based structures. Sensitizers are usually simple ethers and the color developers are weak organic acids, like phenols.[9]

The alternatives used for BPA are bisphenol S and other bisphenol derivatives, which, due to the structural similarity, are assumed to have a similar effect to the human organism and Pergafast 201®. The urea derivative does not have an endocrine effect, but is classified as toxic for water organisms and has a low biodegradability.[9,16]

One solution to this challenge may be to develop a dye system whose components are non-toxic to nature and humans. Another approach, however, may be to develop a completely different system for thermal papers, a dye-free system so that small molecules, which can migrate do not have to be used. Koehler SE employed this strategy and revolutionized the market by developing a new generation of thermal

papers with the brand Blue4est®.[17] It uses a physical effect to create the printed picture. The mechanism of the new concept is schematically displayed in Figure 1.3.

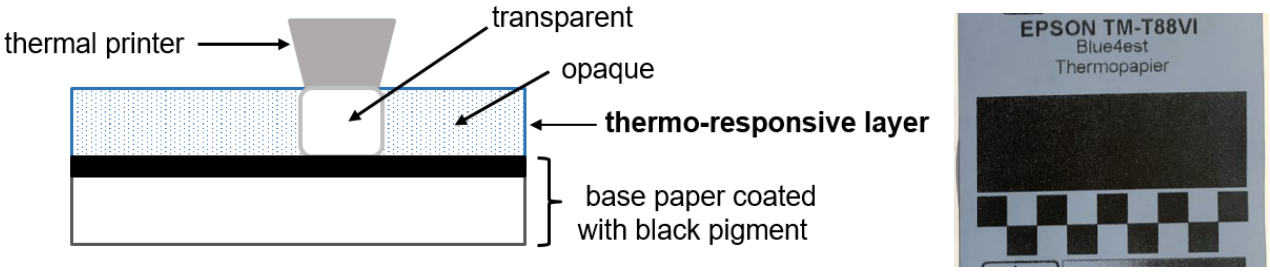

Figure 1.3: Functional mechanism of a novel thermal paper that is not based on leuco dyes (left)[17] and a picture of a Blue4est® thermal paper (right).

Paper having a thin pre-coat of black pigments is coated with an opaque thermo-sensitive layer. This thermo-responsive coating consists of air-filled structures, organic pigments and binders. This way the incident light is scattered on the phase boundaries of the different materials with different refractive indices. Since light is scattered on the coating, the paper appears white. During thermal printing, the desired locations are melted. The air-filled structures are destroyed and the coating becomes transparent, due to the vanishing of the polymer-air interfaces. The underlying base paper that is coated with black pigment becomes visible and the printed image is generated. This system has the advantage that the printed image is more stable during aging (UV light and temperature) than comparable standard thermal paper because the molten structures cannot be reversibly formed back into the original light-scattering state. However, it is more mechanically susceptible than the standard. The novel thermal papers also do not come with the same whiteness. Since air has an insulating effect, the opaque coating cannot be applied with any layer thickness. Otherwise the entire layer will not be switched and thus become transparent. A compromise must therefore be found between opacity and switchability so a slightly blue paper is the result.

In order to research a new system for thermal papers, it is therefore possible to decide between two main routes. When visible light interacts with matter the possible basic interactions are: scattering, reflection, absorption and emission. The first route, analogous to the standard paper with thermochromatic systems, is based on absorption of light. Here, a choice can be made between pigments based on leuco dyes[18,19], cholesteric liquid crystals[20,21] and the corporation of both into polymers. The other main route is to design a system based in thermotropic material like it is used in the new Blue4est® thermal papers. This route is based on the change of light scattering properties due to a temperature stimulus, which does not affect the color but the transparency of the material, e.g. from an opaque to a clear state.[8,22]

Considering the before outlined limitations of existing technologies, it is of utmost challenge to develop more sustainable opportunities for future thermal paper design. A major task to address this challenge

and that plays a central role in this thesis is to develop a water-based coating that covers a black base paper with a maximum film thickness of 10 µm. The use of non-toxic and, if possible, bio-based substances should be taken into consideration, in order to establish highly sustainable new ways for future thermal paper design.

2 Thermotropic Films - State of the Art

2.1 Light Scattering in Thin Films

When it comes to investigating alternative systems for thermal papers, it is important to understand how thin films or coatings that exhibit high scattering are typically produced. This thesis focuses on polymers as the base of the scattering film. Absorption of light can be set aside in this matter since it is only important in black or colored material and has no contribution to the opacity of polymers which cannot absorb light with wavelength greater than 400 nm. Light scattering is an interaction between electromagnetic radiation and heterogeneous matter.[8] If a beam of light is travelling through a medium, the straight-lined beam is slightly shifted by fluctuations in the dielectric constant i.e. refractive index by either phase boundaries or changes in density or concentration. The intensity of the scattering is dependant on the number of the fluctuations, like the difference in refractive index or the size of domains with a certain refractive index. The maximum scattering occurs when the involved scattering centers are in the same order of length than the wave length of light.[8] To obtain a thin film that can be thermally switched from opaque to transparent, a thermotropic material is needed. In the light scattering state, domains are present that have a different refractive index than the matrix material. The domains can be formed either due to a phase separation or can be permanent and at switching temperature the refractive indices are matched thus leading to a transparent state.[8,23,24]

Figure 2.1 shows the possible fluctuations on interfaces in one polymer. They can occur between crystalline/amorphous phases, on crystalline/crystalline phases due to the anisotropy of the crystallites and, the interface between polymer and air and in a blend or copolymer, the other polymers add multiple possible interface fluctuations.

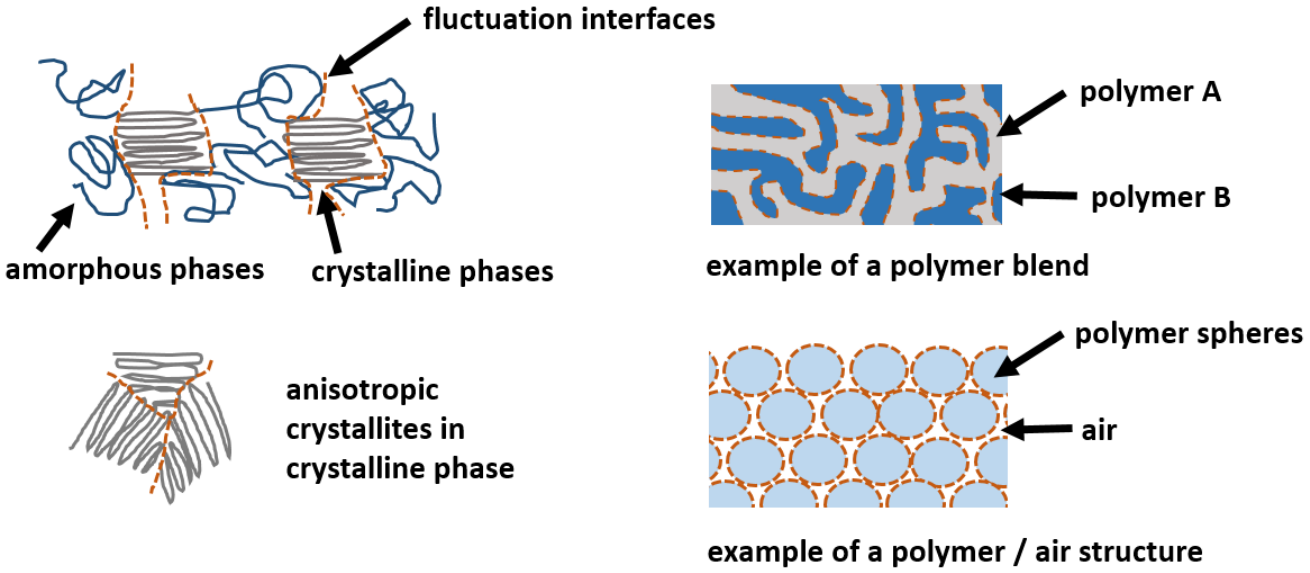

Figure 2.1: Schematic representation of the possible phase boundaries in homopolymers, copolymers and polymer blends. Due to the fluctuation of the refractive index in the different phases, light is scattered.

2.2 Nanostructured and Open Porous Polymer Thin Films

The easiest method for designing interfaces at wich scattering occurs is to use materials with significantly different refractive indices, such as polymers (typically $n=1.3$ to 1.7)[25] and air ($n=1$)[26]. Blue4est® thermal papers work with this principle. Nanostructured films of polymethylmethacrylate (PMMA) were introduced by SYURIK *et al.*[27] who got inspired by the beetle *Cyphochilus*. Colors in nature are often a result of complex nanoscale architectures. Examples for this are opals or brilliant and iridescent colored butterfly wings, where periodic structures lead to these optical properties.[28] The beetle does not have a colorful appearance but has a bright white shell. The shell consists of a low-refractive index anisotropic chitin network, which is highly fibrillated. The beetle-inspired film is made exclusively from PMMA using a solvent-evaporation protocol with a solvent (acetone) and a non-solvent (water). The resulting film shows a high opacity with a thickness of only 4 μm. Figure 2.2 shows the beetle and the inspired PMMA film.

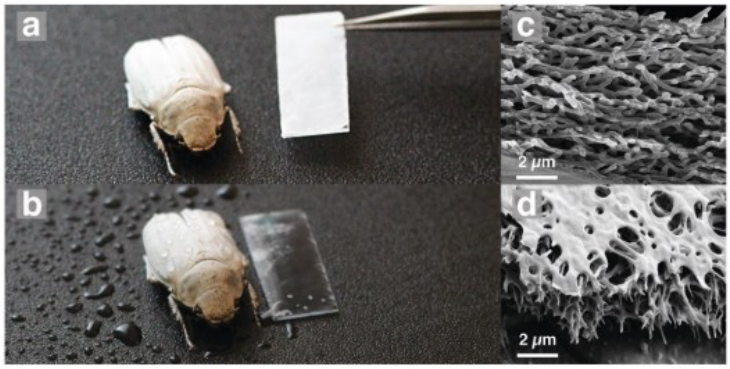

Figure 2.2: a) Like the *Cyphochilus insulanus* beetle (left), microstructured PMMA films (right) show a bright white appearance achieved by efficient multiple scattering. The film shown is 4 µm thick. b) Due to the pores water can penetrate into the structure. Thus, the polymer film turns transparent when wet. The beetle does not change color upon wetting due to a continuous surface layer encasing the scales. A cross-sectional SEM image (Scanning Electron Microscopy) of a scale of a *Cyphochilus* beetle c) and of the PMMA film d) revealing the random networks that cause the bright white coloration by multiple light scattering. Image and caption from SYURIK *et al.*[27].

Another way to introduce light scattering properties into a simple homopolymer film is to incorporate forced convection in the solvent evaporation process after solvent casting. The cellular morphology is attributed to the flow field guided deposition of sequentially generated precipitates that occurs when solvent evaporation is fastened, resulting in selective dissolution.

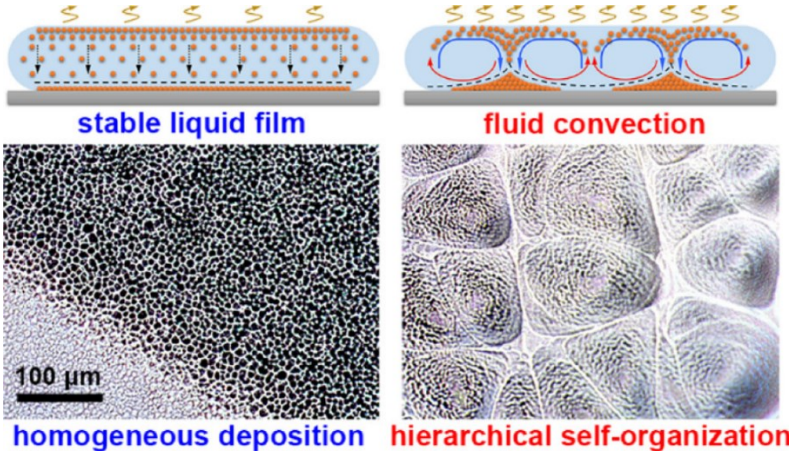

Figure 2.3: Schematic diagram and optical miscroscope images of the resulting films of the deposition mechanism for a homogeneous deposition in a static field (left) and self-organized deposition in the convection field (right). Fluid streamlines in the convection movement are depicted in the schematic diagrams. The downward arrows (blue) denote the lateral mass transfer and consequent boundary enrichment of precipitates. The upward arrows (red) denote the lateral boundary growth direction with the precipitate accumulation toward the nucleus positions. Reprinted (adapted) with permission from *Langmuir* 2018, 34, 19, 5551–5557.[29] Copyright 2018 American Chemical Society.

The same effect occurs when a blend out of two polymers with different solution behaviors is solvent-cast. A hierarchical self-organization with fluidic convection is obtained. This is shown in Figure 2.3 in comparison to a stable liquid film with homogenous distribution.[29] The following SEM images show a film prepared from PMMA, solvent-cast onto a polyethylene terephthalate (PET) foil. Under forced convection with a cold air blower, the films show the characteristic pattern of a hierarchical self-organization. The porous surface structure leads to milky, cloudy films.

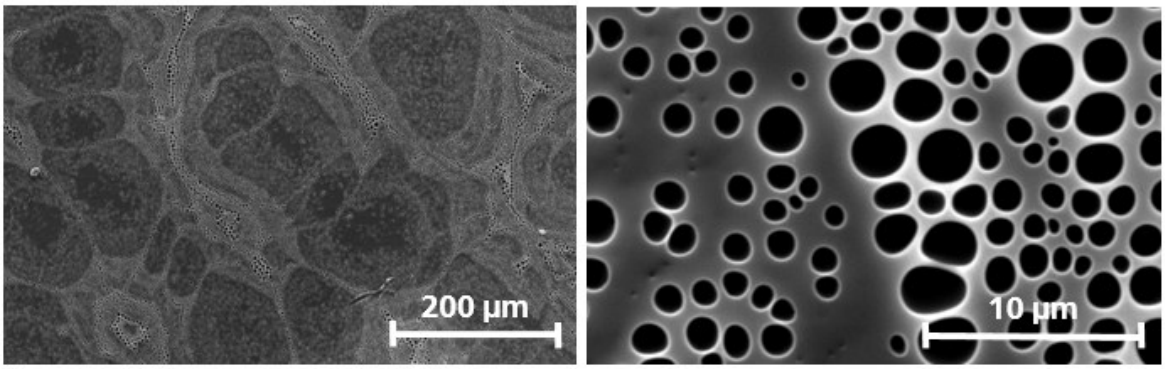

Figure 2.4: SEM image of a (self-prepared) PMMA film that was solvent-cast onto a PET-substrate. During the evaporation of the solvent PET, forced convection with a fan led to the formation of multiple pores, which lead to an opaque film and the distinctive pattern of hierarchical self-organization.

Although porous films are opaque at low layer thicknesses, they have the disadvantage that the opacity can be quickly destroyed by filling the air pores. e.g. reversibly with rapidly evaporating liquids such as water, but also irreversibly with e.g. oil. Compression of the films by mechanical stress also destroys the air voids and the thin polymer films become transparent.

2.3 Light Scattering by Control of Phase Transitions in Thin Films of Polymer Blends

Polymer blends consist of two or more polymers, which typically have different refractive indices (often with only minor differences). Additionally, blends can form special structures due to microphase separation. Both increase the scattering properties of polymer blend films. Examples are polymer blends out of PMMA and polystyrene (PS), which form self-assembled island-like domains of PS in the PMMA matrix during spin-casting from organic solvent[30], and polymer blend films prepared by CHANG and WOO[31] from isotactic polystyrene (*i*PS) and poly-4-methylstyrene (P4MS). They observed that the blend forms an interesting surface structure when it is cast out of solvent: the surface is covered with elevations out of *i*PS with elevations of about 1000 nm in height at a fraction of 50/50. The formation of the surface structure is schematically illustrated in Figure 2.5.

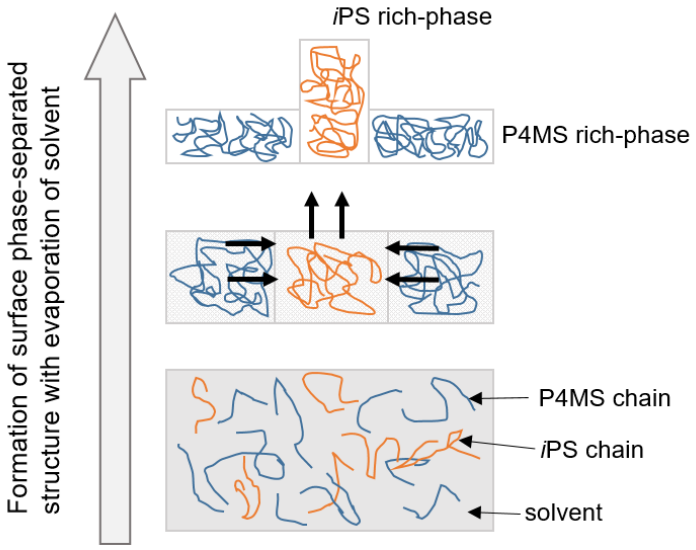

Figure 2.5: Forming of the surface structure of *i*PS and PMMA blend with progressing evaporation of the solvent Tetrahydrofuran (THF). At the bottom both polymers are in solution. With the ongoing evaporation, the phase-separated structure is formed.[31]

This is due to the difference in the solubility of the polymers in the solvent used, as well as the surface free energy. The resulting films were not measured for their scattering properties, but the surface structure, the large surface area and the many phase boundaries may be good candidates for scattering films.

2.4 Light Scattering in Thermo-Responsive Polymers and Polymer Blends

In the field of stimuli-responsive polymers, thermo-responsive macromolecules are of great interest because the stimulus can be applied in a non-invasive and simple manner or because temperature fluctuations occur naturally in the application area.[32] Thermo-responsive polymers are being investigated

by many research groups and are used, for example, in drug delivery systems[33], where the temperature of inflamed tissue triggers a conformational change and the drug is released locally. Thermo-responsive polymers exhibit a miscibility gap in the polymer/solvent phase diagram depending on the temperature (see

Figure 2.6). As the temperature is varied, the interaction between the polymer chains and the solvent changes. The polymer chains become less solvated and tend to associate with each other. This leads to phase separation, with the polymer precipitating out of solution. Turbidity occurs because the separated phases have different refractive indices and scatter the light differently. This leads to a clouding of the solution and the temperature at which the latter occurs is called cloud point temperature T_{CP}. A distinction is made between the lower critical solution temperature (LCST) and the upper critical solution temperature (UCST), which is the maximum/minimum of the bimodal curve. At UCST, polymer and solvent at any ratio are miscible at elevated temperatures. At LCST the miscibility is given at lower temperatures.[34,35]

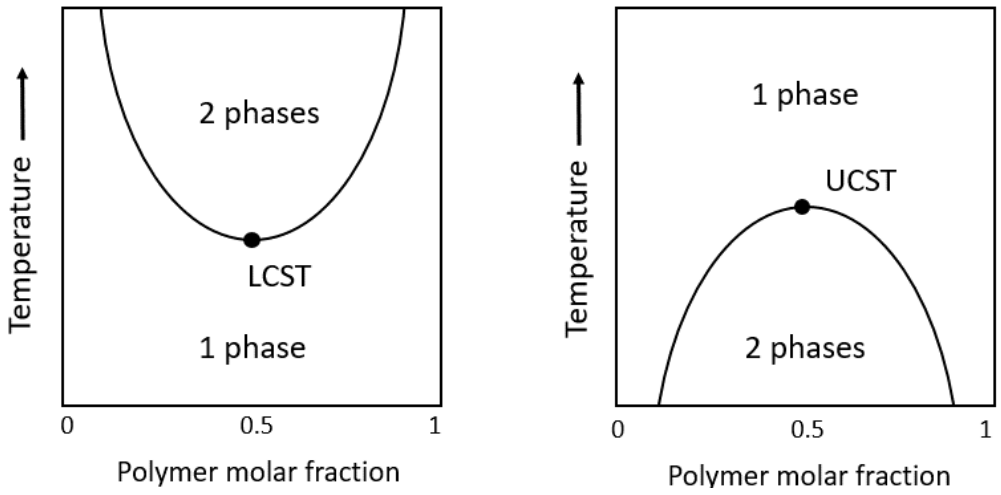

Figure 2.6: Schematic phase diagrams of thermos-responsive polymers in solution with a LCST (left) and UCST respectively. The bimodal curve limits the range in which solvent and polymer are not soluble and two phases are present.

The first polymers with these properties were studied in organic solvents, but the most widely researched systems are based on aqueous solutions to be used in biomedical applications, like drug delivery.[36–38] Perhaps the best-known and studied thermo-responsive polymer is poly-*N*-isopropylacrylamide (PNIPAM), which has an LCST of about 32°C. It is most commonly used in water, as three-dimensional network known as hydrogel.[39,40]

To use a thermo-responsive polymer in a thermo-switchable coating for paper, a polymer/solvent system cannot be used. For this application, polymer blends with a UCST or a LCST are of interest. The polymers undergo phase transitions at their critical temperature, resulting in demixing of the bulk phases (Figure 2.7).[40].

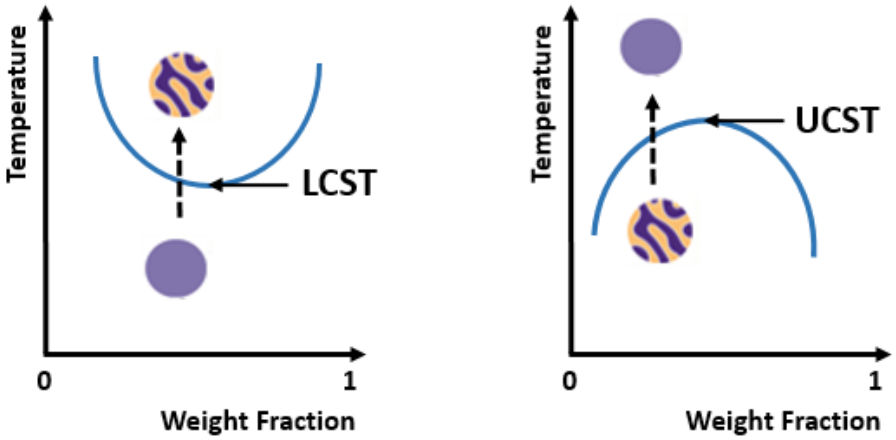

Figure 2.7: Schematic illustration of a LCST or UCST system where the condition of a polymer blend is dependant on the temperature. The LCST and UCST are the temperatures at the lowest respectively highest point of the bimodal curve.[41]

To employ this system for a thermotropic film, a system with an UCST lower than the switching/printing temperature is required. As shown schematically in Figure 2.8, prior to printing, the material is in a demixed state and the light is scattered on the surface boundaries. During thermoprinting the material is heated above UCST and the phases are homogeneously mixed. Therefore no light is scattered on phase boundaries and this state would ideally be frozen during cooling.

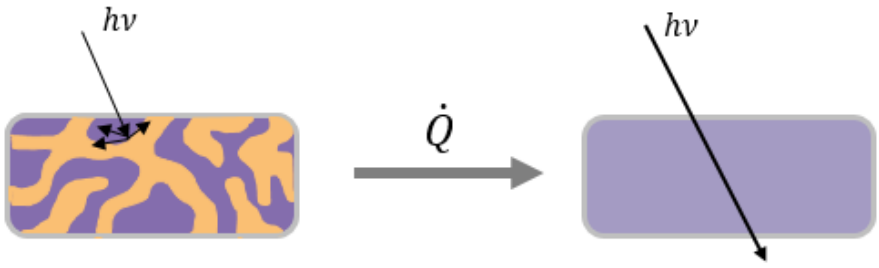

Figure 2.8: Schematic illustration of a possible UCST system used as thermo-tropic coating. Above switching/printing temperature the polymer blend or copolymer exhibits a homogenous phase leading to a minimum of light scattering.

An example of a polymer blend exhibiting UCST properties is a polystyrene/poly(styrene-co-acrylnitrile) (SAN) blend introduced by YANG *et al.*[42]. The polymers are dissolved together in organic solvent at different ratios and are coated on a glass substrate. After evaporation of the solvent, the phase diagram was constructed using small angle light scattering measurements at different temperatures. When the scattering intensity is at its peak, the blend is in a phase-separated state. This shows that this effect could possibly be used for a thermo-optical switchable film. The following pictures (Figure 2.9) shows impressively how the blend is constituted at two different temperatures. Below (left) and above the UCST (right).

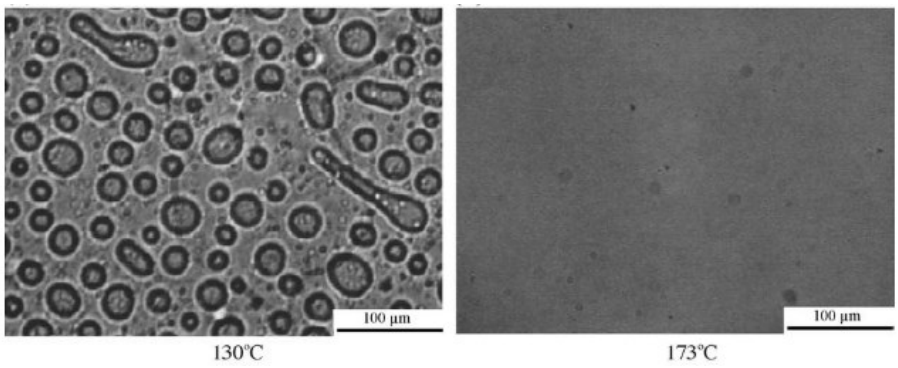

Figure 2.9: Phase contrast photomicrographs of PS/SAN (80/20) blend at different temperatures below (right) and above (right) USCT. Reprinted (adapted) with permission from *Materials Letters* 58 (2004) 3939 – 3944.[42] Copyright 2004 Elsevier.

Another blend with USCT behavior is reported by ZHOU *et al.*[43] , who prepared samples consisting of two layers of random polystyrene-*co*-styrene sulfonate (PS-SS$_x$) and PS. The layers were deposited using a spin coater and the layer thicknesses are 350 nm. The miscibility of the two-layer system was measured at different temperatures. The polymer as well as the two-layer coating is displayed in Figure 2.10.

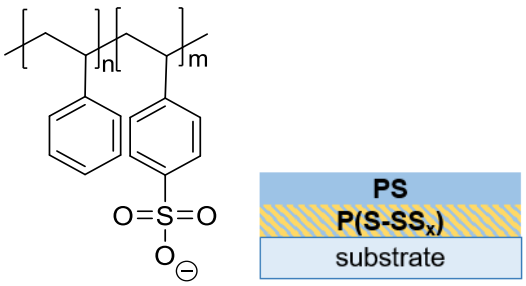

Figure 2.10: Chemical structure of random polystyrene-*co*-styrene sulfonate (P(S-SS$_x$)) and polystyrene (PS) synthetized by ZHOU *et al.*[43](left) and setup of the prepared samples; both layers have a film thickness of 350 nm (right).

With the amount of styrene sulfonate in the copolymer can be used to adjust the UCST and different levels of sulfonation were investigated. The phase diagram was constructed using spectroscopy. The mixing behaviors of the two layers forming a blend with a UCST was observed. The optical properties are not described, but it may lead to a scattering film. If an opaque film can be formed from these polymers, the influence of the film thickness is critical, as the film thickness for a paper coating is limited.

2.5 Crystalline Substances in a Polymer Matrix

In addition to polymer blends, crystalline substances embedded in a polymer matrix can be interesting candidates for thin opaque films. In theory, light is scattered on particles or domains of crystalline substances in a polymer matrix, as shown schematically in Figure 2.11. During thermal printing/heating, the domains or particles are destroyed and finely dispersed into the polymer matrix. To achieve an irreversible switching from the opaque to the transparent state, the domains must be prevented from reforming after cooling. In this context, recrystallization must be taken into account.

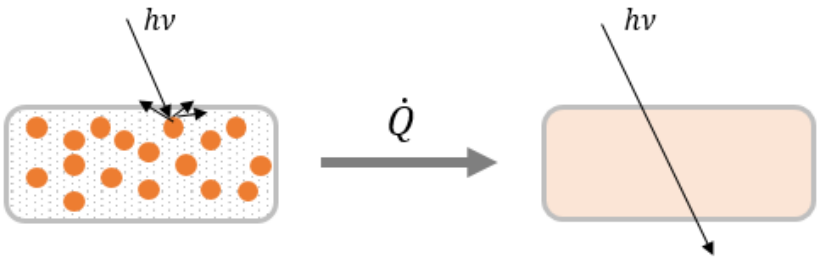

Figure 2.11: Schematic illustration of thermal switching of films consisting of crystalline substances in polymer matrix. The crystalline domains are destroyed during thermal treatment/thermal printing and the incident light is not scattered anymore, leading to a transparent film.

Thermally reversible light scattering films were prepared by Zucchi et al.[44,45]. The matrix consists out of an epoxy resin and the crystalline domains consist of either of polystyrene/naphthalene dispersions or polystyrene/diphenyl dispersions. The films were prepared by polymerization-induced phase separation: the crystalline substances form a dispersion in the epoxy resin due to the low compatibility of PS and the epoxy resin and its high compatibility with the crystallites. The intensity of the transmitted light was measured during several heating/cooling cycles of the films. Both variants show the desired behavior of switching from opaque to transparent even after several cycles. The reversibility is achieved by the melting or recrystallization of the crystalline substances in the confinement of the particles introduced by the dispersions. This example shows that the compatibility and the miscibility are essential for reversibility. Since an irreversible system is needed for the thermotropic coating, this must be taken into account.

2.5.1 Natural and Synthetic Waxes as Crystalline Substance

The combination of a polymer with a crystalline and wax-like substance can be of interest for the design of optically switchable films due to the ability of the waxes to form highly crystalline phases. The waxes must have melting points below the glass transition temperature of the polymer matrix, such as paraffin wax, fatty acids (with melting points above room temperature; starting from C_8)[46] or triglycerides. The resulting coating would not only be partially derived from natural resources, but would also have thermo-responsive properties when heated due to the crystalline nature of the substance.[47] These properties could be thermal, structural or optical. The thermal properties could vary in melting point of the crystalline substance or the glass transition temperature of the polymer. Structurally, the roughness, hydrophobicity or barrier properties may change. The optical changes are a novel and interesting area to study at different temperatures, for a material that is composed of materials with different softening and melting temperatures leading to a different light scattering behavior.

The combination of triglyceride or wax and polymer is mostly commonly researched as phase change material (PCM), where the wax/triglyceride is used as latent heat storage. Thermal energy is transferred when the PCM undergoes a phase transition from solid to liquid. Fatty acids and triglycerides are often

used for this application because they have reproducible melting and freezing behavior, high heat of fusion and they freeze without supercooling.[48–52]

Other fields of study include the waxy material as additive for polymers as a plasticizer[53], process additive for demoulding[54] and extrusion or even the synthesis of monomers for the polymerization of novel polymers from natural resources[55–57]. In the medical research field wax and polymers are combined to create non-biological skin models to mimic the properties of skin topography[58] or drug delivery systems[59]. The wax in the encapsulation material delays the release of the drug. The use of natural materials as coating material for paper packaging is also an interesting research field for the use of polymer and wax. The wax, fatty acid or triglyceride provides a good moisture barrier.[60]

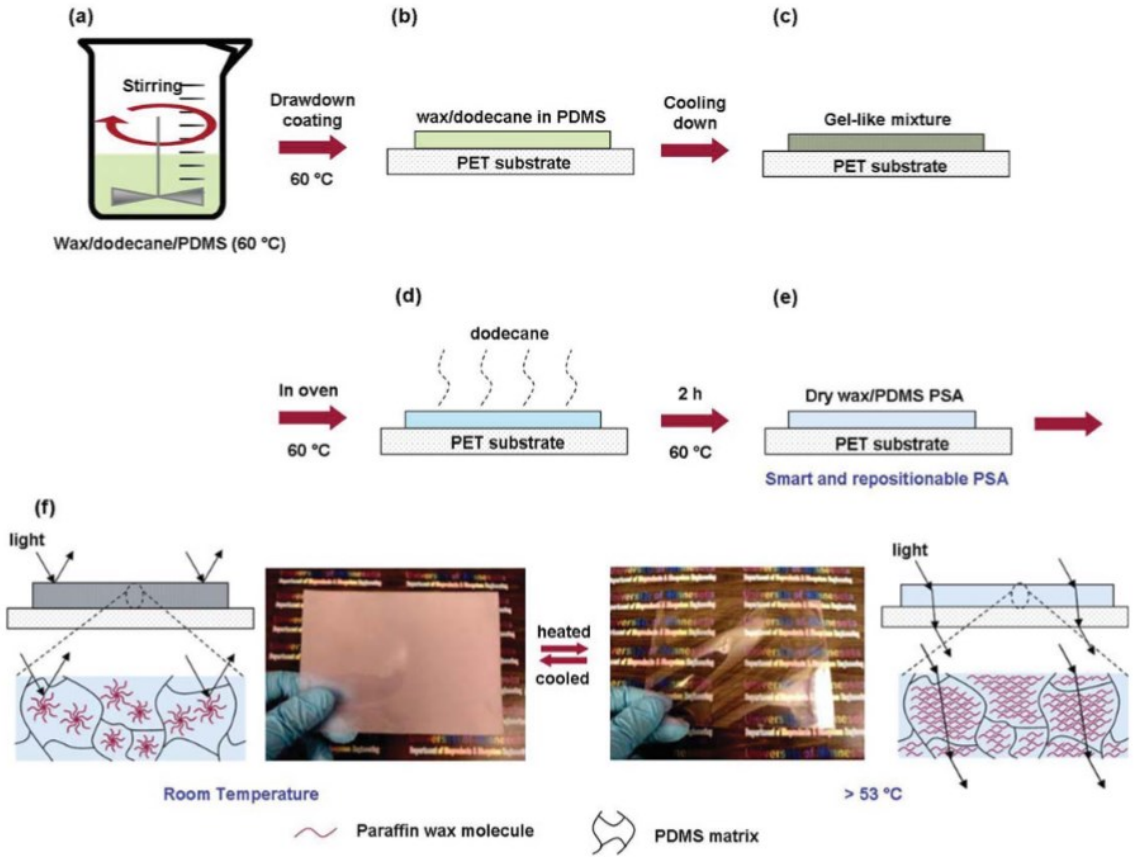

Figure 2.12: Schematic drawing for the preparation of the thermos-responsive and repositionable pressure sensitive adhesive (PSA). (a) uncured PDMS, curing agent, and wax/ dodecane solution at 60 °C; (b) coated on PET substrate (2 mm) with a 7 mm preheated bar; (c) cooling of the films at room temperature for 5 min to form a gel-like film; (d) evaporation of Dodecane in oven at 60 °C; (e) dry PDMS/wax PSA; (f) the PSA can reversibly switch between opaque and transparent. (Left) At room temperature, the paraffin wax solidifies and phase separates from the PDMS matrix. The film is opaque due to light scattering. (Right) At temperatures above 53 °C, the paraffin wax melts and the light-scattering domains are destroyed, forming a transparent film. Reprinted (adapted) with permission from *Journal of Materials Chemistry C, 2013, 1, 1080.*[47] Copyright 2013 Royal Society of Chemistry.

The combination of a polymeric matrix with a wax to create scattering centers to achieve a scattering power leading to opacity was introduced by ZHANG *et al.*[47] to create a pressure sensitive material, which exhibits thermally responsive transparency. They used polydimetlysiloxane (PDMS) as matrix and added

paraffin wax before curing the elastomer. By heating the resulting material above the melting point of the paraffin wax, it is reversibly switched from opaque to transparent (Figure 2.12). This results in a multipurpose optical sensing device for temperatures above the melting point of the paraffin wax used.

One way is to dissolve polymer and wax together and then cast/cure the films. Another option is to add the wax as particles. These particles can be prepared by melt dispersion. HOTTA *et al.*[61–63] studied various fatty acids dispersed in polymer. They investigated these systems for use as thermos-reversible recording media. The films were formed from the dissolved components in a multi-solvent system on a PET substrate. The findings showed that the transparent films become light-scattering if cooling down from temperatures higher than the melting temperature of the fatty acid/ wax. The light-scattering films can be switched back to transparency by heating to just below the melting temperature of the fatty acid and by cooling. The state of the particles at each stage is schematically displayed in Figure 2.13. A mechanism is proposed in which the fatty acids form particles from microcrystals in which air voids cause the scattering effect. When the film is cooled from just below the melting point of the fatty acid, the crystals are relatively large with no voids in the domains. This way, the film appears transparent.

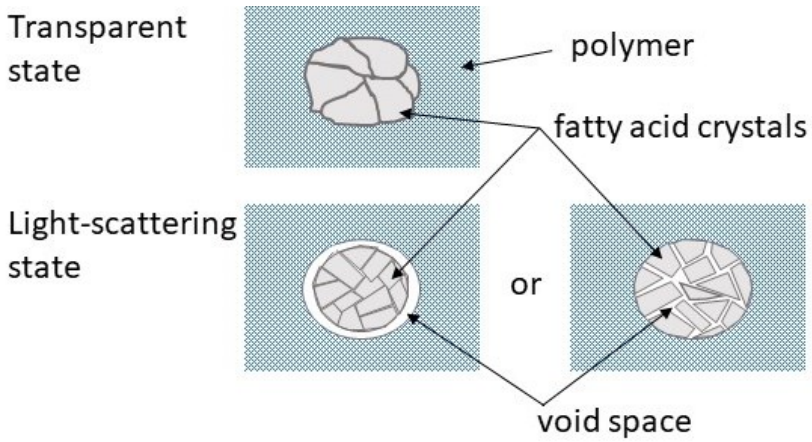

Figure 2.13: Different states of behenic acid dispersed particles in a polymer matrix leading to light scattering and transparent films. Figure inspired by HOTTA *et al.*[62]

The polymer matrix is also important for the mechanism; it is proposed that an incompatibility of the fatty acid and the polymer is required, so that small domains of the waxes are formed homogeneously distributed in the film by phase separation. Thus, the important factors are: the polymer matrix, the thermal properties of the fatty acid and the polymer, and the thermal history of the film. Such a coating is promising for the practical use because the components are non-toxic and widely available. Additionally, the switching of the different optical states is only dependant on the temperature and not on the heating or cooling rates. One drawback is the presence of organic solvents in the coating process. It would be of great interest to study the conversion to an aqueous formulation.

2.5.2 Organic Eutectic Mixtures as Scattering Portion

Another strategy would be to use a special combination of components to use as light scattering components in a thin film: eutectic mixtures. A eutectic mixture is a mixture of two or more chemical compounds in which the ratio of the components is such that at a given temperature they have a lower melting point than either component alone. The temperature at which the mixture melts is called the eutectic temperature T_E.[64] This control of the melting temperature is used with some relevant materials. Examples include soldering tin[65], other alloys[66], melting salts[67], ceramic materials[68], and pharmaceuticals[69]. A special feature of organic eutectic mixtures is their wide application in synthetic chemistry, as they can be used as alternative solvents to conventional organic solvents.[70–73] By definition, a binary eutectic is a two-phase solid that changes directly from a solid to a homogeneous liquid and has one precise melting point. The eutectic point is the lowest solidification temperature of the binary system. A phase diagram of a binary eutectic mixture is shown in Figure 2.14.

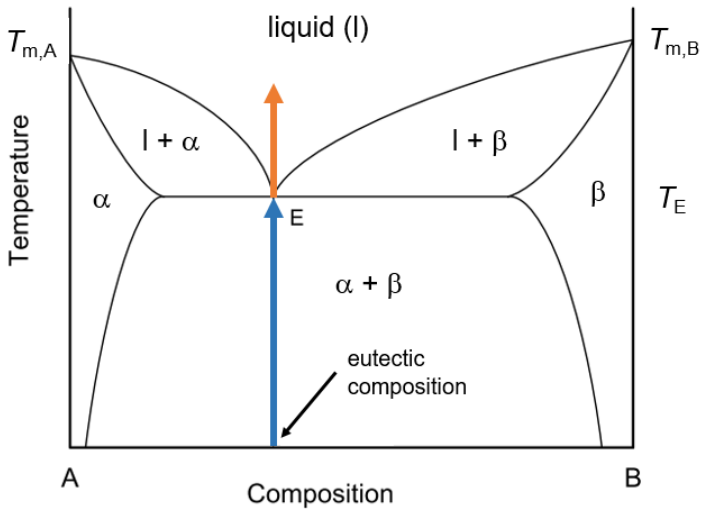

Figure 2.14: Phase diagram of a binary eutectic mixture from A and B. α and β are their solid phases. At the eutectic temperature T_E, only one melting temperature is visible which is lower than those of the pure substances $T_{m,B}$ and $T_{m,A}$. For a thermally switchable coating, a eutectic and its eutectic temperature could be used for a precise and fast switching. This is indicated with the arrows.[74]

For use in thermally switchable films, a eutectic could be interesting, since there are many phase boundaries in the material due to the mixing of substances. In addition, the homogeneous melting behavior of a eutectic mixture would make the switching very precise.

Next to the melting behavior, eutectic mixtures have other interesting properties: the simultaneous crystallization of the components leads to interesting microstructures of the solid phase. The shapes that are formed depend mostly on the entropy, but also on the cooling rate and thermal control of the melt.[73,75] Several researchers have studied the microstructures of eutectics, both organic and inorganic.[73,76–82]

HUNT and JACKSON pioneered in the calculation, prediction and classification of eutectic mixtures based on the melting entropies of the different phases. They investigated both organic and inorganic systems and postulated a theory in which binary organic eutectics can be divided into three groups: lamellar or rod-like structures are formed when both components have low melting entropies. Irregular/complex structures are formed when one phase has a high melting entropy and the other a low melting entropy. If both phases have a high melting entropy, regular structures cannot be formed at all and no coupled growth occurs as in the other two cases.[73]

RAI *et al*. provide another explanation for why different organic eutectic microstructures are formed and show examples of these morphologies (see Figure 2.15). Rod-type crystallization can occur, but also feather-like structures, where it is assumed that the crystals grow only when the supercooling at the interface is small and the interface structure is not diffuse enough to allow the formation of a new layer, e.g. lamellae. The third structure they found is a particulate-type morphology. The particles are formed by thermal insulation of the particle phase from the surrounding phase.[66]

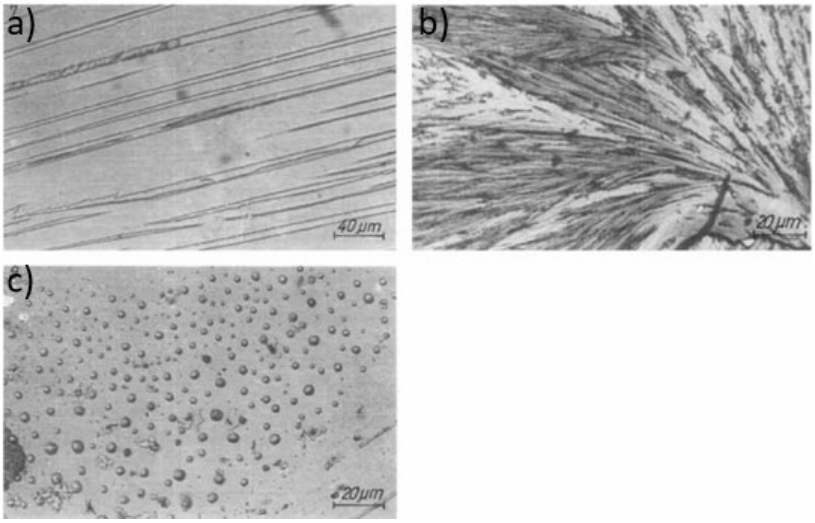

Figure 2.15: Eutectic microstructures of a) rod-type, b) feather-type and c) particulate-type eutectics. Reprinted (adapted) with permission from *Crystal Research and Technology*, 1994, 4, 533.[66] Copyright 1994 WILEY-VCH Verlag GmbH & Co. KGaA.

The results show that the control of a eutectic microstructure is not clearly defined and is highly dependent on the properties of the components. However, if the same thermal conditions are chosen, different eutectic structures can be compared. For the use in a highly scattering thin film, a feather-like structure with components with a high difference in refractive index could help to maximize the interfaces between the components. As eutectics are not usually studied for their optical properties, fundamental investigations are needed to support this hypothesis.

2.6 Preliminary Work

The preliminary work and this thesis were part of a bilateral cooperation between TU Darmstadt and Koehler SE. Several possible routes for novel thermally switchable coatings were considered. Initial experiments with polymer blends showed that the investigated polymer blends did not meet the required performance criteria under the necessary framework conditions, such as the ratio of layer thickness to opacity. Figure 2.16 shows one case: a film consisting of a blend of PMMA and PS (e27, experimental procedure in 8.2). The two polymers were dissolved in methyl ethyl ketone (MEK) and cast onto a PET foil. The resulting film is frosted, and SEM images show a distinct surface structure formed by phase separation during solvent evaporation. However, the film proves incapable of achieving opacity when applied to black substrates. Even when subjected to a thermal treatment above T_g, there was no change in the optical properties, as the structure did not homogenize to achieve transparency.

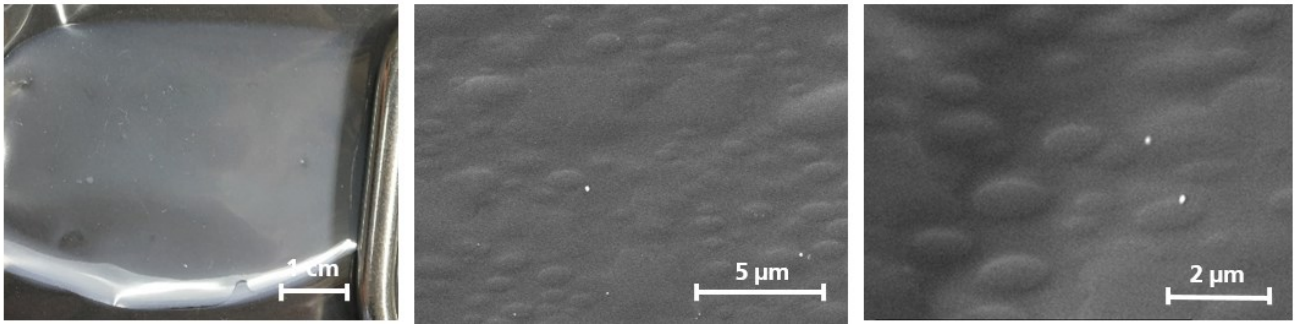

Figure 2.16: Film out of 70 % PMMA and 30 % PS cast out of MEK. The two SEM images on the right display the surface pattern that is fromed due to microphase separation (e27).

Another blend that underwent preliminary testing was a blend of P4MS and PS (e8, experimental procedure in 8.1). The resulting films were transparent, and SEM images showed a lack of surface structure. However, cross-sections of the films demonstrate microphase separation (Figure 2.17).

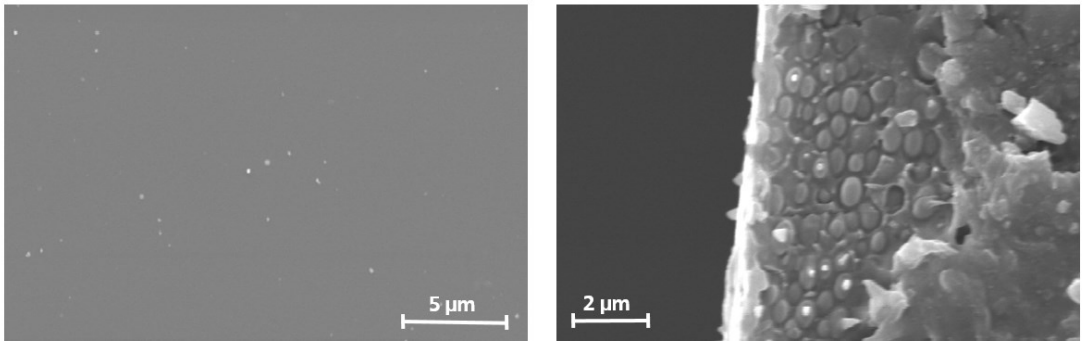

Figure 2.17: SEM images of the surface (left) and cross-section (right) of a film out of 30 % P4MS and 70 % PS, cast out of THF. While the surface is homogeneously closed, microphase separation can be observed in the cross-section (e8).

Further patented preliminary work was carried out by NAU *et al.* who, in a bilateral collaboration with Koehler SE and the Technical University of Darmstadt, worked on a thermos-sensitive recording material.[83] The new material consists of a carrier substrate, which is black or colored on at least one side, and a thermo-responsive layer, where the thermo-responsive layer consists of nanoparticles of at least one cellulose ester. The nanoparticle layer is opaque in its original unaltered state. The opacity of the layer is caused by light scattering on the particles and the difference in refractive index between the polymer and the air present in the open-pored system. When the structure is melted, the shape of the particles and the air cavities are destroyed, resulting in an irreversible, transparent polymer film. cellulose esters have the advantage of being bio-based and more sustainable than petroleum-based polymers. They are also widely available and non-toxic. The switching temperature can be varied by using different cellulose esters such as cellulose acetate, cellulose acetate propionate, cellulose butyrate or cellulose acetate butyrate.[83–85] The particles are formed by nanoprecipitation from organic solvents on a laboratory scale. In order to use them economically on a large scale, a different production method must be chosen, e.g. spray drying. The precipitated particles, together with binders and other additives, are coated onto a model substrate and dried in an oven. Using a CO_2 laser, the opacity of the films could be switched successfully. Printing on a laboratory thermal printer was proven to be difficult because the polymer adhered to the print head, making continuous printing impossible. During thermal printing, the print head is in direct contact with the nanoparticles and the molten polymer adheres to it. On the one hand, these deposits can reduce the lifetime of the printer, and on the other hand, the adhesion effect can distort or compress the printed image. To obtain a reliable print medium, this adhesion effect can be reduced by applying a topcoat. The topcoat should be transparent and have non-insulating and non-thermoplastic properties. However, applying an additional layer is not economical and, depending on the material, can have negative impact on recyclability or biodegradability. A sustainable solution that does not require a topcoat is therefore preferable.

3 Goal and Strategy of the Research

Based on the motivation that was outlined in chapter one, and based on the current state of research and own preliminary work outlined in chapter two, the goal of the thesis was to investigate and develop opaque-transparent thermally switchable coating. They should base on crystalline substances in polymer matrices, as this strategy resulted in promising thin and opaque (light scattering) coatings in preliminary tests. For this purpose, different polymers and crystalline substances were analyzed for their thermal and optical properties and formulations for coatings were prepared. The opacity of the coated substrates was then measured and the switching behavior was investigated. In addition, real-life application conditions were used by ultimately testing the switchability in a standard point-of-sale thermal printer. Following key question has to be answered in the course of this thesis:

> *Can crystalline substances be introduced into a polymer matrix to obtain a thin opaque film that can be thermally switched?*

To answer this question following sub-questions were investigated:

1. *Can a eutectic system be used to have an increased scattering effect in binary mixtures of crystalline substances?*
2. *What is the best strategy for introducing crystalline substances into a thin layer polymer matrix?*
3. *What properties of the polymer matrix and the crystalline substance are required for a coating to undergo irreversible thermal switching in opacity?*
4. *Does the substrate influence thermal switching of a coating?*

In order to answer the questions above, the following approach was taken: The first part of the work was devoted to the study of eutectic mixtures. The question was addressed as to whether binary, organic eutectic mixtures can add measurable value to the scattering effect of a crystalline mixture. Eutectic mixtures had to be identified and then studied on their optical properties. A measurement system and a suitable sample preparation method had to be found with which the scattering factors could be determined. The second part of the thesis deals with the formation of coatings from organic solvent. By using organic solvents, the choice of polymer and crystalline substance is very broad and the structures that are formed during solvent evaporation were investigated. PET film is used as model substrate for the coating formulations, to avoid the influence of paper on the coating process. Paper has a homogeneous surface and its permeability to solvents impacts the formation of films. Only water-based coating formulations can be widely used in the paper industry. Therefore the third part of the thesis deals with the transfer of coatings into aqueous formulations. Finally, the aqueous formulations are coated onto paper. Since water passes through paper, the film formation process is different from that

with PET substrate. The paper samples are also printed in a thermal printer to test the performace of the coating in the real application.

The described approach of the thesis is summarized in the following Figure 3.1.

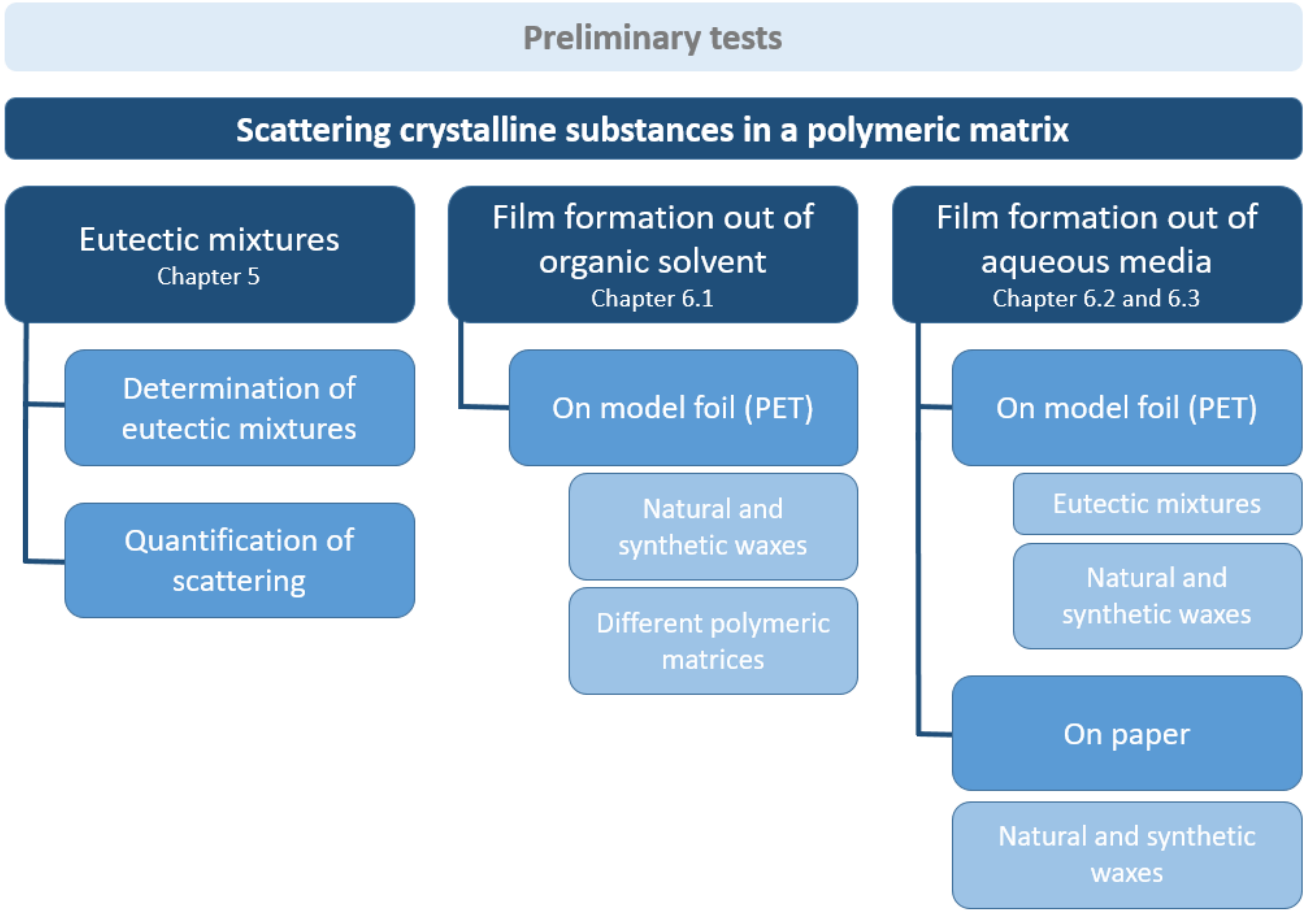

Figure 3.1: Overview of the content and approach of the thesis.

4 Methods

4.1 Theory and Measurement of Light Scattering

Since the goal of this work is to find a system that should have high opacity due to high light scattering even in the thinnest coatings, the interaction of light and matter must be considered in more detail. In addition, it is shown how the scattering factors can be determined.

Scattering describes the deflection of particle or wave radiation by interaction with a scattering center. For example, light can be scattered by atoms, molecules or particles. The strength of the scattering is given by the so-called scattering cross-section. It is, among other things, a measure of the probability that a scattering process will occur and can be interpreted graphically as the "hit area" of a target particle.[86,87]A general distinction is made between elastic and inelastic scattering. Elastic scattering is characterized by an unchanged kinetic energy before and after the impact. This is in contrast to inelastic scattering, where the kinetic energy decreases due to the excitation or ionization of an atom.[86] In the case of wave scattering, a distinction is made between coherent and incoherent scattering. In coherent scattering, there is a fixed phase relationship between the incoming wave and the scattered wave, so they can interfere with each other. This is not the case with incoherent scattering.[86–88]
Scattering is generally to be distinguished from diffraction and refraction, in which deflection of radiation occurs. The different mechanisms are schematically shown in Figure 4.1. In diffraction, the deflection is caused by the property of a wavefront to propagate in all directions along the edge of an object. In the case of refraction, the deflection results from the change of the propagation velocity, e.g. in the case of the change of the density at a phase boundary of two media.[86]

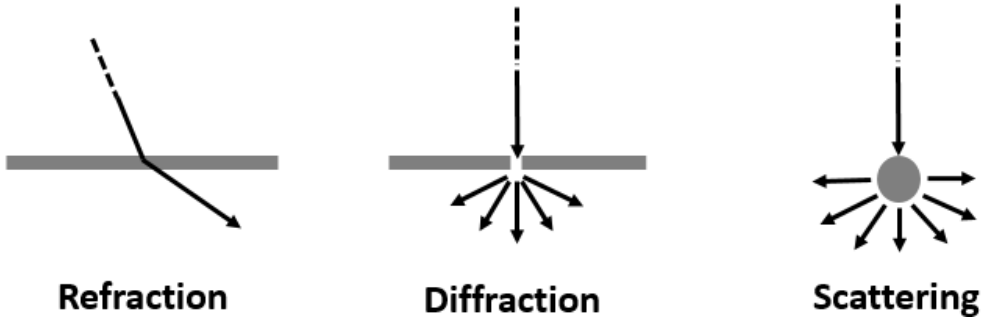

Figure 4.1: Difference between refraction, diffraction and scattering of light. Refraction occurs when light enters a medium and the wave angle changes direction after passing the phase boundaries. Diffraction occurs when light waves are bend at an object. Diffraction is dependant on the wavelength of the light in relation to the size of the object. Light scattering occurs when light is deflected by particles in directions deviating from the incident direction. [86,89,90]

For the scattering of electromagnetic radiation the following highlights the scattering on matter, in particular on particles. Other scattering effects and variants are not discussed in this chapter.

If light hits a particle and is scattered by it, different models are used to describe the occurring processes, depending on the size of the particles. These models are divided into three regimes depending on the dimensionless size parameter α. α is defined as the quotient between the particle circumference $\pi \cdot d_P$ and the wavelength λ:

$$\alpha = \frac{\pi \cdot d_P}{\lambda} \qquad \text{Eq. 1}$$

if $\alpha \ll 1$: particle is much smaller than the wavelength of light → Rayleigh scattering
$\alpha \approx 1$: particle has about the same size as the wavelength of light → Mie scattering
$\alpha \gg 1$: particle is much larger than the wavelength of light → Geometric scattering.[87]

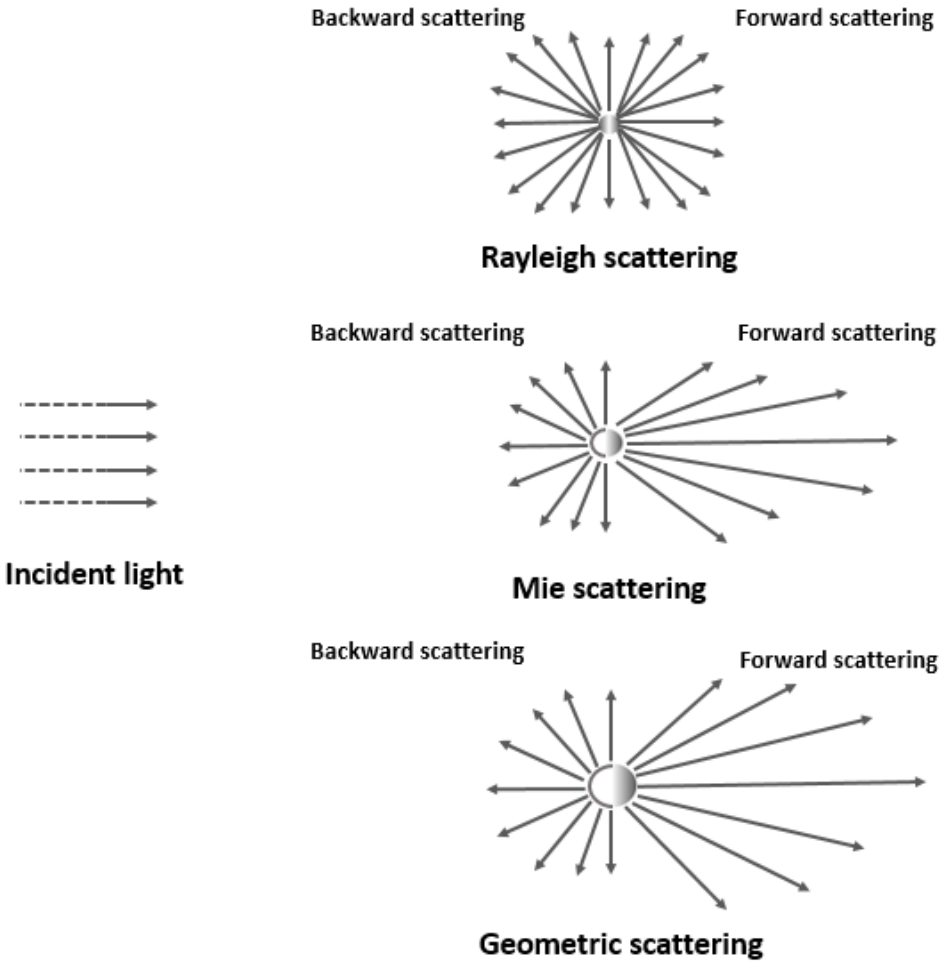

Figure 4.2: Scattering profiles of Rayleigh, Mie and geometric scattering. The scattering profiles are dependent on the particle size compared to the wavelength of the incident light.[87,91]

The scattering patterns of the different scattering types are shown in Figure 4.2. Thus, Rayleigh scattering describes processes in which light in a medium strikes and is scattered by a small, spherical volume with a refractive index different from that of the medium. To apply the model, the size of this volume must be significantly smaller than the wavelength of the light. The upper limit for the validity of

the model is typically 1/10 of the wavelength.[86,87,92] In practise, the shape of the passing volume is negligible in this order of magnitude. The strength of the scattering, i.e. the angle at which the scattered light was deflected from the original path, is strongly dependent on the wavelength of the light and is proportional to $1/\lambda^4$. With the help of Rayleigh scattering, e.g. the blue sky can be explained, which is caused by the scattering of sunlight by the gas molecules in the atmosphere: While the long-wave, red components of the light are scattered less strongly, the blue short-wave components experience a strong deflection and are scattered more strongly. As a result, the sky appears blue from all directions. In addition to the wavelength and other factors, the scattering angle also depends on the polarization, angle and coherence of the incident light.[92]

The scattering of light by particles whose diameter is in the order of magnitude of the wavelength of the light is described by the Lorenz-Mie theory. Unlike Rayleigh scattering, Mie scattering has a weak dependence on the wavelength. However, in this regime the shape of the scattering center is of great importance, which is why the theory only applies to spherical and spheroidal matter. The Mie formalism describes the shape, direction and intensity of the scattered light. The resulting Mie resonances allow conclusions about the size of the particles at which particularly weak or strong scattering is observed.[93] When viewing opaque coatings made of colloidal films of small particles, the opacity is created by particles with dimensions similar to the wavelength of light, so that the scattering that occurs follows the Mie formalism. Since the light in such films is scattered diffusely and independently from the wavelength and all components of visible light are included in the scattered light, the films appear frosted and the coating is opaque after drying. In addition, a bluish tint, caused by the Tyndall effect, can be observed in dilute dispersions of such particles. This so-called opalescence is caused by a small amount of Rayleigh scattering and disappears with increasing colloid size. Due to the wavelength-dependence, the blue portion of the visible light is scattered stronger and the film appears bluish. When such a film dries, the regular arrangement of the particles can produce a variety of colors by interference of the backscattered light. This effect is observed in the coloring of opals and is the reason for structural colors in nature. Examples include the colors of butterfly wings, the colors of peacock feathers, and the blue color of the iris. The prerequisite for this is a narrow particle size distribution.[86,92]

The Kubelka-Munk-theory quantifies the scattering of a surface or material. This is the most widespread theory that deals with the diffuse reflection on turbid media and is based on the light scattering *s* and light absorption *k*. Rudolf Kubelka and Franz Munk investigated the masking behavior of paint coatings and the correlation between coating thickness and opacity. This enables the determination of the minimum layer thickness of a coating at maximum coverage of the substrate.[94] The theory is widely used in the paper industry due to its sufficient prediction accuracy. It is used for scattering quantification of paper coatings, paints, but also plastics and textiles.

The Kubelka-Munk parameters s and k can be determined by measuring the remission of a material using spectral photometry with a diffuse distributed monochromatic light source. The sample itself is also restricted in its properties e.g it must be a homo-reflecting body or Lambert radiator. A Lambert radiator is an ideal diffuse spotlight that emits the incident light uniformly in all directions. Such a radiator is also called an ideal matte surface because it reflects light in all directions, regardless of the incident light direction. Although paper does not completely fulfill the conditions, the Kubelka-Munk theory can still be applied with sufficient accuracy. Exceptions are papers or other materials with glossy surfaces, which have highly distorted reflection characteristics.[86]

The derivation of the Kubelka-Munk equations establishes a correlation between the reflection coefficient, the light scattering coefficients and the light absorption coefficients. Based on the idea of how a light beam is reflected and transmitted in thin layers, the following formulas for diffuse reflection have been derived (visualized in Figure 4.3): A paper of thickness w is placed on a completely black surface with reflection factor R_g. The light intensity of the light source is I_0 and the intensity of the reflected light is J. This gives the reflection factor $R = \frac{I_0}{J}$

$$R = \frac{I_0}{J}. \qquad \text{Eq. 2}$$

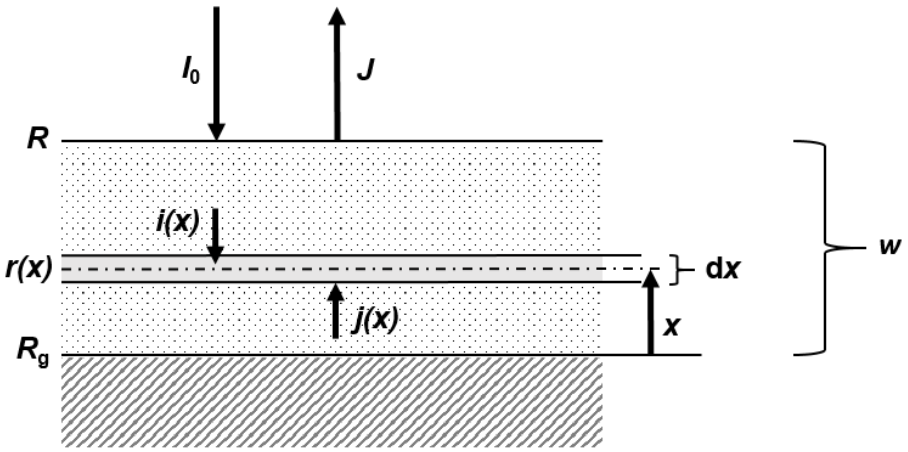

Figure 4.3: Modell for the derivation of the Kubelka-Munk equations.[95]

At a distance x from the substrate, a layer dx is illuminated vertically by a light beam with the intensity $i(x)$ from the light source and $j(x)$ from the reflected light. When light passes through the layer dx, some of the light is absorbed and some is scattered. Thus i and j are reduced by $(s+k)i\mathrm{d}x$ and $(s+k)j\mathrm{d}x$. At the same time, these parts of the scattering $sj\mathrm{d}x$ and $si\mathrm{d}x$ are added to the light intensity i and j:

$$-\mathrm{d}i = -(s+k)i\,\mathrm{d}x + sj\,\mathrm{d}x \qquad \text{Eq. 3}$$

$$\mathrm{d}j = -(s+k)j\,\mathrm{d}x + si\,\mathrm{d}x. \qquad \text{Eq. 4}$$

These two differential equations form the basis of the theory. The complete derivation is not discussed in this context and we continue further with the resulting equations that are used to determine the scattering factors.[94–98]

Derived from this theory, the scattering factors, i.e. the density-related scattering coefficient *s*, the density related light absorption coefficient *k* and the scattering power are to be determined. This is done by measuring the reflectance of the samples on a black and white background using a spectrophotometer. The intrinsic reflection R_∞ is given by:

$$R_\infty = a - \sqrt{a^2 - 1} \text{ and} \qquad \text{Eq. 5}$$

$$a = \frac{1}{2}\frac{(R_S - R_{gs})(1 + R_V R_{gv}) - (R_V - R_{gv})(1 + R_S R_{gs})}{R_{gv}(R_S - R_{gs}) - R_{gs}(R_V - R_{gv})}, \qquad \text{Eq. 6}$$

with R_s: Reflection of sample over black substrate,

R_v: Reflection of sample over white standard,

R_{gs}: Reflection of black substrate (= 0),

R_{gv}: Reflection of white standard.

With the intrinsic reflection R_∞, the scattering coefficients *s* and *k* are determined:

$$s = \frac{1}{m_A\left(\frac{1}{R_\infty} - R_\infty\right)} \ln \frac{(1 - R_S R_\infty)(R_\infty - R_{gs})}{(1 - R_\infty R_{gs})(R_\infty - R_S)} \text{ and} \qquad \text{Eq. 7}$$

$$k = \frac{s\,(1 - R_\infty)^2}{2R_\infty}. \qquad \text{Eq. 8}$$

with m_A : grammage of the sample in kg m^{-2}.

The scattering factors can be used to compare samples and draw conclusions about the quality of the scattering.

4.2 Formulation of Inks to be Used in Paper Coatings

The formulation of the coatings depends on the ingredients and their solubility behavior, or their melting point. The coatings consisting of polymer and crystalline substance from organic solvent are dissolved in a solvent, in which all ingredients can be dissolved. To aid dissolution, especially with high wax content, solutions are treated in a heated ultrasonic bath.

Aqueous solution coating formulations with natural or synthetic waxes are prepared using a dispersing tool (Ultra-Turrax T25, *IKA*). In this process, the wax is heated together with the binder and matrix, polyvinyl alcohol (PVA), in an oil bath above the melting temperature of the wax. The setup is displayed in Figure 4.4. The mixture is then dispersed at a rotation speeds of approximately 13,500 rpm for one minute. The oil bath is then removed and the mixture is cooled in an ice bath at the lowest dispersion speed. The constant mixing prevents agglomeration. With a mixture of fatty acid and PVA, the influence of cooling is investigated. In addition to the standard, ice bath, liquid nitrogen is also used for cooling. This increases the viscosity of the coatings drastically, which interferes with the coating process (inhomogeneous films) and has no benefit in terms of opacity. Therefore, only an ice bath was used to cool the melt dispersions.

Figure 4.4: The dispersion tool during melt dispersion (left) and an exemplary coating composed out of PVA and fatty acid (right).

4.3 Coating Technologies for Paper

The coatings produced are applied to a model film or paper using different coating processes. The most commonly used method is a doctor blade process using a film frame on an automatic film applicator which guarantees a constant coating speed. The applicator and the frames are shown in Figure 4.5. The film frame applicators each have four milled gaps of different heights. These gap heights determine the wet film thickness. With the selected wet film thickness and the adjusted solid content of the applied coating, the theoretical dry film thickness is estimated. This is demonstrated at the end of this chapter.

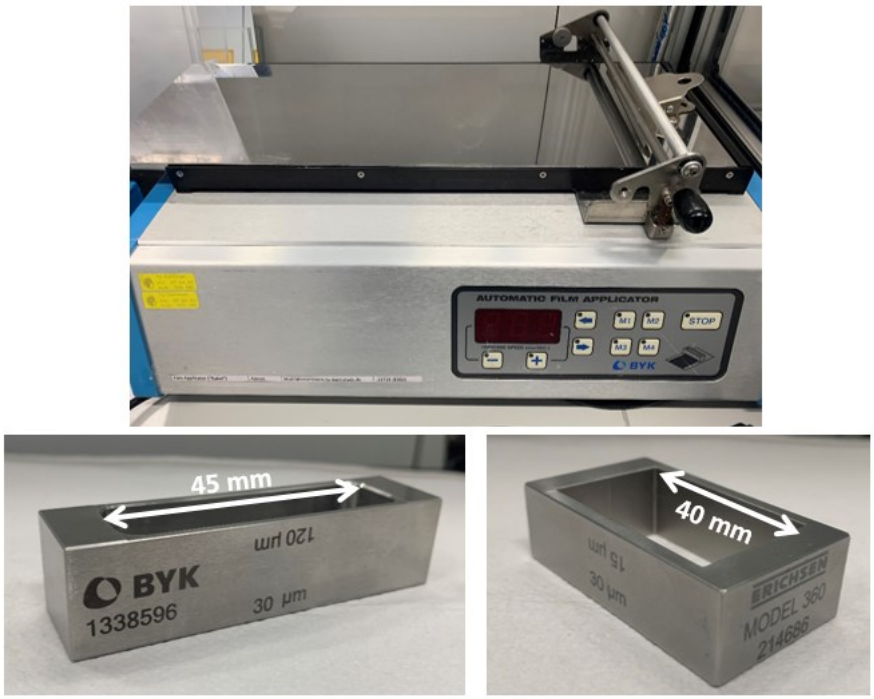

Figure 4.5: The automatic film applicator (top) was used to coat the papers and model films with the film frame applicators (bottom row) with different gap widths (15-120 µm).

Figure 4.6: Mechanism of coating a substrate with a film frame applicator. The coating solution is placed inside the frame and dragged over the substrate.

Figure 4.6 shows schematically the coating process with the film frame applicator. The substrate is stretched on the coating table and the film drawing frame is placed on top. The coating material is transferred into the frame. The slide of the doctoring table pushes the frame over the substrate at a defined speed so that a homogeneous layer is applied through the gap in the frame.

Another option to coat formulations is to use a wire-wound rod. The thickness of the wet film is determined by the thickness of the wire that is wound around the rod. During the coating process, the coating material is placed in front of the rod and the rod is pulled over the substrate by the support of the doctoring table at a defined speed, and the material is pushed in front of the rod. This process results in very homogeneous strokes, but in this thesis the film frame applicator is mainly used, since it requires only a minimal amount of coating formulation with little discard.

For the formulations out of PVA and melt-dispersed palmitic acid (PAc), the real film thicknesses of the dry films were determined using white light interferometry (WLI) in order to check whether the estimated and real film thicknesses correspond to each other. Before measuring the samples, scratches were made in the coatings to be able to measure the difference in height between the coating surface and the substrate. In this case the substrate is PET foil. Then 20 nm of Pt/Pd were sputtered onto the films so they show the necessary reflectance that is needed for the measurement. Figure 4.7 shows how one of the scratches was used to measure the height of the coating. The exemplary samples consist out of different amounts of fatty acid dispersed in PVA. All percentages given in this thesis are mass percentages, unless otherwise stated. The gap height used for the coating is 30 µm which, with the solid content of 30 %, gives a theoretical thickness of approximately 9 µm. The thickness was measured at different spots on three scratches leading to film thicknesses summarized in Table 4.1. The values are close to 9 µm but vary up to 2 µm. This means that the theoretical estimate is close to the actual thickness, but has an experimental error.

Table 4.1: Film thicknesses of exemplary samples to check if the theoretical and real film thicknesses dependant on the solid content of the coating and the gap height of the film frame applicator correspond to each other.

Sample	Solid content of coating	Gap height of film frame applicator	Measured film thickness via WLI
30 % PAc in PVA	30 %	30 µm	9.0 ± 1.4 µm
50 % PAc in PVA	30 %	30 µm	8.6 ± 1.8 µm
90 % PAc in PVA	30 %	30 µm	9.7 ± 0.5 µm

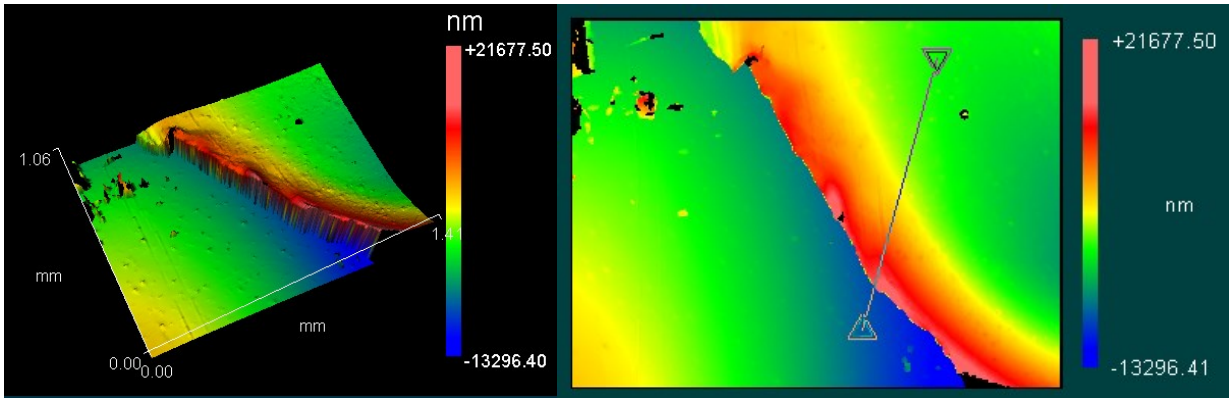

Figure 4.7: White light interferometry images of a sample out of PVA with 30 % melt-dispersed palmitic Acid. The solid content of the coating is 30 %. The coating was applied using a frame gap applicator with a gap width of 30 µm leading to a theoretical thickness of 9 µm.

4.4 Thermal Treatment and Thermoprinting of Coated Samples

Since thermal papers and their thermal switching behavior are the focus of this thesis, the samples produced must be tested for their optical properties when thermally treated. In order to do this easily in the laboratory, a simple drying oven is used. The films are placed on a preheated metal tray. The temperature should be similar to that of a thermal printer. However, thermal printers do not work with a defined temperature, but with a defined voltage at which the print head prints. Therefore, a temperature cannot be specified. Nevertheless, a temperature of 140 °C is chosen to have a constant switching temperature throughout all experiments. If samples perform well and are suitable for the thermal printer, then their performance is tested during printing. Figure 4.8 on the left shows the standard thermal printer used in this thesis (EPSON TM-T88VI). The print head is displayed on the upper right side. After the samples are printed, a test print is made with a commercial thermal paper to see if any of the coating is deposited on the print head. The image on the lower right side shows an image of such a test print, which has clear streaks in the printed locations caused by the deposits on the print head.

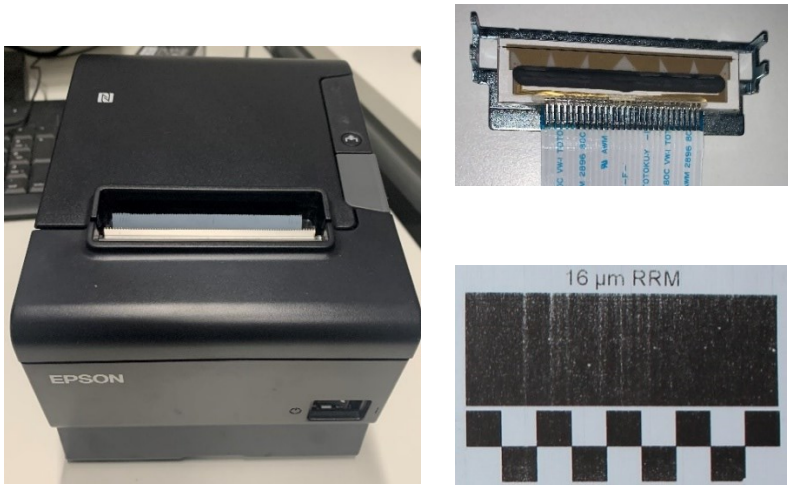

Figure 4.8: Picture of the used standard thermal printer EPSON TM-T88VI (left), a print head of a thermal printer with the black thermal strip (right top) and a test print with streaking caused by deposits on the print head (right bottom).

4.5 Determination of Opacity

In order to quantify the quality of the samples produced, it is necessary to find a method for the determination of the opacity of the coatings in the original, as well as in the switched state. The switched state can either be generated by thermal printing or switching in the oven. For this purpose, transparency can be measured using a remission spectrophotometer. Transparency is given by the light transmission of the sample and calculated from the characteristic reflexion values

$$Tr = \sqrt{(R_\mathrm{v} - R_\mathrm{s}) \cdot \left(\frac{1}{R_\mathrm{gv}} - R_\mathrm{s}\right)}, \qquad \text{Eq. 9}$$

with: Tr : transparency,
R_s : reflexion of the sample over a black substrate,
R_v : reflexion of the sample over white background (white standard) and
R_gv : reflexion of the white standard.

These measurements can only be performed on films that are coated on transparent substrates. However, since the opacity of coatings on paper should also be quantified, the optical density (OD, see Eq. 10) is measured. It is measured with a portable densitometer (SpectroEye by X-Rite) that uses the standardized light D65 and a viewing angle of 10°, and a DIN 16536 density standard. The resulting values are an average of four measurements each on a different spots of the sample.
The optical density is the absorbance of a material which is described by the logarithmic intensity ratio of the light incident on the material to the light transmitted through the material. It can be expressed as follows:

$$OD(\lambda) = \lg \frac{I_0}{I}, \qquad \text{Eq. 10}$$

with: I_0: intensity of the incident light and
I: Intensity of the transmitted light.

Coatings that are intended to have the highest possible opacity require a particularly high optical density. However, if the optical density is determined by the proportion of backscattered light, a low optical density value corresponds to a high opacity.[82.95]. As a standard the optical density values of commercially available thermal papers are determined (Table 4.2). This leads to the target value for the original/non-switched/non-printed coatings of OD < 0.5 and a target value for the switched/printed coatings of OD > 1.3. This is the value of the black base paper for Blue4est® thermal papers.

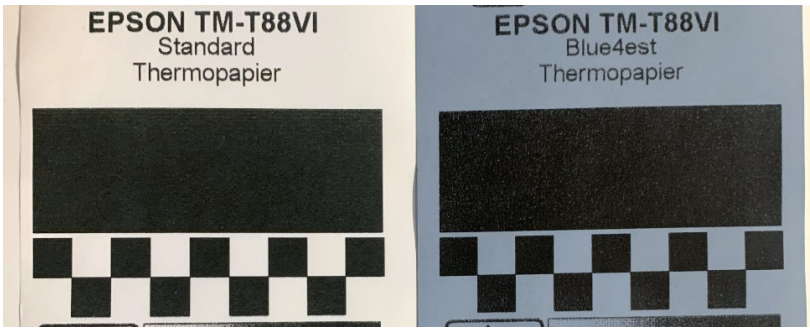

Figure 4.10: Images of a standard thermal paper (left) that is based on leuco dyes and a new type of thermal paper (Blue4est® from Koehler Paper SE) where the printing process is solemnly based on physical processes (right).

Table 4.2: Optical densities of commercially available thermal papers in the original and printed state.

	OD of white paper / non-printed	OD of black paper / printed
Standard thermal paper	0.10	1.04
Blue4est® thermal paper	0.54	1.39

5 Crystalline Eutectic Mixtures and their Scattering Behavior

The main strategy of this work is to use crystalline substances embedded in a polymeric matrix which contribute to the opacity of the thin film. Therefore, a maximum of scattering is needed for the crystallites. One idea to obtain this maximum is to use organic eutectic mixtures, as it has been reported that eutectics can form microstructures.[66,76,82] This means that there is a maximum of interfaces between the components. If a eutectic mixture can be found where the difference in refractive indices is at most, a maximum of light scattering can be obtained. This chapter describes the experiments designed to test this hypothesis.

The first step is to find organic eutectics with components that have a high difference in refractive index. Binary mixtures are used to lower the complexity of the investigations. Many substances were screened for their refractive index n_D if it was low ($n_D < 1.4$) or high ($n_D > 1.6$). Differentical scanning calorimetry (DSC) measurements were carried out to determine whether the substances exhibit eutectic properties in any mass composition and combination.

5.1 Eutectic Mixture of Dimethyl Oxalate and Ethylcarbazole

The dimethyl ester dimethyl oxalate (DMO) and the carbazole derivative 9-ethylcarbazole (EC) were selected for their low, respective high refractive index, which was measured using an Abbe refractometer in the molten state (experimental procedure e34; see 8.3):

- Dimethyl oxalate n_{D60}=1.390
- 9-Ethylcarbazole n_{D80}=1.621

The difference in refractive index of the melts is $\Delta\ n_{D20}$=0.231 which is high enough, but has to be confirmed with the solids if the substances form a eutectic mixture. The chemical structures are shown in Figure 5.1.

Figure 5.1: Structures of dimethyl oxalate (left) and 9-ethylcarbazole (right).

Figure 5.2 shows the DSC thermograms of the pure substances DMO and EC, as well as example curves with three mixtures with amounts of DMO below, over and in the eutectic composition. For the evaluation, the second heating cycle is used, since it is assumed that the substances are homogeneously mixed by the first melting and recrystallize in a well mixed state. The melting points of DMO at 56 °C and EC at 72 °C are clearly decreased in all of the mixtures and at 50 % DMO only one melting peak is visible, which is necessary for a eutectic composition. Many different mixtures were measured to create a phase diagram, to obtain information on the properties of the mixtures. No miscibility gaps were found

and the eutectic range is at compositions from 50 to 60 % DMO with the eutectic melting temperature T_E at 46 °C. For the phase diagram, the peak melting temperatures $T_{m,Peak}$ were used since the melting rate is the highest and can be evaluated more accurately. The onset melting temperature $T_{m,Onset}$ for the peaks that are merely a shoulder, show large deviations depending on where you place the tangent. The diagram is shown in Figure 5.3.

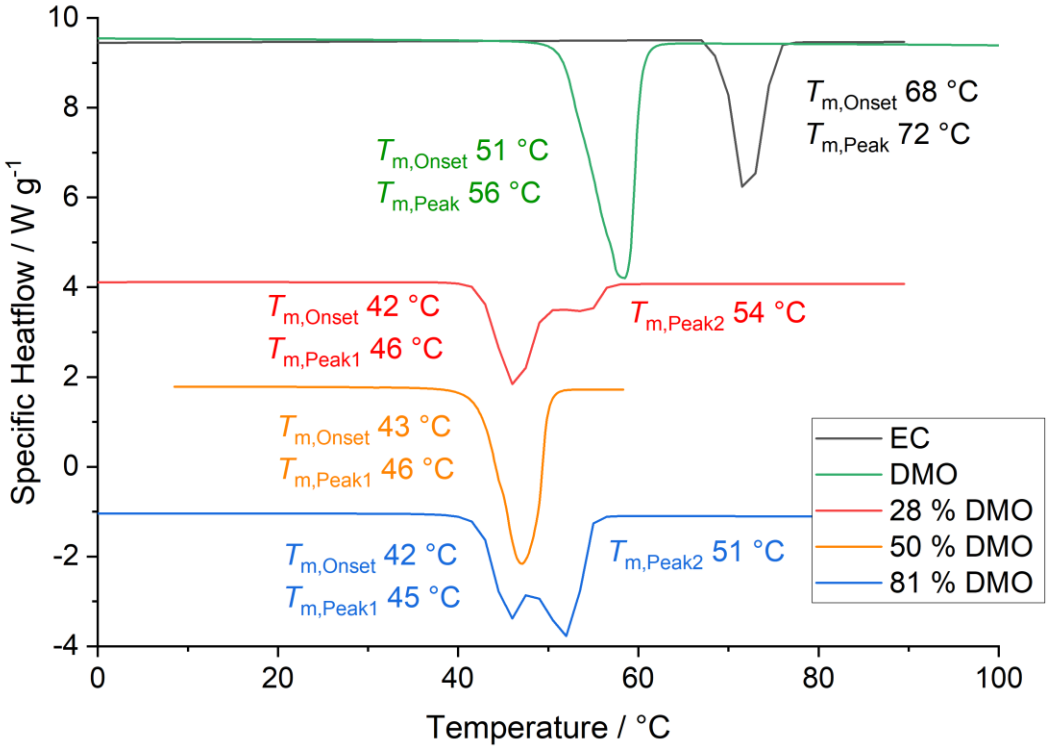

Figure 5.2: DSC thermogram of the pure substances DMO and EC, as well as example curves with different compositions of their mixtures. The amount of DMO describes the composition. The second heating cycle is displayed; the heating rate, as well as the prior cooling rate is 10 K min^{-1}.

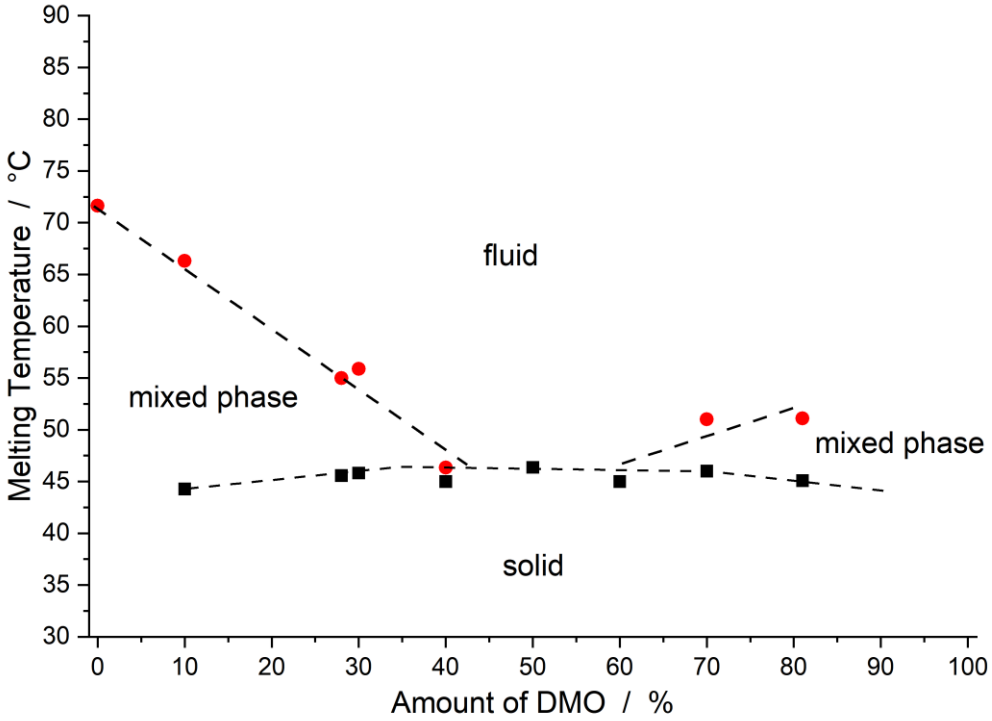

Figure 5.3: Phase diagram of DMO and EC at various compositions. A eutectic mixture with a single melting temperature is found at 50 and 60 % DMO. Therefore, a eutectic range from 50 to 60 % DMO is being assumed.

For the application in a paper coating, the substances are used at room temperature. Since the refractive index values measured with the Abbe refractometer were obtained from the melts at different temperatures, the values had to be confirmed for the substances in a solid state using ellipsometry (experimental procedure e34; see 8.3). A thin layer of the molten substance was deposited on Si-wafers and the thickness of the layer was measured using white light interferometry (WLI). Half of the sample was sputtered with gold for the WLI measurements, since a reflecting surface is needed. The height was determined by measuring scratches in the film (Figure 5.4).

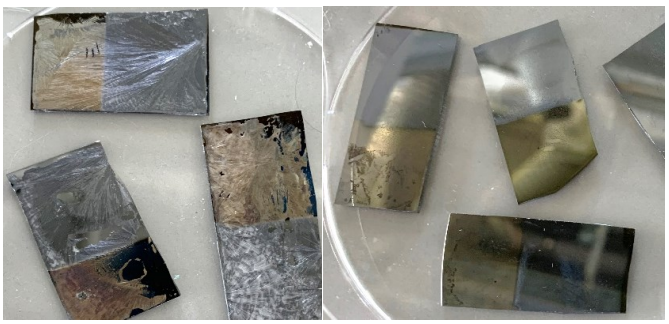

Figure 5.4: Samples of EC (left) and DMO (right) on Si-wafers. Half of the sample was sputtered with 20 nm of gold to obtain a reflecting surface for the measuring of the height via white light interferometry. The ellipsometry measurements were carried out on the non-sputtered part oft he sample (λ (laser) = 658 nm; RT; 15 % rel. H.; e34).

The obtained refractive index is 1.458 ± 0.046 for DMO and 1.638 ± 0.053 for EC. The thickness measurements of the DMO films show a higher deviation since the surface structure had a coarser

morphology than the EC films. The ellipsometry measurements were performed in close proximity to the scratches so that the height of the films is included in the measurement with as little error as possible. The difference in refractive index of the components at room temperature is $\Delta n_{D20}=0.2$ which is slightly smaller than that of the melts. Ellipsometry measurements were also performed with the eutectic and other mixtures of the substances, but a reliable evaluation was not possible because no local maximum could not be found during the measurements due to the high scattering of these samples.

To obtain more information on the optical properties of the DMO and EC mixtures, optical test specimens were prepared for microscopy (experimental procedure e25; see 8.4). The melt was placed on a hot microscope slide and covered with a hot coverslip. Uniform pressure was applied to obtain a homogeneous thickness. The mixtures always crystallized from the outside to the inside. Figure 5.5 displays schematically the preparation of and Figure 5.6 the final test specimens.

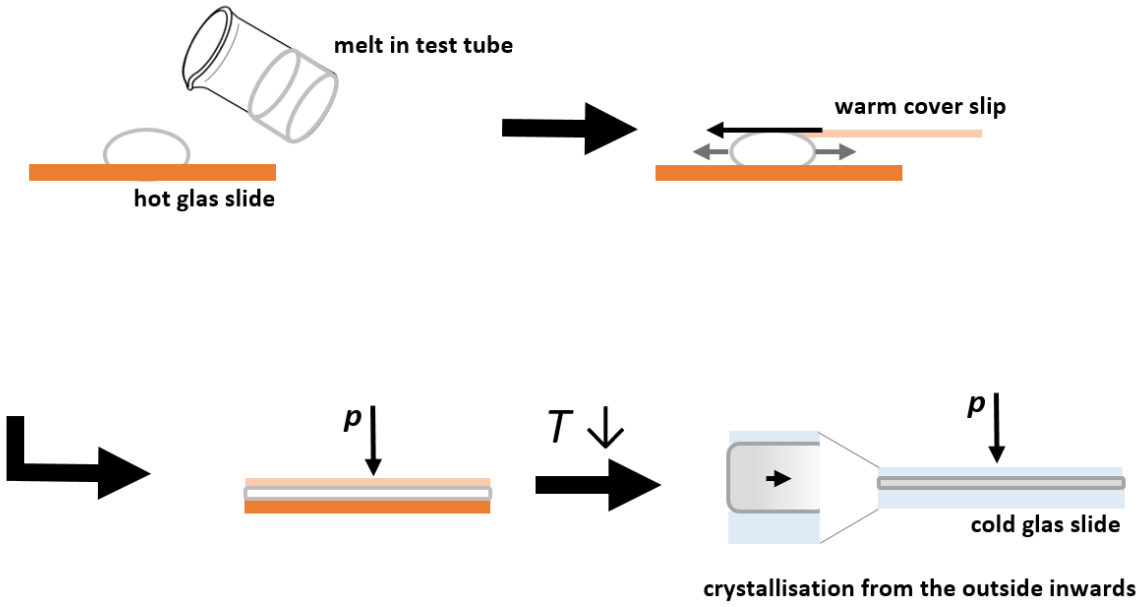

Figure 5.5: Sample preparation of optical test specimens of different mixture compositions of DMO and EC.

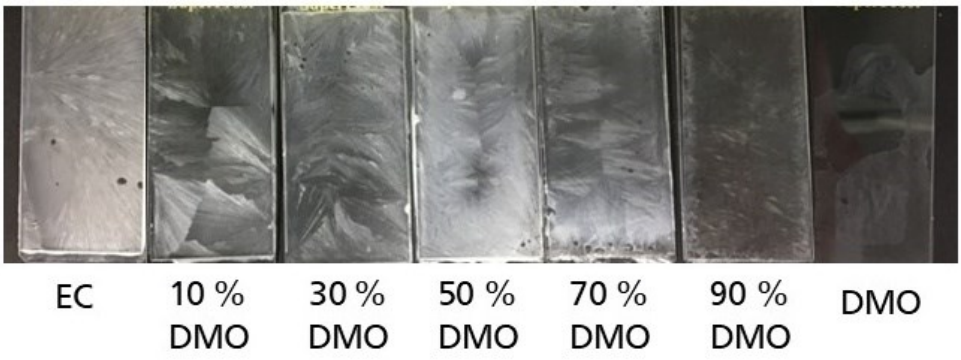

Figure 5.6: Optical test specimens of different mixture compositions of DMO and EC. The eutectic mixture is represented with 50 % DMO.

To see the crystal structures, a microscope equipped with a phase contrast filter and a differential interference contrast (DIC) setup was used. The images of the different compositions are shown in Figure 5.7 and Figure 5.8.

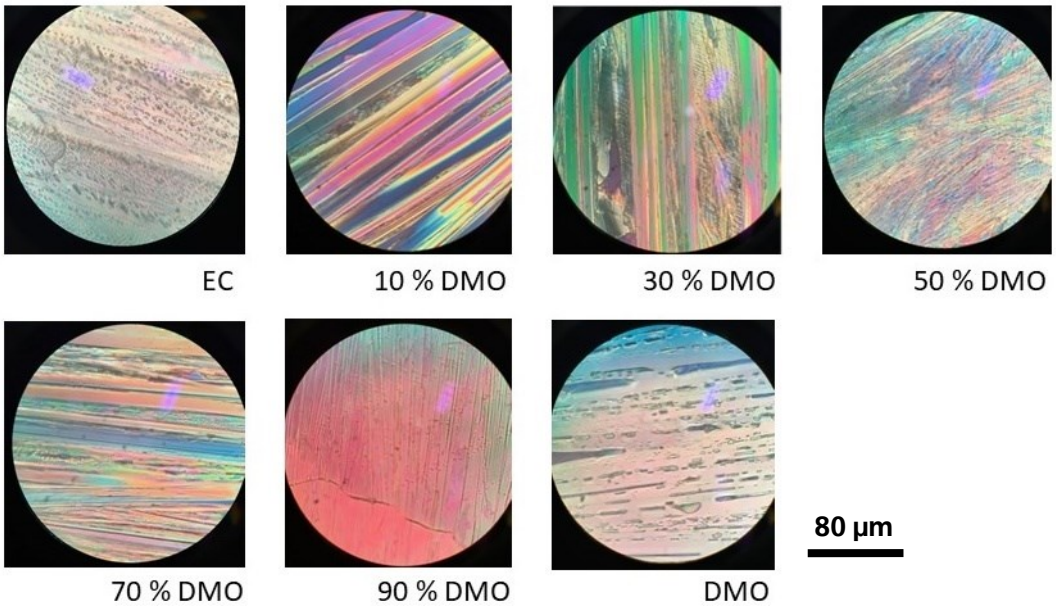

Figure 5.7: Microscope images of samples consisting of different mixtures of DMO and EC. The images were taken using a phase contrast filter.

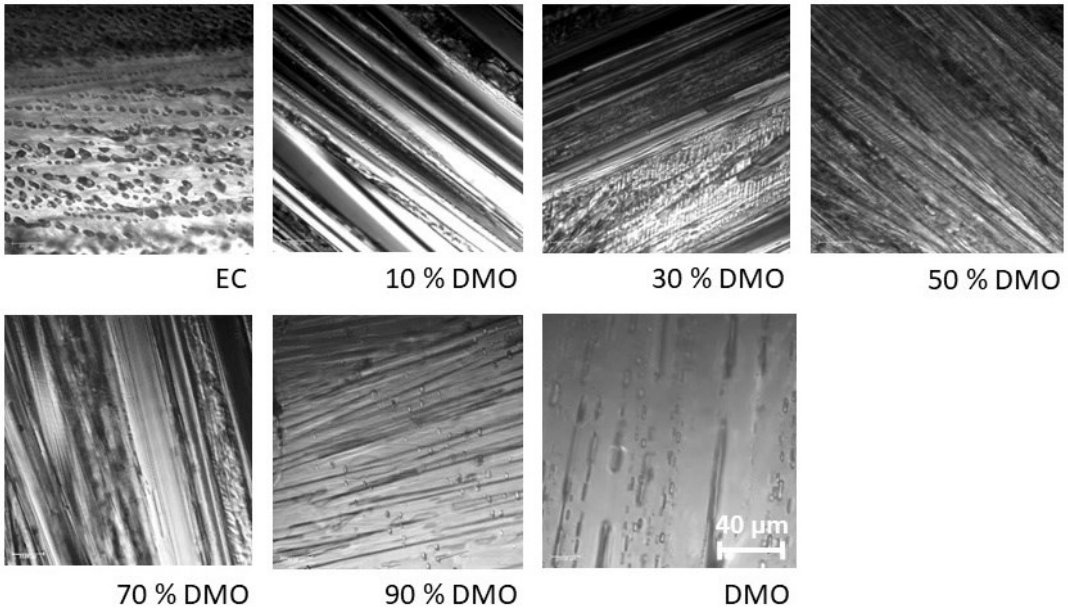

Figure 5.8: Microscope images of samples consisting of different mixtures of DMO and EC. The images were obtained using DIC.

The pure substance EC as well as DMO show a lamellar growth with small inclusions of air or smaller crystallites. With the addition of DMO the lamellar growth increases visibly and in the eutectic mixture at 50 % DMO, the lamellae become very fine. This is due to the simultaneous crystallization observed in this mixture. In the other mixtures, two separate crystallizations were seen and DMO crystallizes around the EC lamellae. The images of the differential interference contrast microscope show the strong

lamellation of the blends and the finer structure of the eutectic blend. The pure substances display air inclusions that could be implemented in the sample preparation by shrinking of the melt. These studies show that there is a different microstructure in the eutectic mixture. But does it have a different scattering behavior than other mixtures, and can it be quantified with a specific measurement setup?

Figure 5.9: Free crystallization of eutectic mixture on PET foil from 70 to 0 °C with a cooling rate of 0.18 K min^{-1}.

Scattering factors, which quantify the scattering properties of a material, are measured using a spectral photometer. As shown in Figure 5.9, the free crystallization of the eutectic mixture forms crystals with a highly textured surface structure. Since this affects the measurement, the melt will be formed behind glass. This way the samples will all have the same surface structure. In addition, different grammages must be used in order to be able to represent the course of the scattering factors as a function of the grammage for comparison purposes. Figure 5.10 shows how the first samples were prepared: frames out of polylactid acid (PLA) with inner edge lengths of 50 mm were printed with a 3D printer. The heights were varied between 0.4 and 2 mm. The frames were attached onto glass slides, heated above melting temperature of the crystalline substances, filled with the melted materials and covered with a coverslip (experimental procedure e29; see 8.5). Only test specimens without air inclusions in the circular measuring area of the spectral photometer (diameter 30 mm) are used. As an example, the eutectic mixture in the PLA frames is shown in Figure 5.11.

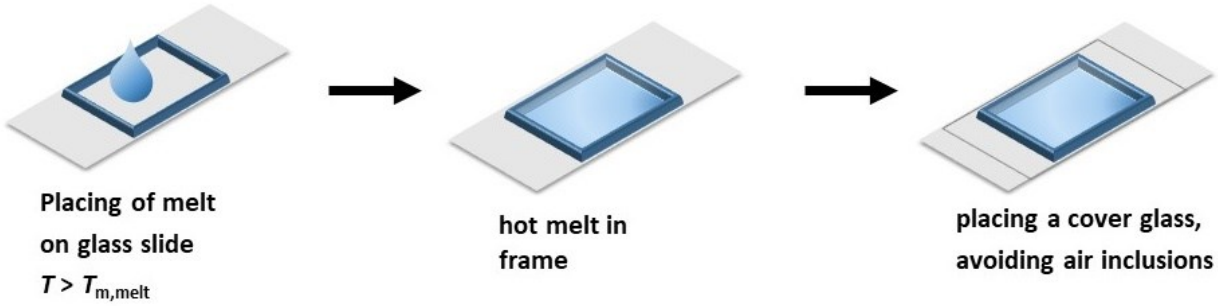

Figure 5.10: Sample preparation of test specimens for the measuring of scattering factors. The melt is filled in PLA frames that are attached on a glass slide.

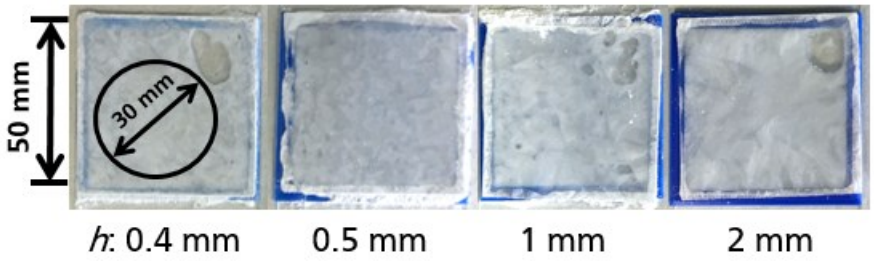

Figure 5.11: Explanatory test specimens of the eutectic mixture of DMO and EC. The grammages are adjusted with different heights of the PLA-frames (e29).

The theory of Kubelka-Munk is described in Section 4.1 of the previous chapter. Derived from this theory, the scattering factors s and k are determined. For this purpose, the reflection factors of the samples are measured in front of a black and a white background using a spectrophotometer. The light source is standard light type C with a cut-off at the wavelength of 420 nm. This way, the diffuse reflection R_∞ can be determined using Eq. 5, Eq. 6 and Eq. 7 (refer to Section 4.1, p.21). A cellulose nitrate membrane is used as the white background so that no fillers or other additives affect the remission measurements. The measurement uncertainty of the spectrophotometer is negligible compared to the sample preparation error. The standard deviation of the measured samples is used as the measurement uncertainty. It is determined by measuring multiple samples of each composition.

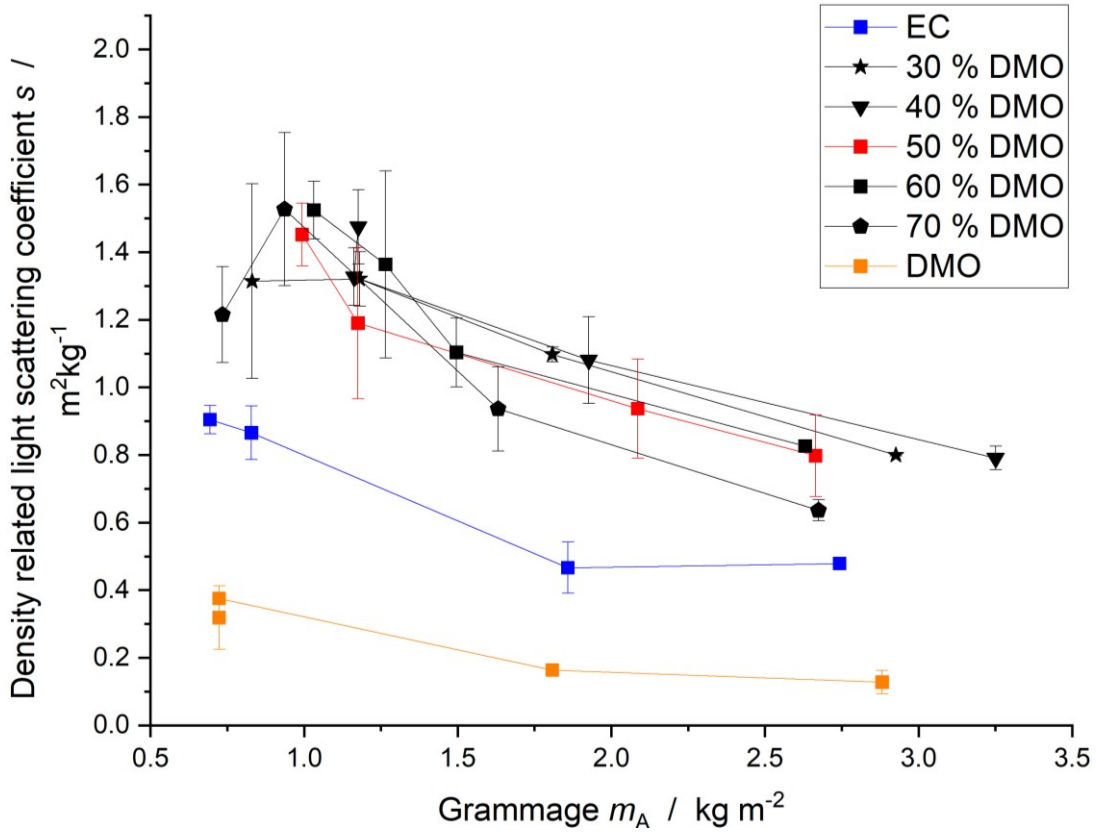

Figure 5.12: Scattering coefficient of samples with DMO and EC in PLA frames dependent on the grammage.

The scattering coefficients of DMO and EC (Figure 5.12) have, as expected, a lower scattering coefficient than their mixtures, where DMO has the lowest values. This is due to its lower refractive index, as well as to its transparency. Its absorption is significantly lower than that of EC, which has a slightly yellow appearance. The mixtures all have an increased scattering coefficient, but the eutectic composition, which is plotted in red for better differentiation, shows a similar behavior.

As can be seen in Figure 5.12 and all subsequent scattering coefficient plots, the scattering increases as the grammage of the sample decreases. The theory of Kubelka and Munk assumes that the scattering coefficients are independent of layer thickness. Thus, the condition for the use of this theory is not fulfilled: the reflected light increases with increasing layer thickness, while at the same time less light is transmitted and absorbed. Since the surface structure in our case is independent of the coating thickness, the amount of reflected light is constant for all grammages. This means that the amount of reflected light must depend on the refractive index of the sample. The thinner the coating is, the stronger this effect is, since only the total reflection R_0 can be measured with the remission photometer.

To minimize the uncertainty in s, the scattering power sm_A,

$$sm_A = s \cdot m_A, \qquad \text{Eq. 11}$$

can be considered. The dimensionless quantity represents an approximately linear curve as shown in Figure 5.13. For the comparison of the mixtures, the consideration of the scattering power sm_A is not relevant, since the effects within the mixtures can also be seen in s. However, the expected course of the scattering of a coating with increasing basis weight, according to Kubelka and Munk, can be observed.

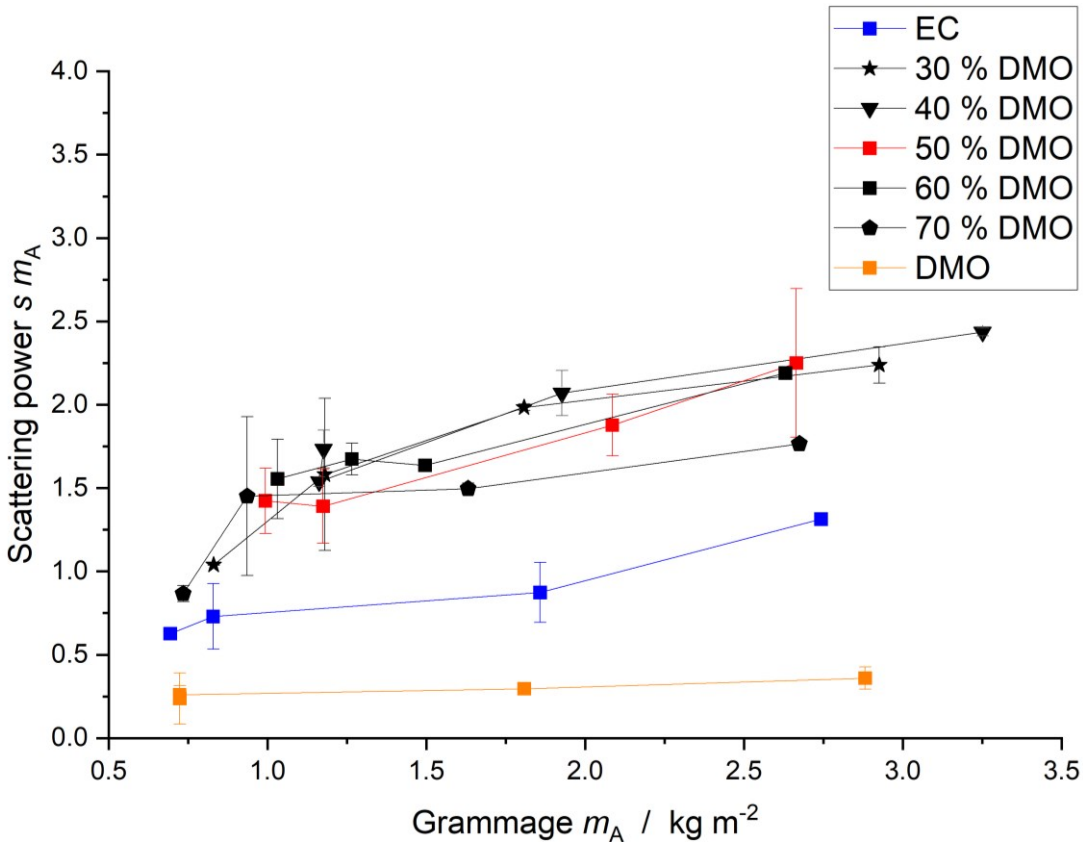

Figure 5.13: Scattering power of samples with DMO and EC in PLA frames dependent on the grammage.

The grammages studied, ranging from 0.7 to 3.2 kg m^{-2}, show interesting effects, but the grammages should be significantly reduced, since the application weights of functional coatings are approximately 10 g m^{-2}. In addition, a clearer differentiation of the compositions is hoped for. For smaller grammages the height of the samples must be reduced. PLA frames smaller than 0.4 mm could not be reproducibly and reliably 3D-printed due to the resolution of the equipment. In addition, they easily warp when the hot melt is poured into the frames during sample preparation. A solution for thinner specimens had to be found. An attempt was made with "free" specimens, similar to those used for the microscope measurements. However, during crystallization between two glass plates, pressure must be applied to prevent air from entering. Thus, the specimens showed deviations in height both in axial and radial direction which led to large errors in the determination of the grammage: a fixed containment is therefore inevitable. Therefore, metal shims were used because they are temperature stable and can be purchased in various thicknesses from 0.1 to 1 mm (experimental procedure e38; see 8.6). Figure 5.14 shows the test specimen setup and Figure 5.15 shows examples of test specimens with various compositions of DMO and EC, where the height of the shim rings is 0.2 mm. The grammage of 10 g m^{-2} will not be reached, but it is closer to real application requirements. In addition, the same heights as for the PLA frames should be used to compare how much the sample geometry influences the measured values.

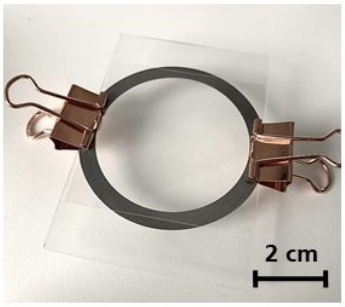

Figure 5.14: Picture of a test specimen setup containing a metal shim ring on a glass slide. The shim rings have an inner diameter of 45 mm.

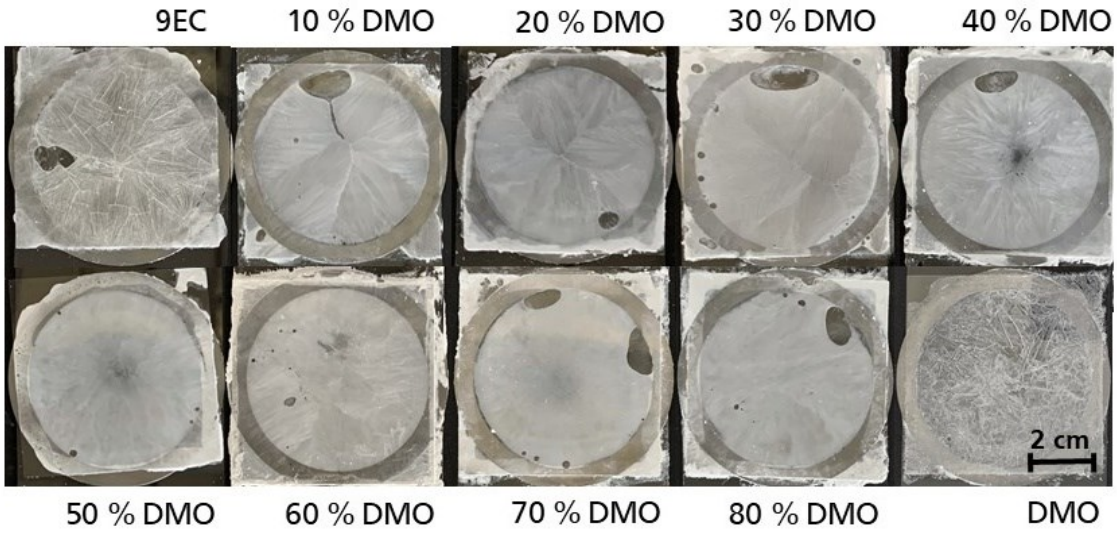

Figure 5.15: Examples of test specimens out of DMO and EC in shim rings with different compositions. These samples are in rings with 0.2 mm in height (e38).

The specimens were measured and evaluated in the same way as the PLA frame samples. The scattering coefficients are shown in Figure 5.16. The determined scattering coefficients show the same characteristic curve, but in this system the pure substances do not show a significantly reduced scattering coefficient. They are at the lower end of the range of mixtures. Nevertheless, the higher scattering effect of EC is also evident here. The samples of 10 to 40 % DMO have a slightly higher scattering coefficient than the other samples which all show a similar curve progression. The eutectic mixture (red curve) shows no increasing scattering in this setup.

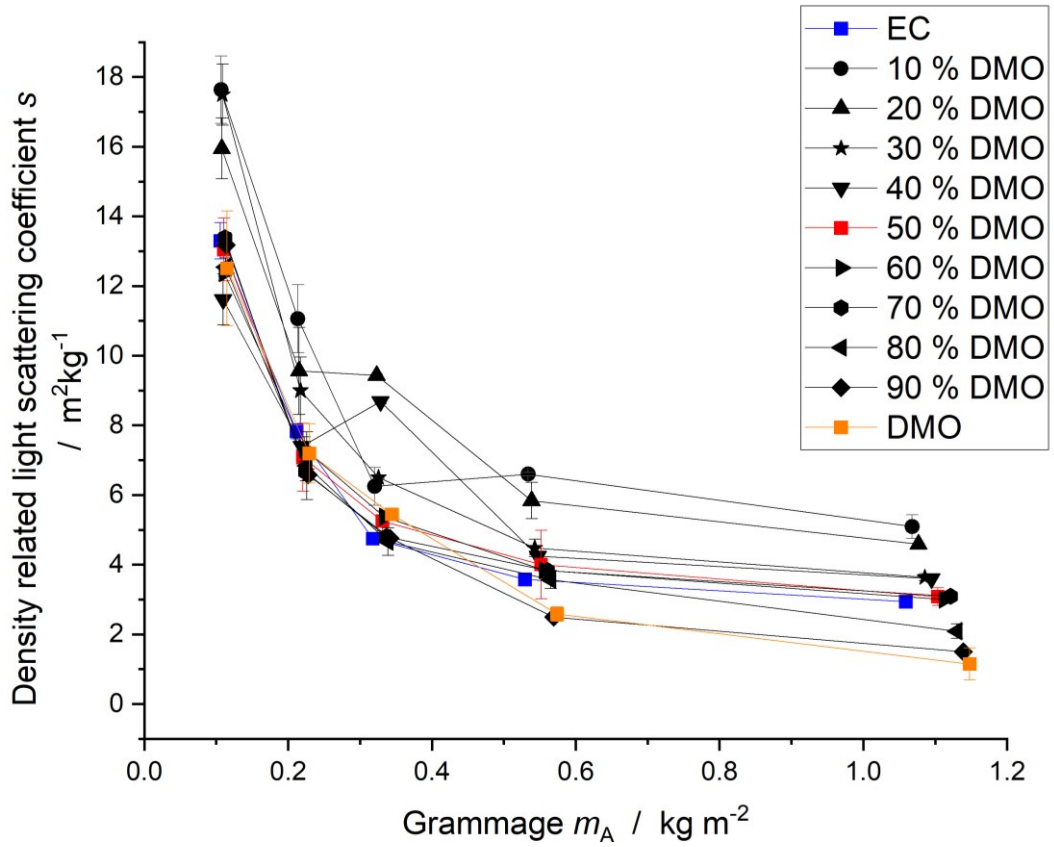

Figure 5.16: Scattering coefficient of samples with DMO and EC in shim rings dependent on the grammage.

Figure 5.17 shows both the scattering coefficients of the PLA frame and the shim ring samples of DMO and EC to compare the results. As can be seen, there is a strong shift to lower scattering coefficients in the PLA frames for the overlapping grammages. This suggests that the sample geometry and preparation have a significant effect on the measurements. The coverslip of the shims lies flat which is not the case with the PLA frames due to the surface structure caused by the 3D print which gives the coverslip some clearance. So the grammage can increase slightly. To reduce this error, the actual layer thickness is measured and used to calculate the grammage. In addition, it is noticeable that this effect is particularly strong in the PLA frames with the lowest height. These are particularly affected by the warping of the PLA when the hot melt is poured in. The samples with the shims are much less prone to errors, so they will be used to study a second eutectic system, although after improving the sample geometry, there are still sources of error in the samples themselves: in particular, air inclusions, which cannot be completely avoided.

All in all, the expected variation of the scattering effect of the compounds as a function of the grammage could be determined, but the increased scattering effect of the eutectic composition could not be quantified within the measurement setup. However, the pure substances show a slightly reduced scattering effect.

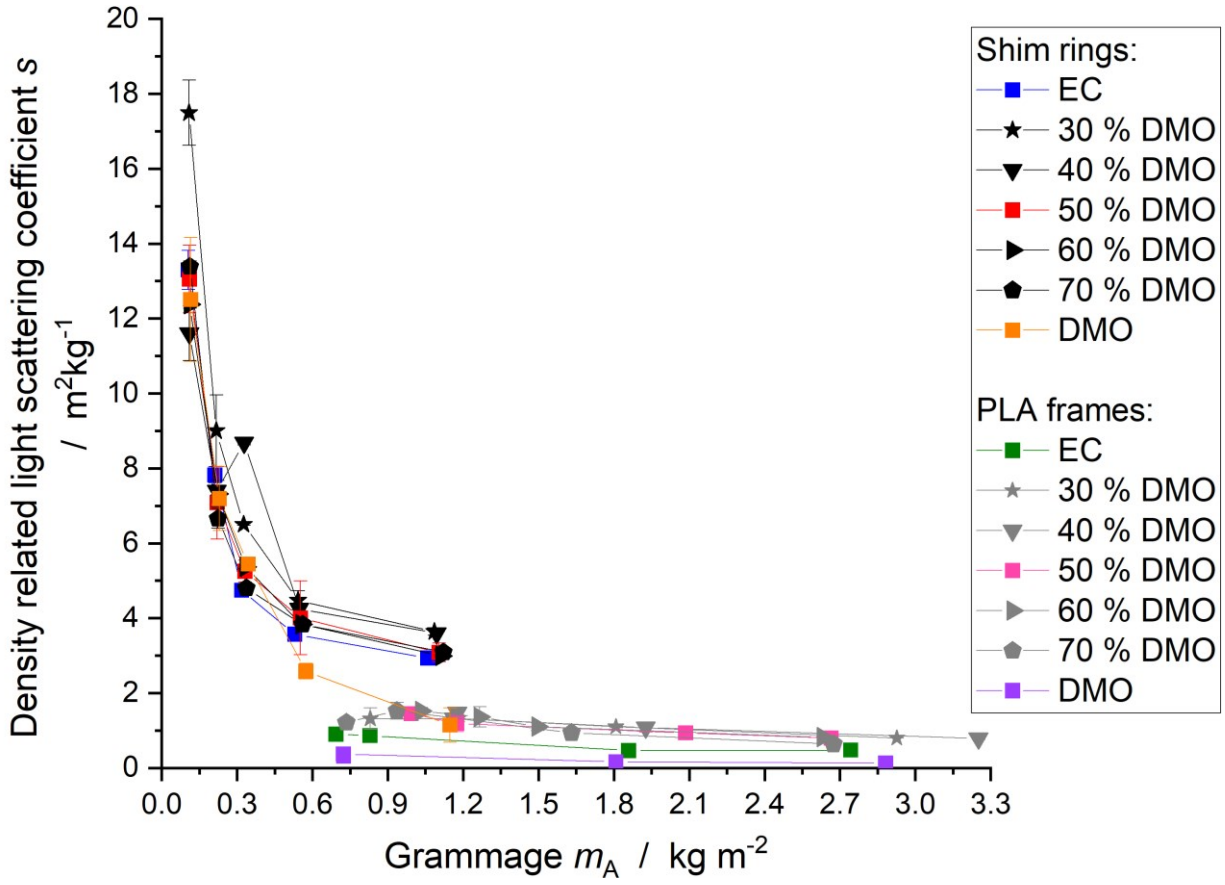

Figure 5.17: Comparison of scattering coefficient of samples with DMO and EC in PLA frames and shim rings depending on the grammage.

5.2 Eutectic Mixture of Urea and Benzoic Acid

For a better understanding of the measurement setup used, test specimens of a second eutectic system are prepared and measured. RAI *et al.* describe a binary eutectic system of urea and benzoic acid (BA), which was determined using cooling curves. 44 % urea is specified as the eutectic mixture with an eutectic melting at 88 °C.[66] First, the composition of the eutectic mixture and the temperature will be investigated using the same techniques as for DMO and EC. Then the scattering factors are determined in order to compare the results of the previous section with a second system to find out if the measurement setup is suitable for these samples. The sample geometry with the shims is used for this purpose. The small difference in refractive index of $\Delta n_{D20}=0.067$ will be neglected:

- Benzoic acid, $n_{D20}=1.540$ [100]
- Urea, $n_{D20}=1.607$ [101]

The chemical structures are shown in Figure 5.18, followed by Figure 5.19 which is the DSC thermogram of exemplary curves with different compositions of BA and urea as well as the pure substances.

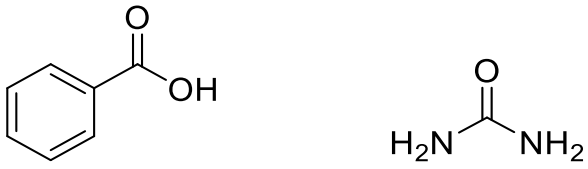

Figure 5.18: Chemical structures of benzoic acid (left) and urea (right).

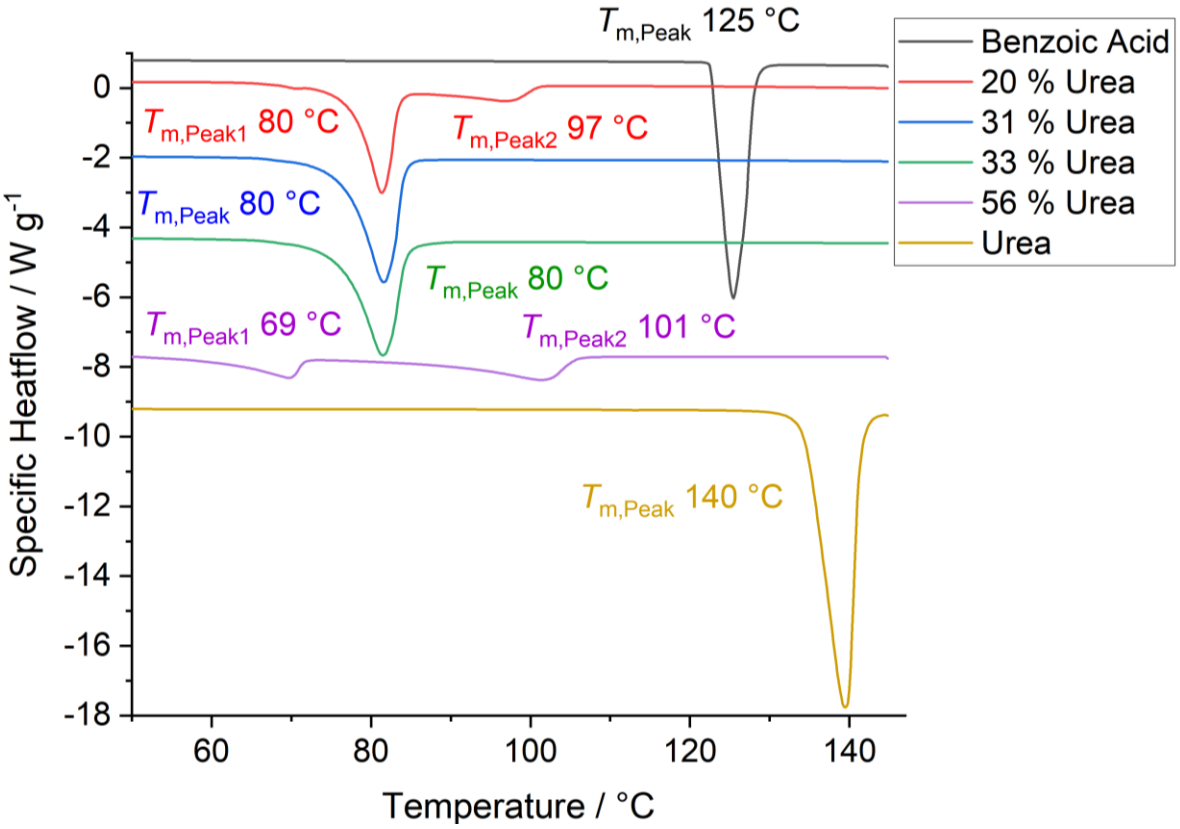

Figure 5.19: DSC thermogram of different compositions and the pure substances benzoic acid (BA) and urea. The second heating cycle is displayed; the heating as well as the prior cooling rate is 10 K min^{-1}.

Unlike literature data suggests, the eutectic composition, that was determined via DSC measurements, is present at 31 and 33 % of urea with the eutectic melting temperature T_E=80 °C. Based on these measurements 31 % urea was used to represent a eutectic mixture in the following measurements. The samples for the remission measurements were prepared analogue to the DMO and EC test specimens (experimental procedure e38; see 8.6): As an example, Figure 5.20 shows images of samples with different compositions.

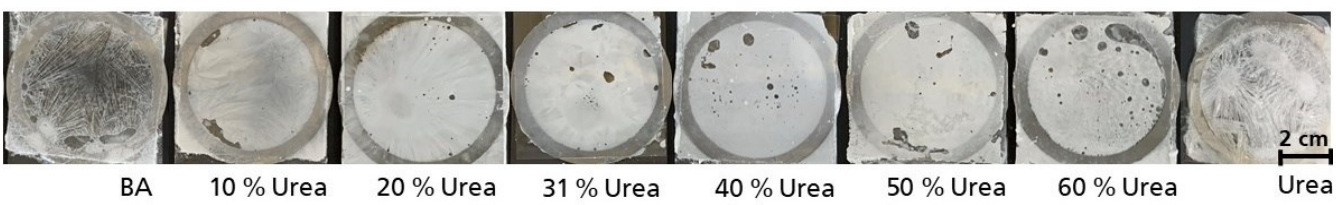

Figure 5.20: Exemplary samples of urea and BA in shim rings with the height of 0.2 mm (e38).

Figure 5.21 shows the determined scattering coefficients of the prepared samples with different compositions of urea and BA. The eutectic mixture with 31 % urea is shown in red for better readability. It is noticeable that the pure substances have a significantly higher scattering coefficient than the mixtures. That means the crystalline structures of the pure substances cause a higher scattering than those of the mixtures. As can be seen from the images of the specimens, BA is colorless, but exhibits strong lamellar crystal growth. Urea also appears much less opaque than the mixtures and a lamellar crystal growth can be observed as well. The opaque blends also show lamellar structures, but these appear to decrease with increasing amounts of urea and are replaced by finer structures. The eutectic composition is indistinguishable from the others and shows no increased scattering behavior.

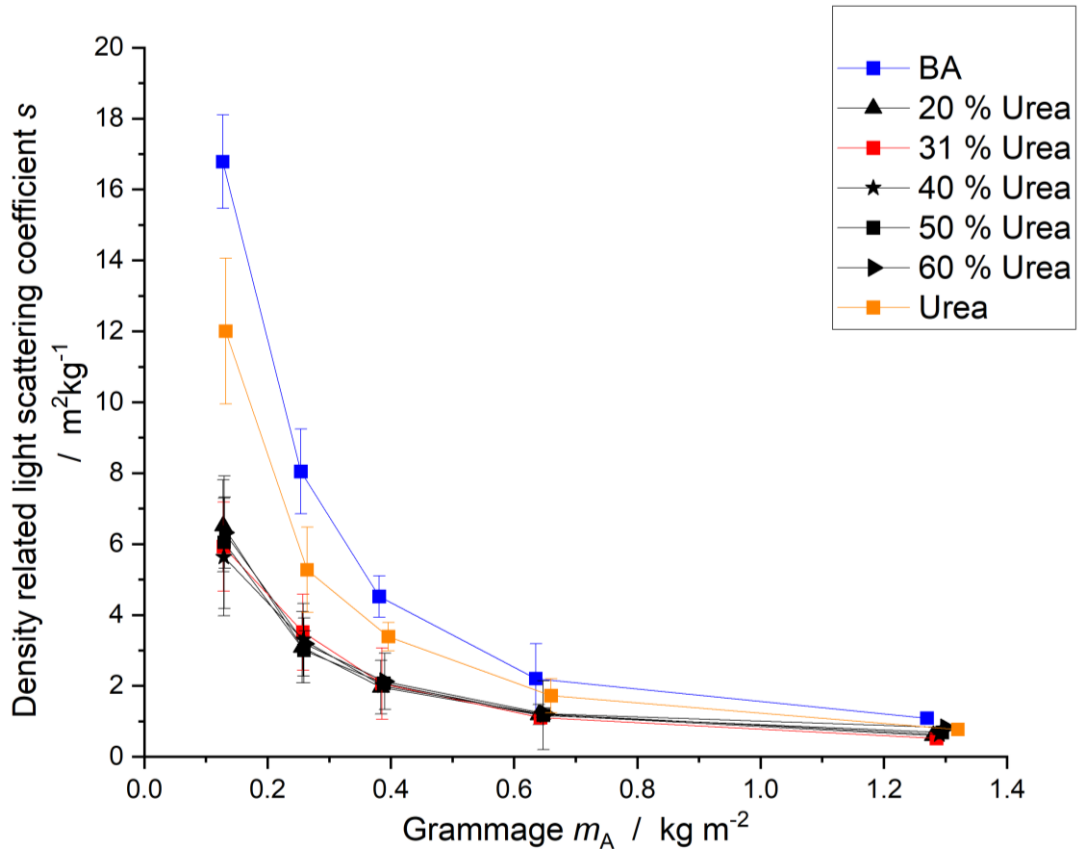

Figure 5.21: Scattering coefficient of samples with urea and benzoic acid (BA) in shim rings depending on the grammage.

The photometer was used to measure the remission, and the expected course of the scattering factors depending on the grammage was obtained. Because the pure compounds behave so differently from the mixtures, this system must be compared with the previous DMO/EC system. This comparison will be covered in the next section.

5.3 Comparison of the Eutectics Dimethyl Oxalate/Ethylcarbazole and Urea/Benzoic Acid

To compare both eutectic systems with their pure substances and different compositions, the scattering factors of selected compositions are plotted in Figure 5.22. Interestingly, the pure substances do not show any major deviations and are in the midfield of the samples. What is clearly different are the mixtures of the two systems.

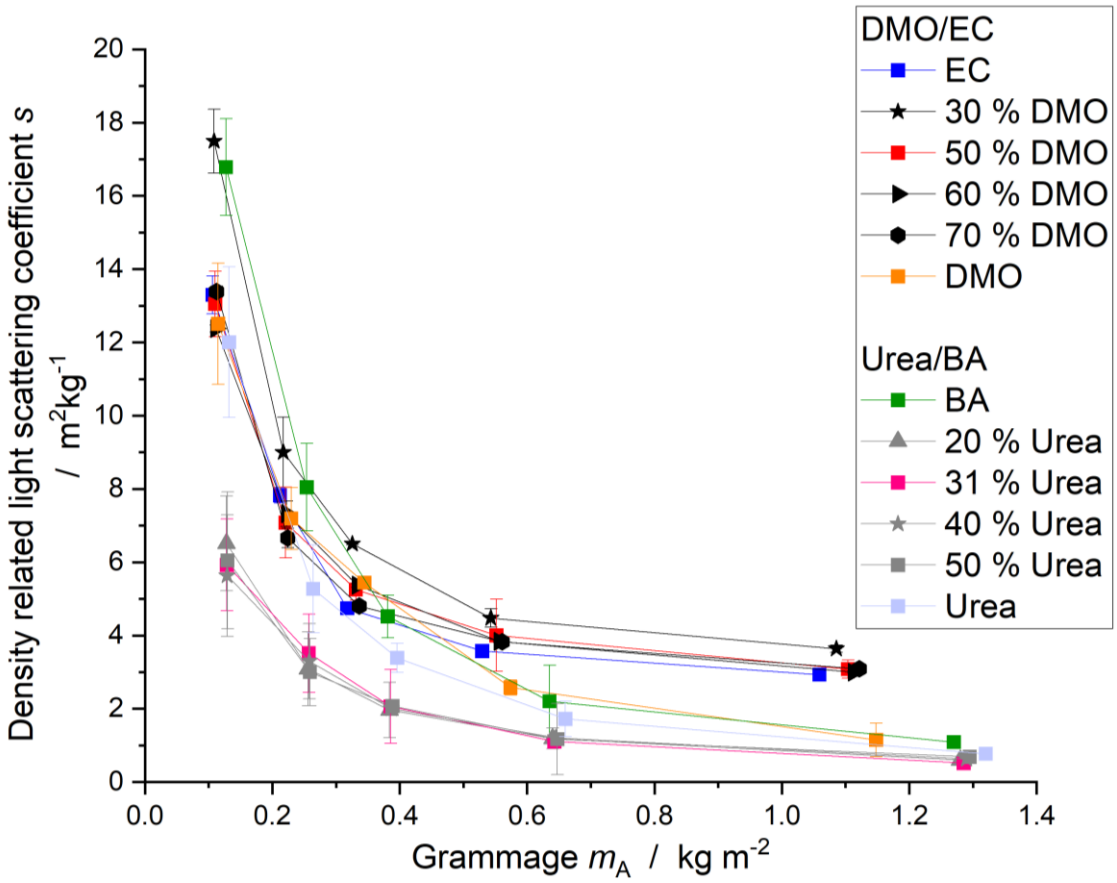

Figure 5.22: Comparison of scattering coefficient of samples with urea and BA, and samples with DMO and EC in shim rings depending on the grammage.

To see this more clearly, the same plot of the scattering coefficients is shown in Figure 5.23 without the pure substances. The big difference in the scattering is in the mixtures. Whereas the urea/BA samples appear much more opaque and fine-grained, the DMO/EC samples show a stronger crystal structure visible to the naked eye. In both systems, no increased scattering effect of the eutectic mixture is found.

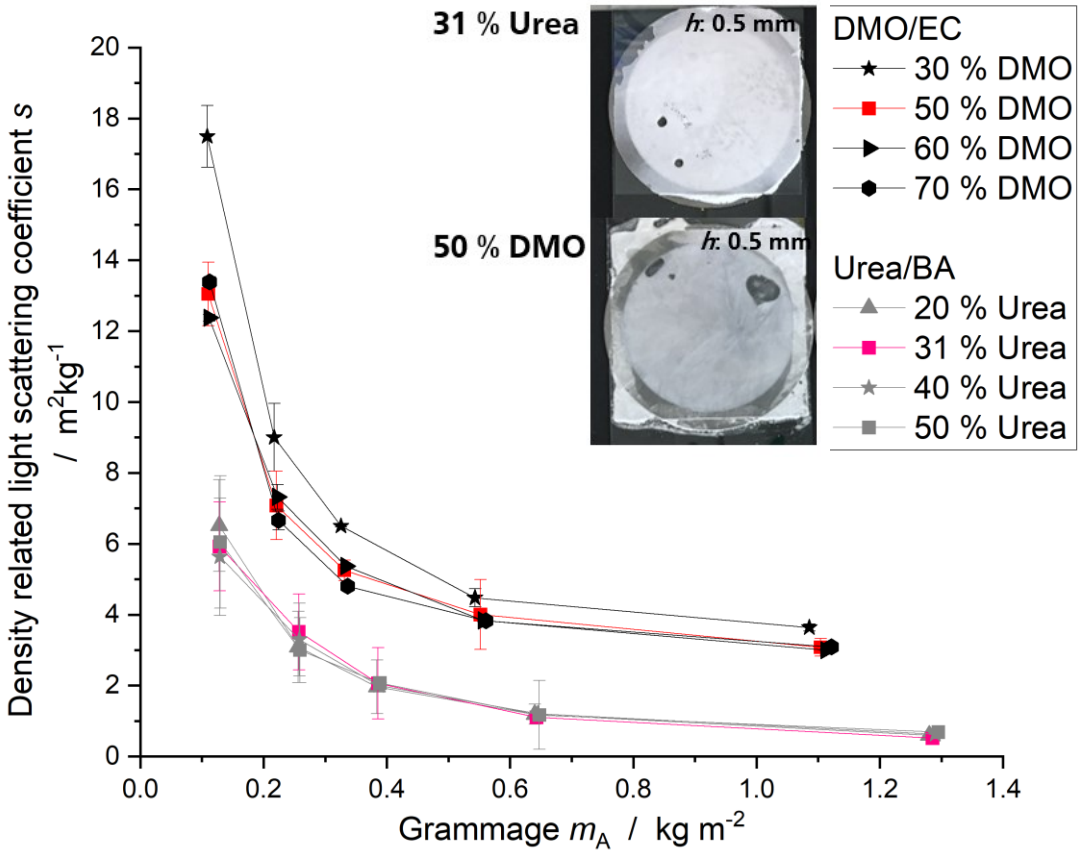

Figure 5.23: Comparison of scattering coefficient of only the mixtures of samples with urea and BA, and samples with DMO and EC in shim rings depending on the grammage.

However, since the measurement uncertainties between the two systems are the same, it is assumed that the different scattering coefficients must depend on the materials and their optical behavior. Table 5.1 shows the refractive indices of the pure components and the difference in refractive index of the substances in the mixtures. While the difference between DMO and EC is 0.195, the difference between urea and EC is only 0.067. Thus, regardless of the mixture, many refractive fluctuations are generated at the crystal-crystal interfaces, causing more scattering.[24]

Table 5.1: Refractive indices of dimethyl oxalate, 9-ethylcarbazole, urea and benzoic acid and the difference of refractive index of the respective substances.

	Dimethyl oxalate	9-Ethylcarbazole	Urea[101]	Benzoic acid[102]
Refractive index n_{D20}	1.45	1.645	1.607	1.540
Δn_{D20}	0.195		0.067	

To verify this, a third mixture of substances, eutectic or regular, with a different Δn_{D20} would have to be measured and evaluated. While these studies are very exciting, the benefit to the development of thermal switching papers is not recognized. Therefore, these studies were not pursued further. A eutectic mixture that was used in coating formulations, is a eutectic of fatty acids. The use of natural waxes as the main component for application in thermal-optical switching papers is novel and in line with the increasing use of natural, bio-based materials in everyday products.

5.4 Eutectic Mixture of Palmitic and Stearic Acid

A eutectic mixture of natural waxes was used to explore the application in thermally switchable papers. The refractive index is not considered further here, since it does not differ much in the range of natural and also synthetic waxes. The system of palmitic (PAc, C_{16}, T_m=64 °C) and stearic acid (SAc, C_{18}, T_m=71 °C) was investigated. The chemical structure of the fatty acids is shown in Figure 5.24. Since literature data are inconsistent on where to find the eutectic composition; 58 % PAc[103], 62 % PAc[104] and 64 % PAc[104] are proposed, own DSC measurements were performed to evaluate the eutectic composition in the same manner as it was used for DMO/EC and urea/BA. The thermograms of SAc, PAc and exemplary mixtures (Figure 5.25) show the steady decrease of the melting temperature until the eutectic mixture is reached. Contrary to literature data, there is no single eutectic point found in one of the mixtures, but rather a wide eutectic range from 40 to 80 % PAc (the resulting phase diagram is shown in Appendix Figure 12.1).

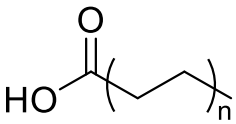

Figure 5.24: Chemical structure of the fatty acids stearic (n=8) and palmitic acid (n=7).

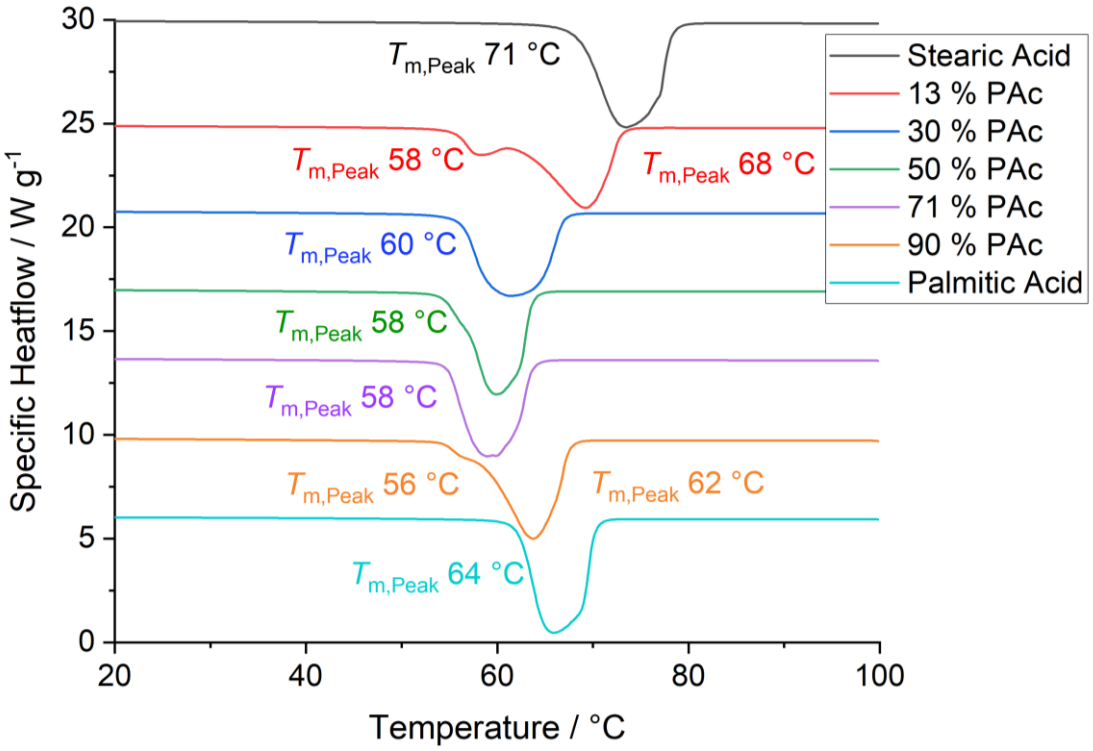

Figure 5.25: DSC thermogram of the pure substances SAc and PAc, as well as example curves with different compositions of their mixtures. The amount of PAc describes the composition of PAc and SAc. The second heating cycle is displayed; the heating as well as the prior heating rate is 10 K min^{-1}.

In order to use fatty acids as a coating on paper, the fatty acid has to be dispersed in aqueous media for health, safety and technical reasons. Therefore, PAc, SAc and mixtures of different compositions have been melt-dispersed together with polyvinyl alcohol (PVA) as emulsifier and binder. The solid content

of the coating formulation is 30 % with 67 % of fatty acid, respectively 33 % of PVA in the dry film. These dispersions were coated on glass slides, covered with a coverslip and pressed to form a film of minimal thickness between the slides (experimental procedure of the dispersions e47, see 8.15). The samples were examined under a microscope with a phase contrast filter. For each composition, one of the test specimens was tempered in an oven at 140 °C for 30 s, to see how the recrystallized structures look like and if they differ from each other. The microscope images are shown in Figure 5.26. The samples that contain the untreated dispersions all look the same, which is in line with expectations. They show a fine-grained structure; the fatty acid particles. The annealed samples show big differences. In the case of pure PAc, as well as in the case of 20 % SAc, formed crystals are visible. In addition, small areas that give the appearance of agglomerated substances (brown spots). These spots are otherwise only observed with pure SAc. The other mixtures, which are eutectic compositions, show no significant change compared to the original samples.

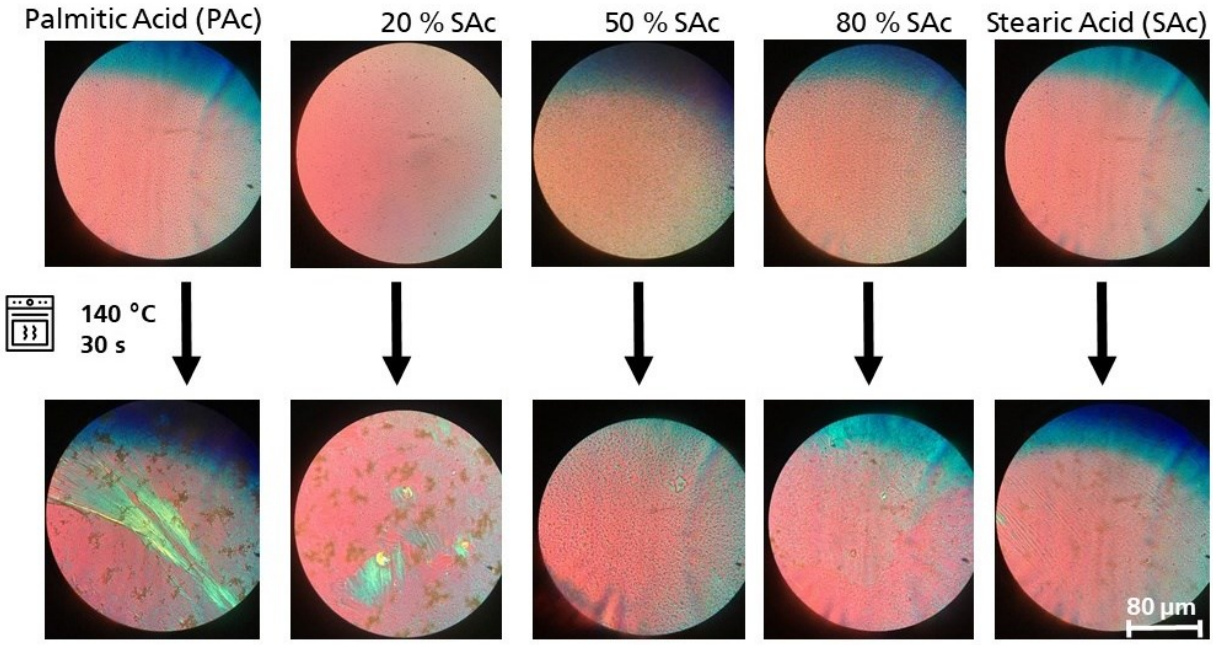

Figure 5.26: Microscope images of samples with melt-dispersed SAc and PAc in PVA. The amount of SAc describes the share of SAc and PAc in the sample. The samples were tempered in the oven at 140 °C for 30 s (below) to see how the fatty acids crystallize (e68).

The strong crystallization effect of the pure palmitic acid dispersion should be considered when applying the coating formulations on foil and paper in the following sections 6.1.3 and 6.2.4. The knowledge gained about eutectic compositions should help in the formulation of coatings in the following chapters. The first step is to use crystalline substances dissolved in organic solvents to see if the structures formed upon evaporation of the solvent are suitable for opaque coatings that can be thermally switched in terms of their optical properties. The second step is to use the eutectic mixtures in aqueous formulations.

6 Film Forming and Characterization of Thermal Switchability

There are several ways to embed crystalline substances in a polymer matrix within a thin coating. The solution behavior, but also the melting temperature, determines in which form and with which solvent the components are present in the formulation for a coating.

For technical applications, aqueous formulations are used almost exclusively for coatings. Since the solvent must evaporate in the drying section of the coating machine after application, it is not advisable to make the formulations from organic solvents for health and safety reasons. Two examples of solvent-based coatings are Neenah Gessner GmbH, which produces methanol-based formulations for specialty papers, and Wacker Chemie AG, which has organic solvent-based release coatings in its product portfolio.[105,106]

For these reasons, the goal of this work is to produce an aqueous formulated coating. However, in order to better understand, the behavior of crystalline substances in polymer matrices, organic solvent coatings will also be investigated. These coatings will be discussed in the following section 6.1.

6.1 Model-Films Prepared on Polymer Foils from Organic Solvents

In this chapter, different waxes are embedded in different polymers, within thin films on model substrates (polymer foil). The polymers are chosen according to their polarities as well as their thermal properties (T_m and/or T_g). The substrate used is a foil out of PET with a thickness of 125 µm and a grammage of 140 g m^{-2}. This transparent and glossy Hostaphan® foil has very good coating properties and is dimensionally stable at the temperatures for thermal switching. It is used to reduce the influence of the substrate on the coating properties, because the surface is smooth and does not absorb the solvent. Paper has an impact on the formation of the coatings due to its inhomogeneous surface and the drying processes due to the capillary effect. In a later section, the coatings are transferred to black paper.

6.1.1 Paraffin Wax Crystallized in Polyvinyl Alcohol and Polystyrene

The idea of using paraffin wax as a crystalline scattering substance was inspired by Zhang *et al.*[47], who embedded paraffin wax in a silicone matrix to create a repositionable film that can be reversibly switched from opaque to transparent. A warning sign or writing under the film becomes visible when the temperature of the surface is above the melting point of the wax. When the surface cools down again, the warning sign becomes invisible again. This sensor material is made of silicone, a thermoset whose cross-linked matrix allows the paraffin wax to melt and recrystallize easily.

For an irreversible function, the matrix itself must be melted or softened during switching so that a rapid solidification of the matrix during cooling fixes the finely distributed wax melt. Therefore, amorphous or semi-crystalline polymers should be used.

The paraffin wax used is a mixture of long-chain alkanes with a melting range of 32 °C to 60 °C. The polymers used are atactic polystyrene (T_g=60 °C) and a partially saponified PVA (T_g=60 °C, T_m=228 °C). The chemical structures of the polymers are shown in Figure 6.1 and the DSC thermograms of the wax and the polymers are shown in Figure 6.2.

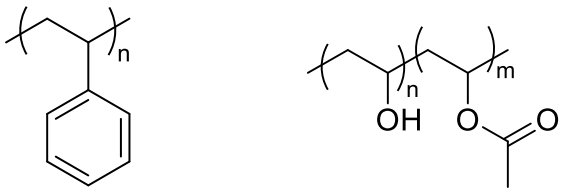

Figure 6.1: Chemical structures of the used polymers as polymeric matrix for paraffin wax. Polystyrene (left) with a M_w of 320 kg mol^{-1} and polyvinyl alcohol (right) with a saponification grade of 88 %.

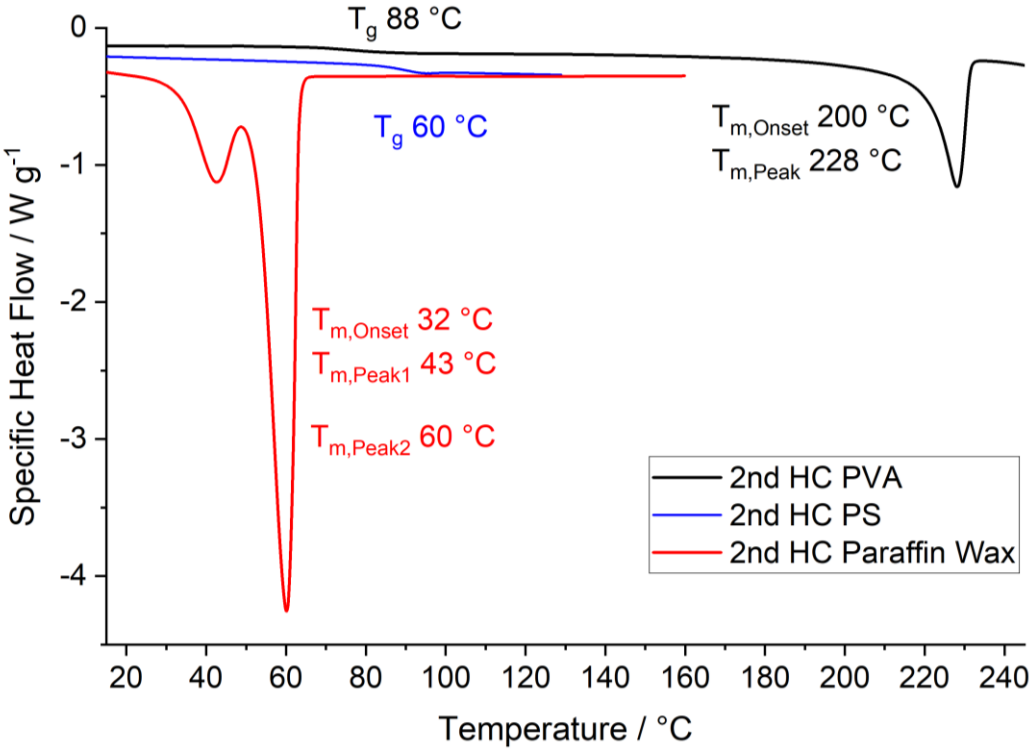

Figure 6.2: DSC thermogram of PS, PVA and paraffin wax. The second heating cycle is displayed; the heating rate as well as the prior cooling rate is 10 K min^{-1}.

To prepare the films out of PVA and paraffin wax, the wax was dissolved in dodecane and the PVA was dissolved in water (experimental procedure e1; see 8.7). The solutions were combined to obtain a solution with a solid content of 12 %. The films were coated on PET foil using a film applicator frame with a gap clearance of 120 µm. The amount of wax in the resulting film is 35 % with a theoretical thickness of 14 µm. Figure 6.3 top left shows the sample with PVA and paraffin wax. The sample shows a good opacity and it has been tempered in an oven at 140 °C for 5 min. There is no visible change, which is supported by the measured optical densities: it shows no significant reduction from 0.45 to 0.44.

The samples with PS were prepared by dissolving PS and paraffin wax in THF and it was coated in the same manner, the theoretical thickness of the sample shown in Figure 6.3 is 14.4 µm with a wax content of 35 % (experimental procedure e6; see 8.13). Switching in the oven leads to an optical change in the film. It irreversibly turns from transparent to more opaque. Therefore, a test series was carried out with different proportions of wax.

Figure 6.4 shows the DSC thermogram of the dried coating formulations of PVA with 35 % wax as well as PS with 35 % wax. The mixture of PVA and wax shows the two melting peaks of the wax which superimposed on the glass transition temperature of the PVA. The PS/wax mixture also shows the two typical melting peaks of the paraffin wax used, but also a T_g of 76 °C. The T_g of the pure PS is 60 °C which means that it has increased by 16 °C. Thus, the movement of the molecular chains are more constrained in the wax that cocrystallizes.

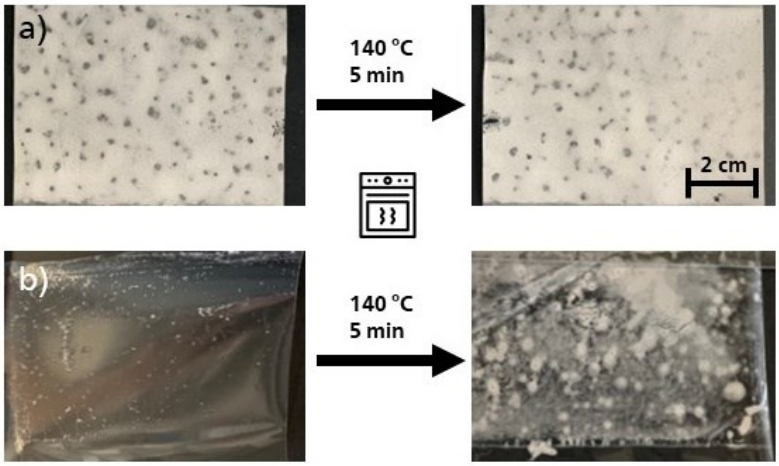

Figure 6.3: paraffin wax in PVA matrix (a, e1) and in PS matrix (b, e9) on the left in the original state and switched in the oven at 140 °C for 5 min. The films were coated on PET foil using a film frame applicator (gap height 120 µm; solid content 12 %).

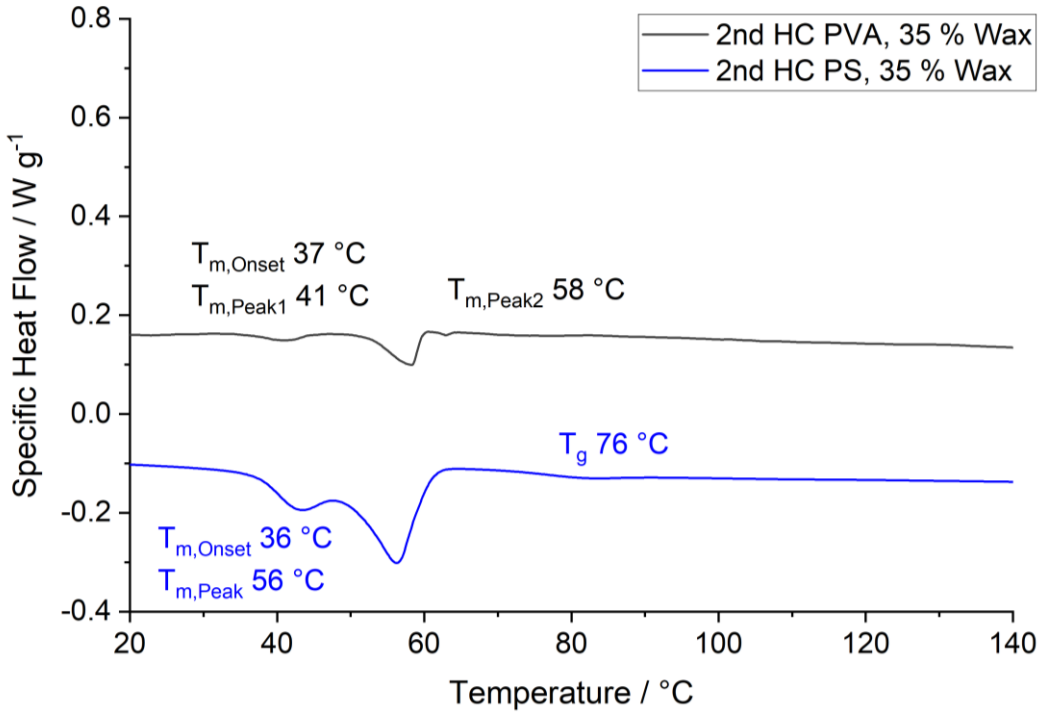

Figure 6.4: DSC thermogram of the coating material in bulk of the samples with PVA and 35 % wax (e1), as well as PS with 35 % wax (e9). The seconds heating cycle is displayed with a heating and prior cooling rate of 10 K min^{-1}.

The PVA and wax films result in highly porous films, as shown in the SEM image in Figure 6.5. This is due to the solvent evaporation protocol that was used to prepare the coating. This was necessary because PVA and wax are polar and non-polar, respectively, and have strongly divergent solution behaviors. The good opacity of the film is caused by the many air voids, resulting from the different evaporation behaviors of the two solvents, dodecane and water. The trapped air causes a strong light scattering due to the difference in refractive indices of the material and air. A similar technique was used by SYURIK *et al.*[27] [11] to recreate a structure similar to a beetles carpace with PMMA and PS.

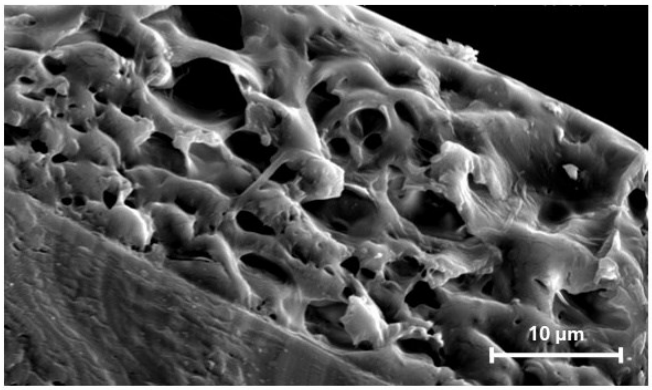

Figure 6.5: SEM image of a cross-section of the sample with PVA and 35 % paraffin wax. A highly porous structure is formed throughout the film.

With this side effect, the scattering effect of the wax cannot be studied. Therefore, only one solvent, THF, is used in the following mixtures (experimental procedure e6, see 8.13).

When preparing the samples with paraffin wax and PS, the amount of wax could not exceed 60 %, because from this point on the mixture solidified directly in the frame gap applicator. The resulting films are displayed in Figure 6.6. In addition, the films did not dry at room temperature and remained sticky and transparent. In Figure 6.7 a SEM image of the surface is displayed. The wax crystals are covered with the polymer and no pores are visible, which is a big difference to the PVA films. After the samples were switched in the oven at 140 °C, they are dry and white spots are formed. At 50 %, the entire surface is covered and an opaque layer is obtained. The optical density of the switched samples was determined to quantify the opacity over a black surface at four random spots. The results are shown in Figure 6.8. As the amount of wax increases, the optical density decreases to 0.61, which would be a fairly good opacity value if it were the other way around.

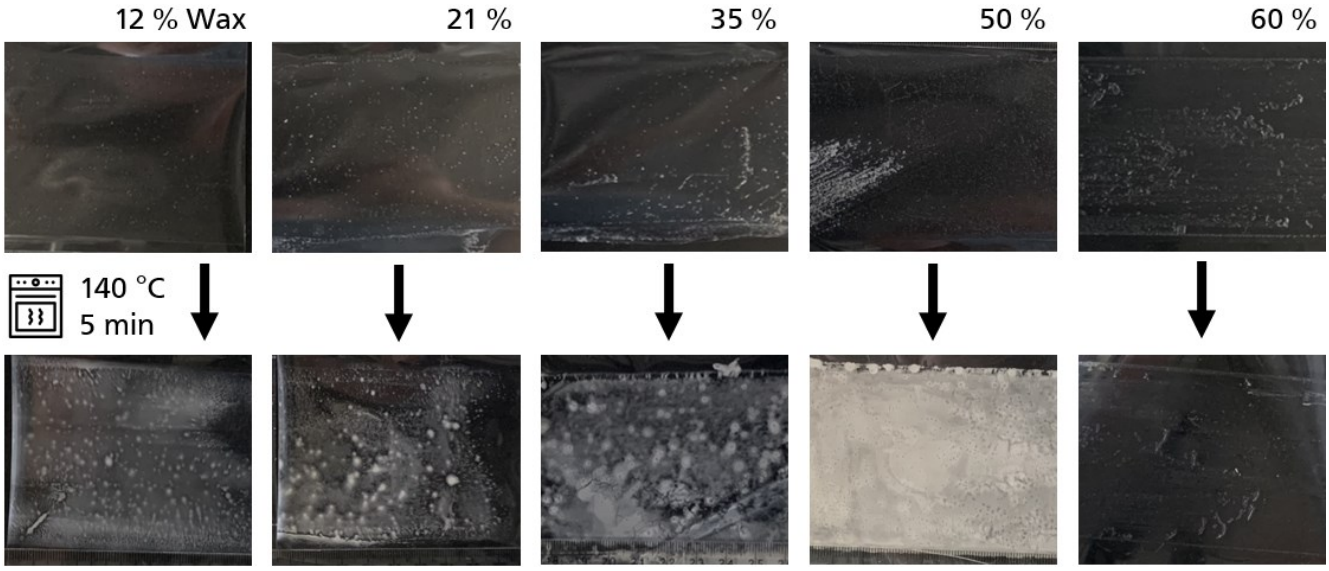

Figure 6.6: Samples with paraffin wax embedded in PS. The films were coated out of THF on PET foil. The original samples are above and the samples that were switched in the oven at 140 °C for 5 min are shown underneath. At 60 % the coating process stopped working because the mixture solidified instantly in the frame applicator (e9).

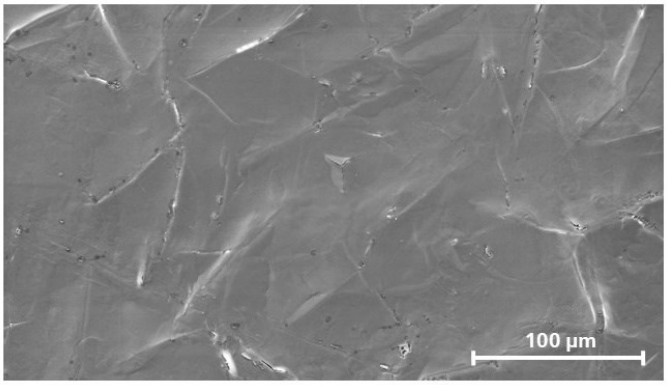

Figure 6.7: SEM images of a sample with 35 % paraffin wax in PS.

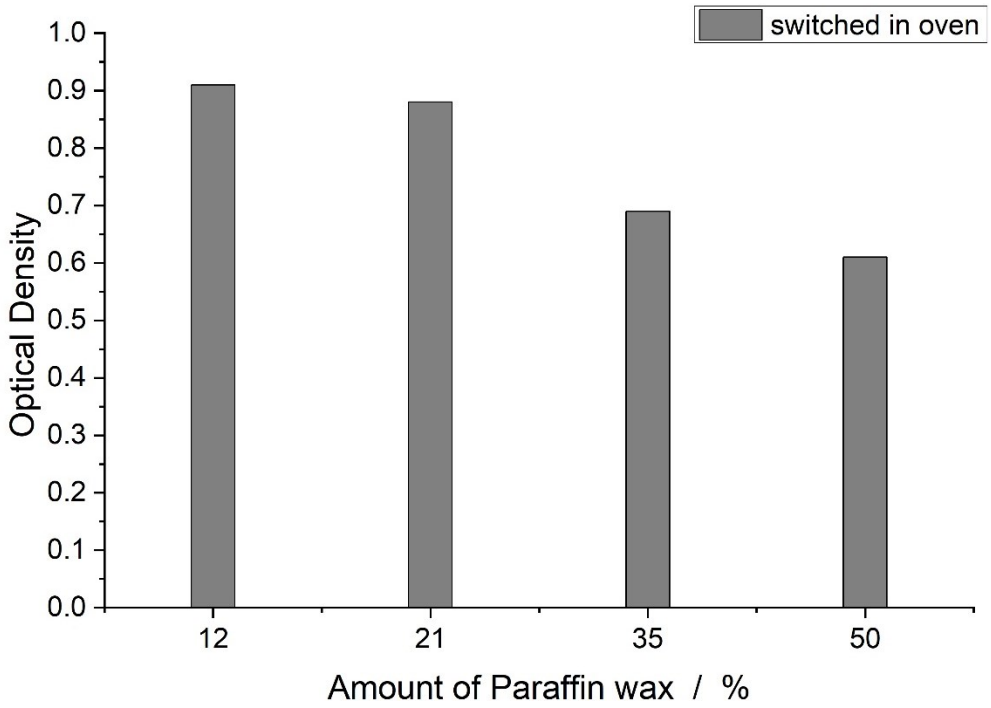

Figure 6.8: Optical density of samples with paraffin wax in PS matrix on PET in switched state (oven; 140 °C, 5 min). The original samples could not be measured since the films did not dry after casting out of THF. The films were coated using a film frame applicator (gap height 120 µm; solid content of coating formulation 12 %).

A comparison between the PVA and PS matrices cannot be made because the preparation has too much influence on the results. The air entrapped in the pores of the wax and PVA films contributes significantly to the opacity. Therefore, no conclusions can be drawn about the interaction between paraffin wax and polymer matrices of different polarities.

6.1.2 Tristearin Crystallized with Amorphous Polymers Coated from Organic Solvent

In this section the natural wax tristearin (TS), or stearin is used as the scattering portion in a polymer matrix to obtain an opaque coating. TS is a triglyceride with three stearic acids and is derived from tallow. Its chemical structure is shown in Figure 6.9. Typically, for triglycerides, TS crystallizes in polymorphs with different melting temperatures. Three possible phases are described in the literature (α, β-prime and β), but only a double melting can be observed in the DSC measurements:

- α phase, T_m = 49 °C
- β phase, T_m = 60 °C
- Literature: α phase 54 °C, β-prime phase 64 to 65 °C, β phase 71 to 73 °C[107,108]

α forms of even acid triglyceride can change directly into the stable β form without passing through the β-prime form.[108] So it is assumed the phases that could be detected via DSC measurements with the used tristearin are the α and β forms.

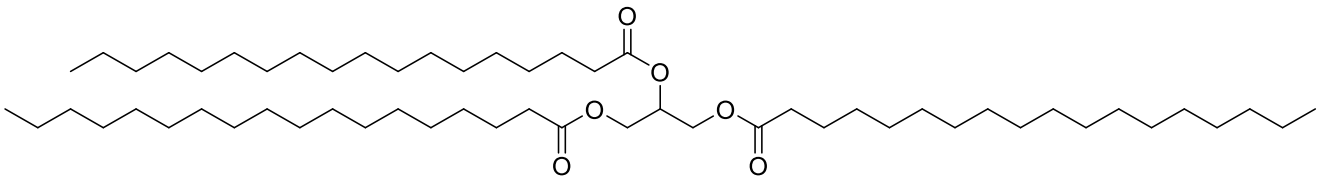

Figure 6.9: Chemical structure of tristearin, a triglyceride with three esterified stearic acids.

a) Introducing Tristearin in Polycaprolactone and Polylactide

For the matrix material polyesters were chosen that not only are amorphous, but are also biodegradable. Polycaprolactone (PCL, Figure 6.10, left) with T_g=-60 °C and T_m= 59 °C and polylactide (PLA, Figure 6.10, right) with T_g=60 °C and T_m=157 °C.

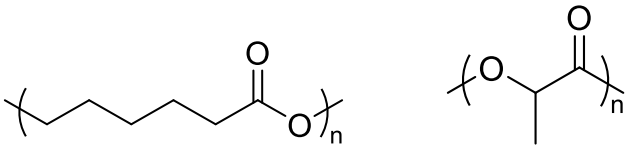

Figure 6.10: Chemical structures of the used polymers: Polycaptrolacton (left) and Polylactide (right).

The DSC thermogram of the polymer materials and a sample of each with 50 % TS is displayed in Figure 6.11. The heating curve of PCL with TS shows the typical two melting peaks of the polymorphous TS and a small melting peak at 61 °C, which belongs to PCL. The heating curve of PLA with TS only shows the melting peaks of TS, the glass transition temperature is superimposed.

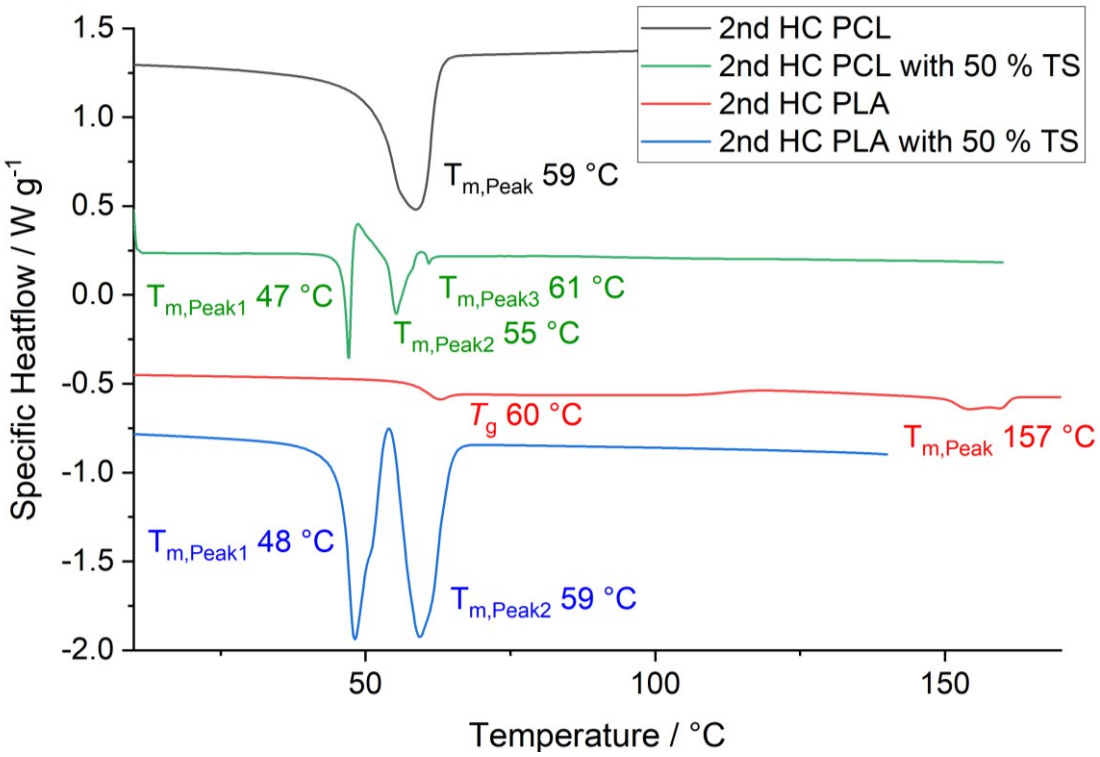

Figure 6.11: DSC thermogram of the PCL, coating material out of PCL and tristearin, PLA as well as the coating material out of PLA and tristearin. The second heating cycles are displayed. The heating rate as well as the prior cooling rate is 10 K min^{-1}.

The sample of PCL with 50 % TS (experimental procedure e10, see 8.9) is shown in Figure 6.12 and it shows the sample in its original and opaque state on the left. PCL and TS were dissolved in THF and coated on PET foil with a film frame applicator with the gap width of 120 µm. This results in a theoretical film thickness of 12 µm (solid content 10 %). The sample was switched in the oven at 140 °C for 5 min and it turned irreversibly transparent (top right). A first attempt at thermal printing was carried out. The result is shown on the lower right.

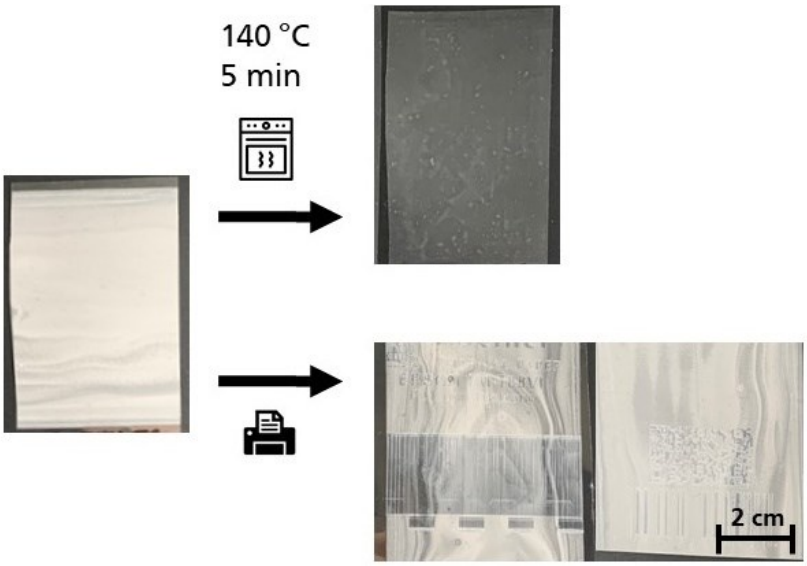

Figure 6.12: Sample of PCL with 50 % TS in the original state (left), switched in the oven (top right) and first attempt of thermoprinting (bottom right)(e10).

The printing was carried out with a standard thermoprinter, but the image is smeared and distorted: the row below the printed horizontal block should show a chessboard pattern. This indicates that the material is sticking to the print head due to the extremely low melting points of the components. To quantify the opacity the optical density was measured. The results are shown in the following graph (Figure 6.13). The OD of the original samples decreases significantly as the amount of TS increases. The OD of the 50 % sample is determined to be 0.48 and is well within the target range. The OD of the switched film is determined to be 1.3, which is also within the target values set by the thermal printing benchmarks. However, the thermoprinted sample clearly shows that the matrix material is too soft during printing. PCL is not only soft, but also liquid at the printing temperatures, being well above its glass transition temperature and melting point. The SEM image (Figure 6.14) shows the TS particles that have formed during evaporation of the solvent. They form spherical shapes that grow into each other to form crescent-shaped structures. In the higher magnification image, the platelet-like crystallized TS can be seen on the larger TS particle in the PCL matrix.

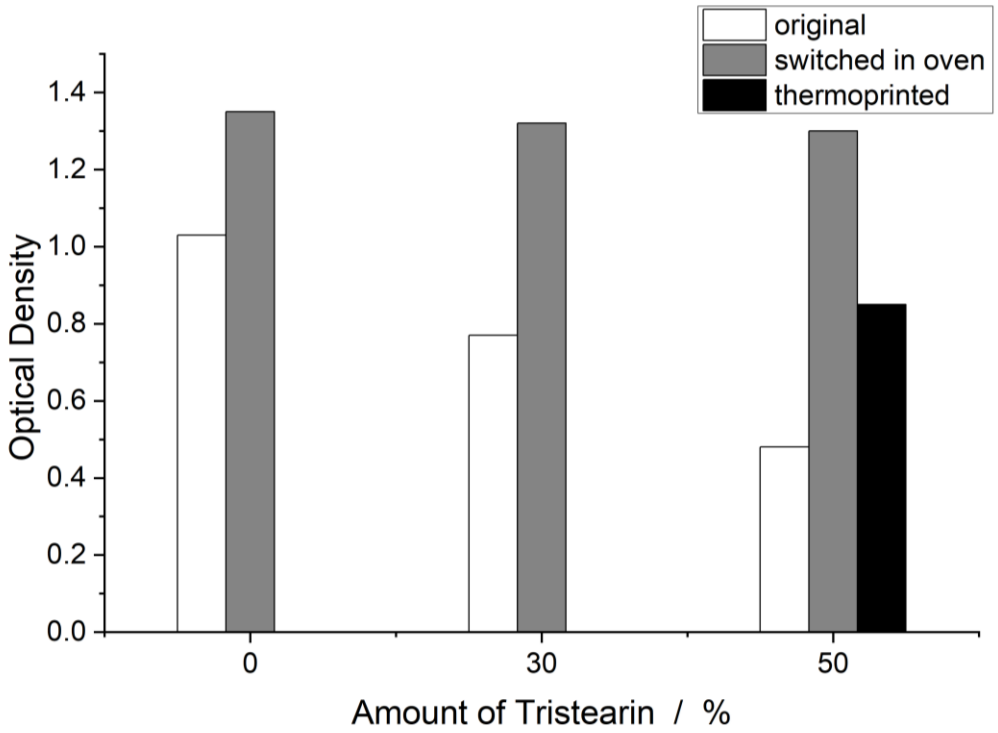

Figure 6.13: Optical Densities of samples out of pure PCL and two different amounts of TS in PCL. Samples were switched in the oven at 140 °C for 5 min. For the sample with 50 % TS, the OD of the thermoprinted samples is displayed.

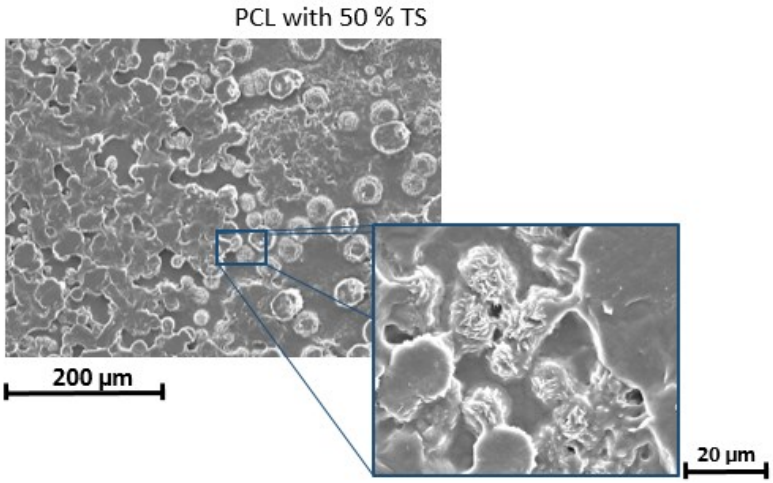

Figure 6.14: SEM image of the sample with 50 % TS in PCL cast out of THF (via film frame applicator).

The advantage of PLA coated together with TS (experimental procedure e31, see 8.8) is, that the switching in the oven (and printing) surpasses its glass transition temperature, whereas the crystalline parts stay solid. The polymer was dissolved in dichloromethane (DCM) together with TS and coated on PET foil using a frame gap applicator with the gap height of 120 µm. Films with various amounts of tristearin are shown in Figure 6.15.

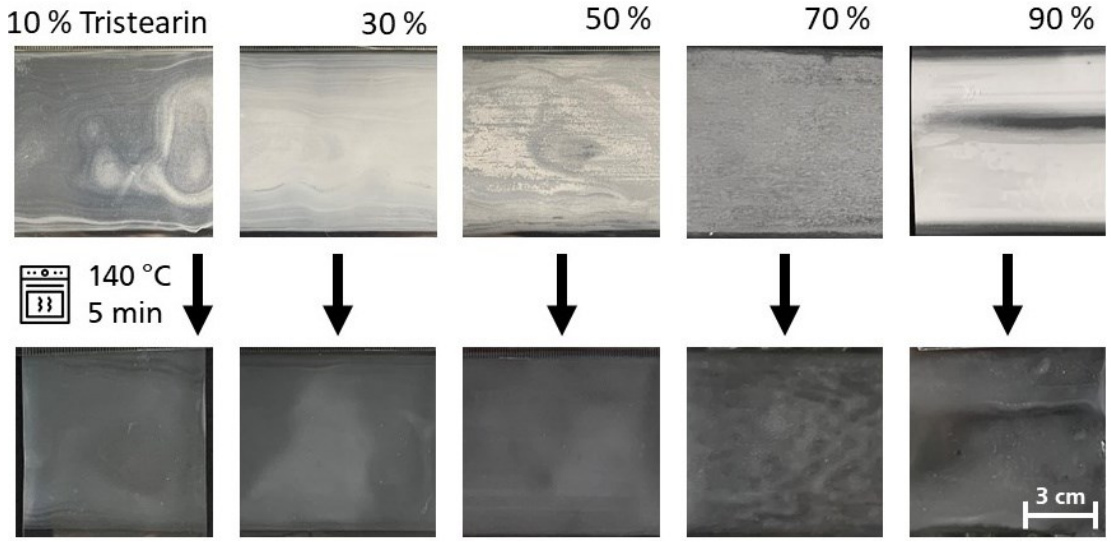

Figure 6.15: Films of PLA with TS cast out of DCM. The original films (upper row) are switched in the oven (bottom row)(e31).

TS crystallizes in typical patterns (ring-like) while DCM evaporates. These inhomogeneous spots can be observed in all films. With an outlier at 80% of TS, the OD measurements (Figure 6.17) show that the OD decreases with increasing TS content, reaching a value of 0.35 at 90 %. However, the values from the switched films show that the films have significant haze. None of the values is greater than 1.4, which is well within the target range. The surface morphology of the 50 % TS sample is shown on the SEM image in Figure 6.16. It was taken from one of the deep white spots and magnified to show the

flower-like structures of TS. Due to the overall porous structure and the structural details that are formed during evaporation of the solvent, the films show a good coverage.

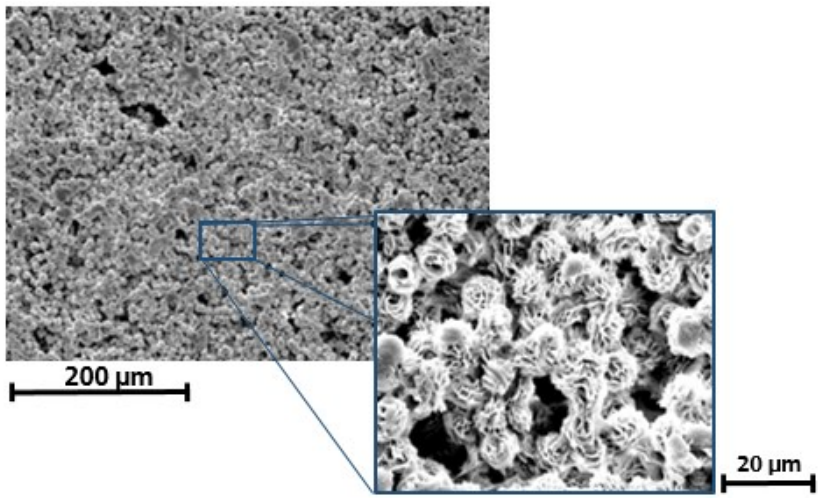

Figure 6.16: SEM image of the sample of PLA and 50 % TS. The magnification on the right shows the flower-like structures of TS that formed during evaporation of DCM.

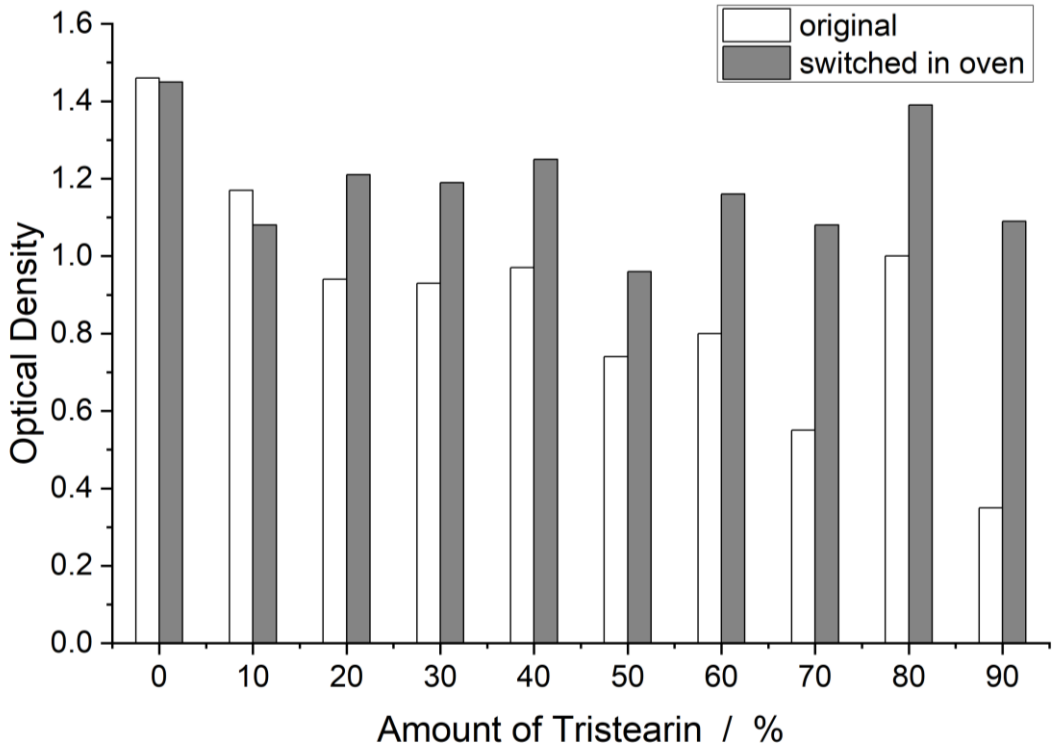

Figure 6.17: Optical densities of samples out of PLA with TS cast out of DMO. The samples were switched in the oven at 140 °C for 5 min.

b) Solvent Cast Films of Tristearin and Polystyrene

Although the coatings with PLA and TS gave some good results, PS will be tested as well to see, if it performs better, similar or worse than PLA. This will lead to a better understanding of the switching behavior of TS. Figure 6.18 shows the DSC thermogram of TS, PS and an exemplary mixture of 35 % TS in PS. The mixture shows the characteristic melting peaks located at almost the same temperatures. The T_g of PS is significantly lowered in the blend with TS: 12 °C compared to the pure PS.

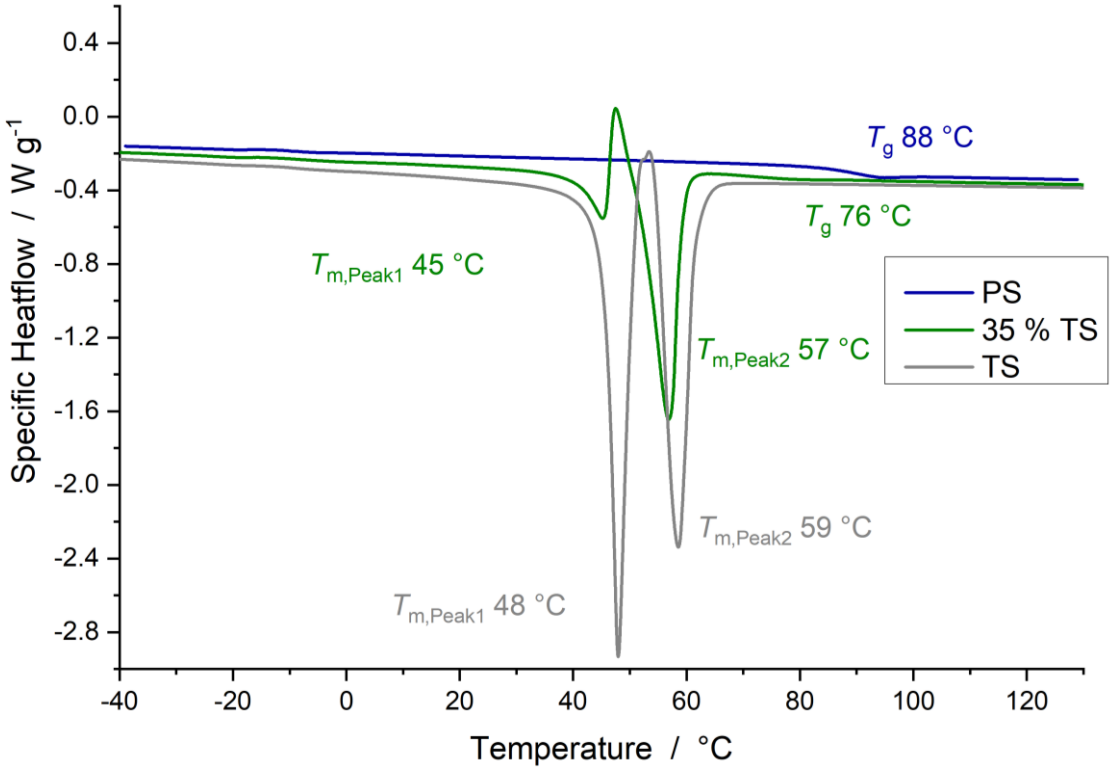

Figure 6.18: DSC thermogram of PS, TS and an exemplary sample with 35 % TS in PS. The second heating cycle is displayed and the heating rate, as well as the prior cooling rate is 10 K min^{-1}.

For the PS and TS system, a phase diagram was constructed to see if the materials have miscibility gaps or other effects at certain compositions. The diagram is shown in Figure 6.19. Melting peaks are evaluated for the melting temperatures of the two modifications of TS. For the plasticization of PS, the T_g is used. The melting temperatures of TS vary only by a few degrees in the compositions. The glass transition temperature of PS varies more, but is so weak above 50 % TS that it cannot be evaluated.

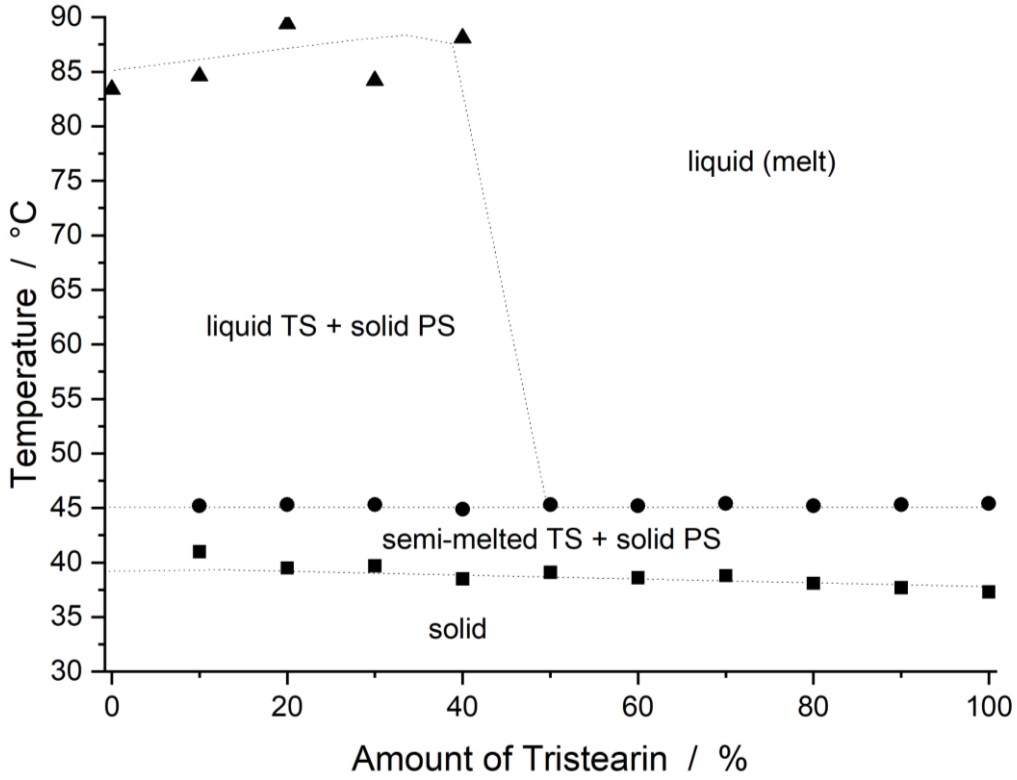

Figure 6.19: Phase diagram of PS and TS based on DSC measurements. The peak melting temperatures of TS and the glass transition temperature of PS is used for evaluation.

The films out of PS and TS were prepared in the same way as the PCL films, but the solutions out of PS, tristearin and THF as well as the film frame applicator (gap width 120 µm) were heated to 60 °C before casting the solutions onto PET foil (experimental procedure e40; 8.10). In this way the material did not solidify directly in the frame applicator at high TS levels. The resulting films are shown in Figure 6.20 (top row). While the pure PS films are completely transparent, the embedded TS, starting at 10 %, leads to a homogeneous film that is not yet opaque, but frosted. The opacity increases with the amount of TS added to the polymer. This is as expected, since TS is the component used to achieve a specific opacity due to an increasing scattering of light. Up to 40 % a homogeneous film is obtained. The surface of the films starts to change at 50 % and the first TS structures start to form on the surface. At 60 % this becomes more pronounced and at 70 % the entire surface is covered by the TS structures that lead to an astonishing opacity of the obtained film. It should be noted that the porosity and brittleness increase drastically from 70 %. These structures are formed by evaporation of the solvent and are destroyed by melting, as shown in the pictures of the switched state (Figure 6.20, bottom row). The switched films show a strong haze that increases with increasing TS content.

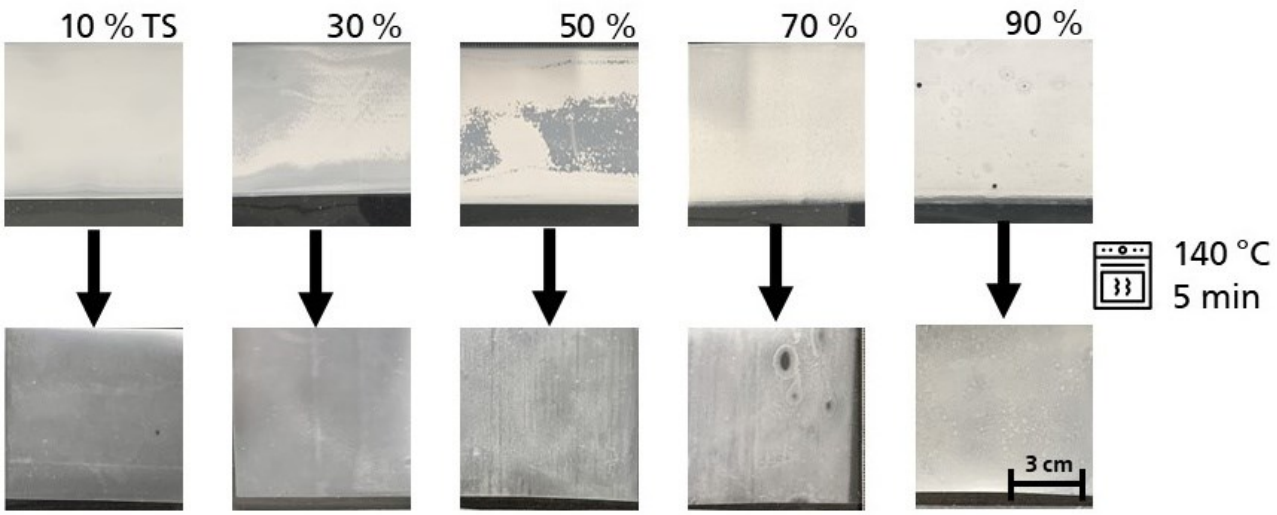

Figure 6.20: Samples of TS in a PS matrix cast out of THF. The original films are on the top and the switched samples (oven, 140 °C for 5 min) are on the bottom. The films were coated via film frame applicator with a gap height of 120 µm (e40).

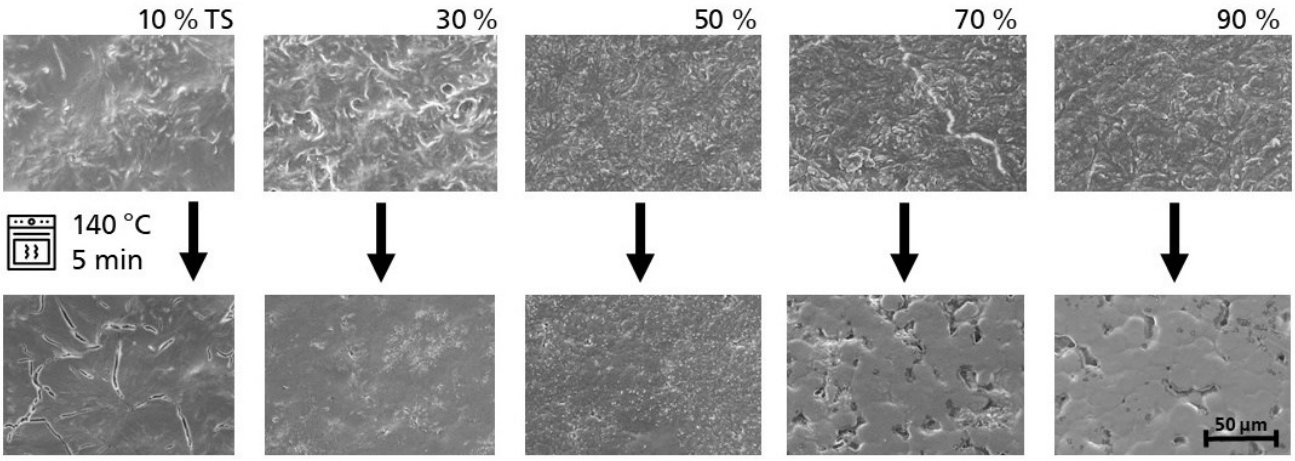

Figure 6.21: SEM images of samples of TS in a PS matrix cast out of THF. The original films are on the top and the switched samples (oven, 140 °C for 5 min) are on the bottom. The films were coated via film frame applicator with a gap height of 120 µm.

The surface structure of the films with different amounts of TS in PS cast from THF can be seen in the SEM images (Figure 6.21). As the amount of TS increases, the surface becomes significantly rougher. Also shown are the surfaces of the films that were switched in the oven. The crystallites previously visible on the surface are no longer visible in the films up to 50 % after annealing and the films appear smoothed. In the films < 50 %, the pores of the coarse tristearin domains are almost closed.

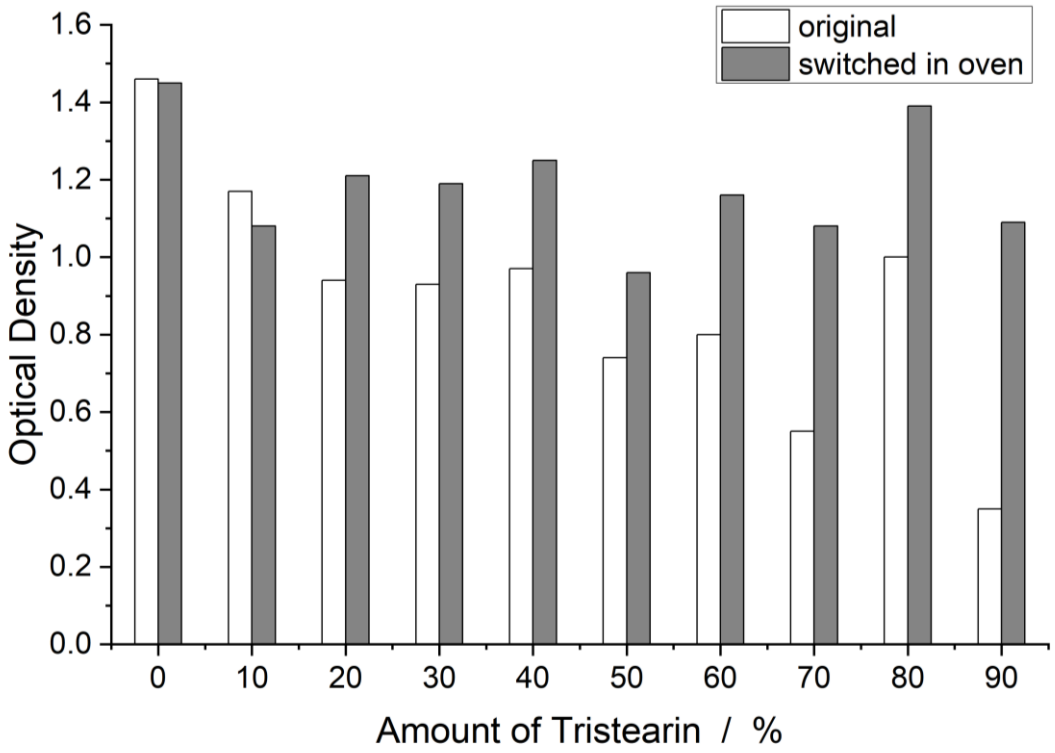

Figure 6.22: Optical densities of the samples out of PS and TS cast out of THF on PET foil in the original and the switched state.

Optical densities were measured to quantify the switching quality of the film. The OD of the non-switched films decreases significantly from 60 % of TS in the coating and drops to < 0.23 at amounts greater than 70 %. The switched samples all show a similar OD around 0.9 to 1.0 which is not within the target values. The difference in OD between the original and switched films increases significantly above 70 %, creating a high contrast that is easily perceived by the human eye.

Compared with the samples out of PLA and TS, the PS/TS coatings have higher opacities, especially at lower amounts of TS. However, the ODs of the switched samples are smaller and in most cases do not exceed 1.0. The optical density measurements together with the sample images lead to the assumption, that the strong opacity is formed by the TS molecules on the surface and not by the molecules dispersed in the polymer matrix itself. Therefore, only films with these TS structures on the surface can exhibit a switching behavior, because heating/switching the films results in mobilization of the matrix and melting of the TS. The wax is dispersed into the matrix and is fixed to form the new matrix with the polymer when the film is rapidly cooled. Therefore, the optical density of the switched state does not depend on the amount of TS in the coating. The amount of TS only affects the formation of the film from the organic solvent and the formation of the specific porous topology that leads to light scattering and hence a remarkable opacity. This is shown schematically in Figure 6.23.

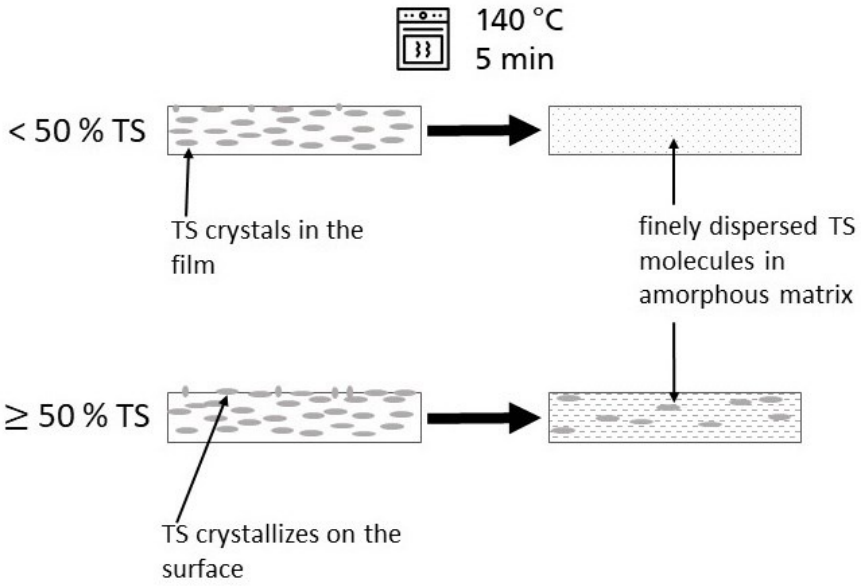

Figure 6.23: Schematic drawing of the crystallization behavior of tristearin in a Polystyrene matrix coated from THF. Amounts greater than 50 % lead to an increasing crystallization on the surface, which leads to structures that increase the opacity of the films.

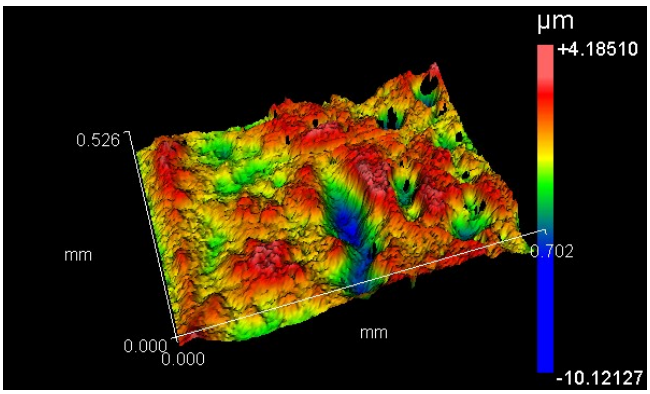

Figure 6.24: Morphology of a sample with 50 % TS in PS. The image was captured using a white light interferometer. The sample was sputtered with gold prior measurements.

The surface morphology of the PS/TS films formed from THF shows interesting structures as can be seen in Figure 6.24 which shows a 3D image of the surface of PS with 50 % TS taken with WLI. It has many pores and forms elevations. This raises the question of how the surface behaves in contact with water. Therefore, the contact angle with water was measured on the films with the different amounts of TS. These are plotted in the following diagram (Figure 6.25). The pure PS film (0 % TS) has a contact angle of 74 ° which corresponds to a moderately hydrophilic surface. The contact angle increases to the hydrophobic range at 108 ° with the addition of 10 % TS and continues to increase with the addition of TS to a local maximum of 129° at 50 % TS. This is due to the addition of the hydrophobic TS. The contact angle then drops to 118° and continues to increase again with the further addition of TS. The reason for the drop is the beginning of the all-over crystallization of the TS on the surface. As the amount of TS increases, the structure becomes coarser, so that the water droplets increasingly stand on the structures. However, superhydrophobicity is not achieved. Pure TS cast from THF has the highest contact angle of

137°. Some of the samples that were switched in the oven at 140 °C were also measured regarding their contact angles, but they do not differ significantly from the untreated films.

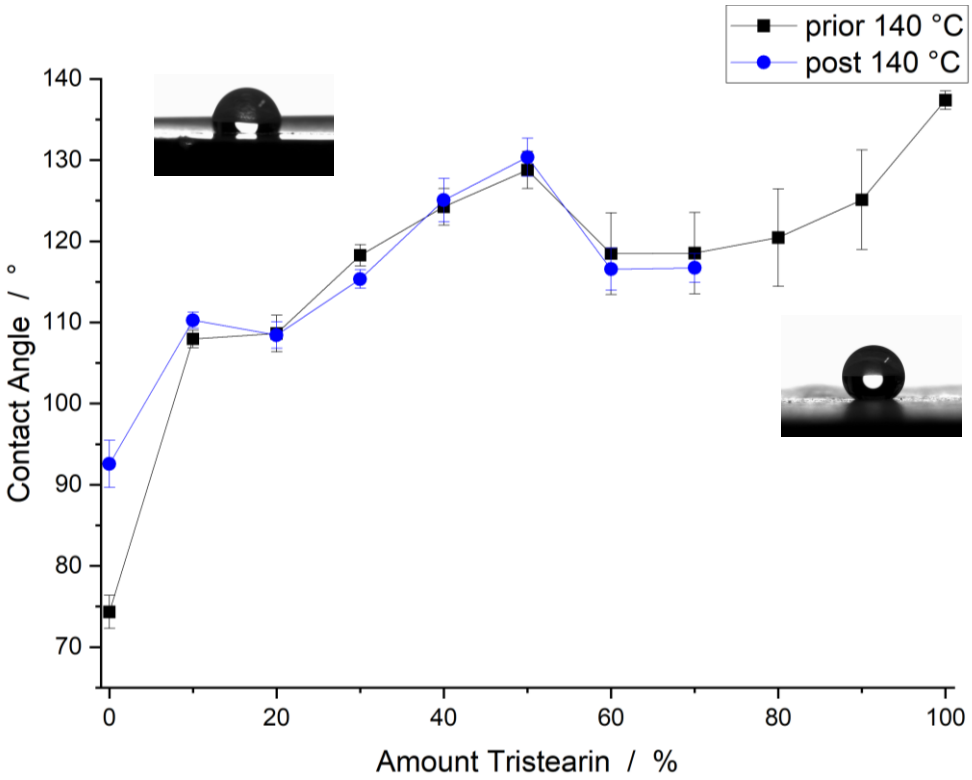

Figure 6.25: Contact angles of the samples of PS and TS out of THF dependent on the composition. The original as well as the switched films were measured. The samples were coated via film frame applicator with a gap height of 120 µm.

As expected, the coating is resistant to water. But how does it react to lipids? This is tested by applying oil droplets to the surface of the coatings and seeing if the black background shows through the droplets or if the opacity remains. For the sake of completeness, water droplets are also deposited. Figure 6.26 shows five of the samples from PS and TS with the oil and water droplets. The results with the water droplets confirm the measured contact angles: the droplets do not penetrate the film and the opacity is maintained. The oil makes the coating transparent. Especially on the parts where there is no surface crystallization of tristearin with amounts of TS < 60 %. The tristearin crystals help to maintain opacity, but the oil slowly sinks into the pores.

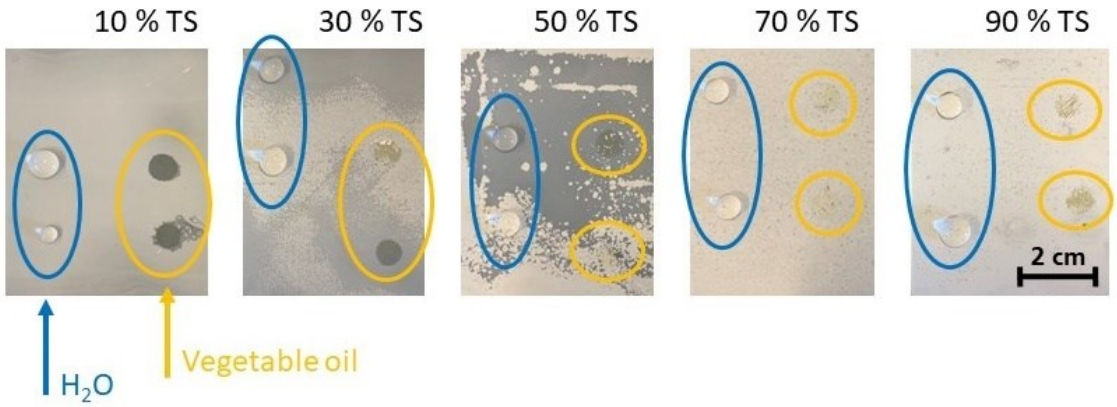

Figure 6.26: Water and oil drops on the samples of PS and TS to see how the coatings and their opacity performs when they come into contact with oil or water. The droplets outlined in blue are water, the ones in yellow are oil. The pictures were taken 5 min after the application.

One idea of how to make porous films that have good opacity, resistant to oil penetration is to seal, or sinter, only the surface. The underlying porosity with the entrapped air must be preserved so that the opacity does not suffer. Various methods have been tested for this surface treatment and the treatments with flash light (VIS), as well as with UV light lead to good results (experimental procedure e70, see 8.11).

For the treatment with visible light (flash light), a *Novacentrix* Pulse Forge 1200, a lab-scale instrument for curing and sintering is used. Parameters used are 400 V (lamp) and 5 pulses at 1 Hz for 1 and 2 ms at a distance of 30 mm from the lamp. Figure 6.27 shows the reference, and the samples treated with flashlight for different pulse times. The films lose opacity with the treatment. The optical density (see Figure 6.29) increases by 0.02 at 1 ms and by 0.05 at 2 ms. This minimizes the opacity, but it is still well within the target range. The most important test, however, is the oil resistance test. In the previous test, the reference showed no penetration into the film because the test period was limited to a few minutes. Here, the films are shown after 4 and 24 hours. The sample treated with 1 ms flash pulses has low oil penetration after 4 hours, but after 24 hours is as high as the untreated sample. On the sample treated with a 2 ms flash pulse, there is no oil penetration into the coating after 4 hours. After 24 hours, the oil droplets show slight penetration into the structure.

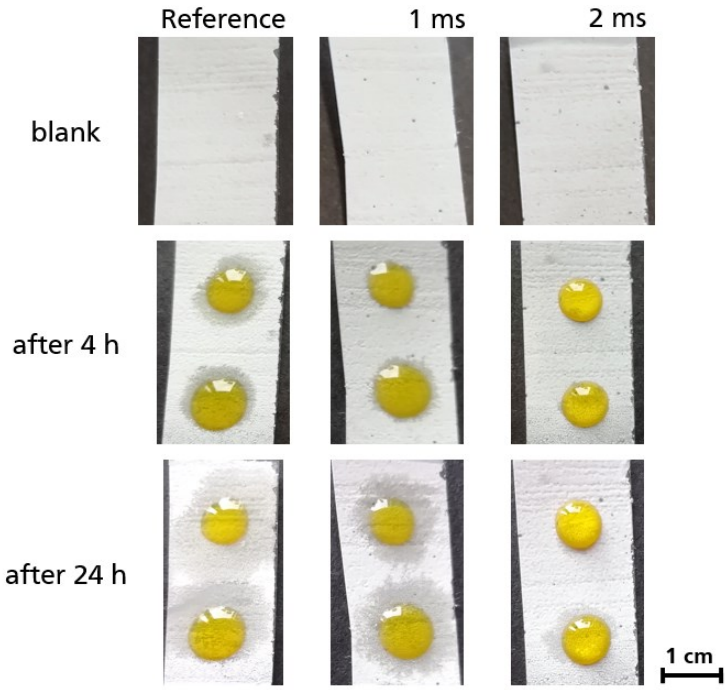

Figure 6.27: Images of the sample out of 80 % TS in PS cast out of THF. The samples were surface treated via flash light for different lengths of time (top row). To see if the treatment has an effect on the resistance against oil, oil droplets were applied on the surface of the films and a picture was taken after 4 h (center row) and after 24 h (bottom row).

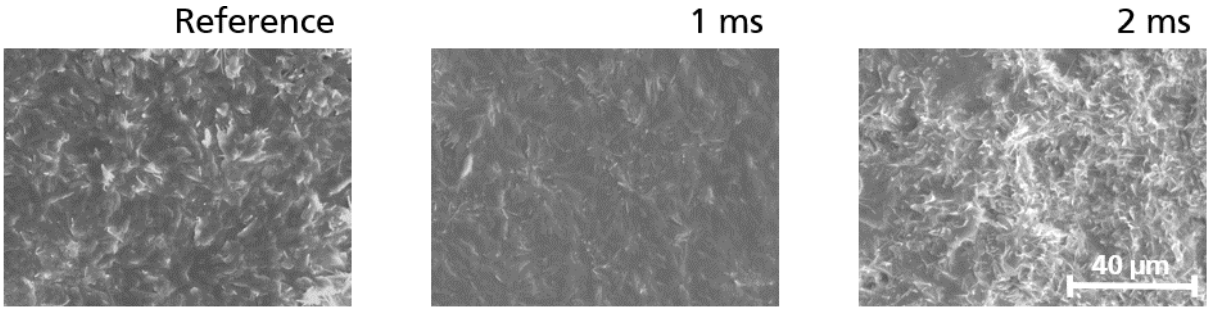

Figure 6.28: SEM-Images of the sample out of 80 % TS in PS cast out of THF. The samples were surface treated via flash light for different lengths of time (1 and 2 ms).

The oil droplet test clearly shows that the surface has been modified and is less susceptible to oil penetration. However, the idea that flash sintering simply closes the surface is not entirely true. The SEM images (Figure 6.28) show that the structures created during the coating process are modified (by the evaporation of the solvent). With 1 ms light pulses, one sees a slightly more homogeneous (sealed) structure with a few TS crystals. With 2 ms light pulses, TS recrystallizes into platelet-like structures. As the films show a much improved oil resistance, the protruding tristearin platelets seem to keep the oil away from the film surface.

Another technique for sintering was tested: treatment with UV light. The samples were placed on the conveyor belt of an *IST Metz* laboratory drying system. The light source is a mercury lamp with a power of 8 kW. Sintering was always performed at full power. The energy applied was controlled by adjusting

the belt speed. The resulting samples with the belt speeds of 25, 20 and 15 m min^{-1} are shown in Figure 6.30.

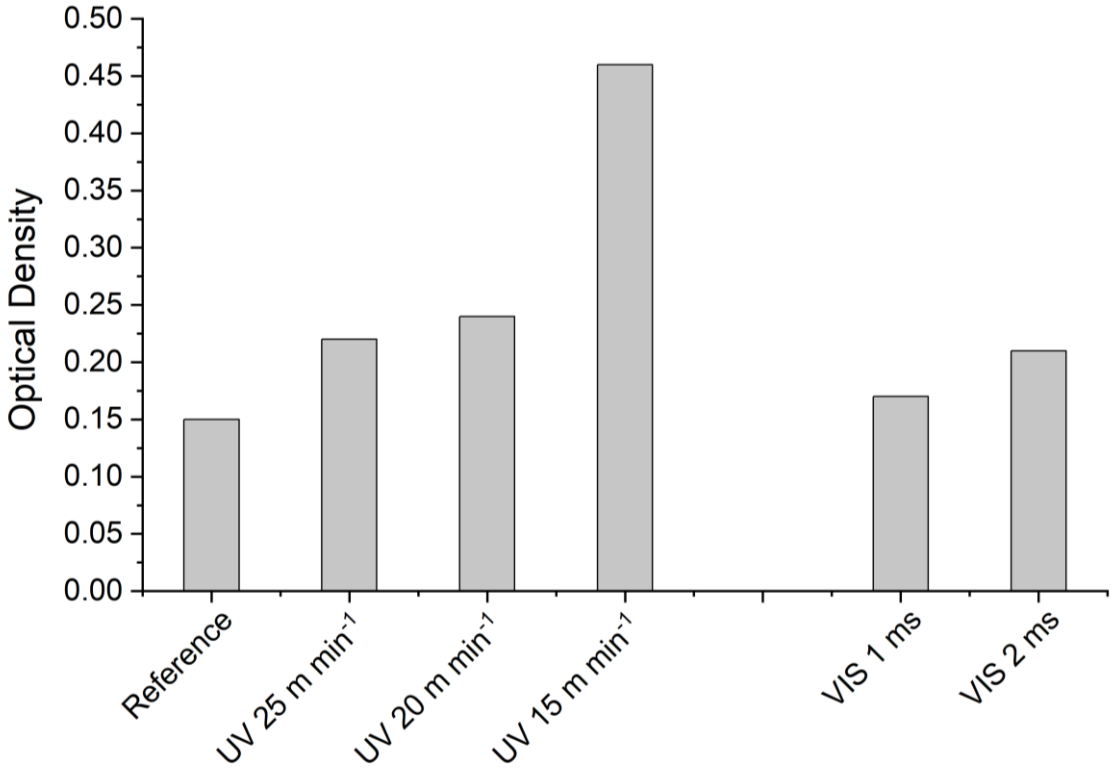

Figure 6.29: Optical density of samples with 80 % TS in PS cast out of THF that underwent a surface treatment to sinter the surface to obtain a better resistance against oil.

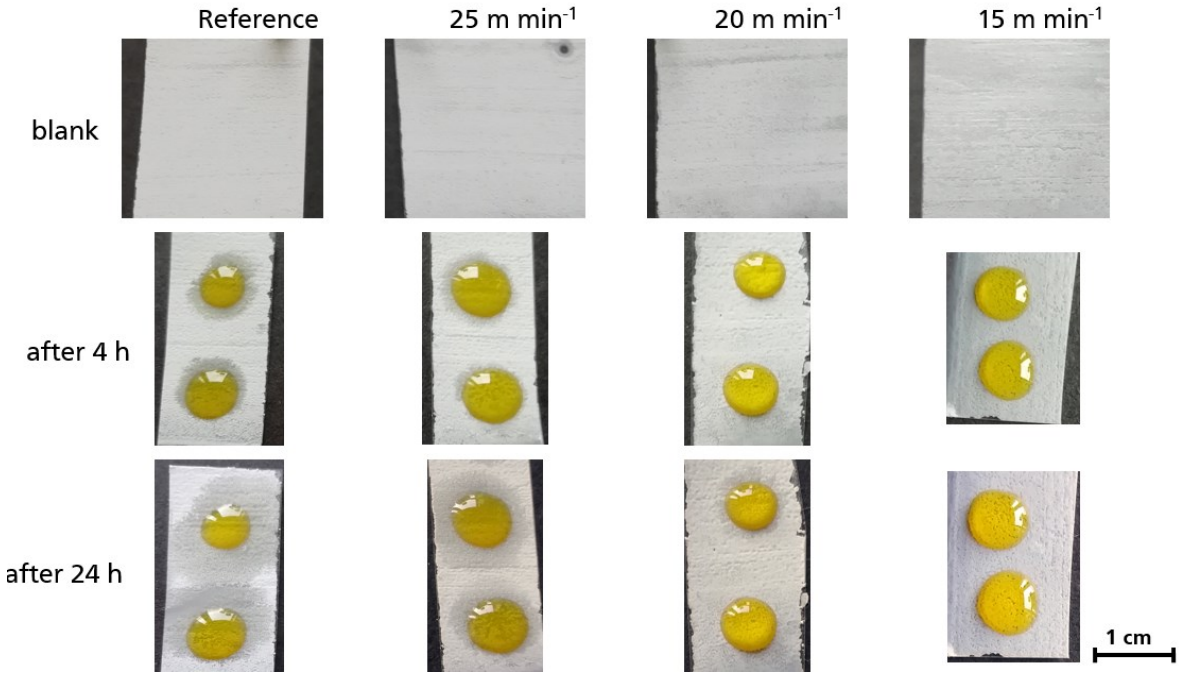

Figure 6.30: Pictures of the samples out of 80 % TS in PS out of THF after surface treatment with a UV-Hg-lamp at different belt speeds which leads to different energy inputs (top row). Below are two pictures of the samples, each with 2 drops of vegetable oil, 4 and 24 hours after application to see, if the oil is penetrating the coating.

As can be seen and measured, the OD of the films increases with slower belt speeds, resulting in higher energy inputs. But in the images with the oil droplets, the improvement in oil resistance can be observed: while the reference sample has already clearly absorbed the oil after 4 hours, the sample with the fastest belt speed shows that significantly less oil has penetrated into the structure after 4 hours, but just as much after 24 hours. At 20 m min^{-1}, only a slight penetration can be observed in the upper oil droplet after 24 hours. The oil resistance is even better at the slowest belt speed of 15 m min^{-1}, but the opacity is significantly worse. The OD (Figure 6.29) of the samples with 25 m min^{-1} and 20 m min^{-1} increase slightly to 0.25 which is still within the target range. However, at 15 m min^{-1} the OD increases to 0.47, which is not acceptable. Therefore, the optimum of good opacity and good resistance to oil can be obtained by using UV light at a belt speed of 20 m min^{-1}.

The SEM images of the films treated with UV light show the same effect as those treated with flashlight: as the amount of energy acting on the surface increases, TS crystallizes in the form of platelets and threads. This prevents the oil from coming into contact with the film surface. This effect is shown schematically in Figure 6.32 to illustrate the proposed process of oil penetration with the original and surface-treated samples.

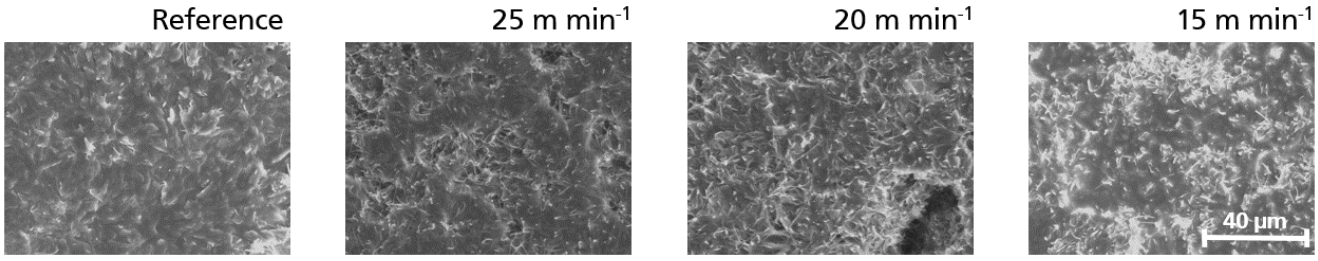

Figure 6.31: SEM images of the samples out of 80 % TS in PS out of THF after the surface treatment with UV light (200 W cm^{-1}) at different belt speeds which lead to different energy inputs.

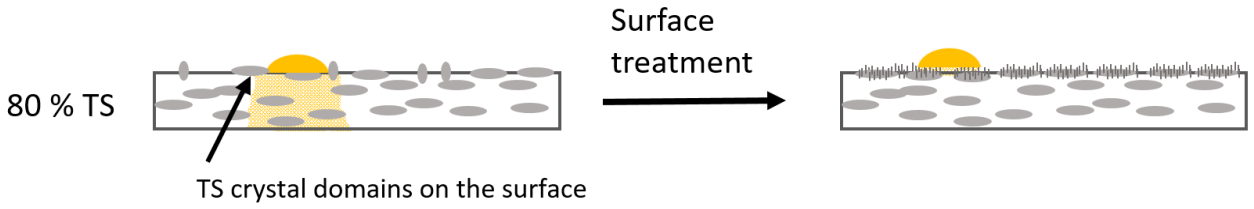

Figure 6.32: Schematically drawn proposed process for surface treatment with UV or flashlight. The resistance against the oil is proposed to come from the formation of platelet-like TS crystals that keep the oil away from the surface.

In summary, both PS and TS are soluble in THF and can be coated as an organic solvent formulation. The resulting films are thermally switchable, with an area-wide clustering of TS on the surface above 50 %, which significantly enhances the switching behavior. This is clearly seen in the contrast of the optical densities. The hydrophobicity of the films increases with increasing TS content, which is due on the one hand to the hydrophobic TS and on the other hand to the surface morphology, which becomes rougher and more inhomogeneous with increasing TS content. Thus, two factors play into the contact angle, which is why the contact angle decreases from 50 % TS content, but then increases again.

However, the measurement uncertainty also increases, since the information about the inhomogeneity of the surface structure is included. This can be well observed in the SEM and the 3D images.

6.1.3 Solvent Cast Films of Fatty Acids and Polystyrene

After the first interesting results with TS, we turned our attention to a simple fatty acid as a component of the switchable coating. In this way, the difference to the sterically more challenging and larger molecule TS will be investigated. The fatty acids used will be stearic acid (SAc), the fatty acid that is esterified in tristearin, and behenic acid (BAc). Due to its longer chain length of C_{22}, Bac has a higher melting point at 80 °C than SAc at 71 °C (C_{18}). The melting points were determined via DSC. The films are coated from THF with a film frame applicator with the gap height of 120 µm on PET foil. The resulting samples are displayed in Figure 6.33 (experimental procedure e9, see 8.12).

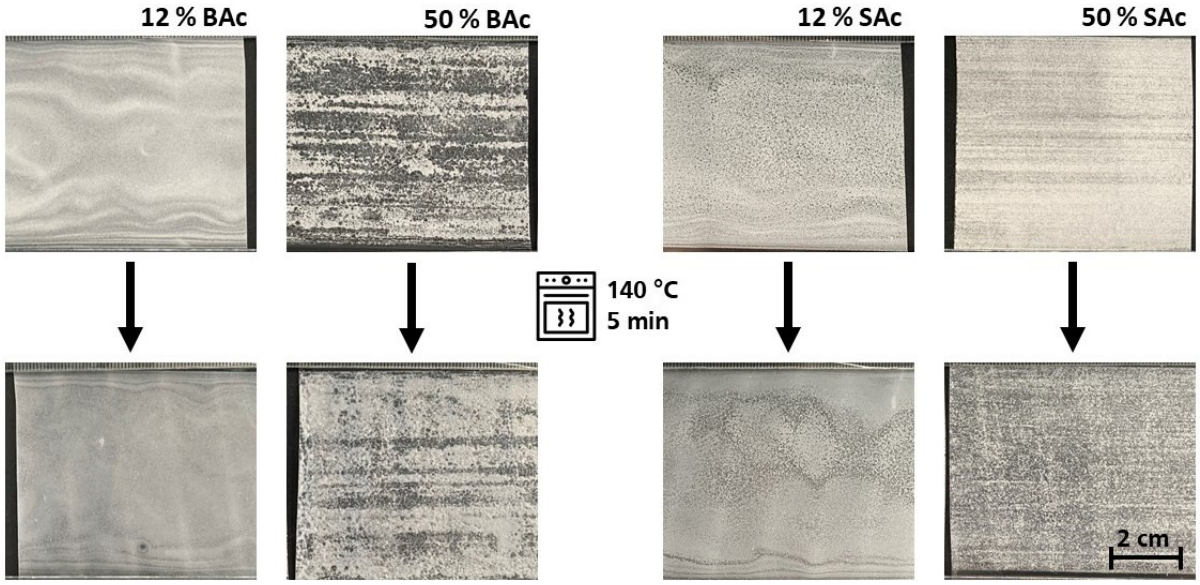

Figure 6.33: Pictures of the samples with PS and BAc (left) and samples with PS and SAc (right). The original samples are in the top row and the samples that were switched in the oven are in the bottom row. The films were coated via film frame applicator with a gap height of 120 µm (e9).

The fatty acids form opaque films, but especially at 50% BAc, a very strong agglomeration of the acid on the surface is observed. As a result, the film becomes very coarse and the opacity is significantly reduced. The films with BAc have a coarser structure than those with SAc and it seems that BAc has a greater tendency to form agglomerates. The experiments carried out have not been able to explain this phenomenon. The coarser structure can also be seen in the SEM image (Figure 6.34). However, the films do not show a good switching behavior at 140 °C in the oven. This contradicts the experience with TS: although TS is much more sterically challenging, the films show a distinct switching behavior, i.e. the molecules are mobile in the polymer matrix during thermal switching. This suggests that polarity, i.e. compatibility or miscibility with the matrix, plays a role. TS is miscible in the plasticized state of PS and

can be finely dispersed, whereas the polar fatty acids do not disperse and remain in their original shape and form. The domains are not altered as the miscibility of fatty acid and PS is not given.

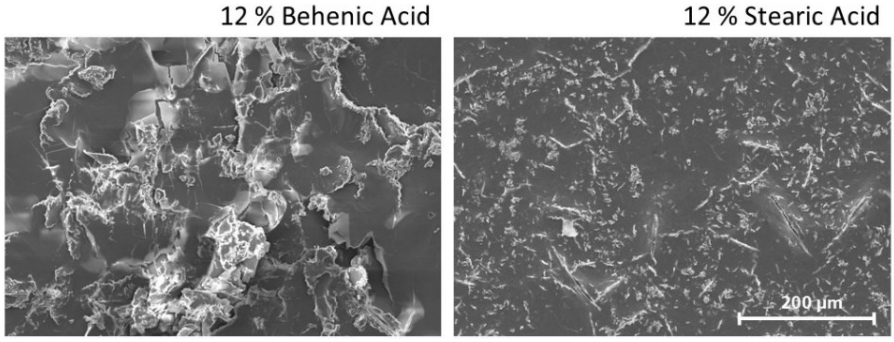

Figure 6.34: SEM image of the surfaces of a sample of PS with 12 % BAc (left) and PS with 12 % SAc (right). The films were coated via film frame applicator with a gap height of 120 µm.

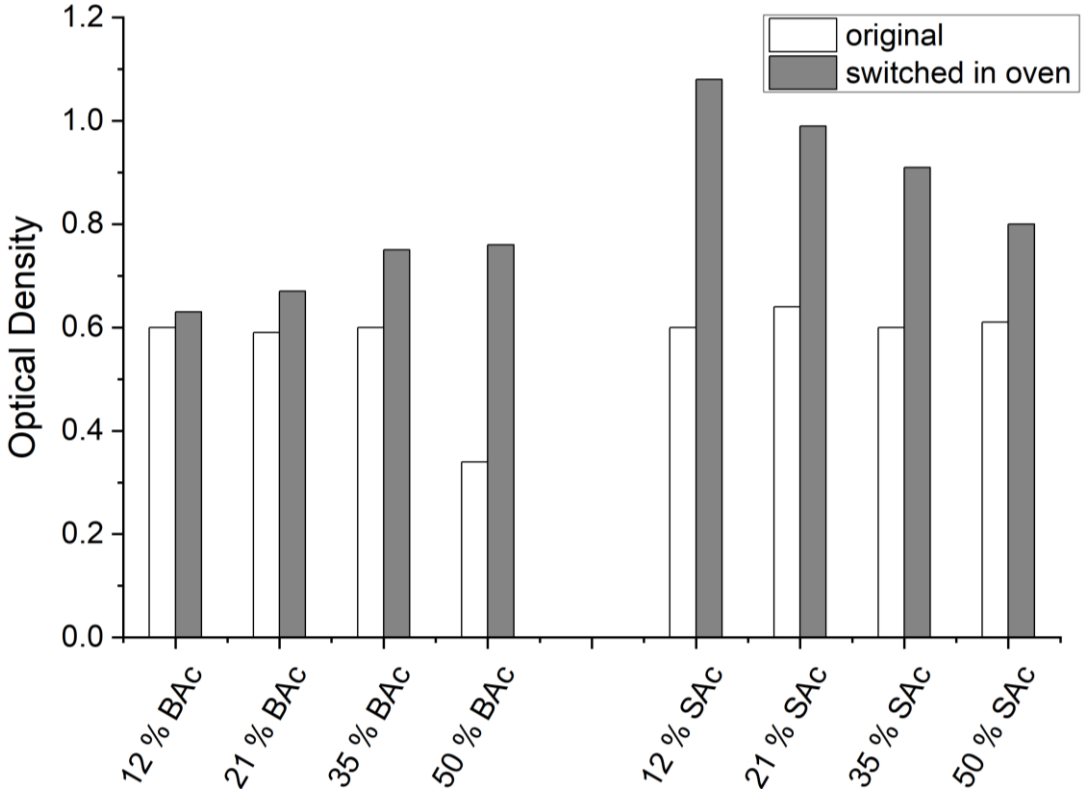

Figure 6.35: Optical densities of the samples with BAc with PS, as well as SAc with PS cast out of THF in the original state and after they have been tempered in the oven at 140 °C for 5 min. The films were coated via film frame applicator with a gap height of 120 µm.

The optical density measurements support the observation of the lack of optical switching of the films with BAc. Only the coating with 50 % BAc shows a larger difference in optical density. However, the value for the original film is significantly lower than the other mixtures due to the large agglomerates, although a better coverage is not given. The optical density value of the films of PS and SAc is not influenced by the amount of SAc in the films. At any concentration, there is a crystallization of SAc on the surface, which is the main contributor to the light scattering and thus to the opacity. The values for

the switched films do not meet the expectations, since they become only minimally more transparent to the naked eye, but the measured contrast between the original and the switched films is very high, up to Δ OD 0.5. This may be due to recrystallization of SAc, which has a different structure when crystallized from solvent than when crystallized by cooling. However, no explanation can be found as to why the measurements show greater contrast than the eye.

6.1.4 Coatings from Organic Solvent - Comparison and Conclusion

TS shows the best optical properties in the original state as well as in the switched state with PS cast from THF. A series of tests were carried out with these samples and, by sintering the surface, it was also possible to obtain good oil resistance while maintaining the same opacity. Although PS and TS films show good results, the formulation needs to be changed to a water-based one. This will be discussed in the next section.

Compared to TS, no strong change in opacity is detectable with fatty acid films do not show a strong change in opacity when the films are switched in the oven. This may be due to the compatibility of the crystalline substance with the matrix material: TS as a non-polar substance is probably better suited for a non-polar PS matrix.

Nevertheless, processing in organic solvents is not effective and the transfer to aqueous systems is necessary. For the natural and synthetic waxes melt dispersion is a good technique to obtain particles that can be processed in aqueous media. In addition, the particle size contributes to the scattering effect, which is extinguished when the particles are destroyed and lose their shape by melting. This makes them promising materials for an irreversible, thermally switchable coating.

Coatings prepared by dissolving the components in organic solvents have the major disadvantage that the optical effect of crystal formation from the solvent as opposed to cooling does not have a large effect on the scattering of light. When a coating performed well, it was always because of a change in shape, e.g. TS crystallizing on the surface versus crystallizing in the matrix.

6.2 Film Formation from Aqueous Dispersion on Model Film

This section covers the step of formulating waterbased coatings. A binder is almost always needed, which in this work is polyvinyl alcohol. PVA also acts as a stabilizer for the dispersions. The polymer matrix can consist of the binder used, PVA, but it can also consist of another water soluble polymer or of polymer particles that are present in the unswitched film in particular shape and are melted during switching. Both concepts were investigated. The polymer particle studied is PS, obtained from emulsion polymerization. In addition, wax particle dispersions in binders will be tested. The waxes used are the already known paraffin wax, TS and fatty acids. The eutectic systems from Chapter 5 were also used in binders to test if these blends will perform in a coating and if they can be thermally switched in their optical properties. The binder used in all formulations is Kuraray Poval® 8-88, a partially saponified PVA.

6.2.1 Films out of Eutectic Crystalline Mixtures and Polyvinyl Alcohol

The mixtures of crystalline substances DMO and EC were studied in Chapter 5.1. They form a eutectic composition at 50 % DMO and 50 % EC. The purpose of this section is to investigate whether the eutectic mixture in a formulation has an advantage over the pure substances or other compositions in terms of thermal switching behavior. When formulating an aqueous coating with the substances, it is important to note that DMO is water-soluble, but EC is not. The mixtures of DMO and EC are melted and after cooling thoroughly mortared. The mixtures or pure substances are then added to an aqueous PVA solution and mixed in a speed mixer. The DMO component dissolves, whereas the EC is dispersed in the coating formulation. Subsequently, the coatings with a solid content of 38 % are applied to PET film by means of a film frame applicator (gap height 120 µm). The resulting coatings in the original and switched states are shown in Figure 6.36 (experimental procedure e43, see 8.14)

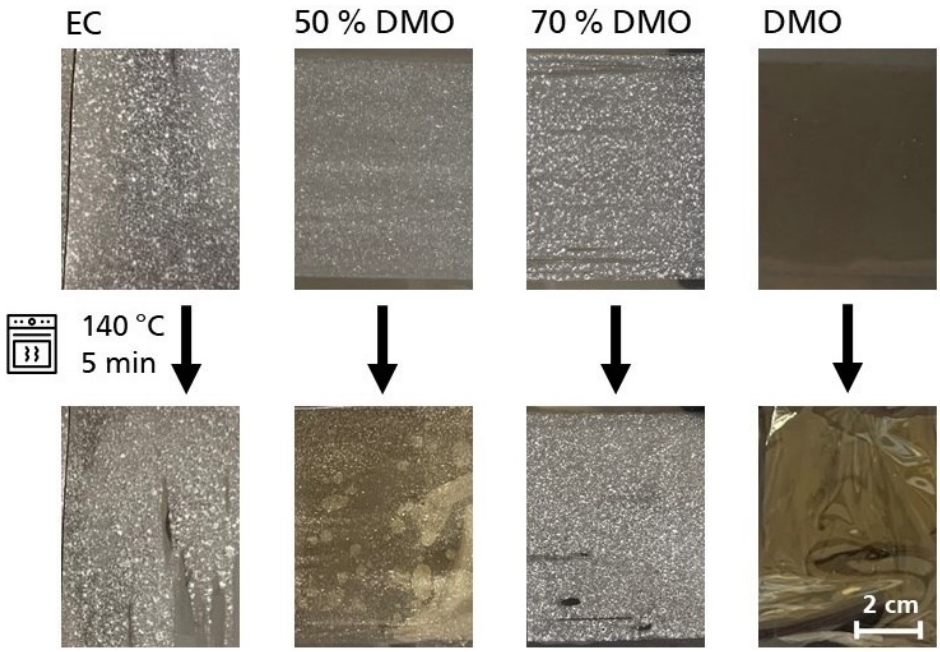

Figure 6.36: Samples of EC, DMO and mixtures out of the substances cast on PET foil out of an aqueous PVA solution. The original films (top row) are tempered in the oven to see if they change during the thermal treatment. The coatings consist of 60 % of DMO, EC or DMO/EC and 40 % PVA. The films are cast out of water with a film frame applicator (gap height 120 µm)(e43).

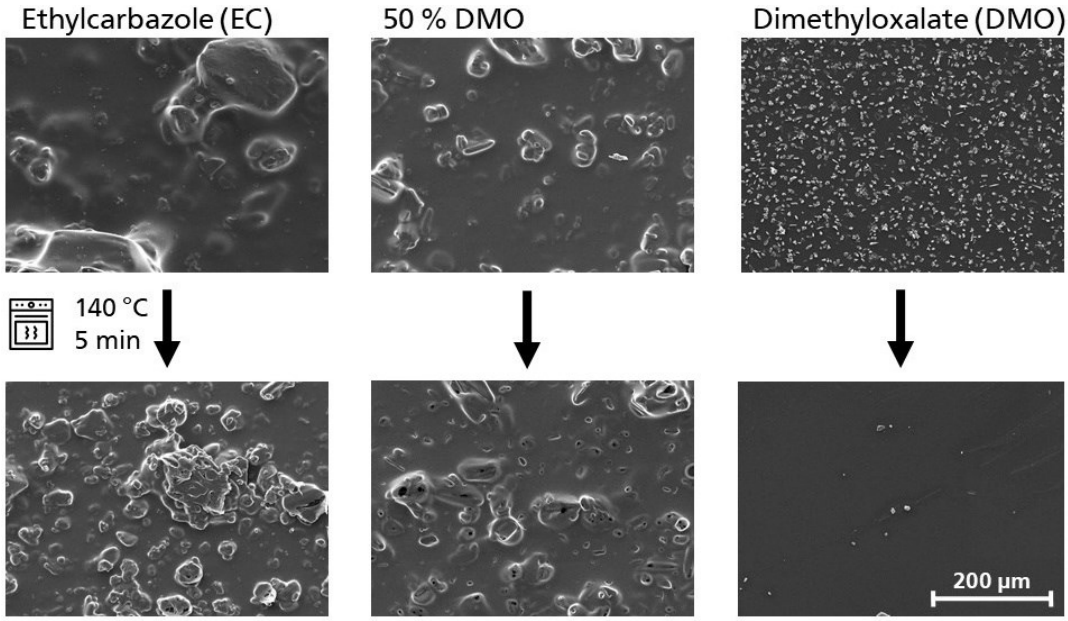

Figure 6.37: SEM images of the samples of DMO, EC as well as a eutectic mixture of DMO and EC in a PVA binder. The original coatings (top row) are tempered in the oven. SEM images of the resulting samples are displayed in the bottom row.

The films with DMO are completely transparent, but show a yellow discoloration after switching in the oven. This is due to the fact that DMO starts to degrade above 100 °C. The film with EC shows clear agglomerations of crystals and a coarse surface. There is no change after switching. The mixtures of DMO and EC also show agglomerations of EC on the surface. Thus, the presence of dissolved DMO in the coating formulation does not affect the agglomeration behavior of the dispersed EC. In the switched state, the film with the eutectic mixture turns yellow, comparable to the DMO pure film. The 70 % DMO

film shows no optical change. These effects can also be seen in the SEM images (Figure 6.37). EC and the eutectic mixture do not show any significant changes after switching. The DMO, which crystallizes in beautiful crystals on the surface when the water evaporates, is no longer visible after annealing. Much of it has been degraded by the temperature.

The optical densities of these samples were not determined because they do not show any opacity. Nevertheless, DSC measurements were performed of the samples to verify that the eutectic mixture is present in the film, even if one of the components is crystallized out of solution along with the PVA and the other component is present only in ground agglomerates. The measurements were carried out in small crucibles in which a round punched-out part of the film on the PET substrate is pressed onto the bottom of the crucible. In this way, the coating itself can be measured directly, rather than the behavior of the bulk. The diagram with the heating curves is shown in Figure 6.38. With DMO, the glass transition temperature of the partially saponified PVA is shifted from 70 to 92 °C. The melting peak is also shifted to higher temperatures. The eutectic blend and the blend with 70 % DMO and EC in PVA show the same curve progression. An unaffected melting peak of EC is obtained at 69 °C, a small melting peak at around 150 °C and a pronounced melting peak at 190 °C. In the blends, no melting peak is seen for DMO or the eutectic blend. This means that no eutectic melting can occur in this film. A modulated DSC measurement was performed to check if DMO is still able to melt in the PVA films. In this measurement method, the temperature is increased and decreased (pulsed) within a given heating rate of 1 K min^{-1}. TOPEM® from *Mettler-Toledo* is used for this purpose. The pulse height and a stochastically changing pulse duration (pulse width) are applied to the sample. Furthermore, since these pulses contain many different frequencies, frequency-dependent (glass transition temperature) processes can be distinguished from frequency-independent processes (melting). However, the main application is to divide the total heatflow into the revering and non-reversing heatflow, which add up to the total heatflow. The diagram of a modulated measurement of a sample of PVA containing 10 % DMO is shown in Figure 6.39.

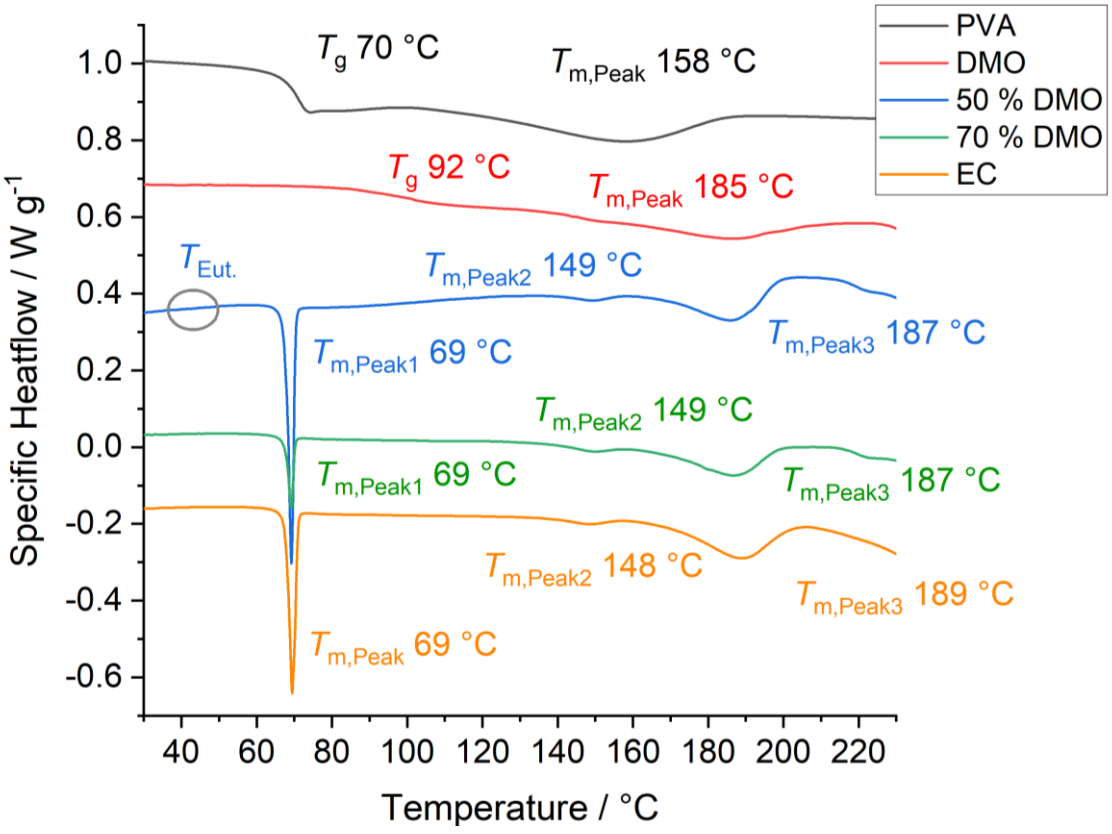

Figure 6.38: DSC thermogram of the pure substances DMO and EC in PVA, the eutectic mixture of DMO and EC in PVA and the PVA itself. The coatings were measured on PET substrate. The second heating cycle is displayed; the heating rate as well as the prior cooling rate is 10 K min^{-1}.

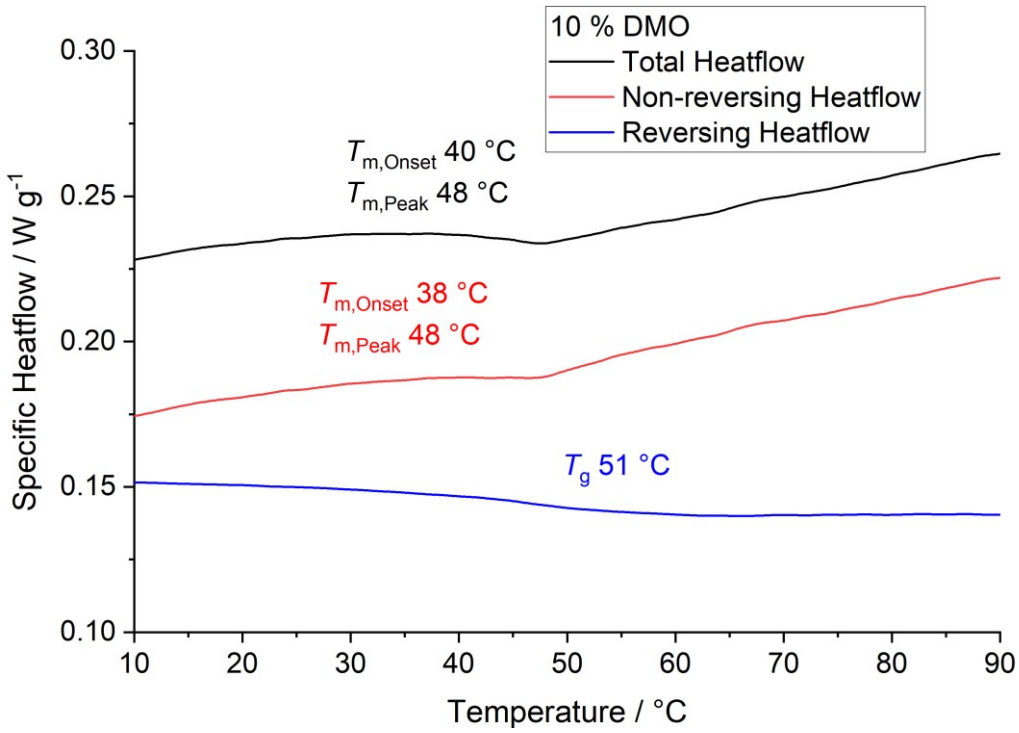

Figure 6.39: DSC thermogram of the modulated measurement of the sample out of PVA with 10 % DMO. The sample was prepared to investigate the melting behavior of DMO in the presence of the used PVA. The total heatflow is divided into non-reversing and reversing heatflow; a heating rate of 1 K min^{-1} is employed.

In this measurement, a clear glass transition temperature can be observed in the reversible heatflow at 51 °C. In contrast, the melting peak of DMO is observed in the non-reversing heatflow at 48 °C. This means that the PVA matrix softens along with the melting of DMO. Measurements with different amounts of DMO in PVA show the shift of the glass transition temperature depending on the DMO present (Table 6.1). The glass transition temperature is significantly lowered with the DMO crystals formed in between the PVA molecular chains during evaporation of the water. The melting temperature of DMO is also lowered; the melting temperature of the pure substance is 57 °C.

Table 6.1: Glass transition temperature measured via DSC of partially saponified PVA depending on the amount of DMO cocrystallizing with the PVA.

Amount of DMO	**T_g of PVA**
0 %	70 °C
10 %	40 °C
20 %	35 °C
30 %	31 °C
40 %	30 °C
50 %	24 °C
60 %	23 °C

The results suggest that it is not advisable to use a suspension with only one the components dissolved and the other as solid. This way the eutectic properties are not maintained. In addition, the large agglomerates of the undissolved EC lead to a highly inhomogeneous surface. Satisfactory coverage could not be achieved and irreversible thermal switching was not possible.

Analogous to the DMO and EC system, benzoic acid and urea are to be coated in PVA. This system presents the same challenge in that one of the components, urea, is water-soluble, while benzoic acid can only be dispersed in the binder. The eutectic mixture of urea and BA and BA are melted and thoroughly mixed (experimental procedure e43; see 8.14). Urea is not melted, as it dissolves in the aqueous solution. The mixtures and pure substances are added to aqueous PVA solution and mixed in a speed mixer. Subsequently, the coatings with a solid content of 38 % are applied to PET film by means of a film frame applicator (gap height 120 µm). The resulting coatings in the original and switched state are shown in Figure 6.40. Coatings of BA, urea and the mixtures also fail to form opaque layers even at 60 % crystalline substance. BA is present in agglomerates on the surface, while the film of urea and PVA shows a relatively homogeneous layer with strong crystal growth. The crystals disappear after the films are annealed in the oven. The films in which only BA or BA and urea are contained in a mixture also have a coarser structure and do not change their appearance with annealing in the oven. However, the SEM images (Figure 6.41) show that the BA agglomerates on the surface after coating are clearly softened into the PVA layer after annealing. Both the eutectic mixture and the urea-only sample show that the previously fine distribution of the crystallites, created by the simultaneous crystallization due to

the evaporation of the water after the coating process, is erased. Large crystal domains with pronounced crystal growth are obtained.

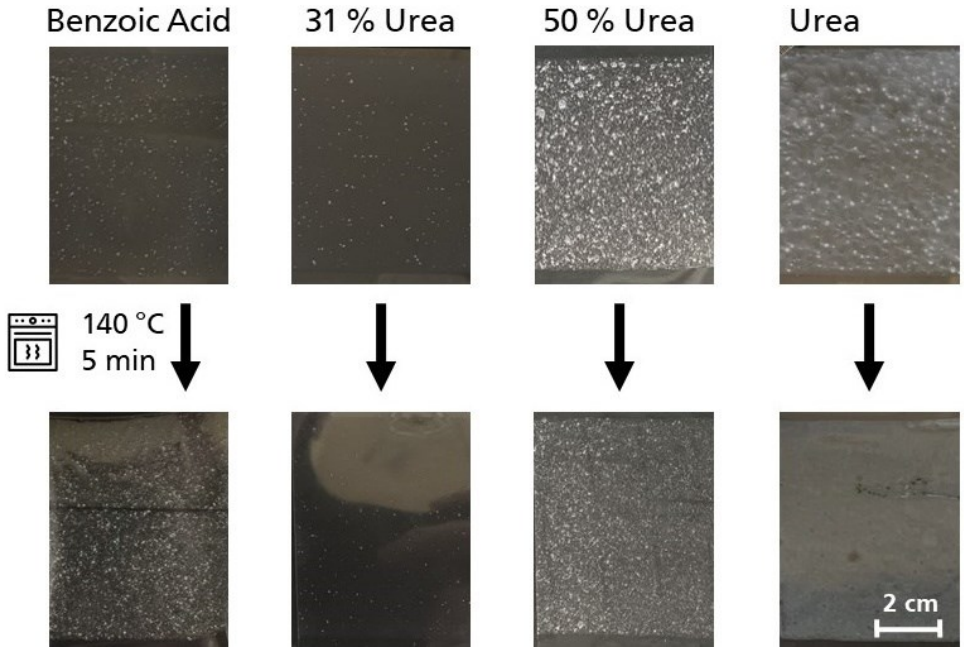

Figure 6.40: Images of the samples of BA, urea and mixtures of urea and BA in PVA. The original films are in the top row and the samples that were tempered in the oven are in the bottom row. The resulting film contain 60 % of crystalline substance and 40 % PVA. The films are cast out of water with a film frame applicator (gap height 120 µm)(e43).

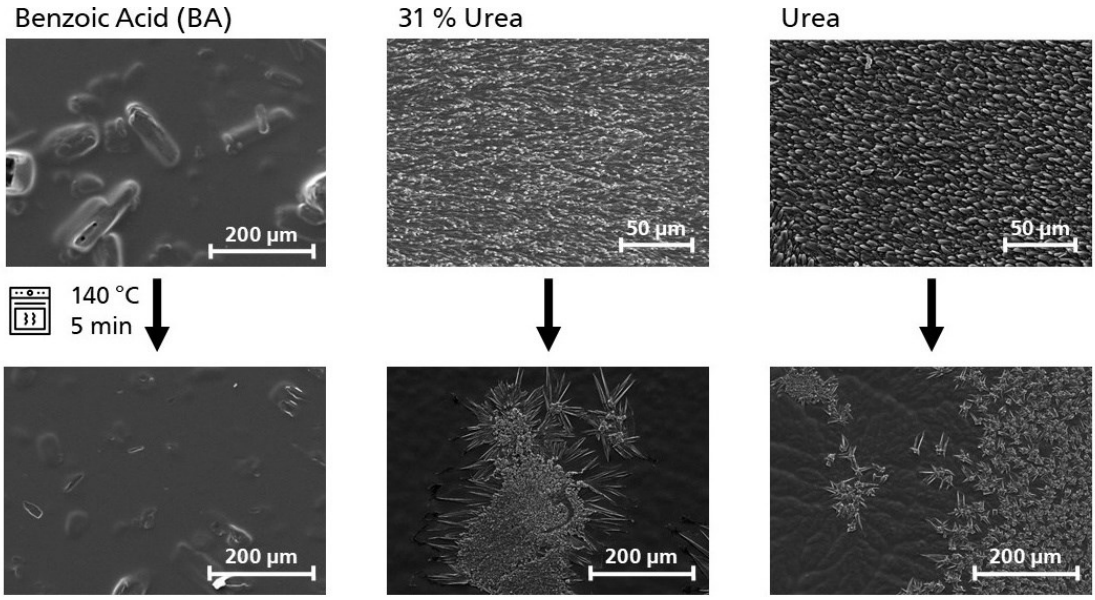

Figure 6.41: SEM images of the samples of BA, urea and the eutectic mixture of urea and BA in PVA. The original films are in the top row and the samples that were tempered in the oven are in the bottom row.

In conclusion, this eutectic system suffers from the same problem of differential solubility. The DSC measurements also failed to show any eutectic melting. Nevertheless, a sample was printed in a standard thermal printer to see if, unlike annealing in the oven, there was a change with this very short thermal treatment. The printout is shown in Figure 6.42 and the printed chessboard pattern is clearly visible,

although the contrast is very low. However, the print test with a standard thermal paper after printing the sample with urea, showed streaks in the print. This means that the printhead was soiled, which is caused when the coating material adheres to the print head during printing.

Figure 6.42: Test print of a sample with 31 % urea in PVA with a standard thermoprinter.

The introduction of the eutectic mixtures into an aqueous formulation was not satisfactory. Urea, the water soluble portion is dissolved, while BA is present as a solid in the PVA/urea solution after dispersion. The coatings are inhomogeneous because of the coarse BA agglomerates. The films with pure BA show no change after annealing, while the films with the eutectic mixture and especially pure urea show a significant change. SEM images show a changed crystal structure, which makes the films appear more transparent after switching. However, due to the brittleness of the films and the very low opacity of the coatings in their initial state, their use as a thermal printable coating is not goal-oriented. Even if a print is visible, the inhomogeneous coatings, the lack of opacity in the initial state, the lack of contrast in the print and the coarse surface are not suitable properties for a thermal paper.
In the following sections, a different approach is taken using natural and synthetic waxes. By melting and dispersing these waxes, not only the material itself but also the shape and size of the particles contribute to the opacity. A different eutectic system is used, but it consists of chemicals with the same solution behavior, i.e. the fatty acids stearic and palmitic acid, which were introduced in Chapter 5.4.

6.2.2 Melt-Dispersed Paraffin Wax in Polyvinyl Alcohol

The first wax to be used melt-dispersed in PVA is paraffin wax. The wax used has a melting range with two distinct melting peaks in the range between 40 to 60 °C. The PVA used is 88 % saponified and has a T_g at 70 °C and T_m at 160 °C. The wax is dispersed in PVA (experimental procedure e65, see 8.17). In melt dispersion, the solid wax is added to a solution of PVA and water, heated above T_m, and mixed at high speed with a disperser after the wax has melted. The mixture is then cooled in an ice bath at low speed so that the particles do not agglomerate during the cooling process.
The thermal properties of the mixture are shown in the DSC heating curve (Figure 6.43). The pure paraffin wax was measured in bulk, and the coating of the wax dispersed in PVA was measured on the PET substrate. The two melting peaks of the paraffin wax are present in the film, but the T_g and T_m of the PVA are not visible in this measurement.

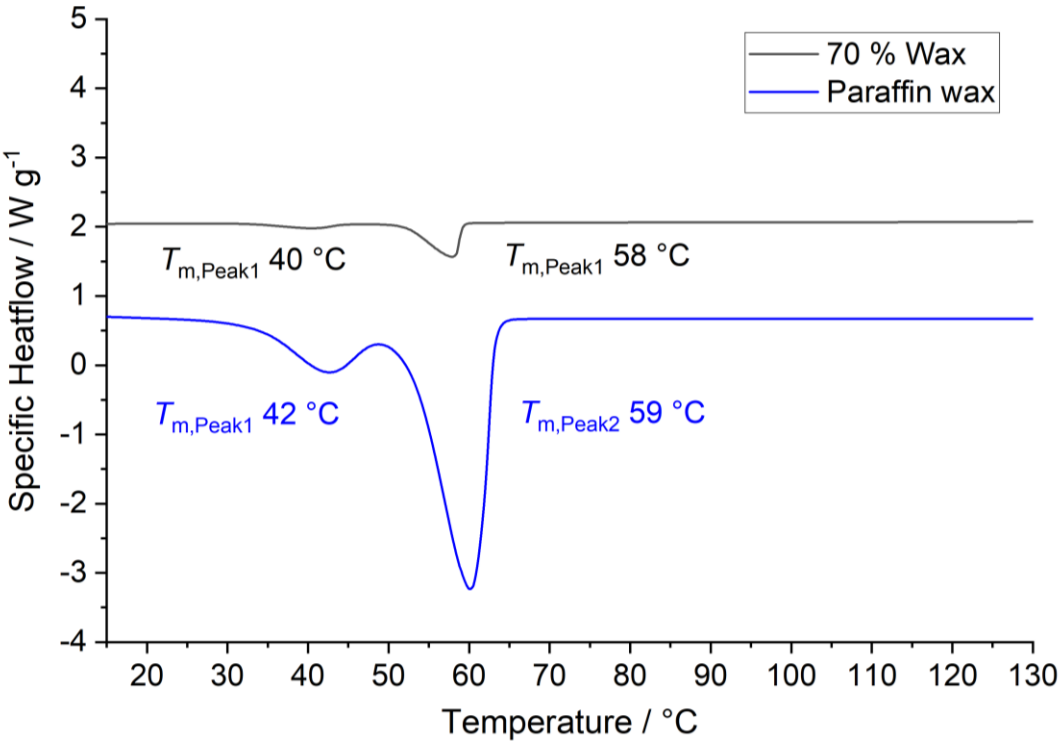

Figure 6.43: DSC thermogram of the sample out of 70 % wax in PVA, as well as paraffin wax itself. The second heating cycle is displayed, the heating and the prior cooling rate is 10 K min^{-1}.

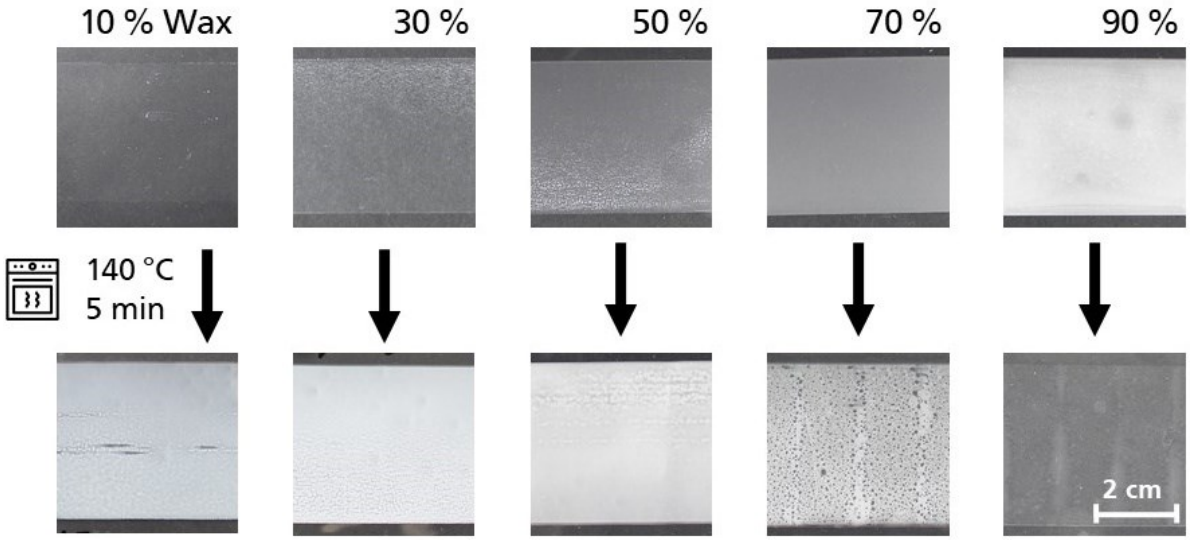

Figure 6.44: Pictures of the samples out of melt-dispersed paraffin wax in PVA. The original films are on the top row and the samples that were switched in the oven in the bottom row. The samples displayed are coated with a film frame applicator (gap height 30 µm). The solid content of the coating formulation is constant at 30 % (e65).

Prior to coating, the wax dispersions are degassed to remove air bubbles. Figure 6.44 shows the resulting films that were coated on PET foil using a film frame applicator with a gap height of 30 µm. The solid content of the coatings is 30 % resulting in a theoretical film thickness of approximately 9 µm. The initial films show an increasing opacity with the increasinging paraffin wax content. At 10 % the films are almost transparent but turn white with a 90 % wax content. After the samples were tempered in the

oven at 140 °C for 5 min, the effect reverses and the films that were rather transparent turn white and opaque. The initially opaque film of the 90 % film on the other hand loses its opacity. The optical densities of the initial and switched samples were measured and plotted in the following graph (Figure 6.45). The ODs of the initial film decrease with the amount of paraffin wax present in the coatings, down to a reasonable opacity with OD of 0.58 with 90 % wax. The value of the OD of the switched film is 1.15 (target value approx. 1.3), which can be explained by the cloudiness of the film. The sample with 90 % paraffin wax was also printed with a standard thermal printer (Figure 6.47). Here, the printed areas achieve an optical density of 1.09, which is only slightly lower than the oven-switched ones.

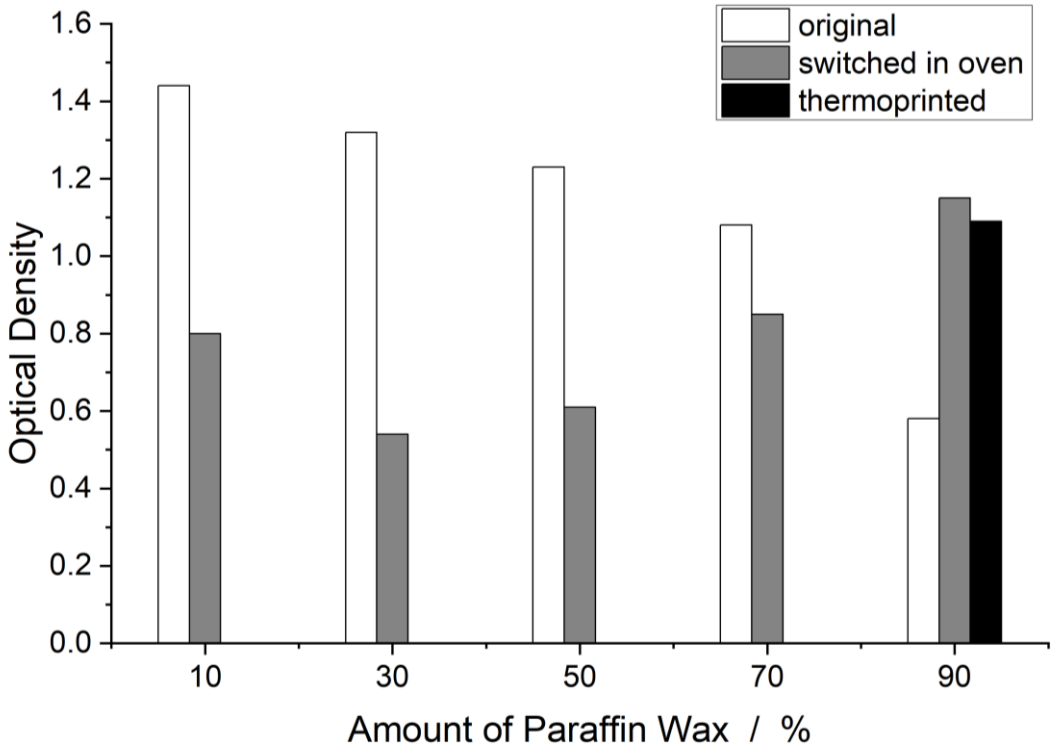

Figure 6.45: Optical densities of samples with different amounts of melt-dispersed paraffin wax in PVA on PET foil. The ODs were measured of the original, switched in the oven (140 °C, 5 min) and a thermoprinted sample. The samples displayed are coated with a film frame applicator (gap height 30 µm). The solid content of the coating formulation is constant 30 %.

The particle size and distribution were determined from SEM images of samples containing 50 % or more wax. Below 50 % wax, no particles are recognisable. The SEM images of the coatings containing 50 and 70 % wax are shown in Figure 6.46; the sample with 90 % wax in Figure 6.47. To determine the sizes, one image of each sample was used to measure the particles. For each image, 30 particles were randomly selected (n=30). The particles grow significantly in size with the increasing amount of wax in the wax-PVA-water-dispersion during melt dispersion (Table 6.2). This is due to less emulsifier, i.e. PVA, stabilizing the surface of the particles.

Table 6.2: Particle size distribution of melt-dispersed paraffin wax in different amounts in PVA. . The solid content is constant 30 %. The values were obtained by measuring particle diameters in SEM images. Per sample one image is measured with n=30.

Amount of paraffin wax in PVA	50 %	70 %	90 %
Size distribution of particles	0.3 to 1.3 µm average 0.6 µm	0.4 to 4.4 µm average 1.5 µm	1 to 17 µm average 4.4 µm

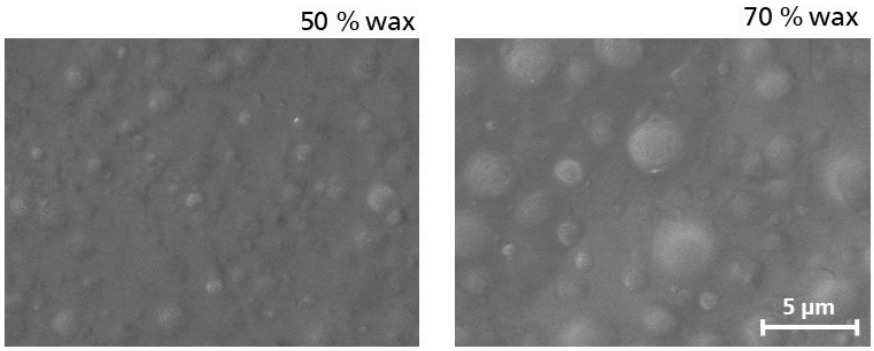

Figure 6.46: SEM images of samples of melt-dispersed paraffin wax in PVA with two different amounts of wax.

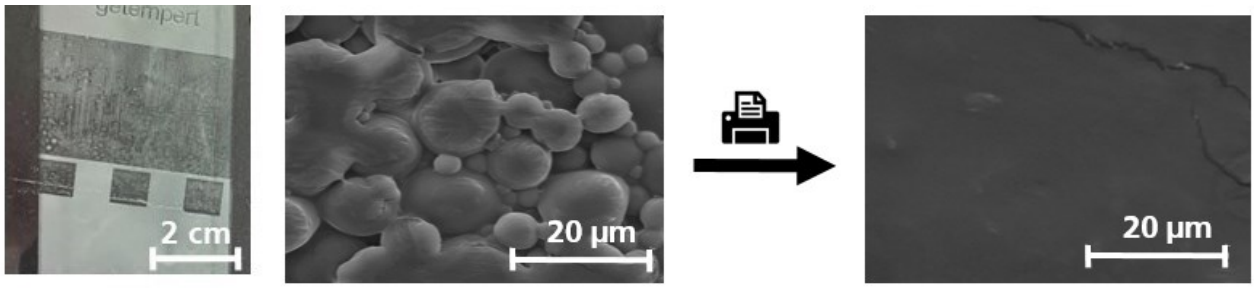

Figure 6.47: Thermoprinted sample of 90 % wax in PVA (left), as well as a SEM image of the same coating of an unprinted (center) and a printed area (right).

Thermal printing on the samples is not smooth, as subsequent print tests with standard thermal papers show a clear deposit of the wax coatings on the print head. However, the print image (Figure 6.47) is clearly visible and the contrast is good. This shows that the approach with a wax is promising. On the right side of the figure is the SEM image of the thermoprinted sample. The structure of the large wax particles is destroyed by the thermoprinting and a homogeneous surface is present.

Since the optical densities of the coated papers with the melt-dispersed paraffin wax in PVA are still too high, the aim is to use a wax that inherently provides better opacity. When comparing bulk materials, paraffin wax is clearly more transparent than tristearin and fatty acids. Therefore TS is used in coatings in the following section: melt-dispersed in PVA and together with PS particles in dispersion.

6.2.3 Tristearin Particle Dispersions with Polystyrene Particles and Polyvinyl Alcohol

a) Melt Dispersion of Tristearin in Polyvinyl Alcohol

In analogy to the paraffin wax samples, TS is melt-dispersed in PVA to be coated on PET foil (experimental procedure e66, see 8.18). The PVA used is 88 % saponified and has a T_g at 70 °C and a T_m at 160 °C. In melt dispersion, the solid TS is added to a solution of PVA and water, heated above the melting point of 60 °C and, after the TS has melted, it is mixed with a disperser at high speed. The mixture is then cooled in an ice bath at low speed so that the particles do not agglomerate during the cooling process. After the mixtures were degassed, the formulations were coated on PET foil using a film frame applicator with a gap height of 30 µm. The solid content is 30 %, resulting in a theoretical film thickness of 9 µm (Figure 6.48). The films form as a slightly opaque layer whose opacity increases only slightly with an increasing TS content despite the high amount of TS. The films that were switched in the oven show an irreversible change, but are still very much cloudy. This is confirmed by the OD measurements (Figure 6.49). The OD drops to 0.6 with 90 % TS and the switched films reach only 1.2. The values are comparable to paraffin wax and show no advantages.

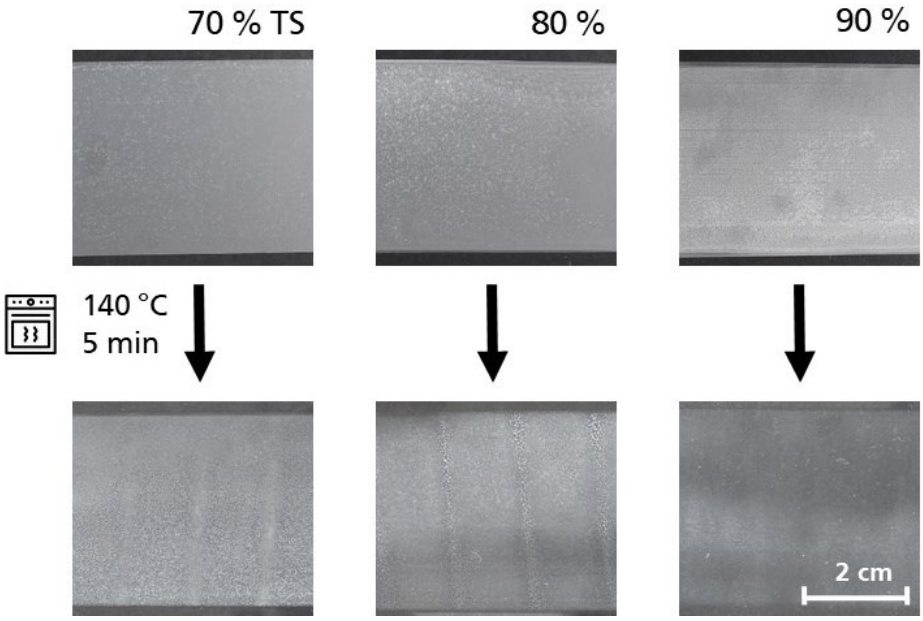

Figure 6.48: Samples out of tristearin and PVA with different amounts of TS. The original samples are in the top row and the samples that were tempered in the oven are displayed in the bottom row. The samples displayed are coated with a film frame applicator (30 µm gap height). The solid content of the coating formulation is constant at 30 % (e66).

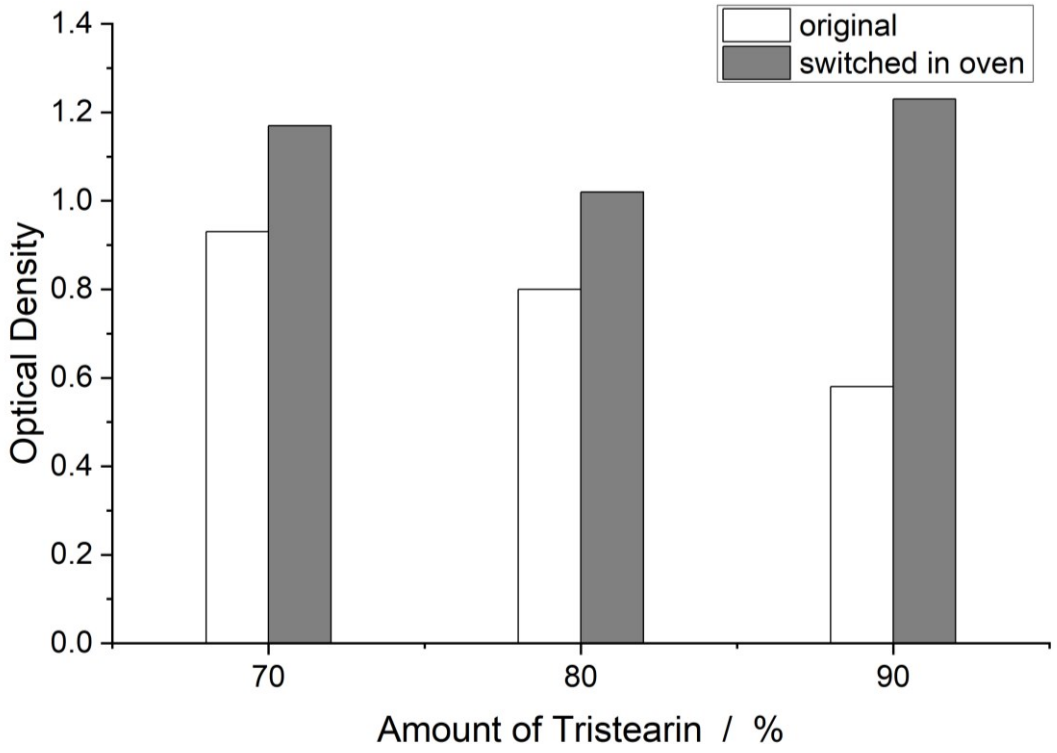

Figure 6.49: Optical densities of samples out of melt-dispersed TS in PVA. The films were measured before and after the switching in the oven at 140 °C for 5 min.

The surface structure can be seen in the SEM images. As the TS content increases, the particle diameter also increases. Based on the SEM images, the particle sizes were measured and listed in Table 6.3. To determine the sizes, one image of each sample was used to measure the particles. For each image, 30 particles were randomly selected (n=30). Due to the reduction of PVA in the formulation which stabilizes the particles in the dispersion, the particle sizes increase significantly and the particle sizes distribution becomes much wider. As a result, the surfaces with the higher amount of TS appear significantly more porous. Less binder in the formulation means that the air voids between the particles cannot be closed. This increased porosity contributes positively to light scattering.

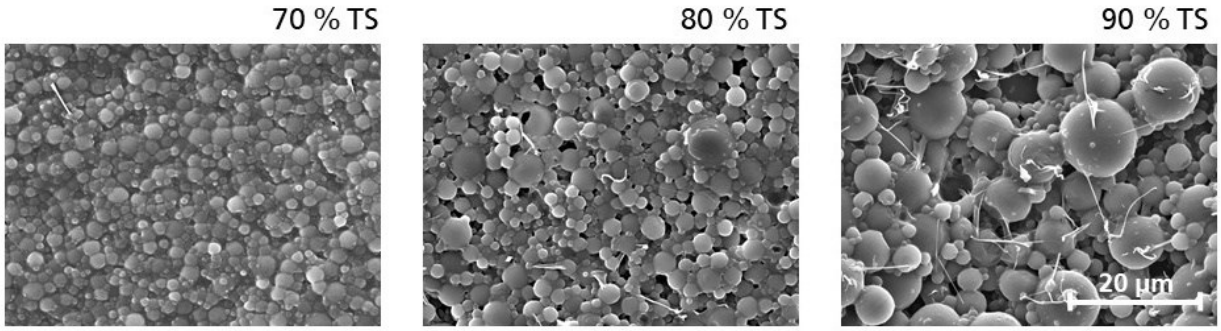

Figure 6.50: SEM images of samples out of melt-dispersed TS particles in PVA.

Table 6.3: Particle size distribution of melt-dispersed TS in different amounts in PVA. The solid content is constant 30 %. The values were obtained by measuring particle sizes in SEM images. Per sample one image is measured with n=30.

Amount of tristearin in PVA	70 %	80 %	90 %
Size distribution of particles	0.3 to 3.1 µm average 1.5 µm	0.4 to 4.1 µm average 1.5 µm	0.7 to 11.5 µm average 3.8 µm

Although TS as a pure substance appears significantly whiter than paraffin wax, the films with melt-dispersed TS have comparable opaque densities in the unswitched and switched states. The lack of transparency may be due to the strong recrystallization of TS into large domains after switching in the oven. However, a fine homogeneous distribution in the matrix is required to obtain a transparent state. Therefore, fatty acids may function better in a polar PVA matrix during switching due to their polarity. Intermolecular interactions are believed to have a major influence and could lead to a reduction of recrystallization due to stronger intermolecular interaction and mixing with the PVA matrix.

b) Melt-Dispersed Tristearin Particles with Polystyrene Particles in Polyvinyl Alcohol

Since the system of PS and TS showed good results when it was coated from organic solvent, we next converted it in an aqueous formulation. For this purpose, PS particles are polymerized by emulsion polymerization. The goal is to synthesize monodisperse particles, so that the resulting films have a sharp switching temperature rather than a wide switching range. The reaction scheme of radical polymerization in emulsion of styrene is shown in the following Figure 6.51.

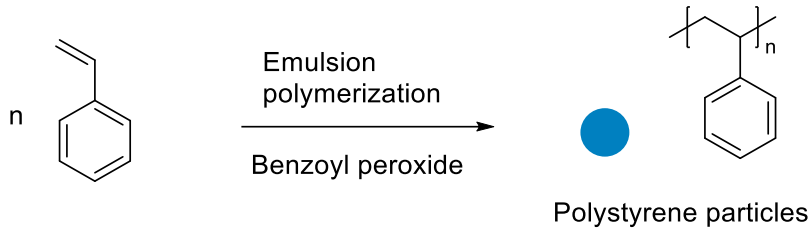

Figure 6.51: Emulsion polymerization of Styrene with Benzoyl peroxide as initiator to gain Polystyrene particles.

In emulsion polymerization, a non water-soluble monomer is dispersed in water above the critical micelle formation concentration (CMC) with the aid of surfactants. *Harkins* published the theory of emulsion polymerization in 1947, which is still valid today.[109] The theory describes a system consisting of water, a slightly water-soluble monomer, emulsifiers and a water-soluble initiator. This free radical polymerization reaction is thereby divided into three phases: the nucleation phase, the growth phase, and the depletion phase.[109]

In nucleation phase I, the monomer is dispersed in water and forms monomer droplets due to poor solubility. The surfactants are present at concentrations above the CMC and form micelles. The surfactants arrange themselves so that their hydrophilic side faces the water and their hydrophobic part

is present inside the micelle. This results in spherical micelles, which are present in a large excess (approx. 10^8 times) compared to the monomer droplets. Due to the hydrophobic character inside the micelles, the poorly water-soluble monomer diffuses from the monomer droplets into the micelles. When the initiator, which is readily soluble in water, is added, it decomposes, immigrates into the micelles and starts polymerization inside. Due to the large excess of micelles over monomer droplets, the probability of initiation in the monomer droplets is negligible. Monomer is consumed in the micelles during polymerization and it is replenished from the monomer droplets by diffusion. The growing micelle is stabilized by diffusion of emulsifier molecules from empty micelles. As the surfactant molecules from the empty micelles are consumed, no further polymerization can be started. The nucleation phase is complete.[99,109,110] The nucleation phase is followed by the growth phase. Polymerization in the micelles constantly consumes new monomer from the monomer droplets. This creates a steady state between the reacted monomer in the particles and the monomer being replenished from the monomer droplets. At the end of the growth phase, the monomer reservoirs are completely depleted. The third phase is the depletion phase. In this phase, the remaining monomers in the latex particles are polymerized out and the reaction rate decreases sharply due to increased termination reactions in the polymerization.[99,109,110] To obtain monodisperse particles, the nucleation phase must be very fast compared to the growth phase. This is the only way to achieve uniform particle growth. Particle size and architecture can also be influenced by the reaction control. In addition to the batch process, emulsion polymerization can be carried out in a semi-continuous process. In this process, a monomer emulsion is slowly added to a pre-dispersion of seed particles. Due to the slow dosing, the polymerization is constantly in the depletion phase. This is why the process is also called "starved-feed" emulsion polymerization. This reaction control means that the particle size can be precisely adjusted by the amount of monomer added. It is also easy to stop the process when the desired particle size is reached.[99] The experimental setup is shown in Figure 6.52, which displays the reactor, the dosing pump and the feed.

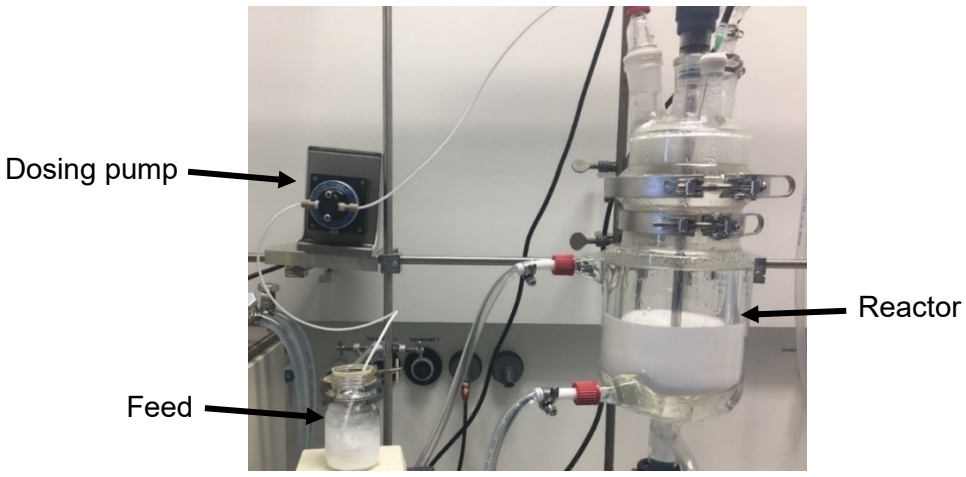

Figure 6.52: Experimental setup for the starved feed emulsion polymerization of styrene. The monomer is stabilized with surfactant and this emulsion feed is slowly added to the reactor by means of a dosing pump.

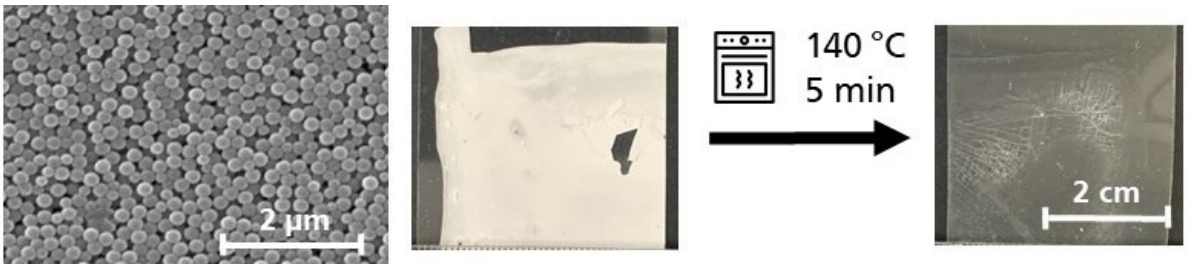

Figure 6.53: SEM image of the resulting PS particles (left) and a sample of dried PS dispersion fresh from the reactor (center) that was switched in the oven (right)(e39).

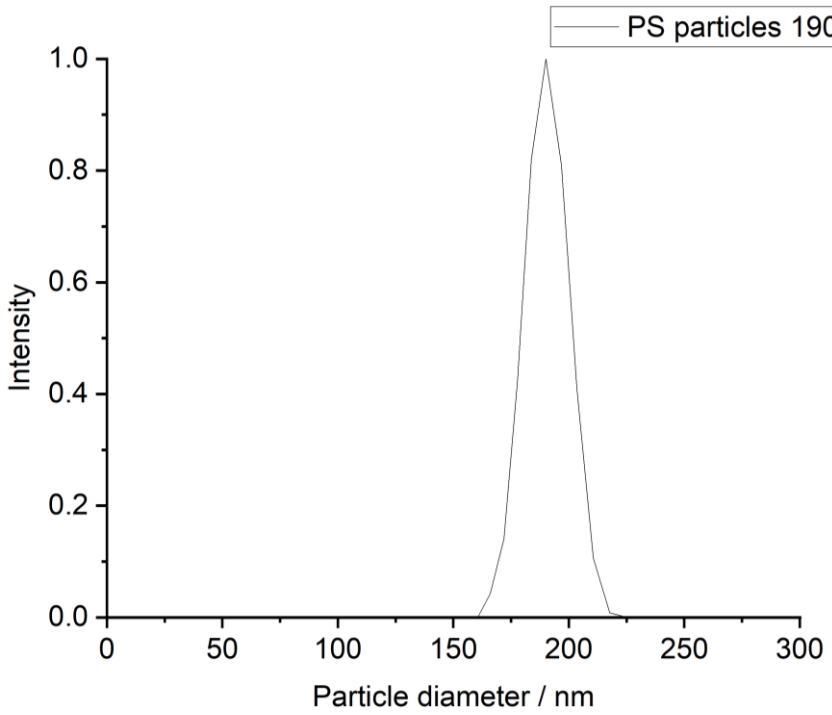

Figure 6.54: Dynamic light scattering measurement of PS-particles e23; EP2 with a diameter of 190 nm. The particles were synthesized using starved feed emulsion polymerization.

The particles (experimental procedure e39, see 8.19) have a monodisperse size distribution, as can be seen in the SEM image in Figure 6.53 (left). The size was measured by dynamic light scattering (DLS, Figure 6.54); the particles have a hydrodynamic diameter of 190 nm. The glass transition temperature is at T_g 102 °C (DSC thermogram, in Appendix Figure 12.4). A gel permeation chromatography (GPC) measurement in THF with PS standard gives a weight average molecular weight M_w=116 kg mol^{-1} (appendix Figure 12.5). Figure 6.53 center shows the pure particle dispersion added to PET. The particles can be switched at 140 °C and produce a transparent film. One of the samples was also thermoprinted, but no image was visible. The thermal sensitivity of the pure PS particles is too low. Therefore, TS is added to reduce the switching temperature (experimental procedure e23, see 8.20). The PS particle dispersion was heated to 80 °C together with water and TS. The mixture is then mixed with a dispersion rod and the TS is melt-dispersed. By rapid cooling with an ice bath, TS particles are obtained in addition to the PS particles. 50 % TS and 50 % PS are used respectively, and the formulations

have a solids content of 13 %. Since no binder is used, which would stabilize the coating formulation, the surfactant sodium dodecyl sulfate (SDS) is added to one of the formulations to investigate whether the presence of the surfactant influences film formation. The film frame applicator used has a gap height of 120 µm.

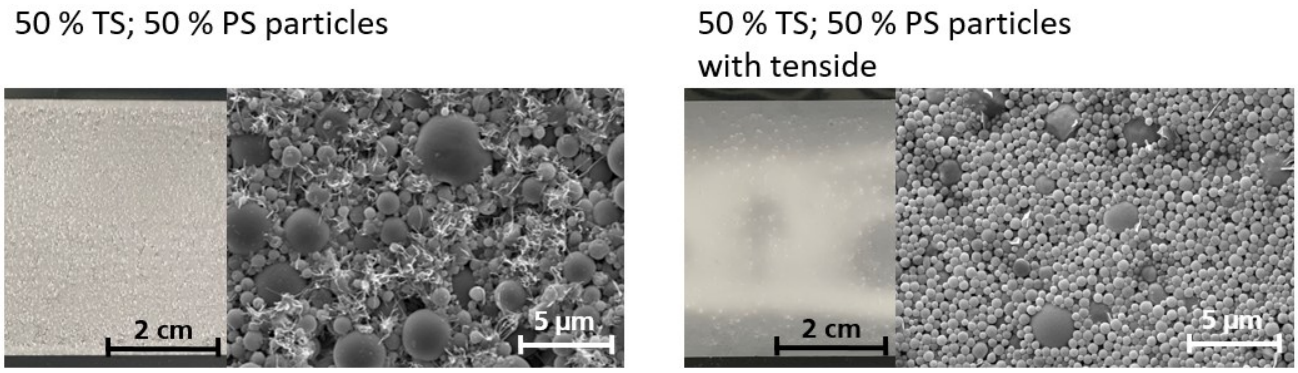

Figure 6.55: Photos and SEM image of the samples constisting of 50 % tristearin and 50 % PS particles. The left sample is formulated without tenside, the right ones were formulated with SDS as tenside. The films were coated using a film frame applicator (gap height 120 µm); solid content of the coating formulations is 13 %.

The coating without tenside (Figure 6.55, right) shows a much coarser structure. TS is not only present in spherical particles, but filamentous structures have also formed. The structure is coarsely porous and the particles are disordered in the network. The sample with SDS, on the other hand, is much more homogeneous and shows a much less porous surface, in which the smaller PS particles are arranged around the large TS particles (Figure 6.55, left). The TS particles are also much smaller than those melt-dispersed without tensides. The surfactants stabilize the TS particles during melt dispersion and suppress the formation of other crystal structures. The use of surfactants can therefore make the surface of the formed films much more homogeneous. However, the system of particles in any form has the disadvantage that oil and water get into the structure, making a possible print image unrecognizable. Therefore, an attempt is made to anneal the samples at different temperatures in order to possibly close the surface of the film without affecting the opacity. This can work if the lower layers contain a sufficient amount of entrapped air. The images of the samples annealed at different temperatures are shown in Figure 6.56. The films with and without surfactant do not differ in thermal sensitivity. The optical density measurements (Figure 6.57) show that there is a leap to higher ODs for the films that were stored at 70 °C. This can be explained by the melting of the TS particles. At 60 and 70 °C the storage time was 10 minutes longer than at higher temperatures due to the melting temperature of TS. The increased annealing temperature ensures that the TS can reshape or recrystallize in the softened, but not yet molten state.

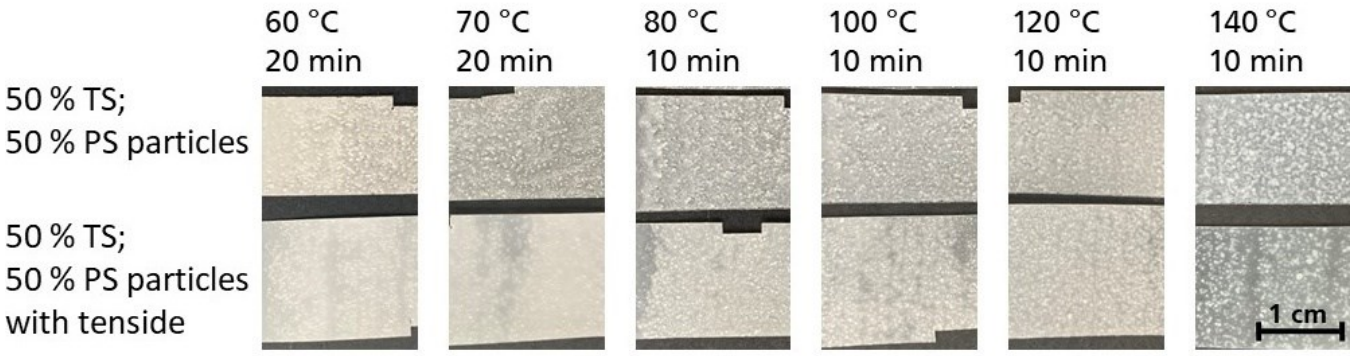

Figure 6.56: Pictures of the samples out of PS particles and 50 % TS coated out of water without (top row) and with tenside (bottom row). The samples were coated with a film frame applicator with 120 µm gap height; 13 % solid content in coating formulations. The samples were tempered in the oven at different temperatures (e23).

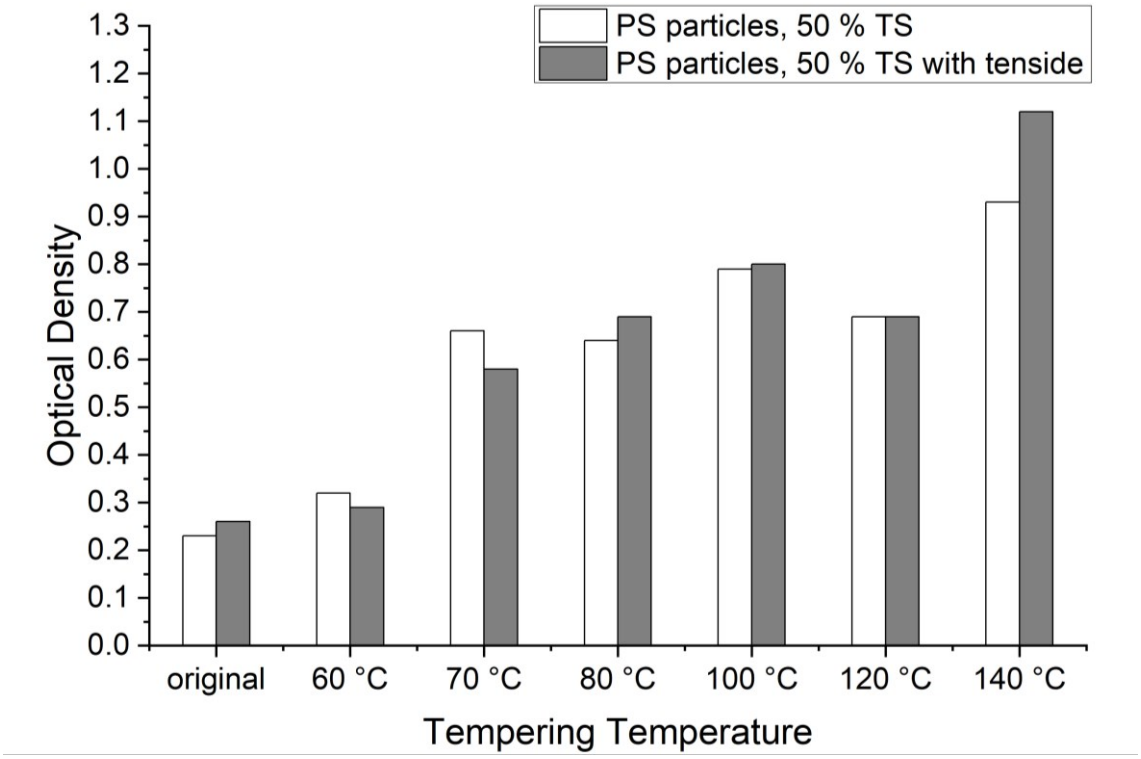

Figure 6.57: Optical density of samples out of PS particles and 50 % TS coated out of aqueous solution with and without tenside (30 µm gap height; 30 % solid content in coating formulations). The values of the OD depending on the tempering temperatures are displayed.

The next leap in OD is observed at 140 °C. This temperature is necessary to melt the PS particles to the point where the covering structure with the particles is completely destroyed. However, the switchting is not complete in these films: the particle agglomerates remain unchanged and therefore the film still appears white. The films with the surfactant vary only minimally in their OD at any given temperature. SEM images were also taken of the samples (Figure 6.58), showing the samples after annealing at the different temperatures. In general, the difference between the samples with and without surfactant can clearly be seen. The significantly larger TS particles resulting from the melt dispersion without surfactant lead to rough surfaces (top), while the films with surfactant are much finer (bottom). Defects caused by

air bubbles formed during the drying process are clearly visible. The samples after annealing at 80 °C show a much more closed surface, but the particle structure is still visible. Above 100 °C the particle structure is gone and a smooth surface is formed. Above 140 °C the defects caused by air bubbles are closed. A less porous surface can be obtained by annealing, but this results in a large loss of optical density and is therefore not applicable. An attempt was made to sinter the surface analogous to the samples with PS and TS from organic solvent (section 6.1.2) was carried out, but only a few particles of the films could be sintered without the films becoming transparent and no oil resistance could be obtained.

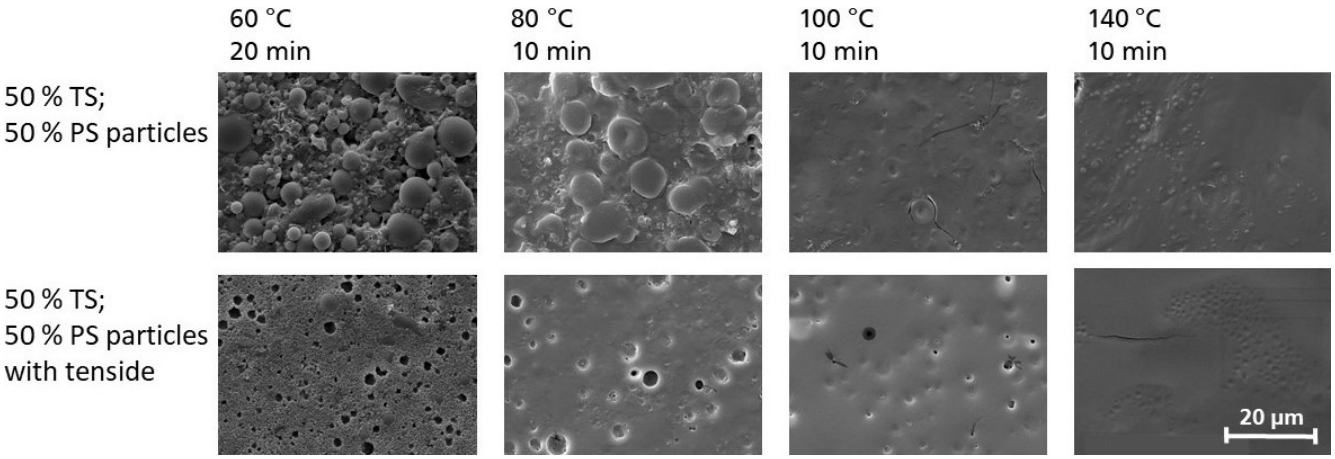

Figure 6.58: SEM images of samples out of PS particles and 50 % TS coated out of water without (top row) and with tenside (bottom row). The samples were tempered in the oven at different temperatures and the images show the changes of the surface.

By synthesizing PS particles and melt-dispersing them with TS an opaque coating can be produced. However, formulations in which the particles agglomerate strongly could be poorly coated. In terms of switchability, there is a challenge with particle agglomerates that do not switch at all or only at high temperatures. The other parts of the film are thermally irreversibly switchable. Since the use of polymer particles maximizes the porosity of the films, another strategy is discussed in the next section: melt-dispersed waxes in PVA which serves as binder and polymer matrix.

6.2.4 Fatty Acids Dispersed in Polyvinyl Alcohol Applied as Coatings on PET foil

a) Combinations of Palmitic and Stearic Acid

In Chapter 5, eutectic mixtures were examined to see to what extent they can contribute to an enhanced scattering effect. It was found that it is not so much the eutectic mixture that has an influence, but rather the greatest possible difference in the refractive indices that is the most important contributor to the enhanced scattering effect. However, the other advantage of eutectic blends, a concrete and precise melting point compared to a wide melting range of the other compositions as well as the pure substances can be used for an alternative thermal paper. Therefore, a eutectic blend of palmitic (C_{16}, T_m=64 °C) and stearic acid (C_{18}, T_m=71 °C) was investigated and the results are shown in the following section

(experimental procedure e47, see 8.15). The system has already been presented in section 5.4 and the eutectic range found by DSC is from 40 to 80 % of PAc in the mixture with T_E=57 °C (phase diagram in the Appendix, Figure 12.1). The compositions were prepared in 10 % increments and the mixtures were melt-dispersed together with PVA (30 % PVA, 70 % fatty acid) above the melting point of the fatty acids using a dispersion bar. The mixtures were cooled in an ice bath to prevent agglomeration of the particles. The mixtures, which had a constant solid content of 30 %, were then coated onto PET using a film frame applicator. Some of the films are shown in Figure 6.59. In the original state and after switching them in the oven.

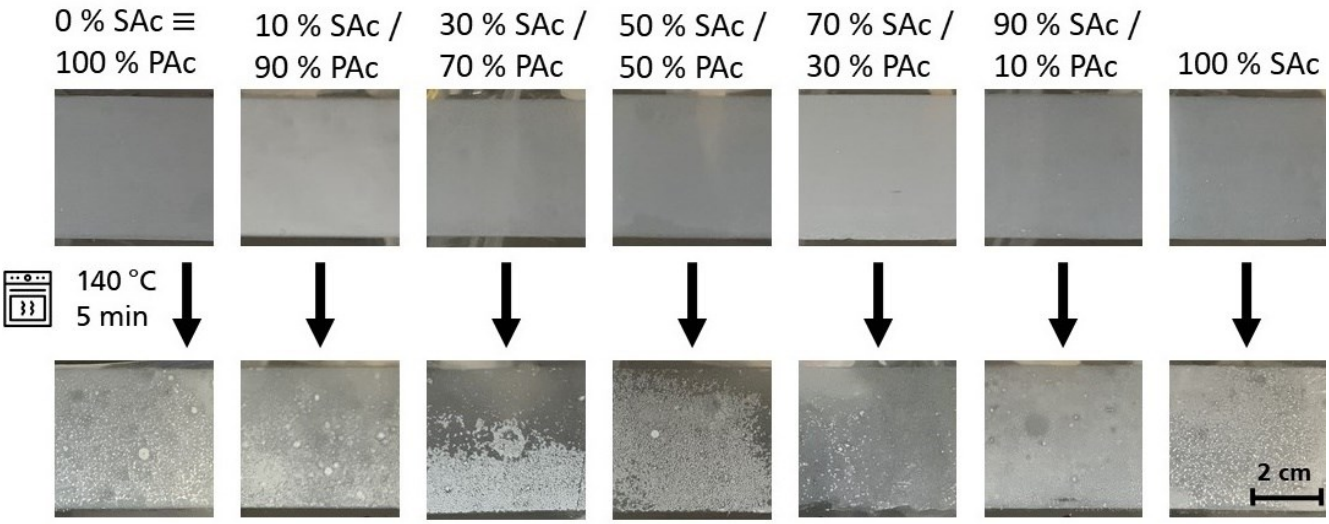

Figure 6.59: Samples out of fatty acids and PVA with different compositions of SAc and PAc. The original samples are in the top row and the samples that were tempered in the oven are displayed in the bottom row. The samples displayed are coated onto PET with a film frame applicator (gap height 30 µm). The solid content of the coating formulation is constant at 30 % (e47).

The coatings with different fatty acid compositions do not show large differences in opacity. The OD values (Figure 6.60) vary by 0.28 from 0.77 to 1.05 over the entire range, with no linkage to the presence or absence of a eutectic composition. This is only a moderate opacity. The switched films show very inhomogeneous domains of crystallized fatty acid on the surfaces. The same applies to the optical densities of the switched films. The values differ by only 0.2 but this is not related to the composition of the fatty acids. The film with 70 % PAc and 30 % SAc has a significantly higher optical density of 1.33 in the switched state. This film has fewer large domains of crystallized fatty acid on the surface.
SEM images of the films are shown in Figure 6.61. The PAc sample shows a mixture of both spherical and ring-like particles. The ring-like particles dominate the surfaces of the other mixtures. The sizes of the particles have not been measured because the ring structures are more existent as fragments. The coating made from pure SAc exhibits spherical particles similar to the coating with pure PAc, but the size of the particles appears to be smaller. The distribution of the fatty acid particles in the films is viewed

using cross-sectional images under the SEM (example image Figure 6.62). The particles are homogeneously distributed throughout the cross-section.

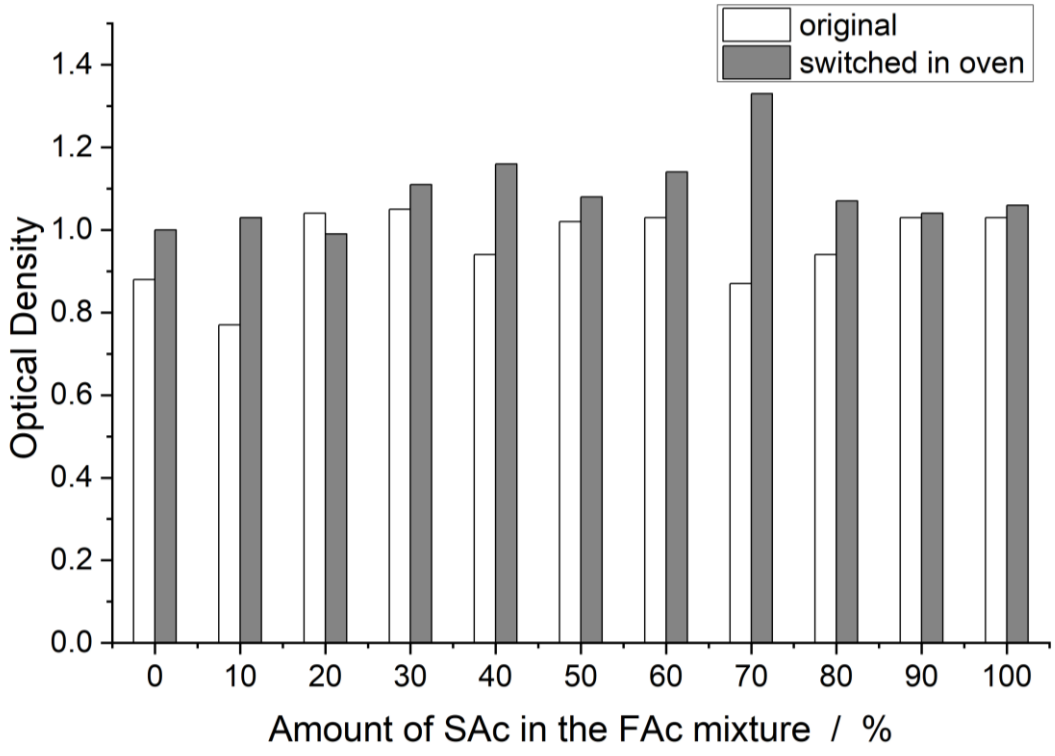

Figure 6.60: Optical densities of samples with 70 % of fatty acid with different compositions of PAc and SAc in PVA coated on PET foil (30 µm gap height; 30 % solid content in coating formulations). The optical densities were measured in the initial and thermo-switched state (oven; 140 °C, 5 min).

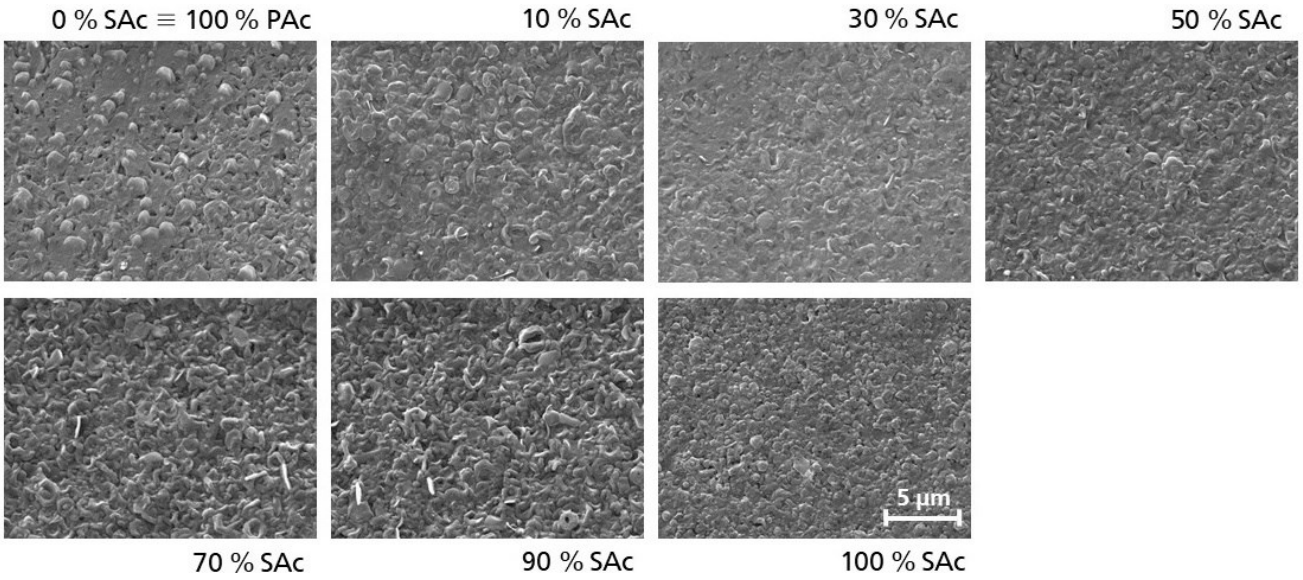

Figure 6.61: SEM images of samples out of 70 % fatty acids and PVA with different compositions of SAc and PAc. The original samples are in the top row and the samples that were tempered in the oven are displayed in the bottom row. The samples displayed are coated onto PET with a film frame applicator (gap height 30 µm). The solid content of the coating formulation is constant at 30 %.

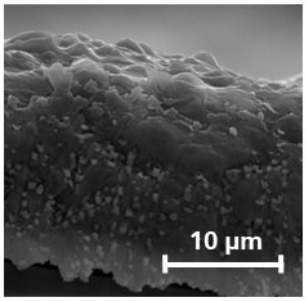

Figure 6.62: SEM image of a cross-section of a sample out of 70 % PAc in PVA. The PAc particles are homogeneously distributed throughout the film.

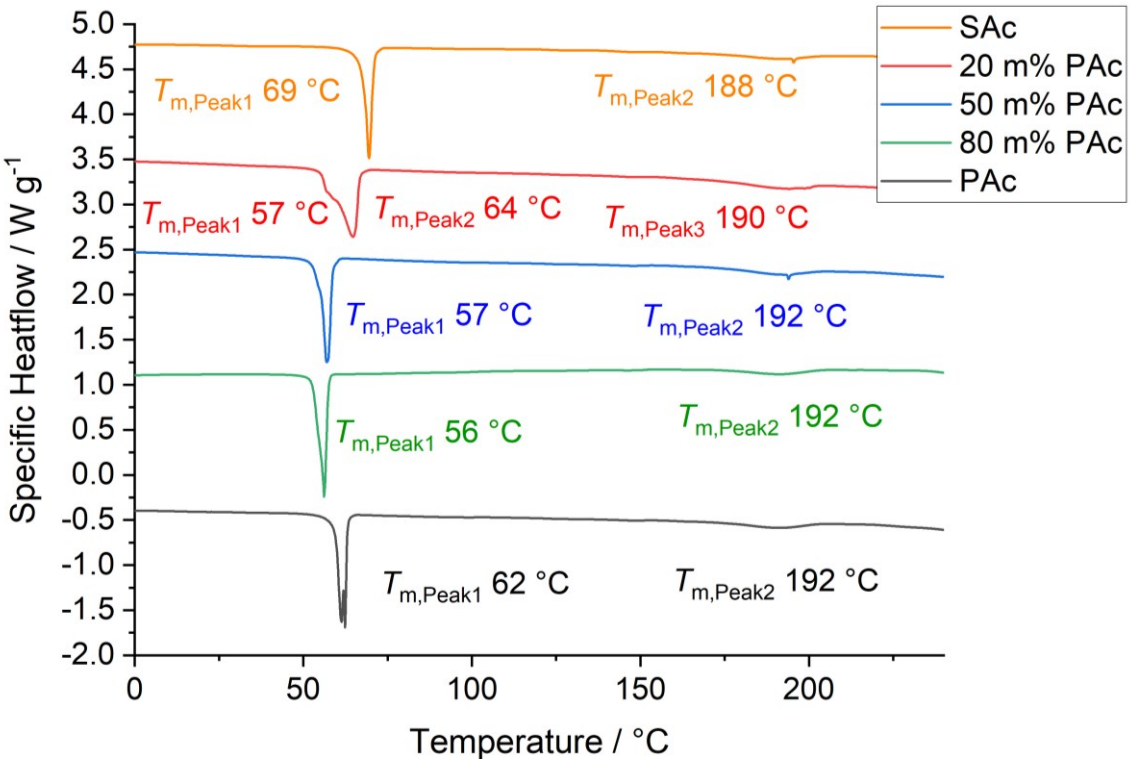

Figure 6.63: DSC thermogram of samples with 70 % of different compositions of SAc and PAc with 30 % PVA coated on PET foil (30 µm gap height; 30 % solid content). The second heating cycle is displayed and the heating as well as the prior cooling rate is 10 K min^{-1}.

DSC thermograms of different compounds are shown in Figure 6.63 (2nd heating cycle). Punched out pieces of the samples were measured in 20 µl crucibles. The eutectic blends (50 and 80 % PAc) show a common reduced melting peak at 56 °C, which also corresponds to the eutectic melting temperature. The other mixture shows two melting peaks. The pure SAc has only the melting peak, whereas PAc shows a double peak. Since it is the second heating cycle, it cannot be a polymorph melting but could stem from the deformation of the punched out sample. The defect can also stem from large crystals melting[111], but since it has no effect on the outcome of the film properties, the measurements were not repeated.

The glass transition temperature of the PVA at 70 °C is superimposed by the melting peaks, but the melting point of the crystalline parts of the PVA is present about 190 °C for all samples. In bulk it is $T_{m,\text{crystalline parts, bulk}}=160$ °C.

Thus, the eutectic composition is still present in these films since the mixtures are equally available to mix during heating and none of the components is present in a different form, e.g. dissolved and finely dispersed in the polymer matrix. The optical densities in the original and switched states are not yet in the required range. Therefore, in the next section, the amount of melt-dispersed fatty acid is varied.

b) Variation of Amount of Palmitic Acid in Polyvinyl Alcohol

To determine the optimum amount of fatty acid in PVA for an opaque, yet switchable coating, pure PAc is melt-dispersed together with PVA in various amounts (experimental procedure e64, see 8.16). The resulting coatings are coated onto PET film using a film applicator frame. The solid content is constant at 30 %. The films coated with a 30 µm gap height are shown in Figure 6.64.

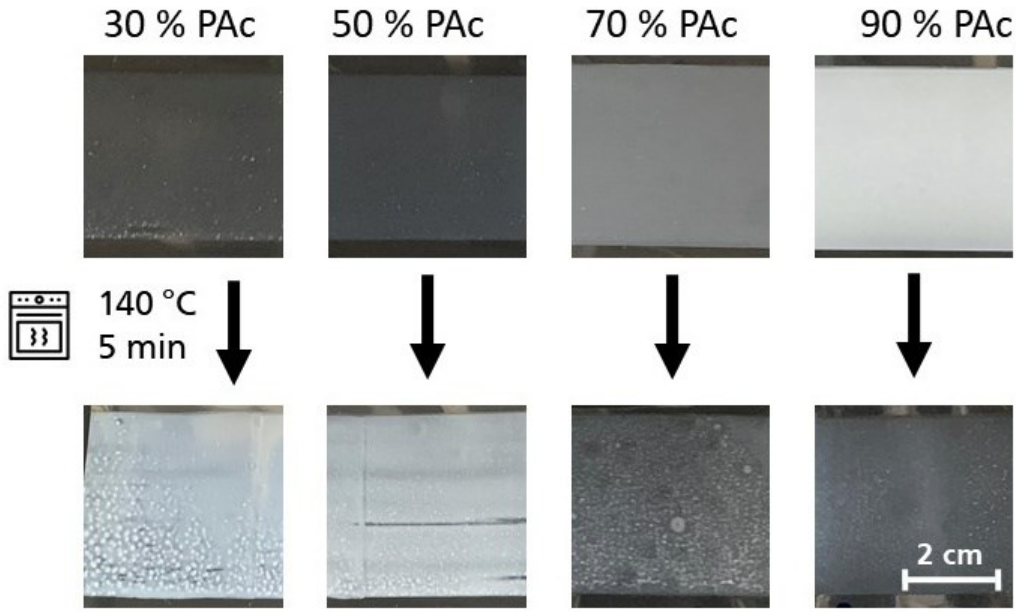

Figure 6.64: Pictures of samples with different amounts of PAc in PVA coated on PET foil (30 µm gap height; 30 % solid content in coating formulation). The films are shown in the initial state (top row) and thermo-switched in the oven (bottom row)(e64).

The films show a constant decrease in optical density, i.e. an increase in opacity (see Figure 6.65). From 80 % PAc, a value of < 0.4 is obtained, which is a very good opacity. However, for the mass fractions up to 70 %, the desired opaque-transparent switching is reversed, i.e. the optical density decreases when switching. The samples with 80 % and 90 % PAc have a difference in the OD of 0.72 and 0.92 respectively. These contrasts between the original and the printed state are already clearly visible, but a contrast of ≥ 1 would be preferable.

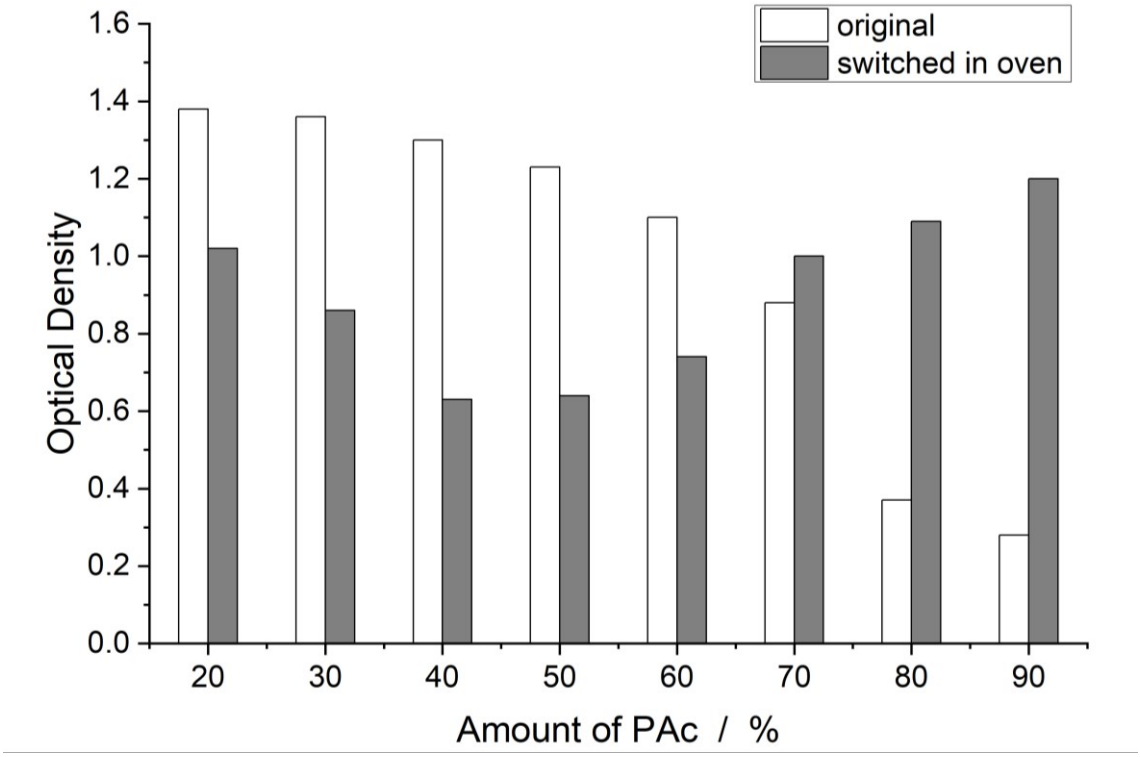

Figure 6.65: Optical densities of samples with different amounts of PAc in PVA coated on PET foil (30 µm gap height; 30 % solid content in coating formulations). The optical densities were measured in the initial and thermo-switched state (oven; 140 °C, 5 min).

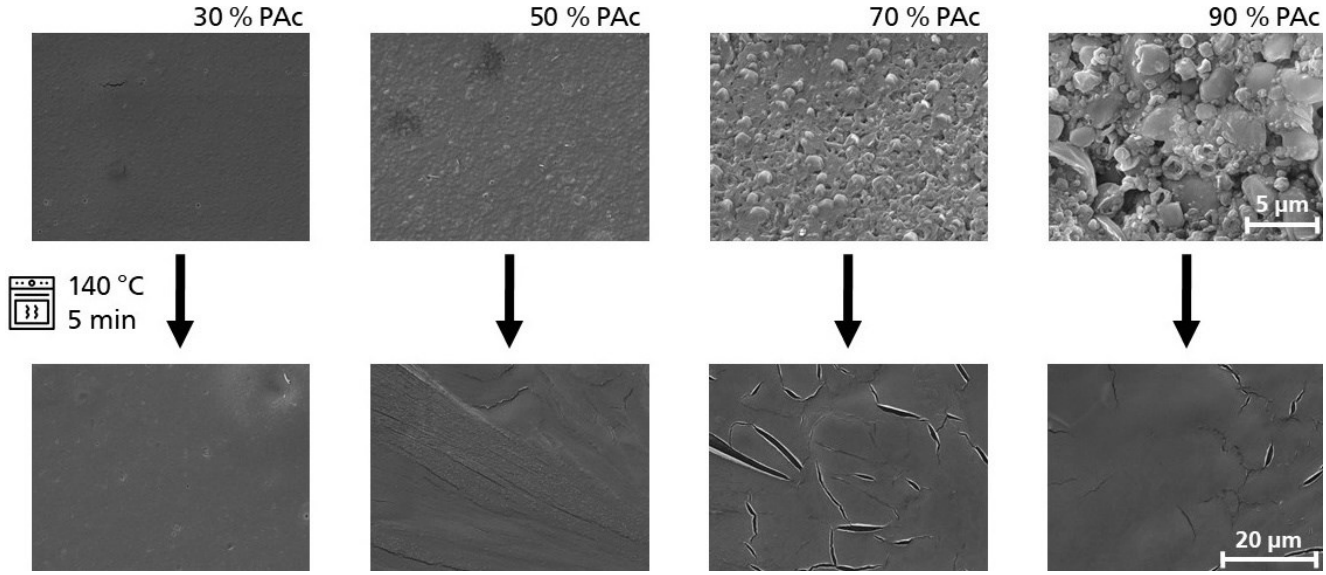

Figure 6.66: SEM images of samples with different amounts of PAc in PVA coated on PET foil (30 µm gap height; 30 % solid content in coating formulation). The surfaces are shown in the initial state (top row) and thermo-switched in the oven (bottom row).

A selection of SEM images is shown in Figure 6.66 which display the surfaces of the original films as well as the surfaces after they were switched in the oven. The particles of PAc are increasingly visible as the amount of fatty acid increases. As the PVA content decreases, the surface structure becomes significantly more porous as the film forming component is reduced. DSC measurements were performed

on the formulations to see if the increased particle shape had an effect on the melting temperature. However, the thermogram shows no difference in the melting temperature during the first heating cycle (see Figure 12.6). Air voids are formed between the particles and ring-shapes structures at levels above 70 %, reaching a maximum at 80 % PAc. The voids and the coarse structure are the reason for the low optical densities of these films. The light is scattered on these structures and the difference in refractive index between air and the fatty acid contributes to the scattering. The switched films show no trace of the particles, and at higher amounts of fatty acids, the films begin to delaminate from their substrate. This is due to the low amounts of PVA required for a stable film. However, delamination is an advantage for use as thermal paper. At these points, recrystallization is not possible, making printing irreversible.

6.2.5 Comparison and Conclusion of Coatings out of Aqueous Media on Model Substrates

The attempt to incorporate the eutectic mixtures investigated for their scattering effect in Chapter 5 into an aqueous formulation was not successful due to the different solubility behavior of the components. In the system of dimethyl oxalate and 9-ethylcarbazole, the DMO is the water-soluble component; in the system of benzoic acid and urea, it is the latter. Since the main goal is to develop a functional coating on an aqueous basis, no other solvent should be used. The limitation is that one of the mixing partners is dissolved in water together with the matrix polymer and the other is more or less coarse in the coating due to mechanical reduction. In this way, no enhanced scattering effect can be produced by the mixture in the coating, and the result is films that are almost completely transparent and cannot be thermally switched. The films in which (eutectic) mixtures of stearic and palmitic acids are melt-dispersed in PVA do not show a trend indicating a clear optimum in the mixtures. However, since the refractive indices also differ only minimally this is also unlikely.

The films, which are produced with the established system of polymer particles that scatter light due to a tailored specific diameter, result in coatings with high opacities. The use of tristearin for a better melting behavior and surfactants for a homogeneous coating surface leads to a better switching behavior compared to pure PS particles. But the fact, that the opacity is solely due to the porosity and the enclosed air makes the system very sensitive to liquids that can penetrate the pore structure. Attempts to anneal only the surface of the samples to obtain oil resistance were not successful. Therefore, this approach, as effective as it is, will not be pursued further.

The lack of opacity in the films with melt-dispersed paraffin wax can be explained, especially in comparison to the fatty acids, by the shape of the particles formed. The smooth spherical particles lead to low porosity only at 90 % wax content, resulting in the best opacity with an OD of only 0.6. Porosity increases as the amount of binder decreases. The fatty acids start to form ring-like, spherical and other fractal shapes as early as 70 %. Thus the roughness and then at even higher amounts the increasing porosity are the reasons for the good opacity with ODs up to 0.3.

The recrystallization of TS and wax leads to a strong haze after switching and decreases the contrast between the switched and original areas of the films. Both substances recrystallize in lager domains and lead to a cloudiness. Maximum contrast is required to achieve a good printing result. The recrystallization of fatty acids is not as strong and they stay finely dispersed in the PVA matrix. Therefore, it is assumed that a stabilizing effect of the matrix is necessary for a durable and high transparency. Although fatty acids are generally considered to be non-polar due to their long alkyl chain, the carboxyl group allows hydrogen bonds to be formed with the polar PVA matrix. The better miscibility and compatibility would then be the reason why no larger domains of wax are formed during thermal switching, which affect the transparency. However, the miscibility is also determined by the amount of fatty acid. If there is an excess of PVA, the formation of large fatty acid domains takes place, which in leads to an increase in opacity. Only with 70 % fatty acid, i.e. fatty acid in clear excess, opaque-transparent switching coatings are obtained.

The first printing tests with films coated on PET show that the substrate is not so well suited for printing. Transport in the printer is slower and the tested coatings showed significant abrasion on the print head. This is why the application of the coating formulations to paper is very important. Coated papers can be assessed for the thermal printing behavior of the coating.

6.3 Film Formation from Aqueous Dispersion on Paper

The use of paper as a substrate for the coating formulations is not only a step towards a realistic application scenario. The coating process, as well as the thermal switching, also differs significantly from the model PET substrate. Paper changes the drying process by removing the water from the coating, resulting in much faster drying. An even greater challenge is the paper's ability to absorb the crystalline substances as a melt during the printing or switching process in the oven. This removes the substances responsible for opacity from the system and leads to stable irreversibility. The synthetic and natural waxes paraffin wax, TS, PAc and SAc are used in this chapter. The new substrate is a base paper used for thermal papers with a grammage of 40 g m^{-2} and a black coating, which should be covered by the applied functional coatings. After opaque-transparent switching, the black paper should be visible again. The initial OD of the black paper is set to 1.39.

6.3.1 Paraffin Wax Dispersed in Polyvinyl Alcohol in a Paper Coating

Paraffin wax was melt-dispersed together with PVA dissolved in water using a disperser (experimental procesure e65, see 8.17). The formulations were coated on black paper using a film frame applicator. The solid content of the coatings was kept constant at 30 %. Examples of the films are shown in Figure 6.67. The optical densities, which quantify the opacity and thermal switching properties are plotted in Figure 6.68. At low amounts of wax the films are completely transparent. The high gloss results in optical densities higher than the black paper itself. A slightly opaque coating with an OD of 0.68 can only be achieved with 90 % wax. However, even here the coating is inhomogeneously cloudy. Furthermore, when switching the samples in the oven, switching from opaque to transparent is also only achieved with 90 % wax. For lower percentages, switching only results in a lower OD. The results are similar to those obtained on PET. Since the same formulations were coated on PET, the particle sizes are the same as those obtained in section 6.2.2.

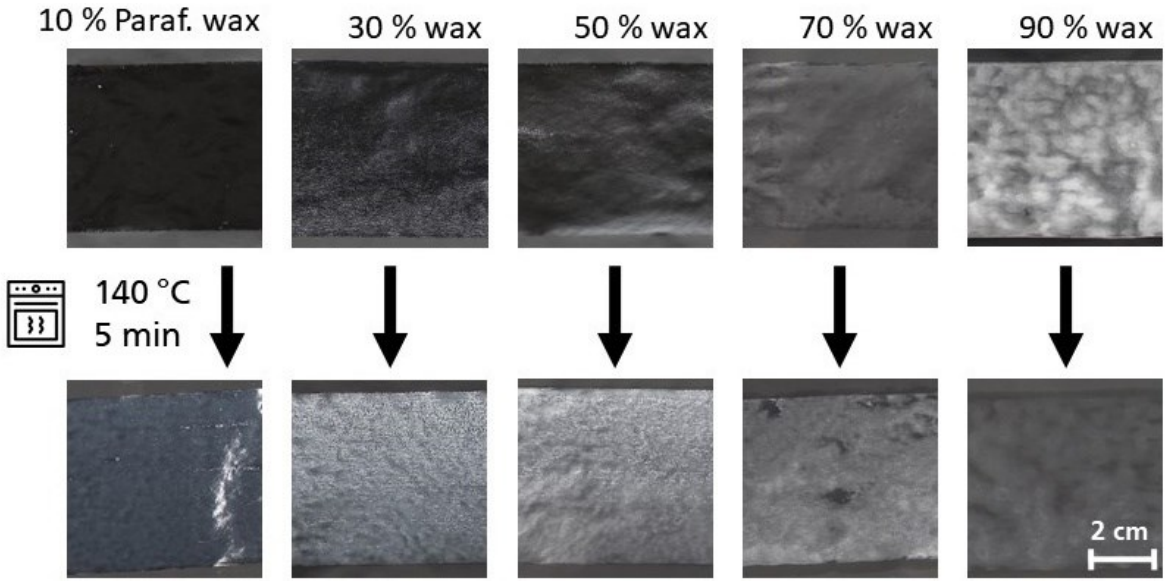

Figure 6.67: Pictures of samples with different amounts of paraffin wax in PVA coated on paper (30 µm gap height; 30 % solid content coating in formulations). The films are shown in the initial state (top row) and thermo-switched in the oven (bottom row)(e65).

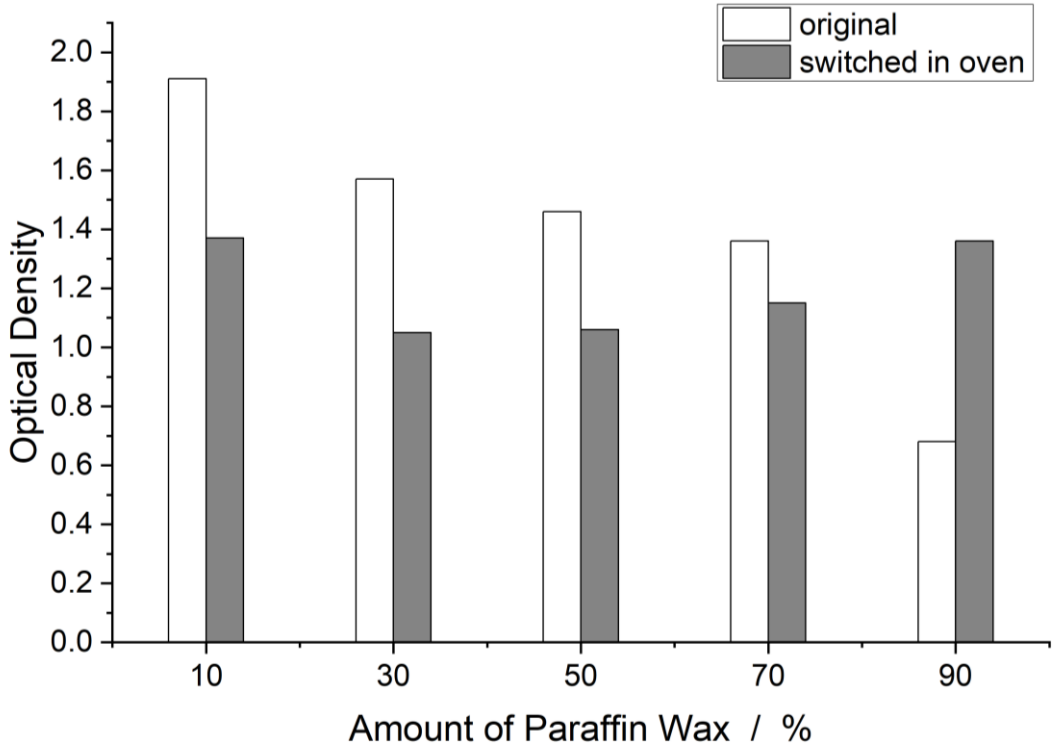

Figure 6.68: Optical densities of samples with different amounts of paraffin wax in PVA coated on paper (30 µm gap height; 30 % solid content in coating formulations). The values of the films in the initial and thermo-switched state (oven; 140 °C, 5 min) are plotted.

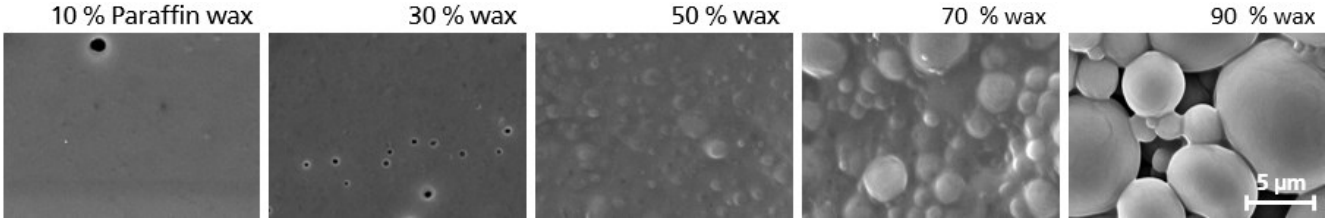

Figure 6.69: SEM images of samples with different amounts of paraffin wax in PVA coated on paper (30 µm gap height; 30 % solid content in coating formulations).

The reason for the opaque film that only forms at 90 % growth, can be seen in the SEM images (Figure 6.69). At 50 % wax, the particles become visible on the film surface and increasingly emerge from the covering layer as the amount of wax increases. At 90 % wax, the amount of PVA is so low that the wax particles are not completely embedded in a matrix. The resulting voids between the particles are up to 10 µm in size. These structures create a scattering effect that leads to the opaque layer. The optical densities achieved and the switching behavior are not in the targeted range. Therefore, these coatings were not further investigated and work continued with TS in PVA.

6.3.2 Tristearin Dispersed in Polyvinyl Alcohol in a Paper Coating

The same formulations and the same film frame applicator as in section 6.2.2 were used to form the coatings on black base paper for thermal papers (experimental procedure e66, see 8.18). 70, 80 and 90 % of TS in PVA were coated, since the smaller amounts do not form opaque films. The samples coated with a gap height of 30 µm are shown in Figure 6.70. The films show increased opacity as the amount of TS increases in the coating formulations. The switched samples have a slightly glossy but transparent appearance. The optical densities of the initial, switched in the oven and thermoprinted samples are plotted in Figure 6.71.

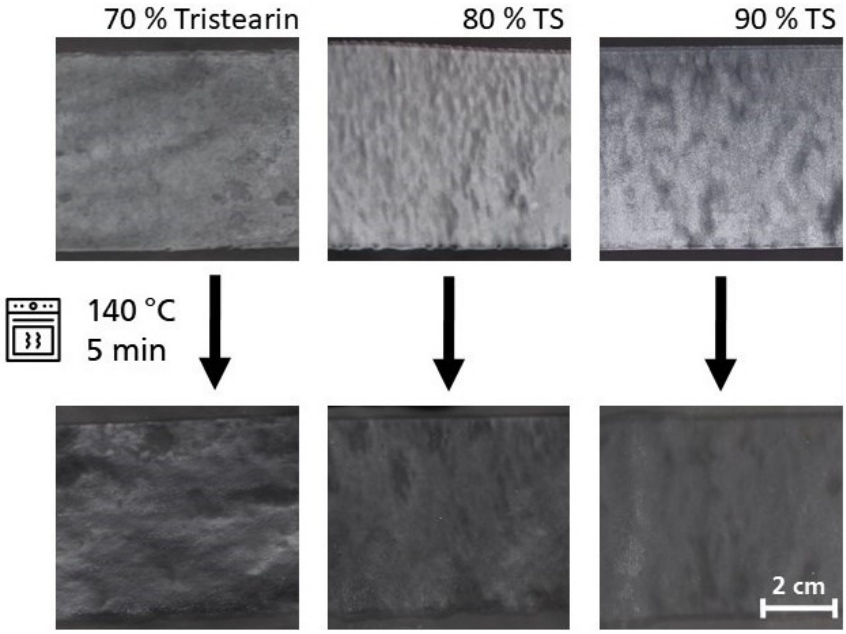

Figure 6.70: Pictures of samples with three different amounts of TS in PVA coated on paper (30 µm gap height; 30 % solid content in coating formulations). The films are shown in the initial state (top row) and thermo-switched in the oven (bottom row)(e66).

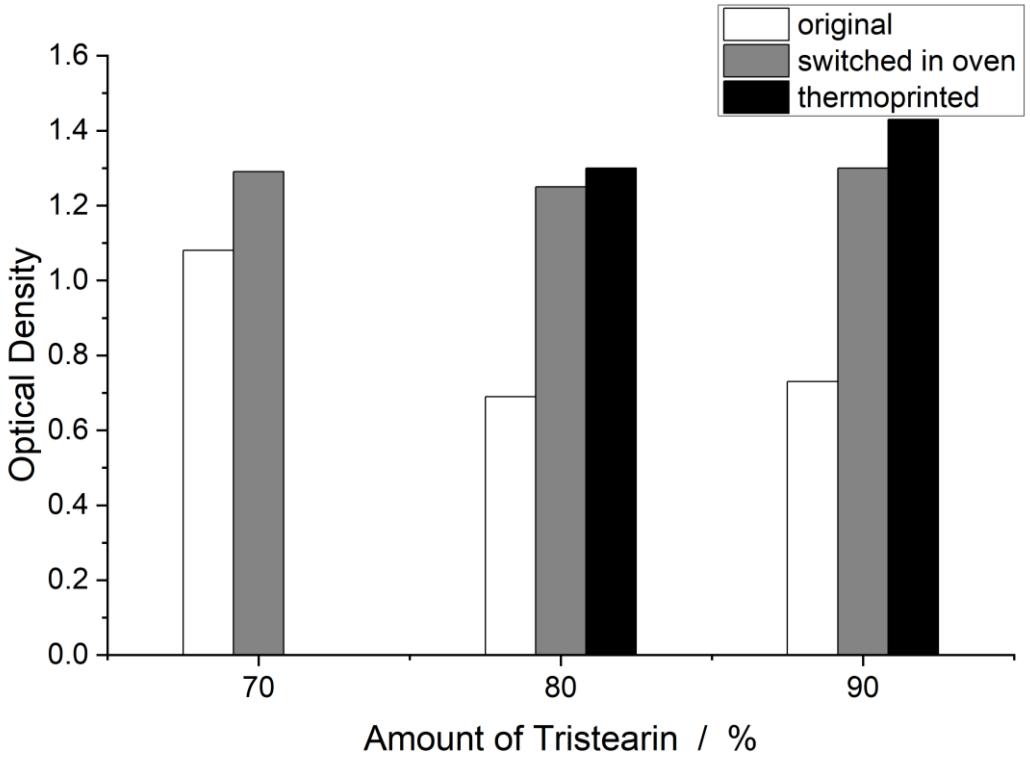

Figure 6.71: Optical densities of samples with three different amounts of tristearin in PVA coated on paper (30 µm gap height; 30 % solid content in coating formulations). The original, switched in the oven (140 °C, 5 min) and thermoprinted samples were measured.

The OD decreases from 70 to 80 % and stays almost the same with more TS added. The switched samples are all in the same range, while the samples that were also thermoprinted have a slightly higher OD. Still, the initial ODs of about 0.7 are still too high for a good opacity. The desired value of approx. 0.5 was not achieved. Figure 6.72 shows the thermoprinted sample of 90 % TS in PVA. The print is very washed out and the textures are bleeding. Other areas, such as the font, were not printed. This may be a sign of an inhomogeneous coating, as the blurred print clearly shows that the coating even switches a bit too early.

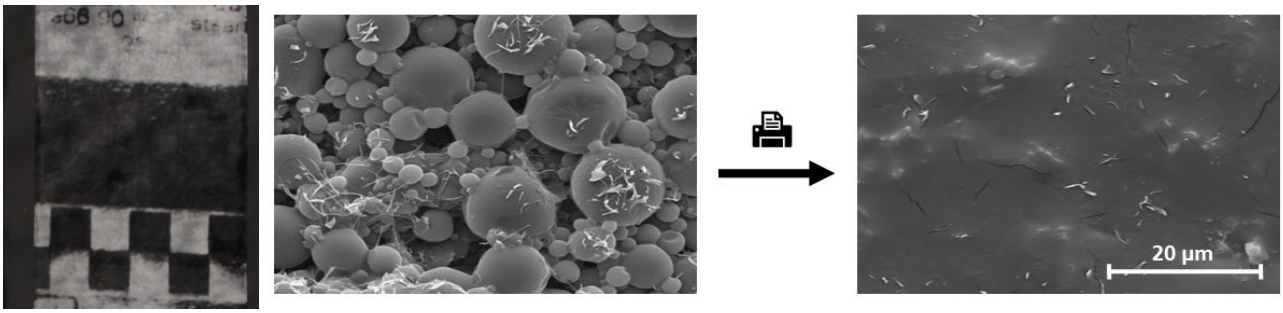

Figure 6.72: Photo (left) and SEM images of a samples with 90 % TS in PVA prior (center) and post thermoprinting (right). The sample is coated on paper (30 µm gap height; 30 % solid content).

The SEM images of the thermoprint (Figure 6.72) show the porous structure of the films with 90 % TS. After printing, a fairly homogeneous layer is present. The air-filled pores and the particles are fused.

Only some filamentous TS crystals are visible. However, this does not affect the transparency of the films. Since a satisfactory OD was not achieved with these coatings, fatty acids are used in the next section as a crystalline substance in the polymer matrix.

6.3.3 Fatty Acids – Various Mixtures Dispersed in Polyvinyl Alcohol in Paper Coatings

The different mixtures of SAc and PAc are coated on paper in the same formulations as used in section 6.2.4 on PET (e47, see 8.15). The fatty acid content is always 70 % and the solid content of the formulations is 30 %. The film application frame is again used as coating technique. In Figure 6.73, the films coated with a gap height of 15 µm are shown after thermal printing. The smaller gap was chosen because the thicker films switch significantly worse than the thinner ones during thermal printing.
The films with pure PAc have a white appearance, while the addition of SAc results in almost transparent films. This may be due to the strong crystallization behavior of PAc that was observed with the phase contrast microscope (section 5.4). Only mixtures with 30 % SAc have a good opacity, which is maintained up to 60 %. With higher amounts of SAc, the films become more transparent again. This can also be seen in the optical density values (Figure 6.74). The most opaque films have an OD of 0.29 to 0.47, which is in the target range. The ODs of all films with different gap heights of 15 to 30 µm are shown in the Appendix Figure 12.8. These films support the findings of Chapter 4: the advantage of a eutectic mixture per se cannot be found, but mixtures in general can increase the scattering in compared to the pure substances. However, the switched films show ODs below 1.0, which is clearly too low to produce a satisfactory print contrast.
To see at what temperature the films switch, temperatures below the standard switching temperature of 140 °C were also used. The films were also annealed at 100 and 120 °C for 5 minutes and the optical density was determined (Figure 6.74). The three temperatures differ only slightly in the ODs after switching.

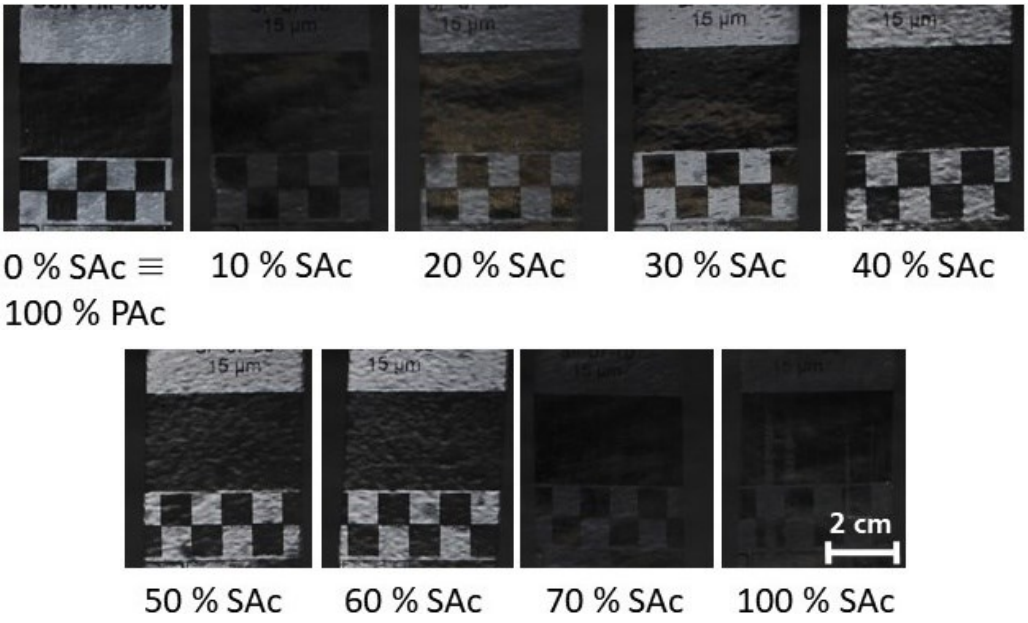

Figure 6.73: Pictures of samples with 70 % fatty acid in PVA. The composition of the fatty acid varies throughout the samples. This is described by the amount of SAc in the fatty acid mixture. The films were coated suing a film frame applicator with a gap height of 30 µm (30 % solid content of coating formulations). The films were thermoprinted using a standard thermoprinter (e47).

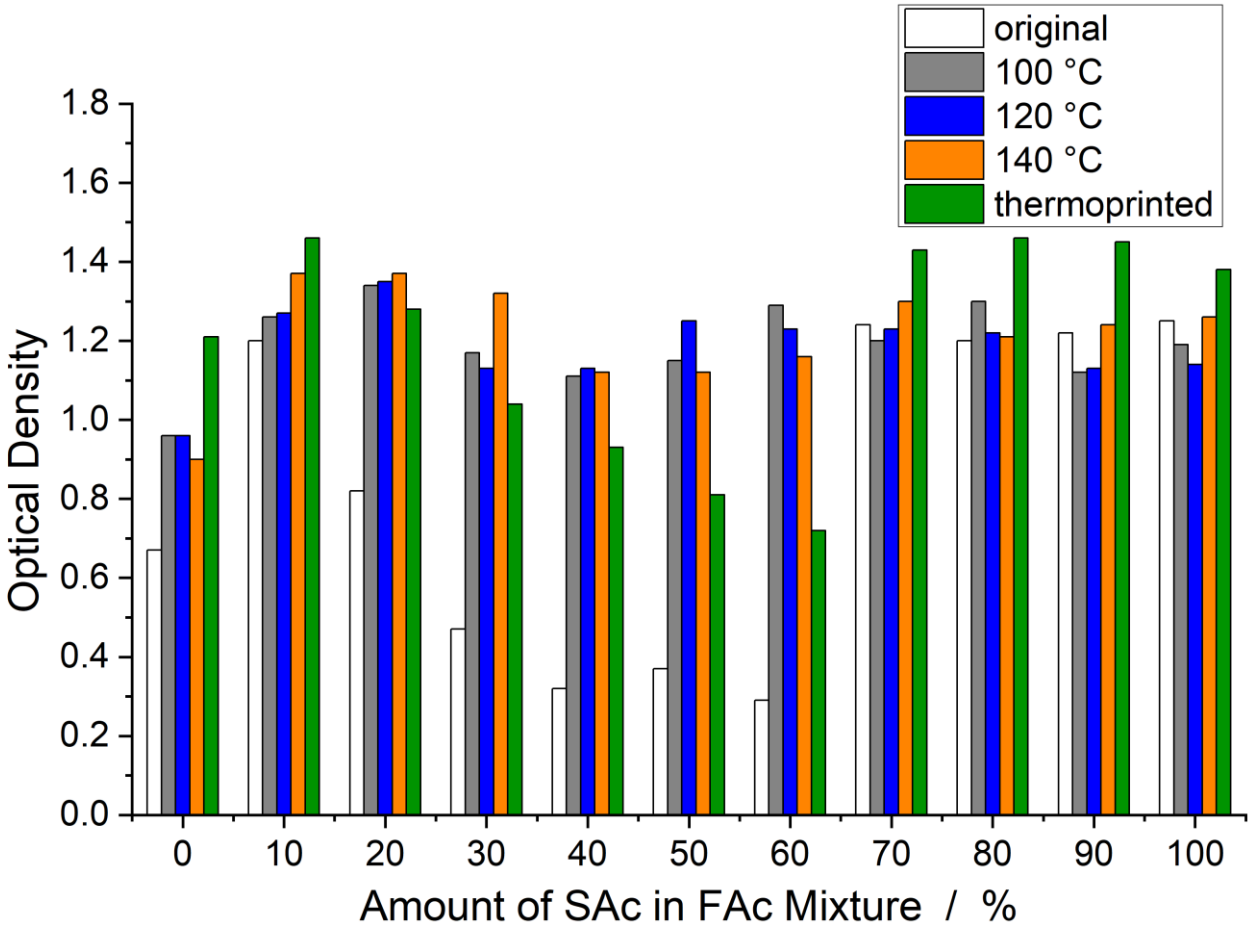

Figure 6.74: Optical densities of samples out of 70 % of fatty acid in PVA. The composition of the fatty acids is varying. The films were coated on black paper with 30 µm gap height. The papers were switched at different temperatures (100, 120 and 140 °C) to find out about the starting temperature for the optical switching. Additionally, every film was thermoprinted and the OD of the printed area is measured.

The eutectic range was found to be between 40 to 80 % SAc in the fatty acid blend in the DSC measurements. The findings observed thus seem not to be correlated to a eutectic mixture. The same formulations that were coated on PET did not show these extreme differences in OD. The question is if the amount of fatty acid shows also completely different results on paper as they do on PET foil. So the formulations with different amounts of PAc (experimental procedure e64, see 8.16) were also coated on paper using the film frame applicator (30 µm gap height). Exemplary films are displayed in Figure 6.75, the optical densities of the original, switched in the oven (at different temperatures) and thermoprinted samples (30 µm gap height) are plotted in Figure 6.76 (ODs of all samples with different coating thicknesses in Appendix Figure 12.9).

Figure 6.75: Pictures of samples with different amounts of PAc in PVA. The coatings with a solid content in the formulations of 30 % were coated on paper with a film frame applicator. The displayed images were coated with a gap height of 30 µm) (e64).

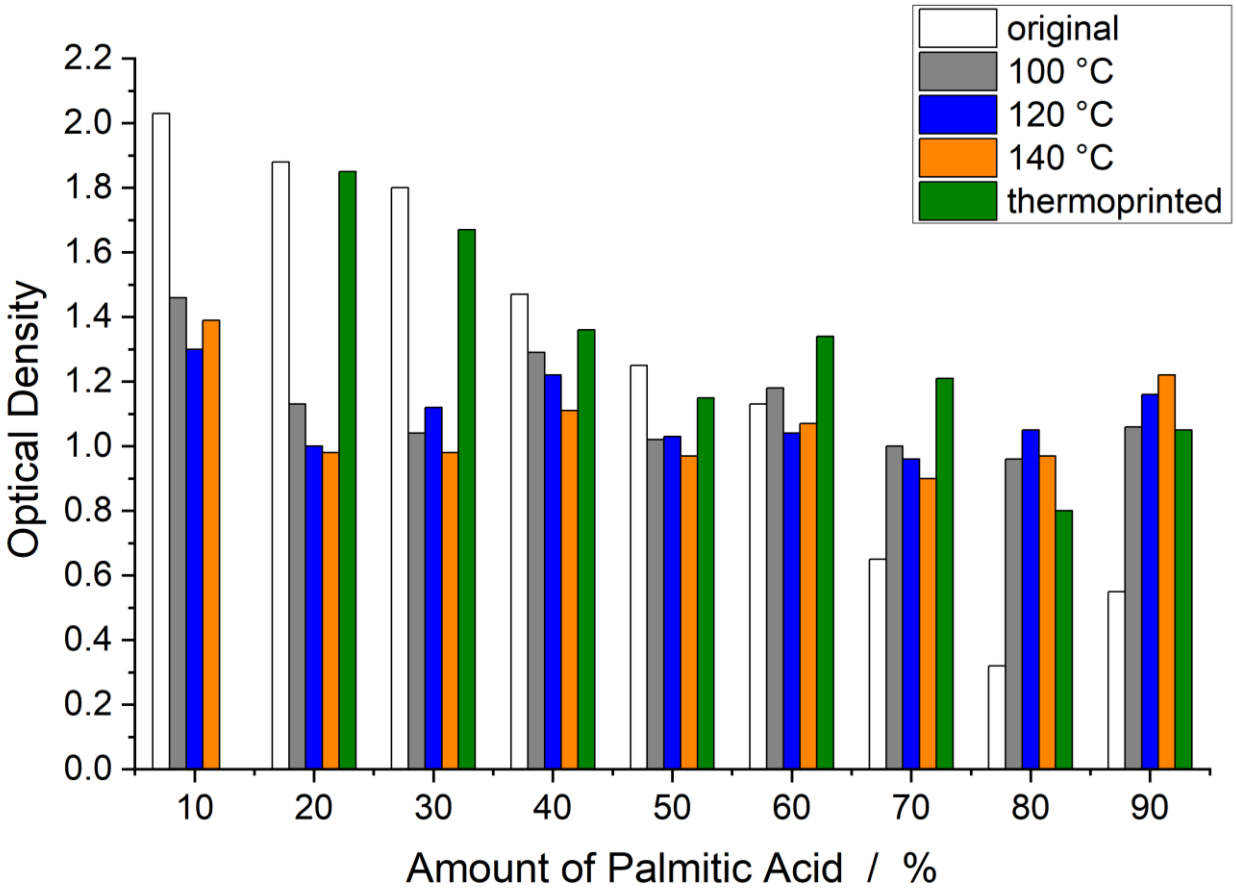

Figure 6.76: Optical densities of samples with different amounts of PAc in PVA (30 % solid content of coating formulations, gap height of film frame applicator 30 µm). The samples were measured in the original state, switched at 100 °C, 120 °C and 140 °C as well as thermoprinted. 10 % PAc showed no print and was therefore not measured.

The samples start to show a good opacity starting at 70 % of PAc (OD=0.65) and the lowest value of OD at 80 % PAc (0.32). This corresponds to an almost pure white film. The temperatures at which the coatings were switched were varied from 100 to 140 °C. All temperatures lead to comparable results in light grey papers with ODs of 1 to 1.2. The graph of the optical densities also includes the values of the same 30 µm films in the thermoprinted state. But the printed areas are blotchy and inhomogeneous, whereas the films that were coated with the smallest gap height of 15 µm show good thermal printing results. The 15 µm thermal printed samples are shown in Figure 6.77 and the corresponding optical densities are shown in Figure 6.78.

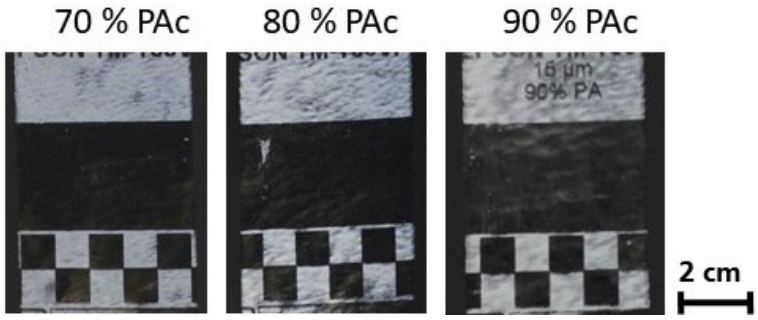

Figure 6.77: Images of thermoprinted samples with 70, 80 and 90 % of palmitic acid (30 % solid content in coating formulation; film frame applicator with 15 µm gap height).

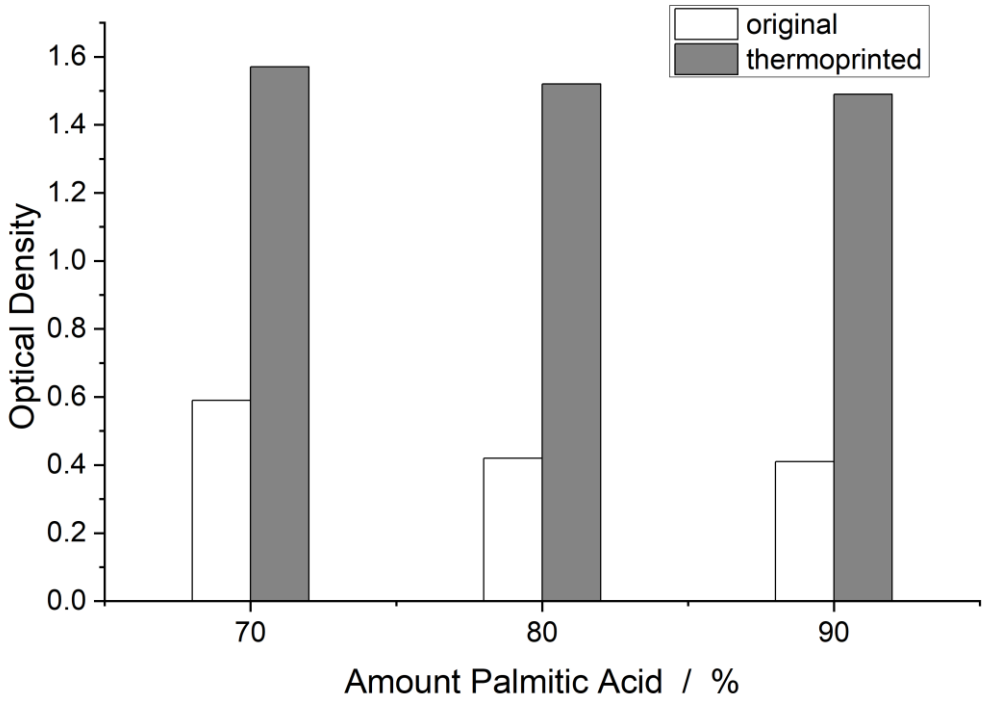

Figure 6.78: Optical densities of samples with different amounts of PAc in PVA. The samples were coated on black paper using a film frame applicator, gap height 15 µm, 30 % solid content in coating formulations.

With the smaller gap height, the optical densities of the films with 80 and 90 % PAc are almost identical in the original (0.42; 0.41) and in the thermoprinted state (1.52; 1.49). The optical densities obtained are within the target values and show a good contrast, which is necessary for a good readability. Test

prints were then made with the thermal printer to see if any deposits had formed on the print head as a result of printing the samples. The prints show no streaks, and the samples themselves show no compression in the print image compared to the normal printouts with standard thermal paper, which would also be a sign of adhesion to the print head. Figure 6.79 shows SEM images of the 70 % PAc thermoprinted sample. On the left side the printed number “29” is visible. The images on the right show the films in the original and printed states in a higher magnification. The ring-like structures of the scattering coating are completely destroyed and a film is formed that starts to delaminate from the base paper by showing many cracks in the surface. This is a good sign in terms of irreversibility, but the effect of the delaminating film on the printer needs to be investigated. The coating must not adhere to the print head during the printing process. This will result in a compressed print image and will shorten the lifetime of the printer.

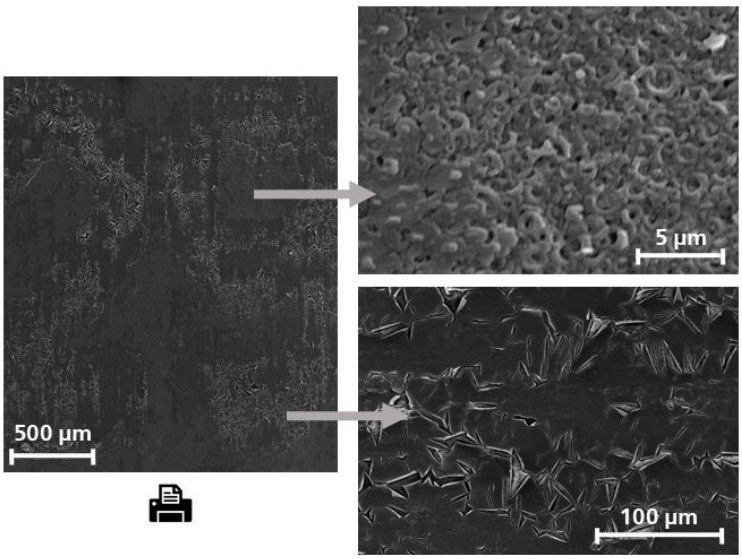

Figure 6.79: SEM images of thermoprinted sample with 70 % of PAc (30 % solid content in coating formulation; film frame applicator with 15 µm gap height). Displayed is an overview of printed numbers (left) the initial surface (top right) and a thermoprinted area (bottom right).

Another important quality factor for a thermal paper is the stability of its optical properties during storage. The papers must remain stable for years at room temperature and under dry conditions. No long-term measurement were carried out, but the films were artificially aged at an elevated temperature of 50 °C for 24, 48 and 62 hours. After each time, the optical density of the films was determined. The results are shown in Figure 6.80. As expected, the optical density should be constant in the best case, because it is assumed that there are no changes in the shape and surface structure of the coating. In the worst case, the OD increases, because parts of the coating start to deform. Looking at the OD of the films, we can see the effect of the deterioration of the opacity at 10 % PAc (OD + 0.1). The duration of storage does not play a major role. At 40 to 60 % PAc, the OD even decreases. Of course, coatings with 70 to 90 % PAc are particularly interesting, because they show a good initial opacity. Fortunately, the optical densities remain relatively stable with changes of less than 0.1. It can therefore be said that the PAc and

PVA films remain stable at 50 °C. However, in order to speak of good stability, the influence of UV light on the films would also have to be studied. These aging tests were not performed in this thesis.

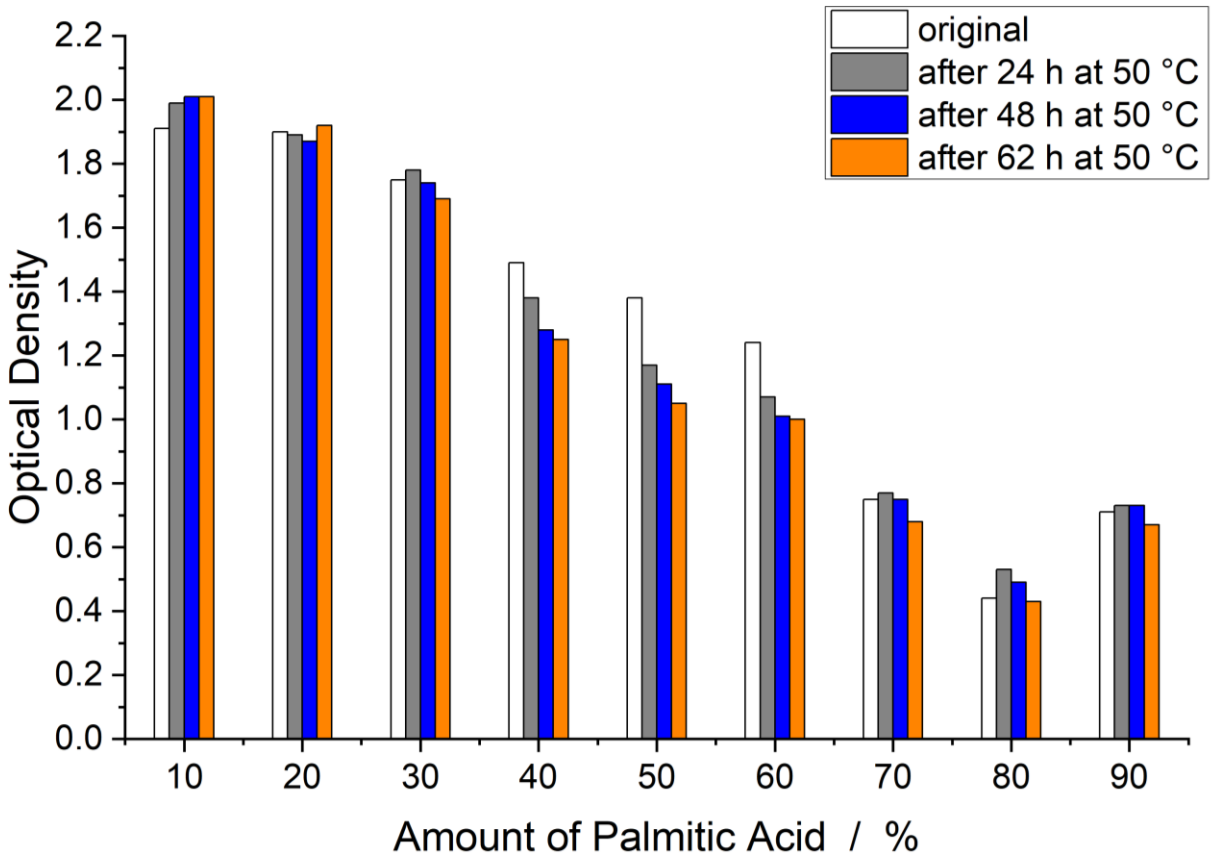

Figure 6.80: Optical densities of samples out of different amounts of palmitic acid in PVA. The films were stored at an elevated temperature of 50 °C for 24, 48 and 62 h. The films were coated on paper using a film frame applicator with a 30 µm gap height (solid content of coating formulation is constant at 30 %).

Since the films perform well in their switching behavior, a test was carried out to determine their stability against water and oil. A droplet of water and an oil droplet were deposited on the samples with different amounts of PAc, as shown in Figure 6.81. It can be seen that water only slightly reduces the opacity of all samples and that the water droplet remains on the film surface. As the water dries after a short time, the original opacity is restored. The oil droplet on the other side immediately spreads on the paper and into the coating of the samples. However, the film with 70 % PAc has a slight advantage: since the coating is less porous (see SEM images of the films, Figure 6.66), the oil takes longer to penetrate into the film and some of the opacity remains. In order to choose a more oil resistant film, a compromise in the initial opacity would have to be made.

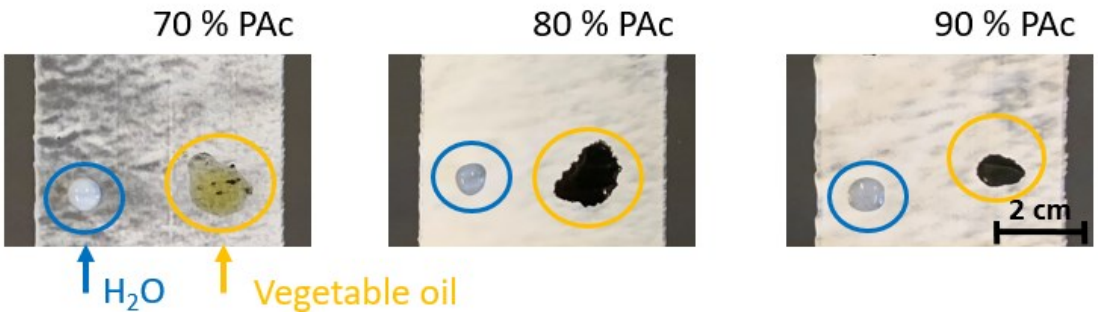

Figure 6.81: Pictures of samples with different amounts of PAc in PVA coated on paper. Water (blue circled) and oil (yellow circled) droplets were put on the surface to see if the liquid interferes with the opacity of the coatings. The films were coated on paper using a film frame applicator with a 30 µm gap height (30 % solid content of coating formulation).

Since the films formed with the film frame applicator always produce a more or less patchy film, another technique is used to coat the papers: a rake rod with a wet film application of 16 µm at the same coating speed (3 m/min). The rod creates much more homogenous coatings, with only small streaks due to the wire sheathing of the rod. Coatings formulations were used that have previously resulted in films with good opacities: 70, 80 and 90 % PAc in PVA. The resulting films are displayed in Figure 6.82. In Figure 6.83, the optical densities of the samples coated with the rake rod and the film frame applicator are compared.

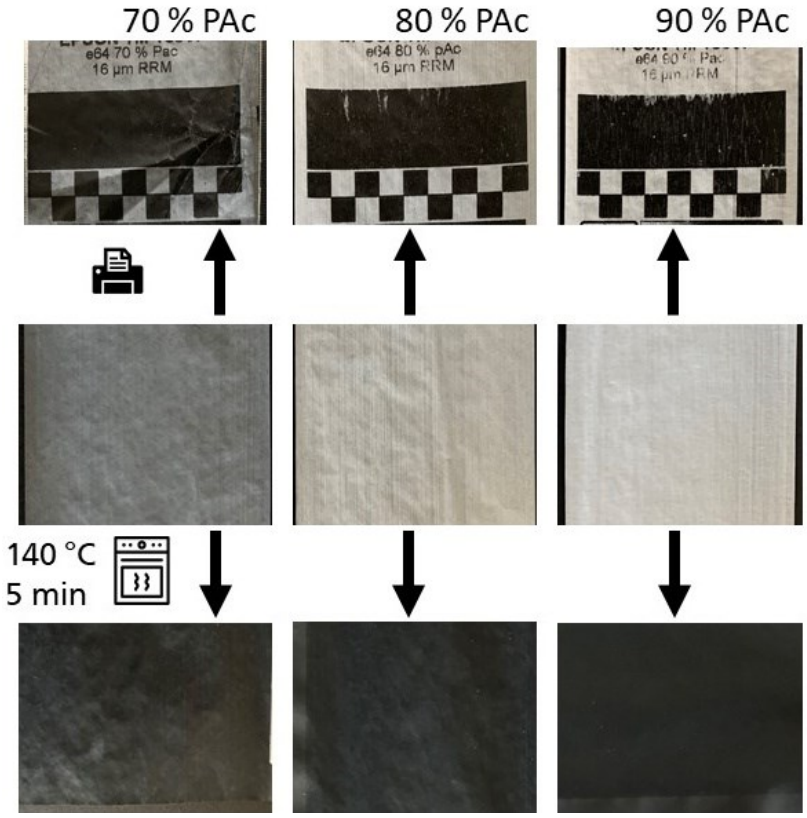

Figure 6.82: Images of samples with different amounts of PAc melt-dispersed in PVA. The coatings were applied with a rod rake (wet film application 16 µm; 30 % solid content in the coating formulations). Displayed are the initial (center row), thermoprinted (top row) and switched in the oven (bottom row).

The papers have a much more homogeneous coating and only small stripes are visible due to the wire sheathing of the rod. The opacity decreases at 80 % PAc and then remains constant. The films show no difference in the oven-switched state, but the quality of the thermoprinted samples is different from the samples that were coated with the film frame applicator. The rake rod is 1 µm thicker in wet application, resulting in approximately 0.3 µm thicker dried coatings. Although the coating is more homogeneous, the thermoprinted samples show some disadvantages compared to the samples coated with the film frame applicator (see Figure 6.77). There are large white areas in the printed areas and the lettering is not as clear.

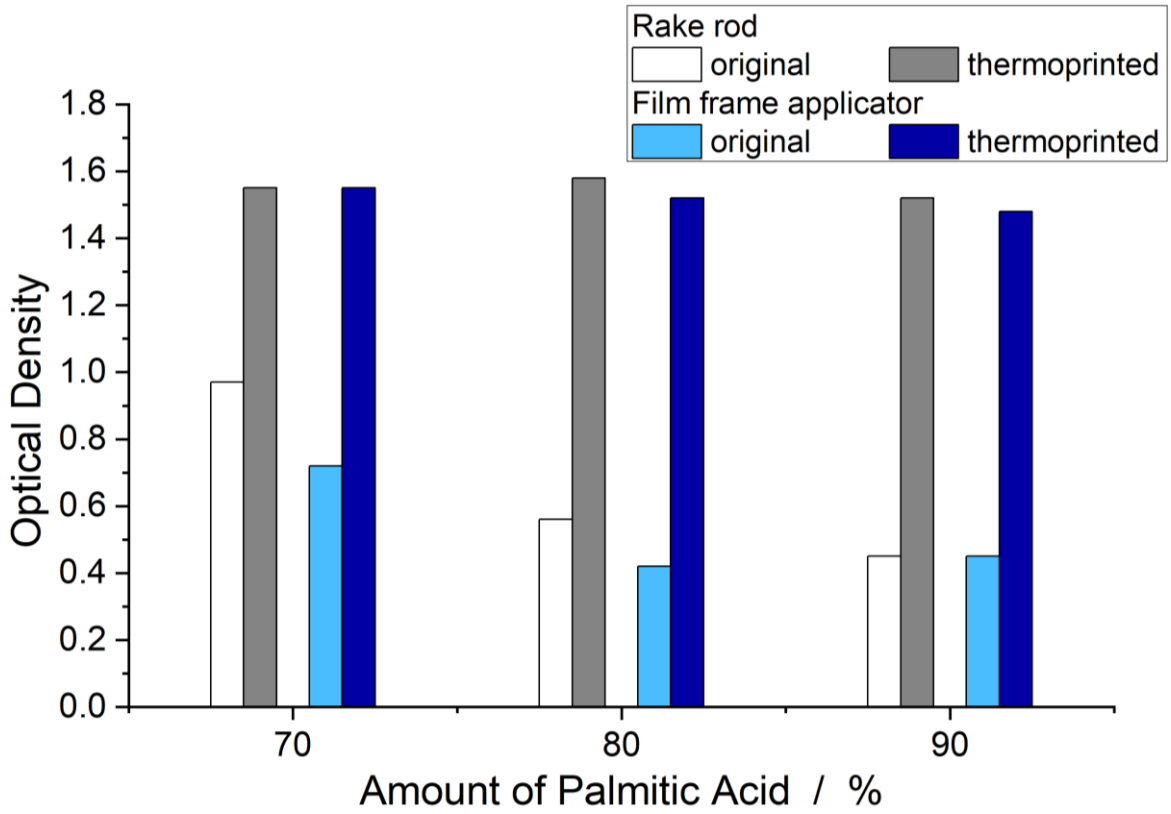

Figure 6.83: Comparison of the samples out of different amounts of PAc in PVA, coated with a film frame applicator (15 µm wet film application) and a rake rod (16 µm wet film application); both in the original and thermoprinted state.

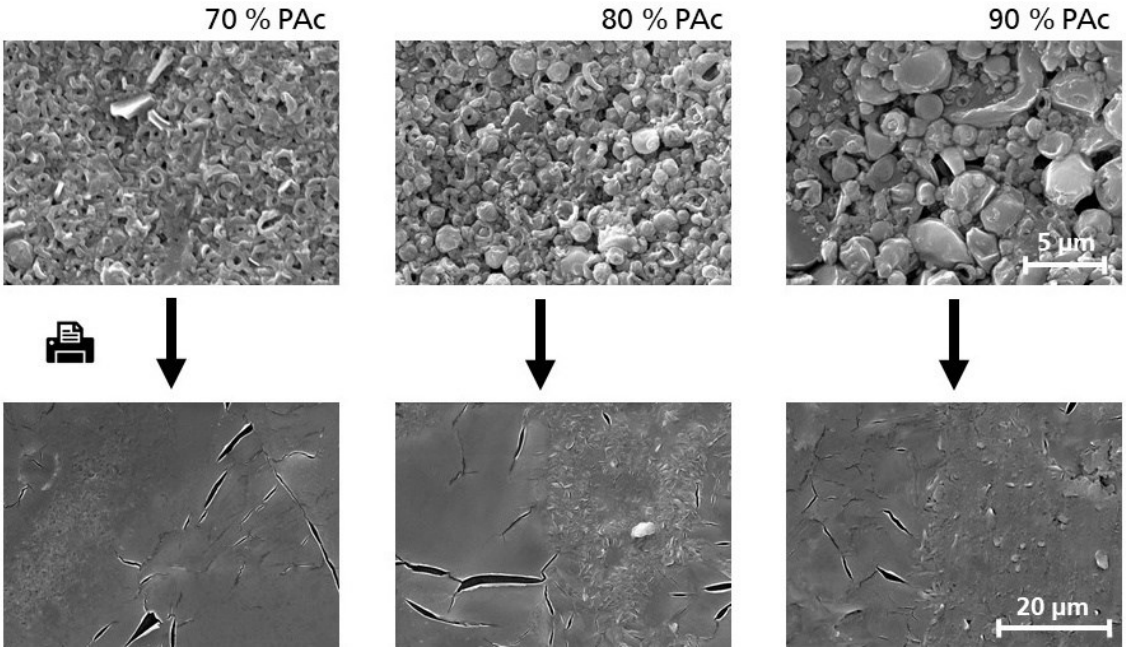

Figure 6.84: SEM images of thermoprinted samples with different amounts of PAc melt-dispersed in PVA. The coatings were applied with a rod rake (wet film application 16 µm; 30 % solid content in coating formulations). Top row: initial film/unprinted area, bottom row: printed area.

The SEM images (Figure 6.84) show that the structure becomes rougher and more porous as the amount of PAc increases, which goes hand in hand with the decreasing amount of PVA. At 70 % PAc, mainly ring-shaped particles are seen, while at 80 % spherical particles are added. At 90 % there is a very coarse mixture of large spherical and pellet-shaped particles. In the printed state, the typical delamination can be seen, but in all blends there are also small areas where the previous coarse structure can still be recognized.

6.3.4 Comparison and Conclusion of Melt-Dispersed Waxes in Polyvinyl Alcohol on Paper

The step from model film to paper is very important in the development of thermal papers. The altered drying processes change the opacity of the coatings compared to PET, and when switching, the aspect that the paper can remove excess wax from the system is a major influence and supports irreversibility. The biggest advantage of using paper, however, is that it allows the ultimate test for coatings to be used as the functional layer for thermal papers: the thermoprinting itself. The results show that the annealing in the oven results in different optical densities than the thermoprinted ones.

For any system of melt-dispersed wax particles, only porosity combined with rough surface structures can produce an opaque layer with optical densities below 0.6 (at film thicknesses below 10 µm). Without air entrapment and crystallites or particles in a closed film, only slight opaque coatings with OD values around 1.0 could be obtained.

Under constant melt dispersion conditions, the particle size of all the waxes studied, i.e. paraffin wax, TS and fatty acids, increases with increasing wax content in the mixture. This is due to the decrease in stabilizing emulsifier, PVA.

Due to the small layer thicknesses and the porosity of the opaque films, there is still the major disadvantage that no resistance to penetrating liquids or pressure can be achieved. The oil resistance test shows that there is a trade-off between durability and opacity. However, since the focus is on opacity and thermal switching, resistance must be compromised.

In terms of switchability and optical densities, PAc in particular performs well at amounts of 80 and 90 % with an optical density contrast greater than 1.0. The high contrast is due to the mixture of spherical, ring and fractured particles that create a coarse surface. The printability is very good and the OD of the printed films is much higher than that of the base paper, as they have a gloss which increases the contrast for the human eye. The printed areas shows delaminates from the base paper in microscope images. This promotes irreversibility, as recrystallization of the fatty acid is no longer possible.

Figure 6.85 shows the proposed melting mechanism of melt-dispersed waxes in polymer. HOTTA and TSUTSUI focused only on fatty acids and how the particles react to thermal influences, since their goal was to create particles that would scatter light or be transparent at room temperature, depending on the thermal treatment to which they were subjected (for use in reversible recording media). The proposed mechanism also takes into account the nature interactions of different polymers and waxes.

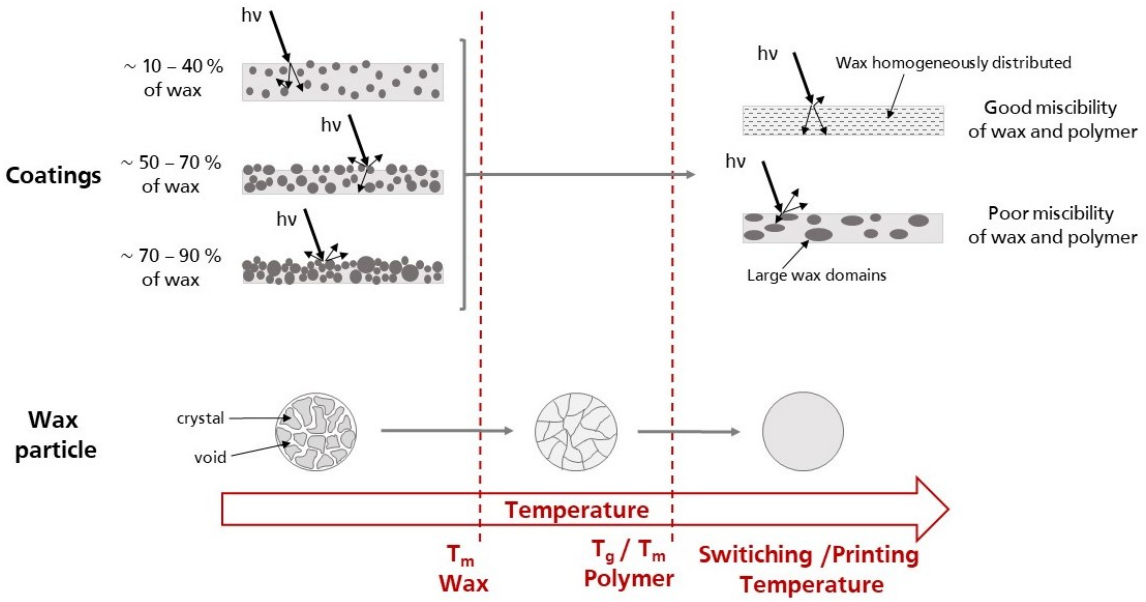

Figure 6.85: Proposed mechanism of melt-dispersed waxes in a polymer matrix during the switching in the oven or thermoprinting. The processes are dependent on the amount of wax and of the miscibility of the wax with the polymer. It is also proposed that the wax particles form air voids after melt dispersion.

In the coating the main factor for a good opacity is a maximum of phase boundaries of different media, which are the polymer, the wax and most importantly, the air. Depending on the amount of wax in the

coating, the amount of air in this construct is increased and the opacity is at its maximum. In the switched state the miscibility of wax and polymer plays an important role in achieving: if the miscibility is poor, large domains of wax are formed, resulting in a film that still scatters light. The amount is independent on the size of the domains.

In addition, the wax particles undergo a change in their state as shown schematically in the lower part of Figure 6.85: TSUTSUI et al.[63] propose that the light scattering bodies consist of polycrystals of the wax and air voids. This occurs when the crystallization takes place below T_g of the polymer because the volume change is associated with the crystallization of the wax. This is always the case with the combinations of paraffin wax, tristearin and fatty acids with polyvinyl alcohol in the previous shown coatings.

7 Summary and Conclusion

The objective of the thesis was to investigate and develop opaque-transparent thermally switchable thin films based on crystalline substances in polymeric matrices. The films were formed from organic solvents or water and were coated on model substrate or paper. In particular, the aim was to find a formulation based on crystalline substances that leads to an opaque film that is capable of covering a black substrate and is irreversibly thermally switchable to a transparent state. In the course of the work, promising substances and systems capable of forming opaque films were found. The quality of the film formation was also generally improved in order to obtain homogeneous coated substrates.

Research questions were posed in Chapter 3. The answers to these questions are used to summarize the findings of the thesis:

1. *Can a eutectic system be used to have an increased scattering effect in binary mixtures of crystalline substances?*

First, binary eutectic mixtures were investigated to find out whether the eutectic structure could enhance the scattering behavior compared to the pure crystalline substances of the eutectic system. The idea was that a mixture of substances with a large difference in their optical density can achieve a maximum scattering effect. Therefore, two binary organic eutectic mixtures were studied in detail. Test specimens of the melts between glass and shim rings were successfully measured in a spectrophotometer. With the measured scattering parameters, the scattering factors of the eutectic mixtures and the pure substances was determined using the Kubelka-Munk theory. For the two eutectics studied, dimethyl oxalate with 9-ethylcarbazole and urea with benzoic acid, differences in scattering were found between the respective mixtures and the pure substances. But the eutectic composition did not show a prominent scattering effect in either system. However, the eutectic composition did not show a significant scattering effect in either system. Therefore, it can be concluded from these measurements that mixtures in general can show an increased scattering effect compared to their pure substances. The eutectic mixtures studied either do not show an increased scattering effect or show an increased scattering effect that is smaller than the experimental error of the setup. An alternative sample preparation could decrease the influence of the setup. Alternative to the glass cover, the melt could be formed in a frame with a defined height and the surface could be carefully polished. The use of the investigated eutectic systems in coating formulations proved to be difficult because of different solubility properties. It would be worthwhile to further study the optical properties of organic eutectic systems. In this way, their interesting and practical thermal properties coupled with their optical properties could be used for potential applications in the future.

1. *What is the best strategy for introducing crystalline substances into a thin layer polymer matrix?*

Subsequently, films were formed on a model surface, on PET foil from organic solvent. The PET foil was used because it has very good coating properties and is dimensionally stable at the temperatures for thermal switching. It is used to minimize the influence of the substrate on the properties of the coating to a minimum, since paper can influence the formation of the films due to its inhomogeneous surface and the drying process due to the capillary effect. The polymers that were tested in their function as organic solvent-cast matrix material were PS, PLA and PCL. They were selected on the basis of their polarities as well as their thermal properties (T_m and/or T_g).

Some interesting formulations were coated on the substrate, which showed promising results in thermal switching. In particular, the films of polystyrene and tristearin from THF show that from a mass ratio of 50 % TS, the surface crystallization of the wax changes from the previously milky films to white, strongly scattering films. However, the switched samples all show a similar OD around 0.9 to 1.0 which is not within the target values (target OD > 1.3). The difference in OD between the original and the switched films increases from 70 % up, creating a high contrast that is easily perceived by the human eye. Compared to the PLA and TS samples, the PS/TS coatings have higher opacities, especially at lower amounts of TS. The optical density measurements together with the sample images suggest that the high opacity is formed by the TS molecules on the surface and not by the molecules dispersed in the polymer matrix itself. Therefore, only films that have these TS structures on the surface can exhibit a switching behavior, because heating/switching of the films results in mobilization of the matrix and the melting of the TS. The wax is dispersed into the matrix and is fixed to form the new matrix along with the polymer when the film is rapidly cooled. This way, the optical density of the switched state does not depend on the amount of TS in the coating. The amount of TS only affects the formation of the film from the organic solvent and the formation of the specific porous topology that leads to the scattering of light and hence a remarkable opacity. It was also possible to improve the resistance of the films to oil. The surface of the films was sintered using UV light to modify the crystalline structure and consequently the surface porosity. As a result, the absorption of oil, which leads to loss of opacity, was significantly reduced. An optimum was found between loss of opacity and improvement of oil resistance at 20 m/min belt speed of the laboratory dryer.

But to develop a coating for paper, the formulation had to be a) based on an aqueous solution and b) work on paper. So the first step was taken and the formulations were changed to water as the solvent. In these formulations, PVA was used as the polymeric matrix, which is the most widely used binder in the industry. With PVA, mainly natural and synthetic waxes were used in the formulations as dispersed particles prepared by melt dispersion. With any system of melt-dispersed wax particles, it can be seen that only when porosity is combined with coarse or porous surface structures can an opaque layer be achieved with optical densities lower than 0.6 (at film thicknesses below 10 µm). Without air entrapment

and crystallites or particles in a closed film, only slightly opaque coatings with OD values around 1.0 can be obtained. Under constant melt dispersion conditions, the particle size of all waxes studied, i.e. paraffin wax, tristearin and fatty acids, increases with increasing wax content in the mixture. This is attributed to a decrease in the amount of the binder PVA.

The recrystallization of tristearin and paraffin wax causes a strong haze after switching and reduces the contrast between the switched and original areas of the films. The waxes recrystallize in lager domains and cause haze. Maximum contrast is required to achieve a good printing result. The recrystallization of fatty acids is not very pronounced and they stay finely dispersed in the PVA matrix. Therefore, it is assumed that a stabilizing effect of the matrix is necessary for a good and durable transparency. Although fatty acids are generally considered to be non-polar due to their long alkyl chain, the carboxyl group allows the formation of Hydrogen bonds with the polar PVA matrix. The better miscibility and compatibility would then be the reason why no larger wax domains are formed during the switching process, which would affect the transparency. However, miscibility is also determined by the amount of fatty acid. If there is an excess of PVA, large fatty acid domains will be formed, which in this case will even increase opacity. Only with 70 % fatty acid, i.e. a clear excess of fatty acid, opaque transparent switching layers are obtained.

In conclusion, the use of organic solvents in the combination of polymer matrix and crystallizing substance leads to coatings that are highly dependent on the form and shape of the crystallizing substance, e.g. flower-like on the surface. During thermal opacity switching, these surface structures are destroyed and opacity is lost. However, the switched films are still very cloudy (OD ~ 0.9 to 1). The use of aqueous melt dispersion has the great advantage that the crystalline substance is introduced into the coating in a controllable shape, which is irreversibly destroyed during thermal printing/treatment. This shape change contributes to the desired change in light scattering and the difference in optical density before and after printing is at its highest.

2. *What properties of the polymer matrix and the crystalline substance are required for a coating to undergo irreversible thermal switching in opacity?*

The experiments show that for a good switchability, there must be compatibility between the polymer and the crystalline substance. Intermolecular interactions can also promote irreversibility. Thermal properties must also be considered: during switching, transport of the melt is essential, so at least parts of the polymer must be fluid. In the best performing coated papers, the melt temperature of the melt-dispersed fatty acid is between T_g and T_m of the PVA used.

3. *Does the substrate influence thermal switching of a coating?*

The first printing tests with films coated on PET show that the substrate is not so well suited for printing. The transport in the printer is not optimal and the tested coatings showed significant abrasion on the print head. Applying the same formulations to PET foil and black paper results in a big difference in the opacity of the samples. However, the biggest advantage of using paper is the thermal printing itself; the paper runs smoothly through the printer and there was less deposit on the print head. The thermal switching is also different: since paper has a capillary effect, the molten waxes can be absorbed by the paper and withdrawn from the surface. This way the coating is not turning back to the opaque state even after a longer storage time. And because non-toxic materials are used, there is no risk to the user's health. In conclusion, the results of this thesis suggest that, in principle, crystallizing substances, such as fatty acids, can be incorporated into thin polymer matrices in order to obtain thermally switchable thin films on paper.

But how can the system be further developed towards a transfer into technologically relevant applications? First, the promising fatty acid and PVA films can be investigated in more detail by extending the test procedures. In addition to optical density, film structure and topography, the switching process is of particular interest. Using a dynamic optical method, e.g. a hot stage microscope, the switching process can be observed with temperature resolution. This makes it possible to document when the switching process starts and when it is completed. In this way, the optical change can be studied as a function of temperature and time. A DSC microscope would also be an option to link the optical changes directly to thermal transitions in the material.

Industrial suitability should be tested with the transfer of the promising fatty acid and PVA systems to a formulation that can be used on a coating machine. This requires precise adjustments with process additives. Next to the coating process the industrial and commercial requirements for the coated papers have to be confirmed by extended printing tests. Even after several meters of thermo-printed paper, there should be no deposits on the printhead and the print should not be distorted or compressed. The stability of the coating in the original opaque and printed transparent state needs to be tested over a long period of time to ensure that they could be used as recording media. This would require harsher conditions that could be simulated UV ageing and storage tests. The change in the optical density after the treatments provide information on the stability. If large quantities of the printed coating is absorbed by the paper, the printed areas will resemble wax-impregnated papers. In this case, recyclability could be compromised because these areas would no longer disintegrate in water during the recycling process. If wax-based coatings are considered for commercially available thermal papers, recyclability tests must be performed of the printed material.

Regarding the production of the coating, the melt dispersion process of the waxes, as well as the material choice can also be further developed and extended. It can be investigated whether the switching temperature can be precisely set by adjusting the particle size using surfactants. Other materials should be tested as crystalline substances: natural waxes like beeswax, carnauba wax, soy and sugarcane based waxes, but also semi-synthetic fatty acid amides may be alternatives. These enable a wider range of crystalline substances with different optical behavior and melting properties. Next to the crystalline component, other polymer matrices or blends can be studied, e.g. the water-soluble film former polyvinylpyrrolidone.

In addition to the production of the coating formulation, the refinement step that takes place after film formation can also be further developed. The oil resistance of the porous melt-dispersed wax systems was studied in this thesis and could be improved with surface treatment with UV light. A larger study with different wax systems could be used to refine this procedure to investigate, if other materials are better suited for sintering the surface without comprising opacity.

8 Experimental Part

If not otherwise specified, percentages given are always weight percent.

Chemicals

All chemicals used were purchased from different companies; the suppliers are stated in the experimental procedures. If not explicitly mentioned, the chemicals were used directly without further purification. Styrene and Methyl methacrylate were destabilized in a glass frit filled with basic alumina.

Coating Substrates

PET foil: 175 μm PET foil Hostaphan® RN 50-350; *Mitsubishi Polyester Film GmbH.*

Base paper: 40 g m^{-2} paper with a black pigment coating; *Koehler Paper SE.*

Differential Scanning Calorimetry

The DSC measurements were performed in a Mettler Toledo instrument (DSC 3). The glass transition temperature is determined via ISO 11357 method. The evaluations were performed using STAR SW 16.00 software.

Scanning Electron Microscope

SEM measurements were performed using the XL30 FEG from Philips. The samples were applied to a sample carrier using a graphite-containing adhesive sticker. The samples were sputtered with a conductive 30 nm thick layer of Pd/Pt before measurement.

Spectrophotometer

The measurements were performed with a Noviprofibre photometer N5950A. The light source used is norm light C with cut-off at 420 nm. The measuring aperture has a diameter of 35 mm. The white standard used in the measurements is a cotton linters paper without additives.

Differential Interference Microscope

The crystal structures of the eutectic mixtures were measured using a Leica TCS SP DIC microscope with phase contrast and lambda-filer

Dynamic Light Scattering

The hydrodynamic diameter of the particles in the dispersions was determined using the Malvern Zetasizer Nano ZS. The samples were measured at 25 °C under an angle of 90 °C in plastic cuvettes.

8.1 Solvent Cast Polymer Blend Films out of PS and P4MS (e8)

Table 8.1: Chemicals used in e8

Chemical	*m* / g	Specification	Supplier
Polystyrene (PS)	2.5	M_w 320 0000 g mol^{-1}	Sigma Aldrich
Polystyrene (PS)	2.5	M_w 35 000 g mol^{-1}	Sigma Aldrich
Poly-4-methylstyrene (P4MS)	2 x 1.07	M_w 72 000 g mol^{-1}	Sigma Aldrich

Solvents used: THF (2 x 40 ml)

The polymer materials were free of additives and were used without further purification.
The polymers were dissolved in Tetrahydrofuran. Two different mixtures were prepared with two PS grades with two different weight average molecular weights. Each mixture contains 70 % PS (2.5 g) and 30 % P4MS (2.5 g) in 40 ml THF. The resulting solid content of the formulation is 9.2 %.
The formulations are coated on PET foil with a film frame applicator with a gap height of 120 μm. The coating speed is 50 mm min^{-1}. The resulting films are dried at room temperature.

8.2 Solvent Cast Polymer Blend Films out of PS and PMMA (e27)

Table 8.2: Chemicals used in e27

Chemical	*m* / g	Specification	Supplier
Polystyrene (PS)	0.298	M_w 35 000 g mol^{-1}	Sigma Aldrich
Polymethyl methacrylate (PMMA)	0.665	M_w 15 000 g mol^{-1}	Sigma Aldrich

Solvents used: Methylethyl ketone (MEK; 44 ml)

0.298 g PS and 0.665 g PMMA are dissolved in MEK with the help of an ultrasonic bath. The resulting concentration is 15 mg ml^{-1}. The formulation is coated on PET foil with a film frame applicator with a gap height of 120 μm. The coating speed is 50 mm min^{-1}. The resulting films are dried at room temperature.

8.3 Measurements of the Refractive Index of DMO and EC (e34)

The refractive index of DMO and EC is measured using an Abbe refractometer and Ellipsometry.

Table 8.3: Chemicals used in e34

Chemical	Specification	Supplier
Dimethyl oxalate (DMO)	Purity > 98.5 %	Thermo Scientific
9-Ethylcarbazole (EC)	Purity > 99 %	TCI Chemicals
Bromonaphthalene	Purity > 97 %	Thermo Scientific

Solvents used: THF

The refractive index of DMO and EC is measured, using an Abbe refractometer. The device is temperature controlled with a thermostat9. The first measurements is performed with the melts of the substances. In a second measurement Bromonaphtalene is used as immersion liquid to identify the refractive index of the solids. The values that were determined are summarized in Table 8.5. With DMO, a refractive index could not be identified since no front was visible.

Table 8.4: Refractive indices of DMO and EC, measured with an Abbe refractometer.

Substance	**Measuring Temperature**	n_D
DMO	50 °C (melt)	1.390
	20 °C (solid with immersion liquid)	no front is visible
EC	80 °C (melt)	1.621
	20 °C (solid with immersion liquid)	1.6195

The refractive index was also determined using ellipsometry. DMO and EC are dissolved in THF (20 mg ml^{-1}) and brought onto Si-wafer. The film thickness is measured using white light interferometry, then the refractive index can be measured using ellipsometry. The measurements were carried out on the non-sputtered part oft he sample λ (laser) = 658 nm; RT; 15 % rel. H.

Table 8.5: Values of the thickness *d* and refractive index *n* of the films of DMO and EC on Si-wafers, measured with white light interferometry and ellipsometry (e34).

	EC	**DMO**
n_1	1.645 ±0.005	1.448 ±0.041
n_2	1.62 ±0.076	1.498 ±0.094
n_3	1.649 ±0.077	1.429 ±0.004
$\bar{n}$	1.638 ±0.053	1.458 ±0.046

8.4 Samples for Optical Measurements of Crystalline Structure – DIC Microscope (e25)

Table 8.6. Chemicals used in e25.

Chemical	**Specification**	**Supplier**
Dimethyl oxalate (DMO)	Purity > 98.5 %	Thermo Scientific
9-Ethylcarbazole (EC)	Purity > 99 %	TCI Chemicals

Table 8.7: Compositions of the samples of e25.

Sample	Mass percentage DMO	*m* (DMO) / g	*m* (EC) / g
EC	0 %	-	1.0001
0.1_DMO_EC	10 %	0.1012	0.9015
0.3_DMO_EC	30 %	0.3017	0.7012
0.5_DMO_EC	50 %	0.5013	0.5018
0.7_DMO_EC	70 %	0.7018	0.3014
0.9_DMO_EC	90 %	0.9034	0.1044
DMO	100 %	1.0024	-

The mixtures with the different compositions are placed in round bottom flasks and are heated until melted via heat gun. Then the melts are put onto heated microscope slides and also preheated cover glasses are slid onto the melt and pressed onto the melts so that a thin substance film is crystallizing between the slides while cooling down.

8.5 PLA-Frames with DMO and EC for Determining Scattering Coefficients (e29)

Table 8.8: Chemicals used in e29.

Chemical	**Specification**	**Supplier**
Dimethyl oxalate (DMO)	Purity > 98.5 %	Thermo Scientific
9-Ethylcarbazole (EC)	Purity > 99 %	TCI Chemicals

The PLA frames are printed out using a filament 3D printer in various heights. The frames are glued on glass slides with power glue. Then the different composistions of DMO and EC, as well as the pure substances are melted in a round bottom flask and poured into the prepared frames on the glass slides which are preheated (at 70 °C). Then a thin cover glass is slid onto the frame and melt so that the entrapped air can be released. The mixtures recrystallize at room temperature. The samples are then measured using a remission spectral photometer. The values obtained and the values calculated are summarized in Table 8.9. Values used for the calculations for the white and black background: $R_v = 0.9588$; $R_s = 0$

Table 8.9: Reflexion values measured with the PLA-frame samples out of DMO and EC.

Mass percentage DMO	**Name sample**	**Height PLA frame**	R_{gs}	R_{gv}	R_{∞}	s / m^2kg^{-1}	k / m^2kg^{-1}
0 % (100 % EC)	3.7	0.4 mm	0.321	0.677	0.460	0.863	0.274
0 % (100 % EC)	3.8	0.4 mm	0.332	0.661	0.459	0.946	0.302
0 % (100 % EC)	3.2	0.5 mm	0.282	0.612	0.393	0.786	0.368
0 % (100 % EC)	3.9	0.5 mm	0.399	0.642	0.496	0.945	0.242
0 % (100 % EC)	3.3	1 mm	0.307	0.523	0.374	0.391	0.205
0 % (100 % EC)	3.10	1 mm	0.391	0.548	0.447	0.542	0.186
0 % (100 % EC)	3.11	2 mm	0.397	0.482	0.425	0.479	0.186
30 %	1.5	0.4 mm	0.388	0.549	0.445	1.026	0.355
30 %	1.6	0.4 mm	0.413	0.613	0.490	1.602	0.424
30 %	1.1	0.5 mm	0.406	0.556	0.460	1.241	0.393
30 %	1.7	0.5 mm	0.477	0.523	0.494	1.401	0.363
30 %	1.8	1 mm	0.458	0.496	0.471	1.076	0.319
30 %	1.9	1 mm	0.467	0.513	0.484	1.120	0.308
30 %	1.10	2 mm	0.423	0.435	0.427	0.802	0.309
30 %	1.11	2 mm	0.408	0.423	0.413	0.797	0.333
40 %	6.1	0.4 mm	0.474	0.571	0.512	1.365	0.318
40 %	6.2	0.4 mm	0.473	0.535	0.496	1.585	0.405
40 %	6.3	0.5 mm	0.446	0.538	0.480	1.242	0.351
40 %	6.4	0.5 mm	0.466	0.564	0.503	1.412	0.347
40 %	6.5	1 mm	0.448	0.487	0.461	0.953	0.300
40 %	6.6	1 mm	0.464	0.492	0.474	1.210	0.354
40 %	6.7	2 mm	0.412	0.420	0.415	0.757	0.312
40 %	6.8	2 mm	0.412	0.421	0.415	0.826	0.341
50%	5.9	0.4 mm	0.409	0.548	0.459	0.966	0.309
50%	5.10	0.4 mm	0.459	0.542	0.490	1.414	0.376
50%	5.4	0.5 mm	0.430	0.578	0.486	1.545	0.420
50%	5.11	0.5 mm	0.441	0.509	0.465	1.359	0.418
50%	5.12	1 mm	0.470	0.510	0.485	0.790	0.217
50%	5.13	1 mm	0.447	0.509	0.469	1.084	0.327
50%	5.14	2 mm	0.426	0.465	0.439	0.677	0.243

Continuation of table:

Mass percentage DMO	**Name sample**	**Height PLA frame**	R_{gs}	R_{gv}	R_{∞}	s / m^2kg^{-1}	k / m^2kg^{-1}
50%	5.15	2 mm	0.405	0.409	0.406	0.918	0.398
50 %	5.16	0.45 mm	0.430	0.612	0.502	1.834	0.453
60 %	7.1	0.4 mm	0.452	0.601	0.511	1.610	0.377
60 %	7.2	0.4 mm	0.473	0.541	0.498	1.439	0.363
60 %	7.3	0.5 mm	0.479	0.555	0.508	1.640	0.391
60 %	7.4	0.5 mm	0.454	0.539	0.485	1.088	0.297
60 %	7.5	1 mm	0.444	0.512	0.468	1.002	0.302
60 %	7.6	1 mm	0.457	0.536	0.486	1.205	0.328
60 %	7.7	2 mm	0.449	0.473	0.457	0.835	0.269
60 %	7.8	2 mm	0.449	0.473	0.457	0.817	0.263
70 %	2.5	0.4 mm	0.397	0.647	0.497	1.457	0.370
70 %	2.6	0.4 mm	0.376	0.652	0.486	0.974	0.264
70 %	2.1	0.5 mm	0.517	0.601	0.551	1.954	0.358
70 %	2.7	0.5 mm	0.407	0.635	0.498	1.101	0.279
70 %	2.2	1 mm	0.466	0.588	0.514	1.061	0.244
70 %	2.8	1 mm	0.446	0.533	0.477	0.812	0.232
70 %	2.9	2 mm	0.443	0.492	0.460	0.667	0.211
70 %	2.10	2 mm	0.452	0.512	0.473	0.605	0.177
100 %	4.7	0.4 mm	0.254	0.764	0.468	0.513	0.155
100 %	4.8	0.4 mm	0.069	0.725	0.196	0.125	0.206
100 %	4.9	0.5 mm	0.209	0.711	0.384	0.500	0.247
100 %	4.10	0.5 mm	0.150	0.735	0.334	0.251	0.167
100 %	4.11	1 mm	0.205	0.702	0.374	0.163	0.085
100 %	4.12	1 mm	0.192	0.717	0.371	0.165	0.088
100 %	4.1	2 mm	0.251	0.658	0.391	0.163	0.077
100 %	4.13	2 mm	0.193	0.675	0.344	0.093	0.058

8.6 Shim Ring Samples out of DMO/EC and Urea/BA for Determining Scattering Coefficients (e38)

Table 8.10: Chemicals used in e38.

Chemical	Specification	Supplier
dimethyl oxalate (DMO)	Purity > 98.5 %	Thermo Scientific
9-*N*-Ethylcarbazole (EC)	Purity > 99 %	TCI Chemicals
urea	Purity > 99 %	Sigma Aldrich
benzoic acid (BA)	Purity 99 %	Alfa Aesar

Shim rings with the heights of 0.1; 0.2; 0.5; 0.5 and 1 mm are glued on glass slides with power glue. Then the different compositions of DMO and EC, different compositions of urea and BA, as well as the pure substances are melted in a round bottom flask and poured into the prepared rings on the glass slides which are preheated (at 70 °C). Then a thin cover glass is slid onto the shim ring and melt so that the entrapped air can be released. The mixtures recrystallize at room temperature.

The samples are then measured using a remission spectral photometer. The values obtained and the values calculated are summarized in Table 8.11 (DMO/EC) and Table 8.12 (urea/BA). Of every composition and shim ring height, two samples were prepared. The table contains the averaged values of the combination composition and shim ring height.

Values used for the calculations for the white and black background: $\boldsymbol{R}_{\mathrm{v}} = 0.9588$; $\boldsymbol{R}_{\mathrm{s}} = 0$

Table 8.11: Reflection factors measured and calculated for the shim ring samples out of DMO and EC.

Mass percentage DMO	**Height shim ring**	R_{gs}	R_{gv}	R_{∞}	s / m^2kg^{-1}	k / m^2kg^{-1}	$m_A s$
0 % (100 % EC)	0.1 mm	0.173	0.735	0.361	13.296	7.503	1.408
	0.2 mm	0.238	0.696	0.402	7.824	3.478	1.657
	0.3 mm	0.256	0.712	0.429	4.746	1.803	1.508
	0.5 mm	0.234	0.672	0.383	3.574	1.779	1.892
	1 mm	0.299	0.560	0.383	2.935	1.462	3.108
10 %	0.1 mm	0.298	0.667	0.436	17.632	6.433	1.883
	0.2 mm	0.305	0.620	0.416	11.062	4.546	2.363
	0.3 mm	0.279	0.656	0.414	6.247	2.597	2.001
	0.5 mm	0.409	0.545	0.457	6.597	2.123	3.522
	1 mm	0.370	0.454	0.396	5.093	2.344	5.438
20 %	0.1 mm	0.261	0.687	0.417	15.947	6.491	1.717
	0.2 mm	0.294	0.649	0.423	9.561	3.773	2.059
	0.3 mm	0.324	0.564	0.405	9.436	4.130	3.048
	0.5 mm	0.394	0.564	0.456	5.841	1.899	3.145
	1 mm	0.435	0.496	0.456	4.595	1.491	4.948
30 %	0.1 mm	0.245	0.670	0.392	17.494	8.261	1.899
	0.2 mm	0.297	0.660	0.431	9.002	3.389	1.955
	0.3 mm	0.315	0.643	0.435	6.502	2.385	2.118
	0.5 mm	0.384	0.616	0.472	4.477	1.323	2.430
	1 mm	0.394	0.519	0.437	3.638	1.320	3.949
40 %	0.1 mm	0.244	0.742	0.440	11.610	4.135	1.271
	0.2 mm	0.385	0.696	0.517	7.399	1.671	1.620
	0.3 mm	0.414	0.587	0.479	8.687	2.456	2.853
	0.5 mm	0.449	0.633	0.524	4.248	0.921	2.325
	1 mm	0.455	0.539	0.486	3.600	0.980	3.940
50 %	0.1 mm	0.310	0.717	0.477	13.048	3.742	1.440
	0.2 mm	0.309	0.702	0.467	7.082	2.160	1.563
	0.3 mm	0.401	0.683	0.520	5.252	1.164	1.739
	0.5 mm	0.429	0.640	0.515	4.005	0.917	2.210
	1 mm	0.440	0.559	0.484	3.082	0.846	3.401

Continuation of table:

Mass percentage DMO	**Height shim ring**	R_{gs}	R_{gv}	R_{∞}	s / m^2kg^{-1}	k / m^2kg^{-1}	$m_A s$
60 %	0.1 mm	0.262	0.727	0.445	12.376	4.289	1.377
	0.2 mm	0.385	0.695	0.516	7.325	1.658	1.630
	0.3 mm	0.376	0.676	0.499	5.371	1.352	1.792
	0.5 mm	0.430	0.647	0.519	3.837	0.857	2.134
	1 mm	0.457	0.568	0.499	2.995	0.754	3.332
70 %	0.1 mm	0.341	0.709	0.495	13.388	3.449	1.501
	0.2 mm	0.329	0.710	0.487	6.660	1.804	1.494
	0.3 mm	0.391	0.696	0.522	4.805	1.053	1.616
	0.5 mm	0.408	0.643	0.502	3.831	0.944	2.148
	1 mm	0.493	0.574	0.525	3.091	0.666	3.466
80 %	0.1 mm	0.268	0.722	0.446	12.545	4.309	1.418
	0.2 mm	0.296	0.705	0.458	6.838	2.195	1.546
	0.3 mm	0.352	0.700	0.497	4.659	1.187	1.580
	0.5 mm	0.421	0.656	0.518	3.571	0.801	2.018
	1 mm	0.439	0.628	0.515	2.090	0.478	2.362
90 %	0.1 mm	0.198	0.720	0.378	13.181	6.751	1.501
	0.2 mm	0.260	0.712	0.433	6.580	2.448	1.499
	0.3 mm	0.303	0.695	0.457	4.760	1.537	1.627
	0.5 mm	0.394	0.719	0.538	2.498	0.495	1.423
	1 mm	0.496	0.696	0.586	1.499	0.219	1.708
100 %	0.1 mm	0.130	0.743	0.313	12.508	9.450	1.436
	0.2 mm	0.147	0.715	0.316	7.193	5.335	1.652
	0.3 mm	0.094	0.719	0.239	5.443	6.593	1.875
	0.5 mm	0.146	0.733	0.327	2.581	1.787	1.481
	1 mm	0.214	0.739	0.410	1.149	0.489	1.319

Table 8.12: Reflection factors measured and calculated for the shim ring samples out of urea and BA.

Mass percentage urea	**Height shim ring**	R_{gs}	R_{gv}	R_{∞}	s / m^2kg^{-1}	k / m^2kg^{-1}	$m_A s$
0 % (100 % BA)	0.1 mm	0.045	0.750	0.154	16.784	39.005	2.132
	0.2 mm	0.051	0.746	0.168	8.047	16.525	2.044
	0.3 mm	0.114	0.722	0.273	4.519	4.382	1.722
	0.5 mm	0.208	0.730	0.396	2.206	1.014	1.401
	1 mm	0.238	0.728	0.425	1.089	0.424	1.383
10 %	0.1 mm	0.171	0.770	0.388	8.759	4.217	1.117
	0.2 mm	0.375	0.795	0.585	3.415	0.502	0.871
	0.3 mm	0.385	0.656	0.494	5.215	1.355	1.995
	0.5 mm	0.244	0.620	0.364	3.794	2.111	2.418
	1 mm	0.323	0.738	0.502	0.999	0.248	1.274
20 %	0.1 mm	0.482	0.803	0.654	6.515	0.595	0.834
	0.2 mm	0.508	0.811	0.675	3.087	0.242	0.790
	0.3 mm	0.520	0.817	0.686	1.968	0.141	0.756
	0.5 mm	0.538	0.817	0.694	1.191	0.080	0.762
	1 mm	0.646	0.826	0.750	0.596	0.025	0.763
31 %	0.1 mm	0.448	0.813	0.645	5.925	0.578	0.762
	0.2 mm	0.514	0.795	0.664	3.514	0.299	0.904
	0.3 mm	0.567	0.814	0.706	2.066	0.127	0.797
	0.5 mm	0.667	0.836	0.767	1.105	0.039	0.710
	1 mm	0.752	0.855	0.815	0.517	0.011	0.665
40 %	0.1 mm	0.543	0.823	0.702	5.635	0.357	0.727
	0.2 mm	0.501	0.802	0.663	3.301	0.283	0.852
	0.3 mm	0.514	0.814	0.680	2.007	0.152	0.777
	0.5 mm	0.653	0.825	0.752	1.209	0.050	0.780
	1 mm	0.721	0.831	0.785	0.631	0.019	0.814
50 %	0.1 mm	0.420	0.809	0.626	6.050	0.678	0.784
	0.2 mm	0.507	0.813	0.676	3.001	0.233	0.777
	0.3 mm	0.509	0.809	0.674	2.070	0.164	0.804
	0.5 mm	0.608	0.823	0.731	1.171	0.058	0.758
	1 mm	0.680	0.815	0.757	0.686	0.027	0.888

Continuation of table:

Mass percentage urea	Height shim ring	R_{gs}	R_{gv}	R_{∞}	s / m^2kg^{-1}	k / m^2kg^{-1}	$m_A s$
60 %	0.1 mm	0.493	0.806	0.662	6.324	0.545	0.822
	0.2 mm	0.514	0.806	0.673	3.192	0.254	0.830
	0.3 mm	0.562	0.809	0.699	2.127	0.138	0.830
	0.5 mm	0.645	0.822	0.747	1.217	0.052	0.791
	1 mm	0.676	0.794	0.740	0.826	0.038	1.073
100 %	0.1 mm	0.045	0.750	0.154	16.784	39.005	2.132
	0.2 mm	0.051	0.746	0.168	8.047	16.525	2.044
	0.3 mm	0.114	0.722	0.273	4.519	4.382	1.722
	0.5 mm	0.208	0.730	0.396	2.206	1.014	1.401
	1 mm	0.238	0.728	0.425	1.089	0.424	1.383

8.7 Solvent Cast Films out of Paraffin Wax and PVA (e1)

Table 8.13: Chemicals used in e1.

Chemical	m / g	Specification	Supplier
polyvinyl alcohol (PVA)	2.6 g	Poval 8-88, 88 % saponified	Kuraray
paraffin wax	1.4 g	Mp. 58-62 °C (ASTM D87)	Sigma Aldrich

Solvent used: Dodecane (5.27 g)

1.4 g paraffin wax is dissolved in 5.27 g Dodecane. 1.4 g PVA is dissolved in 51.6 g water by heating the mixture to 90 °C. After the PVA solution is cooled down to room temperature, the wax solution is stirred into the PVA solution. Then the mixture is immediately coated onto PET foil using a film frame applicator wwith the gap height of 120 μm (speed 50 mm s^{-1}). The resulting films consist out of 35 % wax and 65 % PVA. The solid content of the coated formulation is 6.6 %. The optical density of the original film is 0.45. The film that is tempered in the oven at 140 °C for 5 min has an OD of 0.44.

8.8 Solvent Cast Films out of Tristearin and PLA (e31)

Table 8.14: Chemicals used in e31.

Chemical	Specification	Supplier
Polylactide (PLA)	Pellets for filament production	Strooder
tristearin (TS)	Purity > 97 %	Arctom Chemicals

Solvent used: DCM

PLA and TS are dissolved in DCM (weights and volumes in Table 8.15). The formulation are coated on PET foil, using a film frame applicator with a gap height of 120 μm. The coating speed is 50 mm s^{-1}. The films are dried at room temperature.

Table 8.15: Compositions of samples of e31; films out of PLA and TS.

Mass percentage tristearin	***m* (PLA) / g**	***m* (TS) / g**	***V* (DCM) / ml**	**Solid content / %**
0 %	2	-	20	7
10 %	2	0.223	20	8
20 %	2	0.503	20	8.6
30 %	2	0.862	20	9.7
40 %	2	1.33	20	11
50 %	2	2.005	20	13
60 %	2	3	20	15.8
70 %	2	4.67	20	20
80 %	2	8	25	23
90 %	2	18	25	37.5

Table 8.16: Optical densities of films out of PLA and TS out of e31. Original films and switched in the oven.

Mass percentage tristearin	**Optical density (OD)**	
	Original film	**Switched in oven at 140 °C for 5 min**
0 %	1.46	1.45
10 %	1.17	1.08
20 %	0.94	1.21
30 %	0.93	1.19
40 %	0.97	1.25
50 %	0.74	0.96
60 %	0.8	1.16
70 %	0.55	1.08
80 %	1	1.39
90 %	0.35	1.09

8.9 Solvent Cast Films out of Tristearin and PCL (e10)

Table 8.17: Chemicals used in e10.

Chemical	Specification	Supplier
Polycaptrolactone (PCL)	M_w X g mol^{-1}	Sigma Aldrich
Tristearin (TS)	Purity > 97 %	Arctom Chemicals

Solvent used: THF

PCL and TS are dissolved in THF (weights and volumes in Table 8.18). The formulation are coated on PET foil, using a film frame applicator with a gap height of 120 μm. The coating speed is 50 mm s^{-1}. The films are dried at room temperature.

Table 8.18: Compositions of formulations of e10.

Mass percentage Tristearin	*m* (PCL) / g	*m* (TS) / g	*V* (THF) / ml	Solid content / %
0 %	1	-	10	10
30 %	1	0.43	15	10
50 %	1	1	20	10

Table 8.19: Optical densities of the films of e10; PCL with TS. Original films, switched in oven and one sample thermoprinted.

	Optical density (OD)		
Mass percentage Tristearin	Original film	Switched in oven at 140 °C for 5 min	Thermoprinted
0 %	1.03	1.35	-
30 %	0.48	1.3	0.85
50 %	0.77	1.32	-

8.10 Solvent Cast Films out of Tristearin and PS (e9 and e40)

Table 8.20: Chemicals used in e9 and e40

Chemical	*m* / g	Specification	Supplier
Polystyrene (PS)	-	M_w 320 0000 g mol^{-1}	Sigma Aldrich
Tristearin (TS)	-	Purity > 97 %	Arctom Chemicals

Solvents used: THF

PS and TS are dissolved in THF with the help of an ultrasonic bath (weights and volumes in Table 8.21 and Table 8.22). The amount of solvents is varied to obtain an approximately same viscosity of the resulting solutions. The solutions with a TS content > 60 % have to be kept at approx. 50 °C and in motion so that the TS does not crystallize which disturbs the coating process.

The formulations are coated on PET foil using a film frame applicator with a gap height of 120 μm. The coating speed is 50 mm s^{-1}. The films are dried at room temperature.

Table 8.21: Composition of e9.

Mass percentage tristearin	***m* (PS) / g**	***m* (TS) / g**	***V* (THF) / ml**	**Solid content / %**
12 %	3.75	0.5	15	24
21 %	3.75	1	15	26
35 %	3.75	2	15	30
50 %	3.75	3.75	15	36

Table 8.22: Composition of e40

Mass percentage tristearin	***m* (PS) / g**	***m* (TS) / g**	***V* (THF) / ml**	**Solid content / %**
0 %	2	-	10	18
10 %	2	0.22	10	20
20 %	2	0.5	10	22
30 %	2	0.86	10	24
40 %	2	1.33	10	27
50 %	2	2	10	31
60 %	2	3	15	27
70 %	1.5	3.5	15	27
80 %	1.5	6	20	30
90 %	1	9	20	36
100 %	-	4	15	23

Table 8.23: Optical densities of e40 films in the original and switched state. One sample was also thermoprinted (70 % tristearin)

Mass percentage tristearin	**Optical density (OD)**		
	Original film	**Switched in oven at 140 °C for 5 min**	**Thermoprinted**
0 %	1.45	1.45	-
10 %	0.52	1.14	-
20 %	0.51	0.94	-
30 %	0.44	1.06	-
40 %	0.40	0.94	-
50 %	0.41	0.97	-
60 %	0.38	0.95	-
70 %	0.23	0.86	0.63
80 %	0.19	0.96	-
90 %	0.11	0.95	-
100 %	0.26	-	-

8.11 Surface Treatment of Films out of Tristearin and PS (e70)

Films out of 80 % TS in PS (formed out of THF) are surface treated with flash light (VIS), as well as with UV light. For the treatment with visible light (flash light), a *Novacentrix* Pulse Forge 1200, a lab-scale instrument for curing and sintering is used. Parameters used are 400 V (lamp) and 5 pulses at 1 Hz for 1 and 2 ms with 30 mm of distance from the lamp. For the treatment with UV light, the samples are placed on the conveyor belt of an *IST Metz* laboratory drying system. The illumination source is a mercury lamp with a power of 8 kW. Sintering is performed at full power. Adjusting the belt speed controls the energy applied. The samples are treated with the belt speeds of 25, 20 and 15 m min^{-1}.

Table 8.24: Optical densities of PS/TS films (e40) prior and after surface treatments.

Sample	**OD after treatment**
Reference: 80 % TS in PS (e40)	0.15
UV 25 m min^{-1}	0.22
UV 20 m min^{-1}	0.24
UV 15 m min^{-1}	0.46
VIS 1 ms	0.17
VIS 2 ms	0.21

8.12 Solvent Cast Films out of BAc / SAc and PS (e9)

Table 8.25: Chemicals used in e9 (SAc and BAc).

Chemical	***m* / g**	**Specification**	**Supplier**
Polystyrene (PS)	30	M_w 320 0000 g mol^{-1}	Sigma Aldrich
Behenic acid (BAc)	7.25	Purity >98 %	Croda
Stearic acid (SAc)	7.25	Purity >90 %	Thermo Scientific

Solvent used: THF

PS and the corresponding fatty acid are dissolved in THF (weights and volumes in Table 8.26). The formulation are coated on PET foil, using a film frame applicator with a gap height of 120 μm. The coating speed is 50 mm s^{-1}. The films are dried at room temperature.

Table 8.26: Composition of e9 SAc and BAc formulations.

Mass percentage fatty acid	***m* (PS) / g**	***m* (TS) / g**	***V* (THF) / ml**	**Solid content / %**
12 % SAc	3.75	0.5	15	24
21 % SAc	3.75	1	15	26
35 % SAc	3.75	2	15	30
50 % SAc	3.75	3.75	15	36
12 % BAc	3.75	0.5	15	24
21 % BAc	3.75	1	15	26
35 % BAc	3.75	2	15	30
50 % BAc	3.75	3.75	15	36

Table 8.27: Optical densities of e9 films (PS with BAc and SAc); original and switched in the oven.

	Optical density (OD)	
Mass percentage fatty acid	**Original film**	**Switched in oven at 140 °C for 5 min**
12 % SAc	0.6	1.08
21 % SAc	0.64	0.99
35 % SAc	0.6	0.91
50 % SAc	0.61	0.8
12 % BAc	0.6	0.63
21 % BAc	0.59	0.67
35 % BAc	0.6	0.75
50 % BAc	0.34	0.76

8.13 Solvent Cast Films out of Paraffin Wax and PS (e6)

Table 8.28: Chemicals used in e6.

Chemical	***m*** **/ g**	**Specification**	**Supplier**
Polystyrene (PS)	30	M_w 320 0000 g mol^{-1}	Sigma Aldrich
Paraffin wax	21.55	Mp. 58-62 °C (ASTM D87)	Sigma Aldrich

Solvent used: THF

PS and paraffin wax are dissolved in THF (weights and volumes in Table 8.26). The formulation are coated on PET foil, using a film frame applicator with a gap height of 120 μm. The coating speed is 50 mm s^{-1}. The films are dried at room temperature.

Table 8.29: Composition of e6 films.

Mass percentage paraffin wax	***m*** **(PS) / g**	***m*** **(Wax) / g**	***V*** **(THF) / ml**	**Solid content / %**
12 %	2	0.27	25	9
21 %	2	0.53	25	10
35 %	2	1.08	25	12
50 %	2	2	25	15
60 %	2	3	25	18
70 %	2	4.67	30	20
80 %	1	4	25	18
90 %	1	9	30	27

Since the films do not fully dry, the optical densities could only be measured in the switched state (see Table 8.30).

Table 8.30: Optical densities of e6 films switched in the oven.

	Optical density (OD)
Mass percentage paraffin wax	**Switched in oven at 140 °C for 5 min**
12 %	0.91
21 %	0.55
35 %	0.69
50 %	0.61

8.14 Films out of DMO/EC and Urea/BAc Mixtures in PVA from Aqueous Solution (e43)

Table 8.31: Chemicals used in e43.

Chemical	**Specification**	**Supplier**
Polyvinyl alcohol (PVA)	Poval 8-88, 88 % saponified	Kuraray
Dimethyl oxalate (DMO)	Purity > 98.5 %	Thermo Scientific
9-Ethylcarbazole (EC)	Purity > 99 %	TCI Chemicals
Urea	Purity > 99 %	Sigma Aldrich
Benzoic acid (BA)	Purity 99 %	Alfa Aesar

Solvent used: water

Prior, PVA is dissolved in water at 90 °C to result in a 20 % solution.

The crystalline substance are mixed in the right compositions and are finely mortared. Then the PVA solution is added and the mixture is stirred vigorously. The weights are summarized in Table 8.32. The formulations are coated on PET foil, using a film frame applicator with a gap height of 120 μm. The coating speed is 50 mm s^{-1}. The films are dried at room temperature.

Table 8.32: Compositions of the films of e43.

Mass percentage substance in film	Substance composition	*m* (PVA) / g	*m* (DMO) / g	*m* (EC) / g	*m* (H_2O) / g
43 %	DMO	2	1.5	-	8
	50 % DMO	2	0.75	0.75	8
	70 % DMO	2	1.05	0.45	8
	EC	2	-	1.5	8
60 %	DMO	2	3	-	8
	50 % DMO	2	1.5	1.8	8
	70 % DMO	2	2.1	0.9	8
	EC	2	-	3	8
43 %	urea	2	1.5	-	8
	31 % urea	2	0.75	0.75	8
	50 % urea	2	1.05	0.45	8
	BA	2	-	1.5	8
60 %	urea	2	3	-	8
	31 % urea	2	1.5	1.8	8
	50 % urea	2	2.1	0.9	8
	BA	2	-	3	8

8.15 Films out of SAc / PAc and PVA from Aqueous Solution (e47)

Table 8.33: Chemicals used in e47.

Chemical	***m*** **/ g**	**Specification**	**Supplier**
polyvinyl alcohol (PVA)	22	Poval 8-88, 88 % saponified	Kuraray
stearic acid (SAc)	16.5	Purity >90 %	Thermo Scientific
palmitic acid (PAc)	16.5	Purity >97.5 %	Thermo Scientific

Solvent used: water

Prior, PVA is dissolved in water at 90 °C to result in a 30 % solution which is used to dose PVA to the formulations. The desired amount of PVA solution, fatty acid and water is placed in a 50 ml snap cap jar. The amounts are given in Table 8.34. The jar is put into an oil bath and heated to 60 °C so that all of the fatty acid is melted. Then the jar is taken out of the oil bath and the mixture is dispersed using an Ultra Turrax disperser. After 1 minute, the jar is placed into an ice bath and dispersed for another minute at the lowest speed until it is cooled down. The formulations are degassed using a speed mixer with a negative pressure of 100 mbar. The formulations are coated on PET foil and black paper using a film frame applicator with a gap height of 15, 20, 25 and 30 μm. The coating speed is 50 mm s^{-1}. The films are dried using a hot gun at approx. 40 °C and 30 cm distance from the films.

Table 8.34: Compositions of the films in e47. The resulting films consist out of 60 % fatty acid.

Mass percentage SAc in the fatty acid mixture	***m*** **(SAc) / g**	***m*** **(PAc) / g**	***m*** **(PVA) / g**	***V*** **(H_2O) / g**	**Solid content / %**
0 % SAc	-	3	2	11.67	30
10 % SAc	0.3	2.7	2	11.67	30
20 % SAc	0.6	2.4	2	11.67	30
30 % SAc	0.9	2.1	2	11.67	30
40 % SAc	1.2	1.8	2	11.67	30
50 % SAc	1.5	1.5	2	11.67	30
60 % SAc	1.8	1.2	2	11.67	30
70 % SAc	2.1	0.9	2	11.67	30
80 % SAc	2.4	0.6	2	11.67	30
90 % SAc	2.7	0.3	2	11.67	30
100 % SAc	3	-	2	11.67	30

Table 8.35: Optical densities of the films of e47 on PET foil in the original and switched state.

Mass percentage SAc in fatty acid mixture	**Gap height film frame applicator**	**Optical density (OD) on PET foil**	
		Original film	**Switched in oven at 140 °C for 5 min**
0 % SAc	15 μm	0.91	1.26
0 % SAc	20 μm	0.9	1.19
0 % SAc	25 μm	0.88	0.92
0 % SAc	30 μm	0.88	1
10 % SAc	15 μm	0.87	1.34
10 % SAc	20 μm	0.84	1.26
10 % SAc	25 μm	0.72	1.02
10 % SAc	30 μm	0.77	1.03
20 % SAc	15 μm	1.1	1.38
20 % SAc	20 μm	1.08	1.29
20 % SAc	25 μm	1.05	0.95
20 % SAc	30 μm	1.04	0.99
30 % SAc	15 μm	1.11	1.42
30 % SAc	20 μm	1.1	1.36
30 % SAc	25 μm	1.06	1.13
30 % SAc	30 μm	1.05	1.11
40 % SAc	15 μm	1.01	1.43
40 % SAc	20 μm	0.99	1.34
40 % SAc	25 μm	0.93	1.05
40 % SAc	30 μm	0.94	1.16
50 % SAc	15 μm	1.05	1.42
50 % SAc	20 μm	1.05	1.4
50 % SAc	25 μm	1.01	1.17
50 % SAc	30 μm	1.02	1.08
60 % SAc	15 μm	1.09	1.42
60 % SAc	20 μm	1.07	1.31
60 % SAc	25 μm	1.01	1.04
60 % SAc	30 μm	1.03	1.14

Continuation of table:

Mass percentage SAc in fatty acid mixture	**Gap height film frame applicator**	**Optical density (OD) on PET foil**	
		Original film	**Switched in oven at 140 °C for 5 min**
70 % SAc	15 μm	0.94	1.37
70 % SAc	20 μm	0.92	1.36
70 % SAc	25 μm	0.86	1.26
70 % SAc	30 μm	0.87	1.33
80 % SAc	15 μm	0.95	1.36
80 % SAc	20 μm	0.97	1.25
80 % SAc	25 μm	0.92	1.05
80 % SAc	30 μm	0.94	1.07
90 % SAc	15 μm	1.07	1.28
90 % SAc	20 μm	1.06	1.3
90 % SAc	25 μm	1.01	1.1
90 % SAc	30 μm	1.03	1.04
100 % SAc	15 μm	1.08	1.1
100 % SAc	20 μm	1.06	1.22
100 % SAc	25 μm	1.05	1.02
100 % SAc	30 μm	1.03	1.06

Table 8.36: Optical densities of films of e47 on black paper in the original state, as well as after 5 min in the oven at 100, 120 and 140 °C.

Sample Amount of SAc in the fatty acid mixture	**Gap height film frame applicator**	**$OD_{original}$**	**$OD_{100°C}$**	**$OD_{120°C}$**	**$OD_{140°C}$**
10 % SAc	15 μm	1.91	1.34	1.4	1.34
10 % SAc	20 μm	2.03	1.36	1.38	1.33
10 % SAc	25 μm	2.02	1.37	1.27	1.36
10 % SAc	30 μm	2.04	1.26	1.27	1.37
20 % SAc	15 μm	1.9	1.36	1.38	1.38
20 % SAc	20 μm	1.89	1.38	1.33	1.41
20 % SAc	25 μm	1.89	1.19	1.19	1.33
20 % SAc	30 μm	1.9	1.34	1.35	1.37
30 % SAc	15 μm	1.75	1.28	1.33	1.41
30 % SAc	20 μm	1.79	1.31	1.18	1.4
30 % SAc	25 μm	1.76	1.2	1.17	1.35
30 % SAc	30 μm	1.8	1.17	1.13	1.32
40 % SAc	15 μm	1.49	1.27	1.29	1.31
40 % SAc	20 μm	1.49	1.23	1.21	1.32
40 % SAc	25 μm	1.5	1.2	1.15	1.12
40 % SAc	30 μm	1.47	1.11	1.13	1.12
50 % SAc	15 μm	1.38	1.26	1.24	1.23
50 % SAc	20 μm	1.37	1.18	1.15	1.2
50 % SAc	25 μm	1.34	1.16	1.1	1.12
50 % SAc	30 μm	1.33	1.15	1.25	1.12
60 % SAc	15 μm	1.24	1.3	1.32	1.29
60 % SAc	20 μm	1.25	1.32	1.3	1.29
60 % SAc	25 μm	1.2	1.24	1.19	1.1
60 % SAc	30 μm	1.18	1.29	1.23	1.16
70 % SAc	15 μm	0.75	1.37	1.36	1.4
70 % SAc	20 μm	0.72	1.37	1.34	1.39
70 % SAc	25 μm	0.69	1.24	1.12	1.3
70 % SAc	30 μm	0.67	1.2	1.23	1.3

Continuation of table:

Sample Amount of SAc in the fatty acid mixture	**Gap height film frame applicator**	**$OD_{original}$**	**$OD_{100°C}$**	**$OD_{120°C}$**	**$OD_{140°C}$**
80 % SAc	15 μm	0.44	1.34	1.36	1.34
80 % SAc	20 μm	0.42	1.31	1.33	1.37
80 % SAc	25 μm	0.3	1.29	1.13	1.18
80 % SAc	30 μm	0.3	1.3	1.22	1.21
90 % SAc	15 μm	0.71	1.25	1.31	1.36
90 % SAc	20 μm	0.62	1.29	1.32	1.37
90 % SAc	25 μm	0.44	1.14	1.11	1.19
90 % SAc	30 μm	0.42	1.12	1.13	1.24

8.16 Films out of PAc and PVA from Aqueous Solution (e64)

Table 8.37: Chemicals used in e64.

Chemical	***m* / g**	**Specification**	**Supplier**
Polyvinyl alcohol (PVA)	22	Poval 8-88, 88 % saponified	Kuraray
Palmitic acid (PAc)	16.5	Purity >97.5 %	Thermo Scientific

Solvent used: water

Prior, PVA is dissolved in water at 90 °C to result in a 30 % solution which is used to dose PVA to the formulations. The desired amount of PVA solution, palmitic acid and water is placed in a 50 ml snap cap jar. The amounts are given in Table 8.38. The jar is placed into an oil bath and heated to 60 °C so that all of the fatty acid is melted. Then the jar is taken out of the oil bath and the mixture is dispersed using an Ultra Turrax disperser. After 1 minute, the jar is put into an ice bath and dispersed for another minute at the lowest speed until it is cooled down. The formulations are degassed using a speed mixer with a negative pressure of 100 mbar. The formulations are coated on PET foil and black paper using a film frame applicator with a gap height of 15, 20, 25 and 30 μm. The coating speed is 50 mm s^{-1}. The films are dried using a hot gun at approx. 40 °C and 30 cm distance from the films.

Table 8.38: Composition of formulations of e64.

Mass percentage PAc	***m* (PAc) / g**	***m* (PVA) / g**	***V* (H_2O) / g**	**Solid content / %**
10 %	0.5	4.5	11.67	30
20 %	1	4	11.67	30
30 %	1.5	3.5	11.67	30
40 %	2	3	11.67	30
50 %	2.5	2.5	11.67	30
60 %	3	2	11.67	30
70 %	3.5	1.5	11.67	30
80 %	4	1	11.67	30
90 %	4.5	0.5	11.67	30

Table 8.39: Optical properties of the films of e64 on PET.

Mass percentage PAc	**Gap height film frame applicator**	**Optical density (OD) on PET foil**	
		Original film	**Switched in oven at 140 °C for 5 min**
10 %	15 μm	1.39	1.18
	20 μm	1.38	1.13
	25 μm	1.4	1.12
	30 μm	1.38	1.02
20 %	15 μm	1.36	0.98
	20 μm	1.36	0.99
	25 μm	1.35	0.82
	30 μm	1.36	0.86
30 %	15 μm	1.29	0.64
	20 μm	1.25	0.73
	25 μm	1.27	0.67
	30 μm	1.3	0.63
40 %	15 μm	1.24	0.89
	20 μm	1.25	0.8
	25 μm	1.25	0.63
	30 μm	1.23	0.64

Continuation of table:

Mass percentage PAc	**Gap height film frame applicator**	**Optical density (OD) on PET foil**	
		Original film	**Switched in oven at 140 °C for 5 min**
50 %	15 μm	1.19	0.88
	20 μm	1.18	0.8
	25 μm	1.14	0.68
	30 μm	1.1	0.74
60 %	15 μm	0.91	1.26
	20 μm	0.9	1.19
	25 μm	0.88	0.92
	30 μm	0.88	1
70 %	15 μm	0.47	1.28
	20 μm	0.49	1.26
	25 μm	0.32	0.93
	30 μm	0.37	1.09
80 %	15 μm	0.47	1.38
	20 μm	0.52	1.28
	25 μm	0.21	1.07
	30 μm	0.28	1.2
90 %	15 μm	1.39	1.18
	20 μm	1.38	1.13
	25 μm	1.4	1.12
	30 μm	1.38	1.02

Table 8.40: Optical densities of films of e64 on black paper in the original, switched in the oven and thermoprinted state.

Mass percentage PAc	Gap height film frame applicator	Optical density (OD) on black paper		
		Original film	Swiched in oven at 140 °C for 5 min	Thermoprinted
70 %	15 μm	0.45	1.36	1.48
	20 μm	0.43	1.35	1.38
	25 μm	0.22	1.25	0.76
	30 μm	0.26	1.32	0.88
80 %	15 μm	0.42	1.37	1.45
	20 μm	0.37	1.33	1.46
	25 μm	0.21	1.11	1.1
	30 μm	0.26	1.15	1.13
90 %	15 μm	0.72	1.36	1.55
	20 μm	0.54	1.39	1.51
	25 μm	0.53	1.15	1.54
	30 μm	0.64	1.06	1.54

Table 8.41: Optical densities of films of e64 on black paper in the original state and after tempering the films in the oven for 5 minutes at 100, 120 and 140 °C.

Sample Amount of PAc	Gap height film frame applicator	$OD_{original}$	$OD_{100°C}$	$OD_{120°C}$	$OD_{140°C}$
10 % PAc	15 μm	2.03	1.42	1.44	1.35
10 % PAc	20 μm	2.03	1.48	1.33	1.33
10 % PAc	25 μm	2.03	1.46	1.3	1.39
10 % PAc	30 μm	1.92	1.1	1.05	1.05
20 % PAc	15 μm	1.9	1.06	0.96	0.95
20 % PAc	20 μm	1.9	1.05	1.02	0.93
20 % PAc	25 μm	1.88	1.13	1	0.98
20 % PAc	30 μm	1.8	1.11	1.11	1.14
30 % PAc	15 μm	1.8	1.09	1.04	1.17
30 % PAc	20 μm	1.8	1.02	1	0.98
30 % PAc	25 μm	1.8	1.04	1.12	0.98
30 % PAc	30 μm	1.52	1.42	1.39	1.41

Continuation of table:

Sample **Amount of PAc**	**Gap height film** **frame applicator**	**$OD_{original}$**	**$OD_{100°C}$**	**$OD_{120°C}$**	**$OD_{140°C}$**
40 % PAc	15 μm	1.43	1.45	1.29	1.26
40 % PAc	20 μm	1.48	1.37	1.31	1.41
40 % PAc	25 μm	1.47	1.29	1.22	1.11
40 % PAc	30 μm	1.28	1.09	1.11	1.09
50 % PAc	15 μm	1.28	1.09	1.06	1.06
50 % PAc	20 μm	1.25	1.05	1.03	1.03
50 % PAc	25 μm	1.25	1.02	1.03	0.97
50 % PAc	30 μm	1.27	1.3	1.16	1.14
60 % PAc	15 μm	1.17	1.25	1.18	1.19
60 % PAc	20 μm	1.16	1.16	1.02	1.01
60 % PAc	25 μm	1.13	1.18	1.04	1.07
60 % PAc	30 μm	0.75	1.07	1.1	1.08
70 % PAc	15 μm	0.72	1.03	1.02	1.02
70 % PAc	20 μm	0.67	0.95	0.93	0.87
70 % PAc	25 μm	0.65	1	0.96	0.9
70 % PAc	30 μm	0.32	1.09	1.13	1.02
80 % PAc	15 μm	0.45	1.02	1.1	1.01
80 % PAc	20 μm	0.29	0.98	1.05	0.99
80 % PAc	25 μm	0.32	0.96	1.05	0.97
80 % PAc	30 μm	0.76	1.18	1.23	1.21
90 % PAc	15 μm	0.69	1.17	1.21	1.25
90 % PAc	20 μm	0.42	1.06	1.08	1.14
90 % PAc	25 μm	0.55	1.06	1.16	1.22
90 % PAc	30 μm	2.03	1.42	1.44	1.35

To see if the cooling of the formulations during melt dispersion has an impact on the optical properties; two formulations are repeatedly melt-dispersed and are cooled down using liquid nitrogen.

Table 8.42: Comparison of optical densities of films of e64 cooled down during melt dispersion with an ice bath (standard) and liquid nitrogen.

Sample Amount of PAc	Gap height film frame applicator	$OD_{original}$	$OD_{100°C}$	$OD_{120°C}$	$OD_{140°C}$
50 % PAc – liq. N_2	15 μm	1.42	1.04	1.03	1.27
50 % PAc – liq. N_2	20 μm	1.42	1.06	1.04	1.2
50 % PAc – liq. N_2	25 μm	1.47	0.87	0.84	0.91
50 % PAc – liq. N_2	30 μm	1.47	0.88	0.89	0.94
90 % PAc – liq. N_2	15 μm	0.44	1.32	1.24	1.21
90 % PAc – liq. N_2	20 μm	0.4	1.3	1.27	1.23
90 % PAc – liq. N_2	25 μm	0.35	1.33	1.35	1.28
90 % PAc – liq. N_2	30 μm	0.33	1.32	1.26	1.24

Table 8.43: Optical densities of films of e64 that are stored in an oven at 50 °C. The ODs are measured after 24, 48 and 62 h.

Sample Amount of PAc	Gap height film frame applicator	OD_{24h}	OD_{48h}	OD_{62h}
10 % PAc	15 μm	1.99	2.01	2.01
20 % PAc	15 μm	1.89	1.87	1.92
30 % PAc	15 μm	1.78	1.74	1.69
40 % PAc	15 μm	1.38	1.28	1.25
50 % PAc	15 μm	1.17	1.11	1.05
60 % PAc	15 μm	1.07	1.01	1
70 % PAc	15 μm	0.77	0.75	0.68
80 % PAc	15 μm	0.53	0.49	0.43
90 % PAc	15 μm	0.73	0.73	0.67

8.17 Films out of Paraffin Wax and PVA from Aqueous Solution (e65)

Table 8.44: Chemicals used in e65.

Chemical	Specification	Supplier
Polyvinyl alcohol (PVA)	Poval 8-88, 88 % saponified	Kuraray
Paraffin wax	Mp. 58-62 °C (ASTM D87)	Sigma Aldrich

Solvent used: water

Prior, PVA is dissolved in water at 90 °C to result in a 30 % solution which is used to dose PVA to the formulations. The desired amount of PVA solution, paraffin wax and water is placed in a 50 ml snap cap jar. The amounts are given in Table 8.45. The jar is placed into an oil bath and heated to 60 °C so that all of the wax is melted. Then the jar is taken out of the oil bath and the mixture is dispersed using an Ultra Turrax disperser. After 1 minute, the jar is put into an ice bath and dispersed for another minute at the lowest speed until it is cooled down. The formulations are degassed using a speed mixer with a negative pressure of 100 mbar. The formulations are coated on PET foil and black paper using a film frame applicator with a gap height of 15, 20, 25 and 30 μm. The coating speed is 50 mm s^{-1}. The films are dried using a hot gun at approx. 40 °C and 30 cm distance from the films.

Table 8.45: Composition of the formulations in e65.

Mass percentage PAc	***m* (Wax) / g**	***m* (PVA) / g**	***V* (H_2O) / g**	**Solid content / %**
10 %	0.44	4	10.36	30
30 %	1.71	4	13.34	30
50 %	3	3	14	30
70 %	4.5	1.93	15	30
90 %	5	0.56	12.97	30

Table 8.46: Optical densities of the films of e65 on PET in their original , switched in the oven and some in the thermoprinted state.

Mass percentage paraffin wax	**Gap height frame applicator**	**Optical density (OD) on PET foil**		
		Original film	**Switched in oven at 140 °C for 5 min**	**Thermoprinted**
10 %	15 μm	1.43	0.96	-
	20 μm	1.44	0.92	-
	25 μm	1.43	0.79	-
	30 μm	1.44	0.8	-
30 %	15 μm	1.37	0.66	-
	20 μm	1.36	0.67	-
	25 μm	1.19	0.48	-
	30 μm	1.32	0.54	-
50 %	15 μm	1.19	0.7	-
	20 μm	1.2	0.69	1.15
	25 μm	1.2	0.52	-
	30 μm	1.23	0.61	1.09
70 %	15 μm	1.03	1.13	-
	20 μm	1.03	1.19	-
	25 μm	1.05	0.8	-
	30 μm	1.08	0.85	-
90 %	15 μm	1.07	1.3	-
	20 μm	0.99	1.28	-
	25 μm	0.56	1.2	-
	30 μm	0.58	1.15	0.88

Table 8.47: Optical densities of the films of e65 on black paper in their original and switched in the oven state.

Mass percentage paraffin wax	Gap height frame applicator	Optical density (OD) on black paper	
		Original film	Switched in oven at 140 °C for 5 min
10 %	15 μm	2	1.5
	20 μm	1.91	1.5
	25 μm	1.95	1.49
	30 μm	1.91	1.37
30 %	15 μm	1.69	1.31
	20 μm	1.7	1.25
	25 μm	1.61	1
	30 μm	1.57	1.05
50 %	15 μm	1.46	1.19
	20 μm	1.44	1.23
	25 μm	1.46	1.01
	30 μm	1.46	1.06
70 %	15 μm	1.41	1.28
	20 μm	1.36	1.2
	25 μm	1.35	1.14
	30 μm	1.36	1.15
90 %	15 μm	0.97	1.41
	20 μm	0.84	1.39
	25 μm	0.83	1.35
	30 μm	0.68	1.36

8.18 Films out of Tristearin and PVA from Aqueous Solution (e66)

Table 8.48: Chemicals used in e66.

Chemical	Specification	Supplier
Polyvinyl alcohol (PVA)	Poval 8-88, 88 % saponified	Kuraray
Tristearin (TS)	Purity > 97 %	Arctom Chemicals

Solvent used: water

Prior, PVA is dissolved in water at 90 °C to result in a 30 % solution which is used to dose PVA to the formulations. The desired amount of PVA solution, tristearin and water is placed in a 50 ml snap cap jar. The amounts are given in Table 8.49. The jar is placed into an oil bath and heated to 60 °C so that all of the tristearin is melted. Then the jar is taken out of the oil bath and the mixture is dispersed using an

Ultra Turrax disperser. After 1 minute, the jar is put into an ice bath and dispersed for another minute at the lowest speed until it is cooled down. The formulations are coated on PET foil and black paper using a film frame applicator with a gap height of 15, 20, 25 and 30 μm. The coating speed chosen is 50 mm s^{-1}. The films are dried using a hot gun at approx. 40 °C and 30 cm distance from the films.

Table 8.49: Composition of the formulations in e66.

Mass percentage PAc	***m* (TS) / g**	***m* (PVA) / g**	***V* (H_2O) / g**	**Solid content / %**
70 %	4.5	1.93	15	30
80 %	5	1.25	14.58	30
90 %	5	0.56	12.97	30

Table 8.50: Optical densities of the films of e66 on PET in their original and switched in the oven state.

Mass percentage tristearin	**Gap height frame applicator**	**Optical density (OD) on PET**	
		Original film	**Switched in oven at 140 °C for 5 min**
70 %	15 μm	0.97	1.29
70 %	20 μm	0.97	1.27
70 %	25 μm	0.93	1.06
70 %	30 μm	0.93	1.17
80 %	15 μm	0.92	1.34
80 %	20 μm	0.84	1.31
80 %	25 μm	0.81	1.07
80 %	30 μm	0.8	1.02
90 %	15 μm	0.84	1.23
90 %	20 μm	0.78	1.3
90 %	25 μm	0.57	1.1
90 %	30 μm	0.58	1.23

Table 8.51: Optical densities of the films of e66 on black paper in their original and switched in the oven state. Some films were measured after being thermoprinted.

Mass percentage tristearin	Gap height frame applicator	Optical density (OD) on black paper		
		Original film	Switched in oven at 140 °C for 5 min	Thermoprinted
70 %	15 μm	1.19	1.35	
70 %	20 μm	1.15	1.34	
70 %	25 μm	1.09	1.25	
70 %	30 μm	1.19	1.35	
80 %	15 μm	0.82	0.35	
80 %	20 μm	0.92	1.35	
80 %	25 μm	0.64	1.27	1.25
80 %	30 μm	0.69	1.25	1.3
90 %	15 μm	0.97	1.35	
90 %	20 μm	0.91	1.32	
90 %	25 μm	0.69	1.29	1.31
90 %	30 μm	0.73	1.3	1.43

8.19 Emulsion Polymerization of Styrene (e39)

Table 8.52: Chemicals used in e39.

Chemical	Specification	Supplier
Styrene	Purity 99 %, stabilized	Thermo Scientific
Sodium dodecyl sulfate (SDS)	Purity > 99 %	Sigma Aldrich
Dowfax 2A1	-	Dow
Potassium hydroxide (KOH)	-	Chemical Shop OC TU Da
Sodium disulfite	-	Sigma Aldrich
Sodium persulfate	Purity > 98 %	Sigma Aldrich

Table 8.53: Composition of the various batches of emulsion polymerization.

	EP1	**EP2**	**EP3**
	m **/g**	***m*** **/g**	***m*** **/g**
Receiver			
Water	280	280	90
Styrene	4	4	1.3
SDS	0.07	0.07	0.02
Initiator			
Sodium disulfite	0.16	0.16	0.1
Sodium persulfate	0.8	0.6	0.05
Feed			
Water	90	90	30
Styrene	60	60	10
SDS	0.23	0.23	0.076
Dowfax 2A1	0.23	0.23	0.076
KOH	0.2	0.2	0.06

The weights of the components of the different batches of the polymerization are to be found in Table 8.53. Styrene is destabilized and cooled down to 0 °C together with water and SDS. A 500 ml glass reactor with stirrer is preheated to 80 °C with a thermostat. The receiver is put into the reactor and the initiator is added immediately and stirred vigorously. After a few minutes the mixture starts to become cloudy. Beforehand, the feed is prepared by mixing all the components using an Ultrasonic mixing bar so that a homogenous emulsion is forming. The feed is added continuously with added with the help of a pump with the volumetric flow rate of $\dot{V} = 1$ ml/min. Figure 8.1 shows the experimental setup of the polymerization.

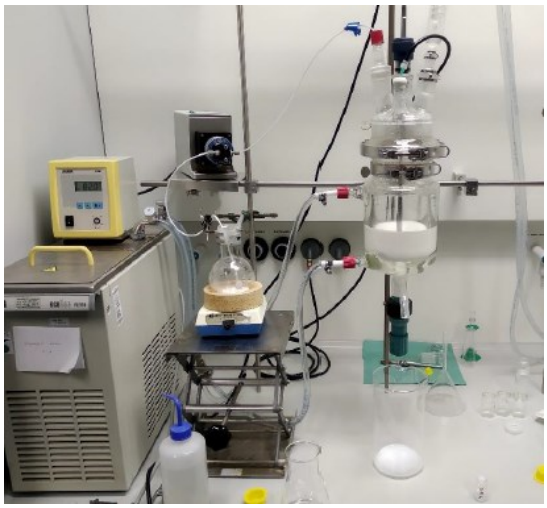

Figure 8.1: Experimental setup of the starved feed emulsion polymerization.

8.20 Tristearin with PS-Particles with and without Tenside (e23)

Table 8.54: Chemicals used in e23.

Chemical	Specification	Supplier
Tristearin (TS)	Purity > 97 %	Arctom Chemicals
PS-particles	Solid content 7 %	see e39 EP2
Sodium dodecyl sulfate (SDS)	Purity > 99 %	Sigma Aldrich

Solvent used: water

The PS-dispersion, tristearin and if needed SDS are placed in a 50 ml snap cap jar and heated to 63 °C in an oil bath (weights found in Table 8.55). After the tristearin has melted, the two-phase mixture is melt-dispersed using an Ultra Turrax disperser tool. After one minute, the jar is put into an ice bath while continuing to disperse it to make sure the particles do not agglomerate during cooling. The formulations are coated onto PET foil using a film frame applicator with a gap height of 120 μm. The coating speed is 50 mm s^{-1}. The resulting films are dried at room temperature.

Table 8.55: Composition of the formulations in e23.

Mass percentage PAc	*m* (PS) / g	*m* (TS) / g	*m* (SDS) / g	*V* (H_2O) / g	Solid content / %
PS particles with 50 % TS	1.05	1.05	-	13.95	13
PS particles with 50 % TS and tenside	1.05	1.05	0.08	13.95	13

Table 8.56: Optical densities of the films of e23.

	Optical density (OD) on PET foil	
Tempering Temperature and Time	**PS particles with 50 % TS**	**PS particles with 50 % TS and tenside**
RT	0.23	0.26
60 °C / 20 min	0.32	0.29
70 °C / 20 min	0.66	0.58
80 °C / 10 min	0.64	0.69
100 °C / 10 min	0.79	0.8
120 °C / 10 min	0.69	0.69
140 °C / 10 min	0.93	1.12

9 References

(1) Wiegand & Partner GmbH. *Tonermacher - So Funktioniert Thermodruck*. https://www.tonermacher.de/wissen/so-funktioniert-thermodruck (accessed 2024-01-12).

(2) Microplex Printware AG. *Microplex Printware AG - Thermal Printers - Our Product Range*. Microplex Printware AG |. https://microplex.de/en/thermal-printers/ (accessed 2024-01-12).

(3) Hengstler GmbH. *Im Vergleich: Thermodrucker, Tintenstrahldrucker oder Laserdrucker*. https://www.hengstler.de/de/technologie/printer/drucktechnologie.php (accessed 2024-01-12).

(4) Kanzan Spezialpapiere GmbH. *The Thermal Imaging Process*. https://www.kanzan.de/en/products/thermal-papers/thermal-technology/the-thermal-imaging-process (accessed 2024-01-12).

(5) Globe Newswire. *Global Thermal Paper Market - Astute Analytica*. https://www.globenewswire.com/en/news-release/2022/11/07/2549428/0/en/Global-Thermal-Paper-Market-to-Value-3-189-69-Million-by-2030-Astute-Analytica.html (accessed 2023-11-05).

(6) RICOH INDUSTRIE FRANCE SAS. *The different layers of a thermal paper*. https://www.ricoh-thermal.com/en/technical-supports/different-layers-thermal-paper (accessed 2023-11-12).

(7) Koehler Paper SE. *Funktionsprinzip - Wie funktioniert der Thermodruck?* https://www.koehlerpaper.com/de/produkte/Thermopapiere/Funktionsprinzip-herkoemmliche-Thermopapiere.php (accessed 2023-11-12).

(8) Seeboth, A.; Lötzsch, D. *Thermochromic and Thermotropic Materials*; Taylor & Francis Group: Boca Taron, Florida, 2013.

(9) Eckardt, M.; Simat, T. J. Phenolische Und Nicht-Phenolische Farbentwickler Sowie Extrahierbare Sensitizer in Thermopapieren - Eine Marktübersicht, Poster, Dresden 2015.

(10) Eckardt, M.; Simat, T. J. Bisphenol A and Alternatives in Thermal Paper Receipts - a German Market Analysis from 2015 to 2017. *Chemosphere* **2017**, *186*, 1016–1025. https://doi.org/10.1016/j.chemosphere.2017.08.037.

(11) White, M. A.; LeBlanc, M. Thermochromism in Commercial Products. *J. Chem. Educ.* **1999**, *76* (9), 1201–1205.

(12) Goldinger, D. M.; Demierre, A.-L.; Zoller, O.; Rupp, H.; Reinhard, H.; Magnin, R.; Becker, T. W.; Bourqui-Pittet, M. Endocrine Activity of Alternatives to BPA Found in Thermal Paper in Switzerland. *Regul. Toxicol. Pharmacol. RTP* **2015**, *71* (3), 453–462. https://doi.org/10.1016/j.yrtph.2015.01.002.

(13) Biedermann, S.; Tschudin, P.; Grob, K. Transfer of Bisphenol A from Thermal Printer Paper to the Skin. *Anal. Bioanal. Chem.* **2010**, *398* (1), 571–576. https://doi.org/10.1007/s00216-010-3936-9.

(14) ECHA Europe. *Bisphenole*. https://echa.europa.eu/de/hot-topics/bisphenols (accessed 2023-11-05).

(15) ECHA Europe. *6'-(dibutylamino)-3'-methyl-2'-(phenylamino)spiro[isobenzofuran-1(3H),9-(9H)-xanthen]-3-one*. https://echa.europa.eu/de/registration-dossier/-/registered-dossier/22813 (accessed 2023-11-05).

(16) United States Environment Protection Agency. Bisphenol A Alternatives in Thermal Paper. **2015**.

(17) Koehler Paper. *Thermal Technonolgy - The Structure of Blue4est Thermal Paper*. https://www.koehlerpaper.com/en/products/Thermal-paper/Functional-principle-Blue4est.php (accessed 2023-11-05).

(18) Zhu, C. F.; Wu, A. B. Studies on the Synthesis and Thermochromic Properties of Crystal Violet Lactone and Its Reversible Thermochromic Complexes. *Thermochim. Acta* **2005**, *425* (1–2), 7–12. https://doi.org/10.1016/j.tca.2003.08.001.

(19) MacLaren, D. C.; White, M. A. Dye–Developer Interactions in the Crystal Violet Lactone–Lauryl Gallate Binary System: Implications for Thermochromism. *J Mater Chem* **2003**, *13* (7), 1695–1700. https://doi.org/10.1039/B302249H.

(20) Sage, I. Thermochromic Liquid Crystals. *Liq. Cryst.* **2011**, *38* (11–12), 1551–1561. https://doi.org/10.1080/02678292.2011.631302.

(21) White, T. J.; McConney, M. E.; Bunning, T. J. Dynamic Color in Stimuli-Responsive Cholesteric Liquid Crystals. *J. Mater. Chem.* **2010**, *20* (44), 9832. https://doi.org/10.1039/c0jm00843e.

(22) Seeboth, A.; Lötzsch, D.; Ruhmann, R.; Muehling, O. Thermochromic Polymers--Function by Design. *Chem. Rev.* **2014**, *114* (5), 3037–3068. https://doi.org/10.1021/cr400462e.

(23) *Optical Interference Coatings*; Kaiser, N., Pulker, H. K., Eds.; Springer Series in Optical Sciences; Springer: Berlin, Germany; Heidelberg, Germany; New York, 2003; Vol. 88.

(24) Pritchard, R. The Transparency of Crystalline Polymers. *SPE Trans.* **1964**, 66–71.

(25) Ritchie, A. W.; Cox, H. J.; Gonabadi, H. I.; Bull, S. J.; Badyal, J. P. S. Tunable High Refractive Index Polymer Hybrid and Polymer–Inorganic Nanocomposite Coatings. *ACS Appl. Mater. Interfaces* **2021**, *13* (28), 33477–33484. https://doi.org/10.1021/acsami.1c07372.

(26) Ciddor, P. E. Refractive Index of Air: New Equations for the Visible and near Infrared. *Appl. Opt.* **1996**, *35* (9), 1566–1573.

(27) Syurik, J.; Jacucci, G.; Onelli, O. D.; Hölscher, H.; Vignolini, S. Bio-inspired Highly Scattering Networks via Polymer Phase Separation. *Adv. Funct. Mater.* **2018**, *28* (24), 1706901. https://doi.org/10.1002/adfm.201706901.

(28) Hayashi, M.; Shibata, K.; Kawarazaki, I.; Takasu, A. Simple Strategy for Dual Control of Crystallization and Thermal Property on Polyesters by Dispersing Metal Salts Via Multiple

Coordination Bonds. *Macromol. Chem. Phys.* **2018**, *219* (15), 1800127. https://doi.org/10.1002/macp.201800127.

(29) Fang, Q.; Ye, F.; Yang, X. Hierarchical Morphology of Polymer Blend Films Induced by Convection-Driven Solvent Evaporation. *Langmuir ACS J. Surf. Colloids* **2018**, *34* (19), 5551–5557. https://doi.org/10.1021/acs.langmuir.8b00600.

(30) Walheim, S.; Böltau, M.; Mlynek, J.; Krausch, G.; Steiner, U. Structure Formation via Polymer Demixing in Spin-Cast Films. *Macromolecules* **1997**, No. 30, 4995–5003.

(31) Chang, L. L.; Woo, E. M. UCST Behavior in Blend Systems of Isotactic Polystyrene/Poly(4-Methyl Styrene) in Comparison with Atactic Polystyrene/Poly(4-Methyl Styrene). *Colloid Polym. Sci.* **2003**, *281* (12), 1149–1156. https://doi.org/10.1007/s00396-003-0890-5.

(32) Roy, D.; Brooks, W. L. A.; Sumerlin, B. S. New Directions in Thermoresponsive Polymers. *Chem. Soc. Rev.* **2013**, *42* (17), 7214. https://doi.org/10.1039/c3cs35499g.

(33) Chen, W.; Qu, L.; Chang, D.; Dai, L.; Ganguli, S.; Roy, A. Vertically-Aligned Carbon Nanotubes Infiltrated with Temperature-Responsive Polymers: Smart Nanocomposite Films for Self-Cleaning and Controlled Release. *Chem Commun* **2008**, No. 2, 163–165. https://doi.org/10.1039/B715079B.

(34) Bordat, A.; Boissenot, T.; Nicolas, J.; Tsapis, N. Thermoresponsive Polymer Nanocarriers for Biomedical Applications. *Adv. Drug Deliv. Rev.* **2019**, *138*, 167–192. https://doi.org/10.1016/j.addr.2018.10.005.

(35) Concilio, M.; Beyer, V. P.; Becer, C. R. Thermoresponsive Polymers in Non-Aqueous Solutions. *Polym. Chem.* **2022**, *13* (47), 6423–6474. https://doi.org/10.1039/D2PY01147F.

(36) Hoogenboom, R. Temperature-Responsive Polymers: Properties, Synthesis and Applications. In *Smart Polymers and their Applications*; Elsevier, 2014; Vol. 659, pp 15–44. https://doi.org/10.1533/9780857097026.1.15.

(37) Pajula, K.; Taskinen, M.; Lehto, V.-P.; Ketolainen, J.; Korhonen, O. Predicting the Formation and Stability of Amorphous Small Molecule Binary Mixtures from Computationally Determined Flory-Huggins Interaction Parameter and Phase Diagram. *Mol. Pharm.* **2010**, *7* (3), 795–804. https://doi.org/10.1021/mp900304p.

(38) Chang, L. L.; Woo, E. M. Surface Morphology and Flory-Huggins Interaction Strength in UCST Blend System Comrising Poly(4-Methyl Styrene) and Isotactic Polystyrene. *Polymer* **2002**, No. 44, 1711–1719.

(39) Ashraf, S.; Park, H.-K.; Park, H.; Lee, S.-H. Snapshot of Phase Transition in Thermoresponsive Hydrogel PNIPAM: Role in Drug Delivery and Tissue Engineering. *Macromol. Res.* **2016**, *24* (4), 297–304. https://doi.org/10.1007/s13233-016-4052-2.

(40) Haq, M. A.; Su, Y.; Wang, D. Mechanical Properties of PNIPAM Based Hydrogels: A Review. *Mater. Sci. Eng. C Mater. Biol. Appl.* **2017**, *70* (Pt 1), 842–855. https://doi.org/10.1016/j.msec.2016.09.081.

(41) Gibson, M. I.; O'Reilly, R. K. To Aggregate, or Not to Aggregate? Considerations in the Design and Application of Polymeric Thermally-Responsive Nanoparticles. *Chem. Soc. Rev.* **2013**, *42* (17), 7204–7213. https://doi.org/10.1039/c3cs60035a.

(42) Yang, Q.; Mao, Y.; Li, G.; Huang, Y.; Tang, P.; Lei, C. Study on the UCST Behavior of Polystyrene/Poly(Styrene-Co-Acrylonitrile) Blend. *Mater. Lett.* **2004**, *58* (30), 3939–3944. https://doi.org/10.1016/j.matlet.2004.08.024.

(43) Zhou, N. C.; Xu, C.; Burghardt, W. R.; Composto, R. J.; Winey, K. I. Phase Behavior of Polystyrene and Poly(Styrene- Ran -Styrenesulfonate) Blends. *Macromolecules* **2006**, *39* (6), 2373–2379. https://doi.org/10.1021/ma052348q.

(44) Zucchi, I. A.; Resnik, T.; Oyanguren, P. A.; Galante, M. J.; Williams, R. J. J. Comparison of Optical Properties of Thermally Reversible Light Scattering Films Consisting in Dispersions of Polystyrene/Naphthalene Domains or Polystyrene/Liquid Crystal (EBBA) Domains in Epoxy Matrices. *Polym. Bull.* **2007**, *58* (1), 145–151. https://doi.org/10.1007/s00289-006-0516-4.

(45) Zucchi, I. A.; Galante, M. J.; Williams, R. J. J. Thermally Reversible Light Scattering Films Based on the Melting/Crystallization of Organic Crystals Dispersed in an Epoxy Matrix. *Eur. Polym. J.* **2006**, *42* (4), 815–822. https://doi.org/10.1016/j.eurpolymj.2005.09.030.

(46) Knothe, G.; Dunn, R. O. A Comprehensive Evaluation of the Melting Points of Fatty Acids and Esters Determined by Differential Scanning Calorimetry. *J. Am. Oil Chem. Soc.* **2009**, *86* (9), 843–856. https://doi.org/10.1007/s11746-009-1423-2.

(47) Zhang, J.; Pu, G.; Dubay, M. R.; Zhao, Y.; Severtson, S. J. Repositionable Pressure-Sensitive Adhesive Possessing Thermal-Stimuli Switchable Transparency. *J. Mater. Chem. C* **2013**, *1* (6), 1080. https://doi.org/10.1039/c2tc00471b.

(48) Sharma, A.; Tyagi, V. V.; Chen, C. R.; Buddhi, D. Review on Thermal Energy Storage with Phase Change Materials and Applications. *Renew. Sustain. Energy Rev.* **2009**, *13* (2), 318–345. https://doi.org/10.1016/j.rser.2007.10.005.

(49) Mishra, P.; Stockmal, K.; Ardito, G.; Tao, M.; van Dessel, S.; Granados-Focil, S. Thermo-Optically Responsive Phase Change Materials for Passive Temperature Regulation. *Sol. Energy* **2020**, *197* (10), 222–228. https://doi.org/10.1016/j.solener.2019.12.064.

(50) Mochane, M. J.; Luyt, A. S. Preparation and Properties of Polystyrene Encapsulated Paraffin Wax as Possible Phase Change Material in a Polypropylene Matrix. *Thermochim. Acta* **2012**, *544*, 63–70. https://doi.org/10.1016/j.tca.2012.06.017.

(51) Hassan, A.; Ismail, N.; Mourad, A.-H. I.; Rashid, Y.; Laghari, M. S. Preparation and Characterization of Expanded Clay-Paraffin Wax-Geo-Polymer Composite Material. *Mater. Basel Switz.* **2018**, *11* (11). https://doi.org/10.3390/ma11112191.

(52) Konuklu, Y.; Paksoy, H. Ö. Polystyrene-Based Caprylic Acid Microencapsulation for Thermal Energy Storage. *Sol. Energy Mater. Sol. Cells* **2017**, *159* (2), 235–242. https://doi.org/10.1016/j.solmat.2016.09.016.

(53) Keshavaraj, R.; Twock, R. W.; Narayan, R. S. Neural-Network-Based Model Approach for Density of High-Molecular-Weight Esters Used as Plasticizers. *Adv. Polym. Technol.* **1995**, *14* (3), 215–225.

(54) Guler, K. A. Effects of Wax Coating on the Surface Quality of EPS Patterns for Solid Mould Investment Casting. *Mater. Test.* **2013**, *55* (3), 193–196.

(55) Rajput, S. D.; Hundiwale, D. G.; Mahulikar, P. P.; Gite, V. V. Fatty Acids Based Transparent Polyurethane Films and Coatings. *Prog. Org. Coat.* **2014**, *77* (9), 1360–1368. https://doi.org/10.1016/j.porgcoat.2014.04.030.

(56) Khot, S. N.; Lascala, J. J.; Can, E.; Morye, S. S.; Williams, G. I.; Palmese, G. R.; Kusefoglu, S. H.; Wool, R. P. Development and Application of Triglyceride-Based Polymers and Composites. *J. Appl. Polym. Sci.* **2001**, No. 82, 703–723.

(57) Maisonneuve, L.; Lebarbé, T.; Grau, E.; Cramail, H. Structure–Properties Relationship of Fatty Acid-Based Thermoplastics as Synthetic Polymer Mimics. *Polym. Chem.* **2013**, *4* (22), 5472. https://doi.org/10.1039/c3py00791j.

(58) Eudier, F.; Grisel, M.; Savary, G.; Picard, C. Design of a Lipid-Coated Polymeric Material Mimic Human Skin Surface Properties: A Performing Tool to Evaluate Skin Interaction with Topical Products. *Langmuir ACS J. Surf. Colloids* **2020**, *36* (17), 4582–4591. https://doi.org/10.1021/acs.langmuir.0c00133.

(59) Kumar, S. A.; Jagdale, S. C. Formulation and Evaluation of Aceclofenac Sustained Release Tablets. *Int. J. Pharm. Sci. Rev. Res.* **2014**, *28* (2), 59–63.

(60) Khwaldia, K.; Arab-Tehrany, E.; Desobry, S. Biopolymer Coatings on Paper Packaging Materials. *Compr. Rev. Food Sci. Food Saf.* **2010**, No. 9, 82–91.

(61) Hotta, Y.; Yamaoka, T.; Morohoshi, K. Morphogenetic Study of Particle Domains in Thermoreversible Recording Media Composed of Polymeric Films with Dispersed Fatty Acis. *Chem. Mater.* **1997**, No. 9, 91–97.

(62) Hotta, Y.; Yamaoka, T.; Morohoshi, K.; Amano, T.; Tsutsui, K. Mechanistic Study of Thermoreversible Recording Media Composed of Polymeric Films with Dispersed Fatty Acids. *Chem. Mater.* **1995**, No. 7, 1793–1799.

(63) Tsutsiu, K.; Hotta, Y.; Sato, K. Melt Crystallization of Behenic Acid in Microspheres Dispersed in Polymer. *J. Crstal Growth* **1996**, No. 163, 440–444.

(64) Yu, D.; Xue, Z.; Mu, T. Eutectics: Formation, Properties, and Applications. *Chem. Soc. Rev.* **2021**, *50* (15), 8596–8638. https://doi.org/10.1039/D1CS00404B.

(65) Kang, S. K.; Rai, R. S.; Purushothaman, S. Interfacial Reactions during Soldering with Lead-Tin Eutectic and Lead (Pb)-Free, Tin-Rich Solders. *J. Electron. Mater.* **1996**, *25* (7), 1113–1120. https://doi.org/10.1007/BF02659912.

(66) Rai, U. S.; Shekhar, H. Solidification Behavior of Binary Organic Eutectic Alloys. *Cryst Res Technol* **1994**, *29* (4), 533–542.

(67) Xu, X.; Dehghani, G.; Ning, J.; Li, P. Basic Properties of Eutectic Chloride Salts NaCl-KCl-ZnCl2 and NaCl-KCl-MgCl2 as HTFs and Thermal Storage Media Measured Using Simultaneous DSC-TGA. *Sol. Energy* **2018**, *162*, 431–441. https://doi.org/10.1016/j.solener.2018.01.067.

(68) Stubican, V. S.; Bradt, R. C.; Kennard, F. L.; Minford, W. J.; Sorrel, C. C. Ceramic Eutectic Composites. In *Tailoring Multiphase and Composite Ceramics*; Tressler, R. E., Messing, G. L., Pantano, C. G., Newnham, R. E., Eds.; Springer US: Boston, MA, 1986; pp 103–114. https://doi.org/10.1007/978-1-4613-2233-7_9.

(69) Cherukuvada, S.; Nangia, A. Eutectics as Improved Pharmaceutical Materials: Design, Properties and Characterization. *Chem Commun* **2014**, *50* (8), 906–923. https://doi.org/10.1039/C3CC47521B.

(70) Rai, U. S.; Rai, R. N. Physical Chemistry of Organic Eutectics. *J. Therm. Anal.* **1998**, *53*, 883–893.

(71) Di Carmine, G.; Abbott, A. P.; D'Agostino, C. Deep Eutectic Solvents: Alternative Reaction Media for Organic Oxidation Reactions. *React. Chem. Eng.* **2021**, *6* (4), 582–598. https://doi.org/10.1039/D0RE00458H.

(72) Magnin, P.; Trivedi, R. Eutectic Growth: A Modification of the Jackson and Hunt Theory. *Acta Met. Mater* **1991**, *39* (4).

(73) Hunt, J. D.; Jackson, K. A. Binary Eutectic Solidification. *Trans. Metall. Soc. Aime* **1966**, No. 236, 843–851.

(74) Edler, F.; Machin, G.; Pearce, J.; White, D. R. *Guide on Secondary Thermometry: Specialised Fixed Points above 0 °C - Consultative Committee for Thermometry under the Auspices of the International Committee for Weights and Measures*; 2017.

(75) Ludwig, A.; Leibbrandt, S. Generalised 'Jackson–Hunt' Model for Eutectic Solidification at Low and Large Peclet Numbers and Any Binary Eutectic Phase Diagram. *Mater. Sci. Eng. A* **2004**, *375–377*, 540–546. https://doi.org/10.1016/j.msea.2003.10.108.

(76) Akamatsu, S.; Plapp, M. Eutectic and Peritectic Solidification Patterns. *Curr. Opin. Solid State Mater. Sci.* **2016**, *20* (1), 46–54. https://doi.org/10.1016/j.cossms.2015.10.002.

(77) Sharma, B. L.; Kant, R.; Sharma, R.; Tandon, S. Deviations of Binary Organic Eutectic Melt Systems. *Mater. Chem. Phys.* **2003**, *82* (1), 216–224. https://doi.org/10.1016/S0254-0584(03)00199-8.

(78) Sharma, B. L.; Tandon, S.; Kant, R.; Sharma, R. Quantitative Essence of Molecular Interactions in Binary Organic Eutectic Melt Systems. *Thermochim. Acta* **2004**, *421* (1–2), 161–169. https://doi.org/10.1016/j.tca.2004.02.026.

(79) Marinescu, D.-C.; Pincu, E.; Meltzer, V. Thermal Analysis of Binary Liquid Crystals Eutectic System Cholesteril P-Phenoxi Phenyl Carbamate–Cholesteril p-Biphenyl Carbamate. *J. Therm. Anal. Calorim.* **2012**, *110* (2), 985–990. https://doi.org/10.1007/s10973-011-1980-0.

(80) Smith, P.; Pennings, A. J. Eutectic Solidification of the Quasi Binary System of Isotactic Polypropylene and Pentaerythrityl Tetrabromide. *J. Polym. Sci. Polym. Phys. Ed.* **1977**, No. 15, 523–540.

(81) Sharma, B. L.; Sharma, N. K.; Bassi, P. S. Microstructure of Binary Organic Eutectics. *J. Cryst. Growth* **1984**, No. 67, 633–638.

(82) Law, D.; Wang, W.; Schmitt, E. A.; Qiu, Y.; Krill, S. L.; Fort, J. J. Properties of Rapidly Dissolving Eutectic Mixtures of Poly(Ethylene Glycol) and Fenofibrate: The Eutectic Microstructure. *J. Pharm. Sci.* **2003**, *92* (3), 505–515.

(83) Nau, M.; Biesalski, M.; Horn, M. Thermoresponsive Papierbeschichtungen auf Basis von Cellulosederivaten. DE 10 2018 111 495 B4 2020.04.09, 2018.

(84) Nau, M.; Seelinger, D.; Biesalski, M. Independent Two Way Switching of the Wetting Behavior of Cellulose-Derived Nanoparticle Surface Coatings by Light and by Temperature. *Adv. Mater. Interfaces* **2019**, *6* (17), 1900378. https://doi.org/10.1002/admi.201900378.

(85) Geissler, A.; Loyal, F.; Biesalski, M.; Zhang, K. Thermo-Responsive Superhydrophobic Paper Using Nanostructured Cellulose Stearoyl Ester. *Cellulose* **2014**, *21* (1), 357–366. https://doi.org/10.1007/s10570-013-0160-8.

(86) Tipler, P. A.; Mosca, G.; Wagner, J. *Physik*; Springer Berlin Heidelberg: Berlin, Heidelberg, 2015. https://doi.org/10.1007/978-3-642-54166-7.

(87) Bleck-Neuhaus, J. *Elementare Teilchen*; Springer Berlin Heidelberg: Berlin, Heidelberg, 2010. https://doi.org/10.1007/978-3-540-85300-8.

(88) Bleck-Neuhaus, J. *Elementare Teilchen*; Springer Berlin Heidelberg: Berlin, Heidelberg, 2013. https://doi.org/10.1007/978-3-642-32579-3.

(89) Meschede, D. *Gerthsen Physik*; Springer-Lehrbuch; Springer Berlin Heidelberg: Berlin, Heidelberg, 2015. https://doi.org/10.1007/978-3-662-45977-5.

(90) *Optical Measurements*; Mayinger, F., Ed.; Springer Berlin Heidelberg: Berlin, Heidelberg, 1994. https://doi.org/10.1007/978-3-662-02967-1.

(91) Fahey, T.; Islam, M.; Gardi, A.; Sabatini, R. Laser Beam Atmospheric Propagation Modelling for Aerospace LIDAR Applications. *Atmosphere* **2021**, *12* (7), 918. https://doi.org/10.3390/atmos12070918.

(92) Bohren, C. F.; Huffman, D. R. *Absorption and Scattering of Light by Small Particles*; Wiley-VCH: Weinheim, 2007.

(93) Mie, G. Beiträge Zur Optik Trüber Medien, Speziell Kolloidaler Metallösungen. *Ann. Phys.* **1908**, *330* (3), 377–445. https://doi.org/10.1002/andp.19083300302.

(94) Kubelka, P.; Munk, F. Ein Beitrag Zur Optik Der Farbanstriche. *Z. Für Tech. Phys.* **1931**, No. 11a, 593–601.

(95) Pauler, N. *Optische Papiereigenschaften*; AB Lorentzen & Wettre: Stockholm, 1991.

(96) Kubelka, P. New Contributions to the Optics of Intensely Light-Scattering Materials. Part 1. *J. Opt. Soc. Am.* **1947**, *38* (5), 448–457.

(97) Malcic, V.; Barbaric-Mikocevic, Z.; Itric, K. Kubelka-Munk Theory in Describing Optical Properties of Paper. *Tech. Gaz.* **2011**, *18* (1), 117–124.

(98) Granberg, H.; Béland, M.-C. Modelling the Angle-Dependent Light Scattering from Sheets of Pulp Fibre Fragments. *Nord. Pulp Pap. Res. J.* **2004**, *19* (3), 354–359.

(99) Lechner, M. D. *Makromolekulare Chemie*, 4. überarbeitete und erweiterte Auflage.; Gehrke, K., Nordmeier, E., Translators; Springer eBook Collection; Birkhäuser Basel: Basel, 2010. https://doi.org/10.1007/978-3-7643-8891-1.

(100) Chemister.ru. *Database - Dimethyloxalate - Physical Properties*. http://chemister.ru/Database/properties-en.php?dbid=1&id=679 (accessed 2023-11-05).

(101) Rosker, M. J.; Tang, C. L. Widely Tunable Optical Parametric Oscillator Using Urea. *J Opt Soc Am B* **1985**, *2* (5), 691–696.

(102) Chemister.ru. *Properties of the Substance: Benzoic Acid*. Database: Properties of Chemical Sustances. http://chemister.ru/Database/properties-en.php?dbid=1&id=679 (accessed 2024-01-13).

(103) Zhang, N.; Yuan, Y.; Du, Y.; Cao, X.; Yuan, Y. Preparation and Properties of Palmitic-Stearic Acid Eutectic Mixture/Expanded Graphite Composite as Phase Change Material for Energy Storage. *Energy* **2014**, *78*, 950–956. https://doi.org/10.1016/j.energy.2014.10.092.

(104) Baran, G.; Ahmet, S. Phase Change and Heat Transfer Characteristics of a Eutectic Mixture of Palmitic and Stearic Acid as PCM in a Latent Heat Storage System. *Energy Convers. Manag.* **2003**, *44*, 3227–3246.

(105) Neenah Gessner GmbH. *Neenah Gessner GmbH - Technologies*. https://www.neenah-gessner.de/en/technologies/ (accessed 2023-12-03).

(106) Wacker ChemieAG. *Technical Data Sheet - DEHESIVE-811 Wacker Chemie AG*. https://www.wacker.com/h/de-de/medias/DEHESIVE-811-en-2021.10.05.pdf (accessed 2023-12-03).

(107) Lutton, E. S. The Polymorphism of Tristearin and Some of Its Homologs. *J. Am. Chem. Soc.* **1945**, *67* (4), 524–527. https://doi.org/10.1021/ja01220a008.

(108) Malkin, T. The Polymorphism of Glycerides. *Prog. Chem. Fats Other Lipids* **1954**, *2*, 1–14. https://doi.org/10.1016/0079-6832(54)90003-8.

(109) Harkins, W. D. A General Theory of the Mechanism of Emulsion Polymerization. *J. Am. Chem. Soc.* **1947**, *6* (69), 1428–1444.

(110) Scheid, D.; Lühe, M.; Gallei, M. Synthesis of Breathing Metallopolymer Hollow Spheres for Redox-Controlled Release. *Macromol. Rapid Commun.* **2016**, *37* (19), 1573–1580. https://doi.org/10.1002/marc.201600338.

(111) Schawe, J.; Riesen, R.; Widmann, J.; Schubnell, M.; Jörimann, U. DSC-Kurven Interpretieren Teil 1: Dynamische Messungen. *UserCom - Mettler Toledo GmbH Anal.* **2000**, *11* (1), 1–7.

10 Index of Figures

11 Index of Tables

12 Appendix

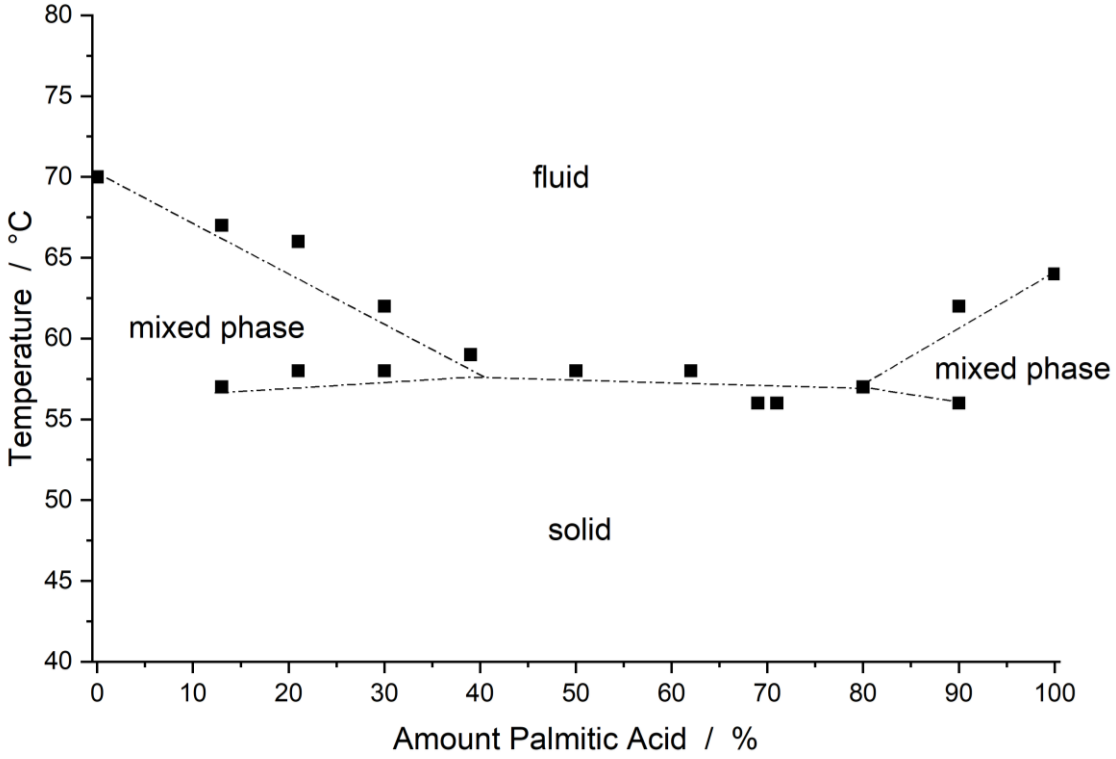

Figure 12.1 Phase diagram of palmitic (PAc) and stearic acid (SAc). The melting temperatures are determined via DSC measurements. The peak temperature of the melting peaks are used as melting temperatures. A eutectic range was found starting from 40 to 80 % PAc.

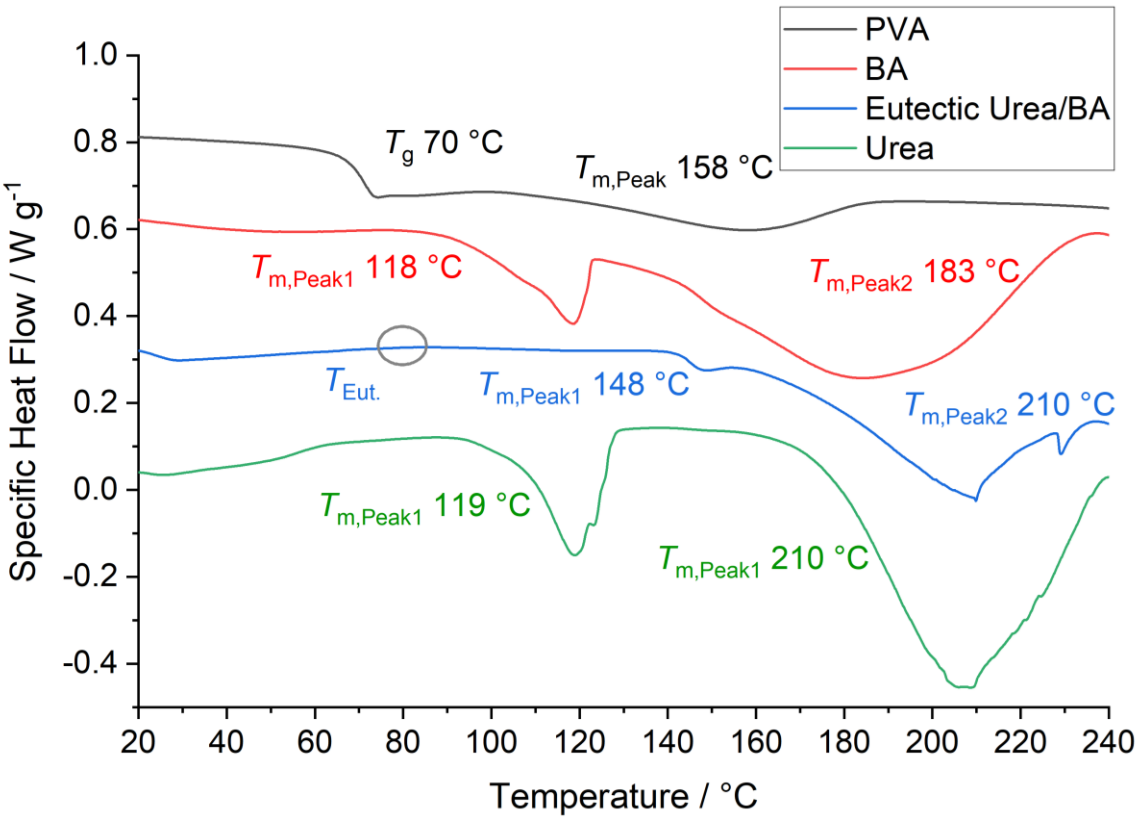

Figure 12.2: DSC thermogram of benzoic acid (BA) and urea in PVA, the eutectic mixture of BA and urea in PVA and pure PVA. The second heating cycle is displayed; the heating rate as well as the prior cooling rate is 10 K min^{-1}.

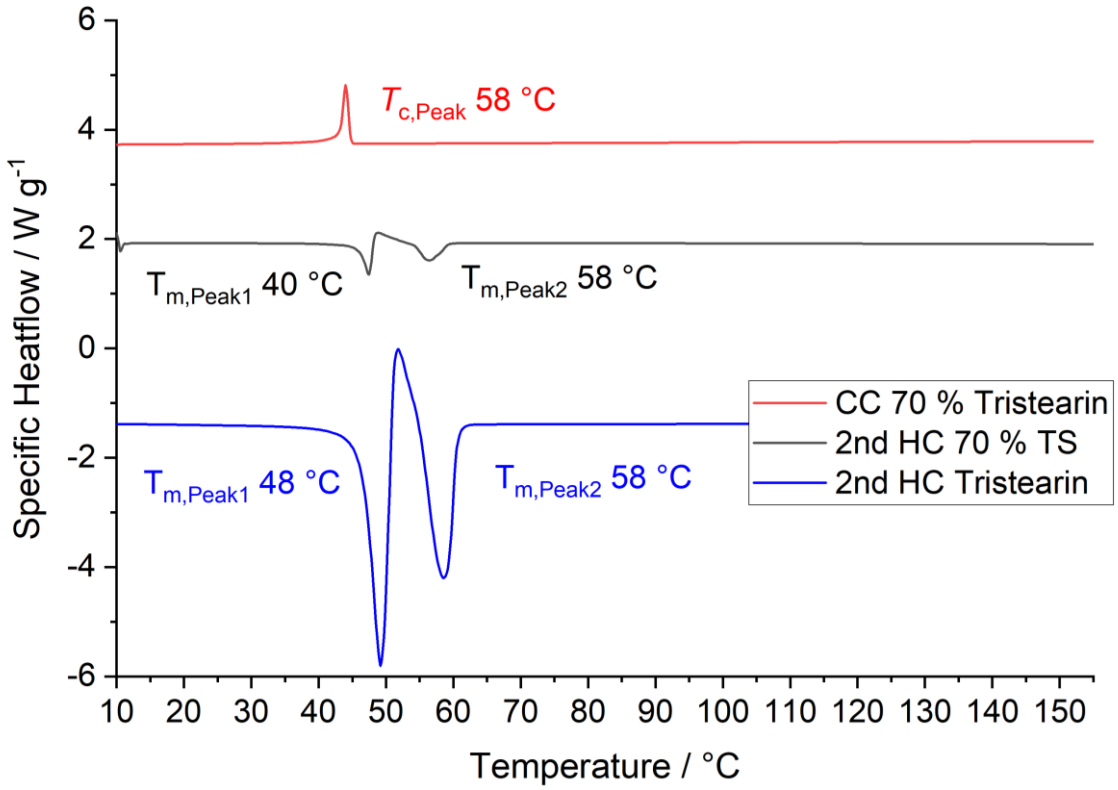

Figure 12.3: DSC thermogram of 70 % of tristearin (TS) melt-dispersed in PVA on PET and pure TS. Displayed is the second heating cycle with a heating, as well as prior cooling rate of 10 K min^{-1} (e66).

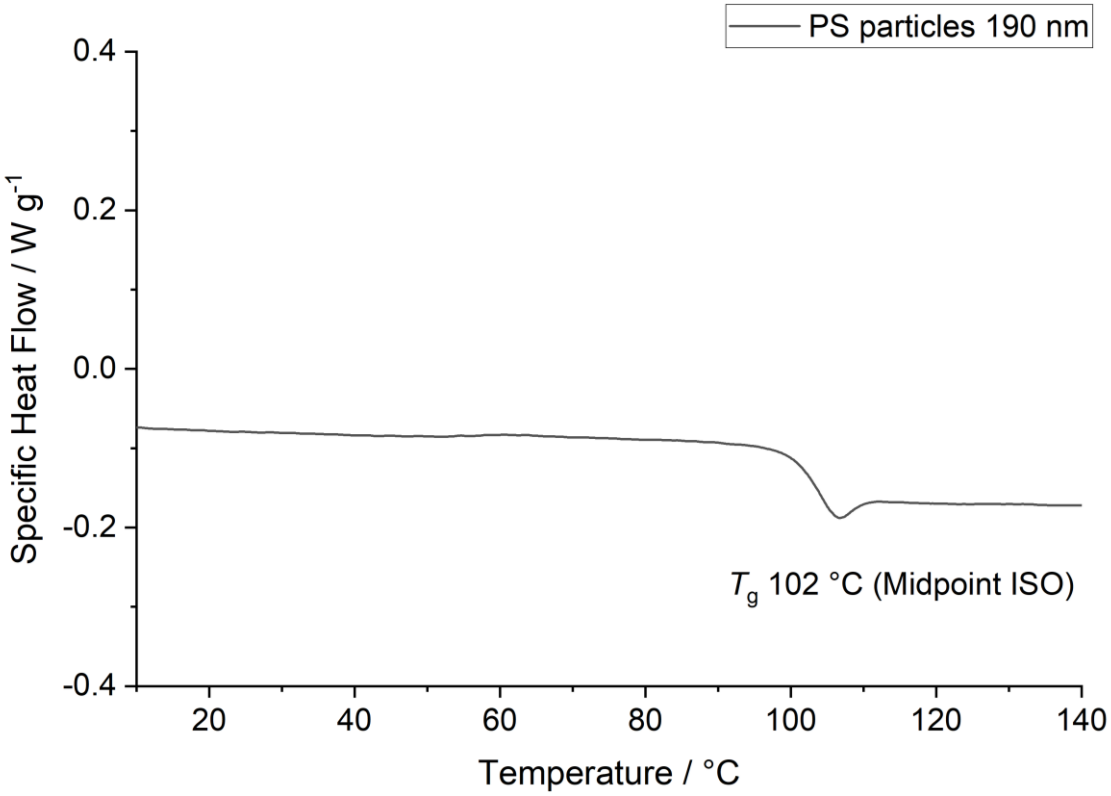

Figure 12.4: DSC thermogram of PS particles (e23). The second heating cycle is displayed, the heating as well as the prior heating rate is 10 K min^{-1}.

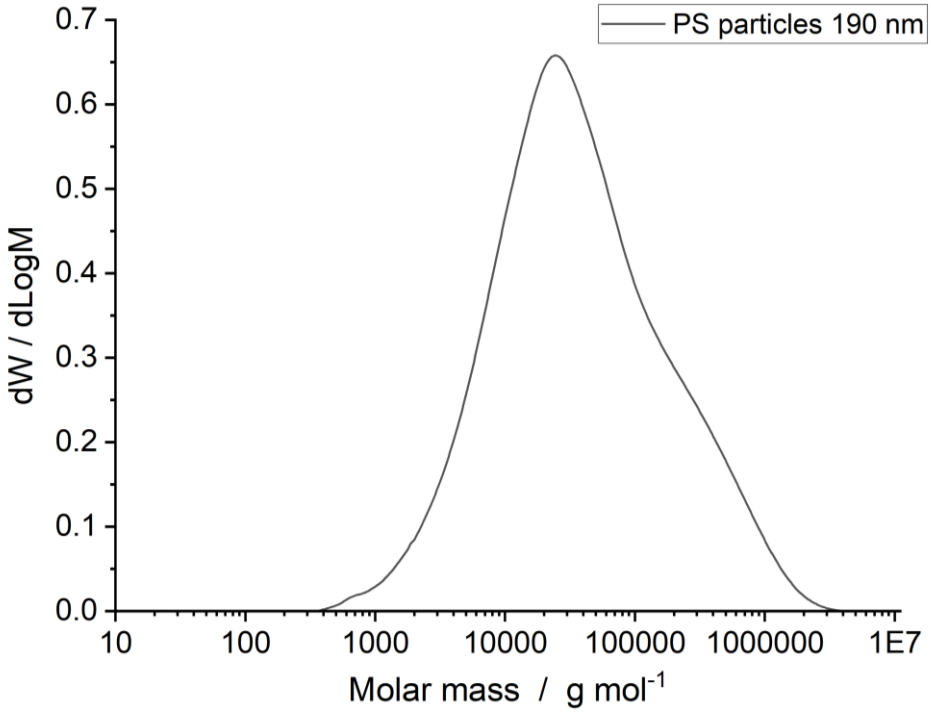

Figure 12.5: GPC elugram of PS-particles e23; EP2 (disssolved in THF; RID detector)

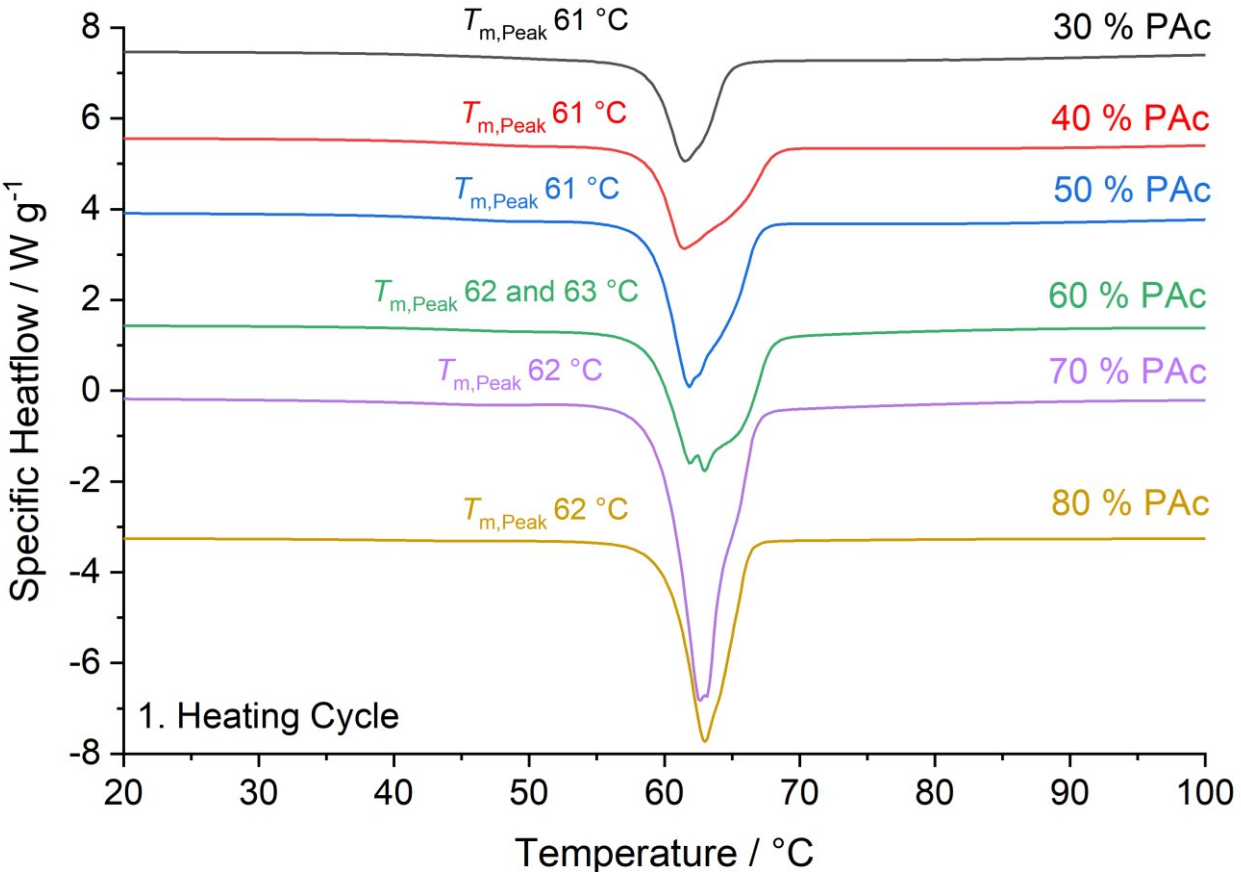

Figure 12.6: DSC thermogram of different amounts of palmitic acid (PAc) in PVA. The first heating cycle is displayed, to see if the particle size of the PAc, which increases with the concentration of PAc, has an influence of the melting temperature. The heating and the prior cooling rate is 10 K min^{-1}.

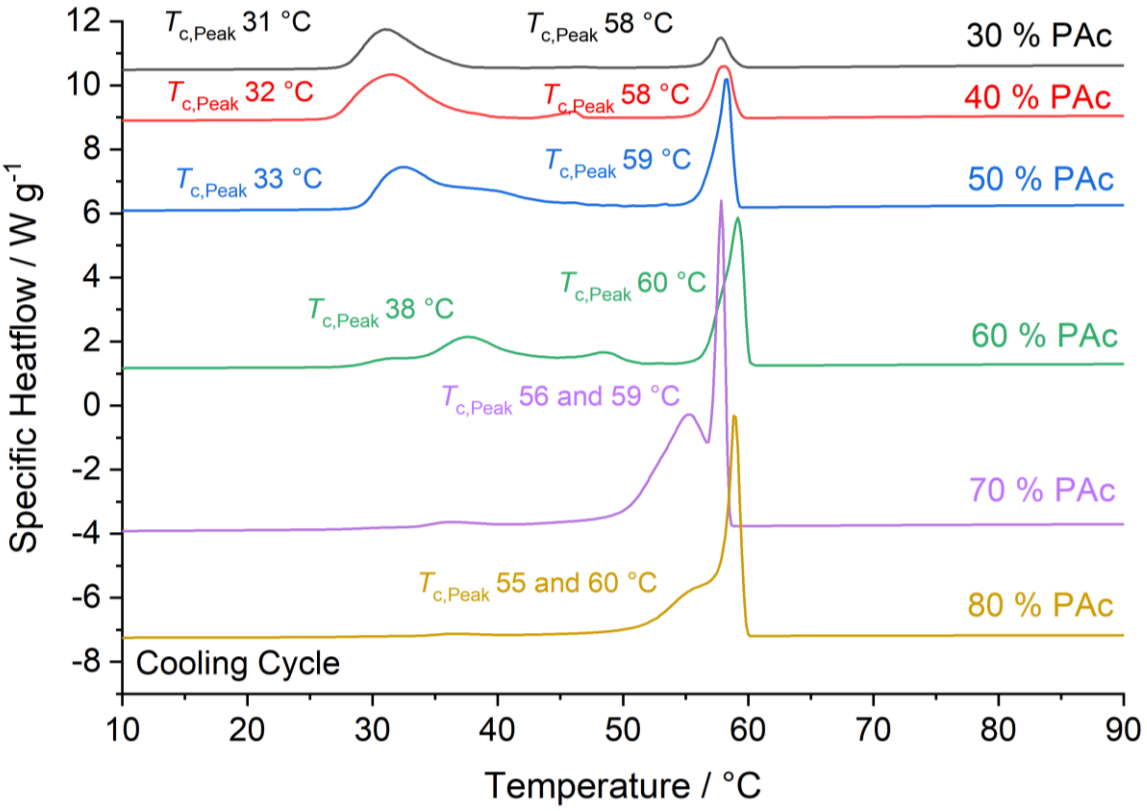

Figure 12.7: DSC thermogram with the crystallization temperatures of the different amounts of palmitic acid (PAc). The first cooling cycle is displayed.The cooling and the prior heating rate is 10 K min^{-1}.

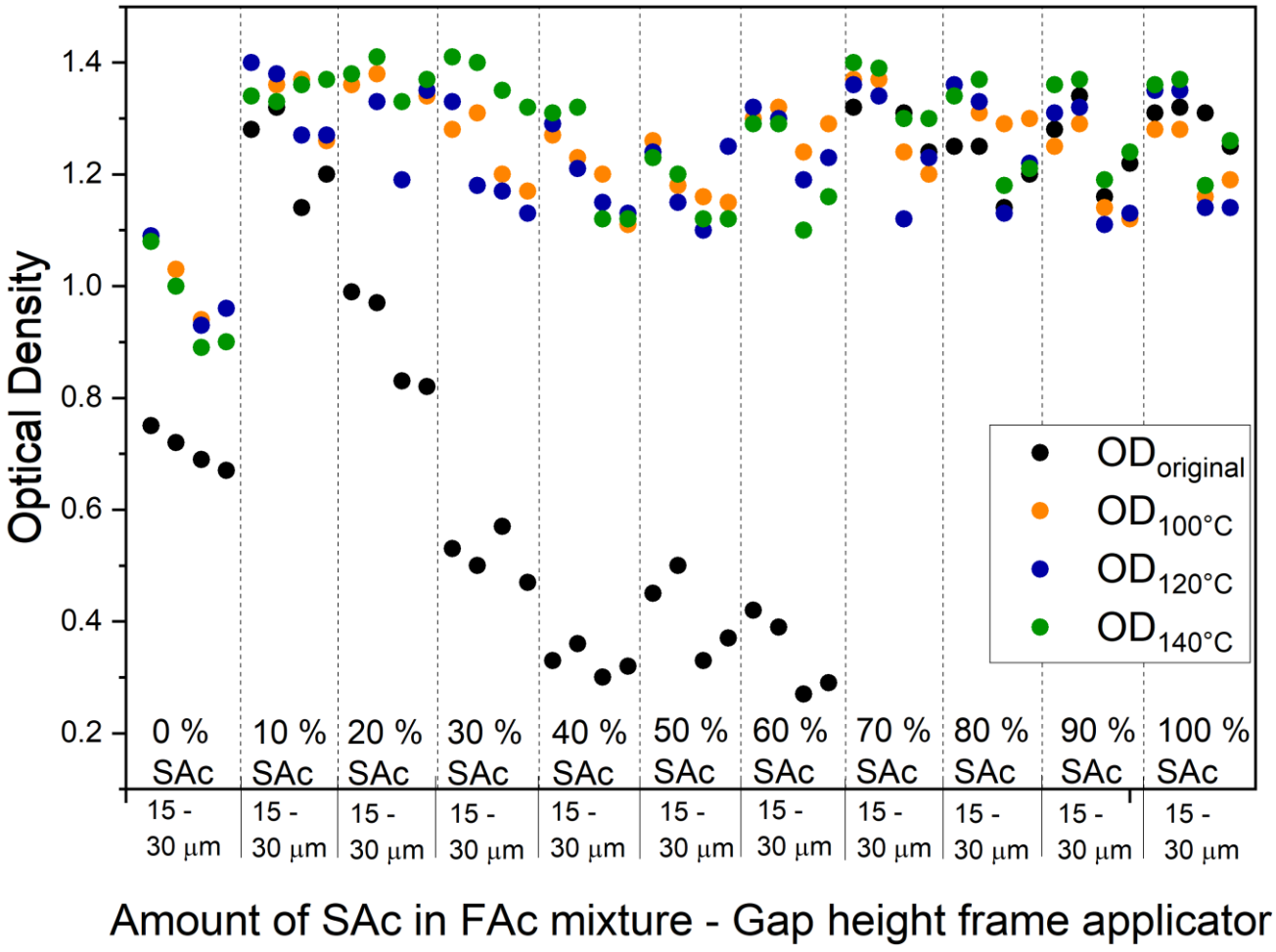

Figure 12.8: Optical densities of samples out of 70 % of fatty acid in PVA. The composition of the fatty acids is varying, which is indicated by the amount of SAc in the fatty acid mixture. They are coated on black paper with four different gap heights (15, 20, 25 and 30 µm; 30 % solid content in coating formulation). These values are in between the dotted lines from small to biggest from left to right.

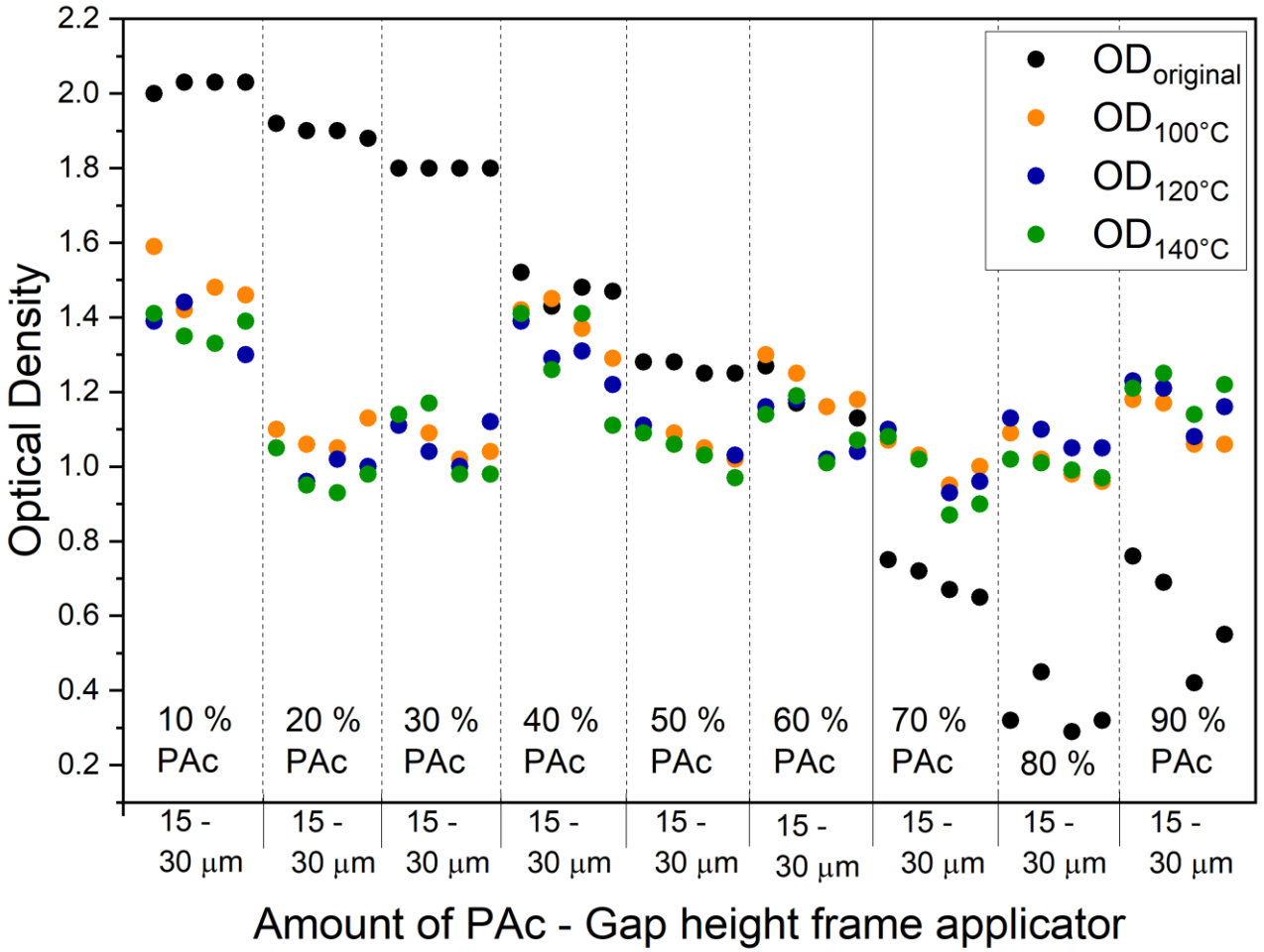

Figure 12.9: Optical densities of samples with different amounts of PAc in PVA. The composition of the fatty acids is varying. They are coated on black paper with four different gap heights (15, 20, 25 and 30 µm; 30 % solid content in coating formulation). These values are in between the dotted lines from small to biggest from left to right.

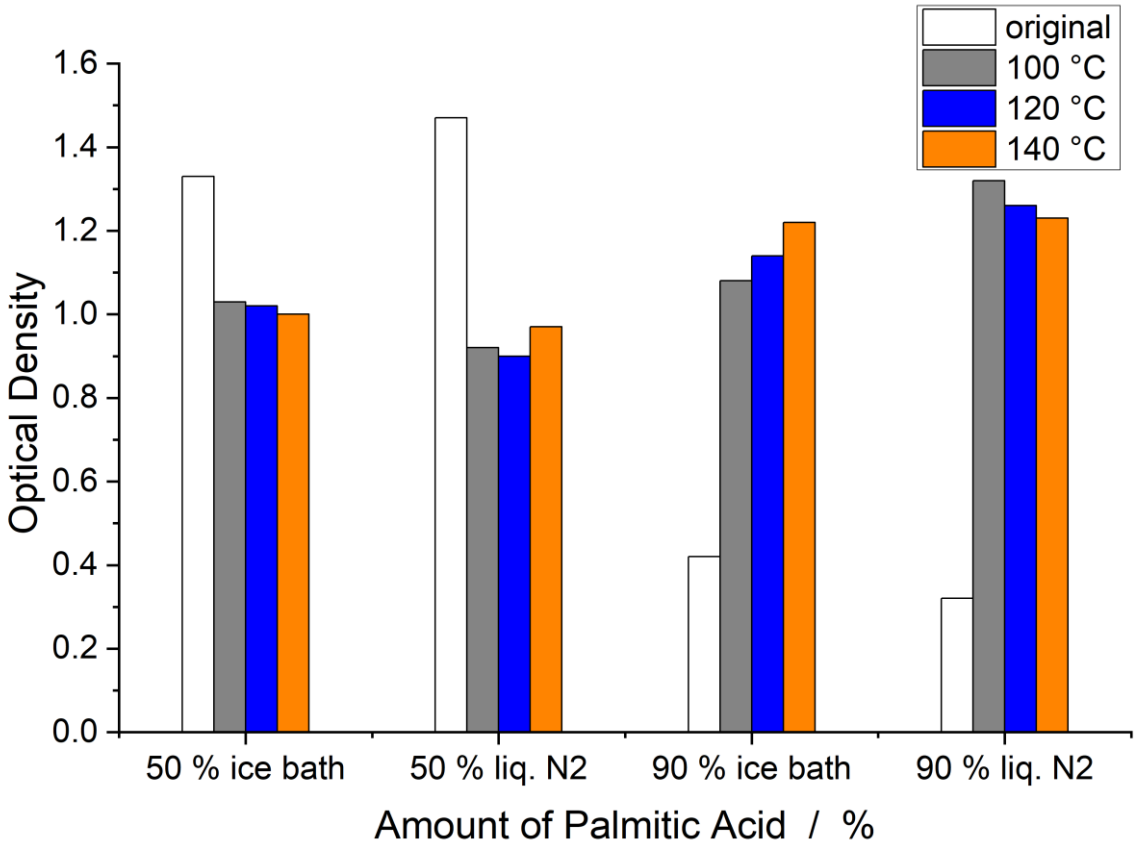

Figure 12.10: Optical densities of samples with different amounts of PAc in PVA. The coatings were cooled down after the melt dispersion with an ice bath and liquid nitrogen to see if the cooling process has an influence of the opacity and switchability of the coatings. The formulations are coated on paper with a film frame applicator; gap width 30 µm, 30 % solid content in coating formulations.